

A COUPLING MATRIX VISION FOR
MOBILE FILTERING DEVICES WITH
MICRO-ACOUSTIC WAVE TECHNOLOGIES.
A SYSTEMATIC APPROACH

Mercedes Jimenez Blasco

July 31, 2015



Universitat Autònoma de Barcelona

Department of Telecommunications and Systems Engineering

**A COUPLING MATRIX VISION FOR
MOBILE FILTERING DEVICES WITH
MICRO-ACOUSTIC WAVE TECHNOLOGIES.
A SYSTEMATIC APPROACH**

a Ph.D. Thesis of the Universitat Autònoma de Barcelona in the program of
PhD in Telecommunications and Systems Engineering

Mercedes Jimenez Blasco

Thesis Supervisor:

Dr. Pedro de Paco Sánchez

July 2015

*“Mystery creates wonder
and wonder is the basis
of man’s desire to understand”*

— Neil Armstrong

ABSTRACT

With a spectrum more and more overcrowded, filters and duplexers are drivers of the technology in the discrete device mobile market. The user segment of wireless communication systems takes profit of the outstanding performance of filtering devices based on acoustic resonators.

Usually, the design of acoustic wave devices have been mainly entrusted to optimization techniques because of the stringent constraints imposed by the technological feasibility of SAW and BAW resonators and the challenging electrical specifications. A stringent transmission response and very restrictive technological factors lead the design to a more and more complex and challenging task.

The aim of the work is focused on easing the filters/duplexers designs and making it more efficient. Consequently, the initial formulation of the problem was focused on the technological feasibility of acoustic wave filters. Providing a systematic methodology is useful to accelerate the learning curve of new entrant designers.

Microwave filters with high selectivity are possible if their transfer functions incorporates finite transmission zeros. The inclusion of non-resonant nodes gives the possibility of designing filters with the maximum number of finite transmission zeros without implementing direct couplings between source and load. Furthermore, inline configuration with NRN allows the extraction of the elements analytically.

The common ladder filter configuration exhibits characteristic similarities regarding inline prototype networks with resonant and non-resonant nodes, which are the property of modularity, to control transmission zeros by independent resonators, and fully canonical response without a direct source-load coupling.

The elements of the bandpass network are given by explicit equations in terms of those in in-line prototypes with non-resonating nodes that can

be synthesized analytically. As a consequence it is possible to define a direct synthesis methodology to obtain the bandpass electric parameters of a general RF filter that is based on acoustic resonators.

This work presents a methodology that provides a systematic synthesis procedure for designing ladder filters and duplexers based on acoustic wave resonators. The methodology uses a nodal approach based on resonating and non-resonating nodes. The coupling matrix representation with a mix of different nature nodes, resonant and non-resonant, is able to efficiently manage the technological restrictions.

The procedure is time efficient, precise in the outcomes and provides a deep understanding of the particular interactions between technological constraints and device performance.

A complete software package with fast, accurate and easy-to-use simulator has been developed, enabling starting point design success.

As a result of the systematic methodology, we have developed a design method that combines and systematically manages a filtering network composed of extracted-pole blocks with coupling resonators blocks, so it is ladder cells with CRF sections.

Moreover, the methodology has been successfully extended to take into consideration filtering power dividers by means of two different topologies: ladder configuration and CRF sections.

The proposed methodology offers a solution that combines a complete spectrum fulfillment with topologies ready to accommodate technological constraints of micro-acoustics technologies. The methodology has been developed natively oriented to manage with the technology, such as accommodating electromechanical coupling constraints, leveraged in rigorous synthesis foundations.

RESUMEN

Con el espectro radioeléctrico cada vez más saturado, los filtros y duplexores son elementos claves de la tecnología en el mercado de dispositivos discretos para la telefonía móvil. El segmento de usuario de los sistemas de comunicaciones inalámbricas aprovecha las destacadas propiedades de los dispositivos filtrantes basados en resonadores acústicos.

Generalmente, el diseño de dispositivos de onda acústica ha sido asumido por técnicas de optimización debido a las restrictivas limitaciones impuestas por la viabilidad tecnológica de los resonadores SAW y BAW, así como las exigentes especificaciones eléctricas. Una respuesta de transmisión muy restrictiva y factores tecnológicos muy limitantes conducen a hacer el diseño más y más complejo y una tarea muy desafiante.

El objetivo del trabajo está enfocado en facilitar el diseño de filtros/duplexores y hacerlo más eficiente. En consecuencia, la formulación inicial del problema se ha centrado en la viabilidad tecnológica para implementar filtros de onda acústica. Proporcionar una metodología sistemática es útil para acelerar la curva de aprendizaje de nuevos diseñadores.

Los filtros de microondas con elevada selectividad son posibles si sus funciones de transferencia incorporan ceros de transmisión finitos. La introducción de nodos no-resonantes (NRN) da la posibilidad de diseñar filtros con el máximo número de ceros de transmisión finitos sin tener que implementar acoplamientos directos entre la fuente y la carga. Además, las configuraciones en línea con NRN permiten la extracción de los elementos analíticamente.

La típica configuración de filtro ladder presenta similitudes características de acuerdo con las redes de prototipo en línea con nodos resonantes y no-resonantes, que son las propiedades de modularidad, para controlar los ceros de transmisión con resonadores independientes, y respuestas completamente canónicas sin acoplamiento fuente-carga directo.

Los elementos de la red pasobanda son dados por ecuaciones explícitas en términos de aquellos en los prototipos en línea con NRN que pueden ser sintetizados analíticamente. Como consecuencia, es posible definir una metodología de síntesis directa para obtener los parámetros pasobanda eléctricos de un filtro RF general que está basado en resonadores acústicos.

Este trabajo presenta una metodología que proporciona un procedimiento de síntesis sistemático para diseñar filtros y duplexores ladder basados en resonadores de onda micro-acústica. La metodología de diseño utiliza un enfoque nodal basado en NRN y nodos resonantes. La representación de la red mediante una matriz de acoplamiento mixta de nodos resonantes y no resonantes es capaz de gestionar de forma eficiente las restricciones tecnológicas.

El procedimiento es eficiente en tiempo, preciso en los resultados y proporciona un profundo entendimiento de las particulares interacciones que se producen entre las restricciones tecnológicas y el funcionamiento del dispositivo.

Un completo paquete de software, con un simulador rápido, preciso y de fácil uso, ha sido desarrollado, permitiendo obtener diseños de primera etapa exitosos.

Como resultado de la metodología sistemática, hemos desarrollado un método de diseño que combina y sistemáticamente gestiona redes filtrantes compuestas de bloques de polo extraído con bloques de resonadores acoplados, es decir, celdas ladder con secciones CRF.

Además, la metodología ha sido extendida exitosamente para tener en cuenta el diseño de divisores de potencia con respuesta filtrante por medio de dos topologías diferentes: la configuración ladder y las secciones CRF.

La metodología propuesta ofrece una solución que combina el completo cumplimiento de las máscaras de espectro con topologías preparadas para acomodar las restricciones tecnológicas de la tecnología micro-acústica. La metodología ha sido desarrollada orientada nativamente a gestionar la tecnología, como es el ajuste de la limitación en el acoplo electromagnético, y basada en fundamentos de síntesis rigurosos.

ACKNOWLEDGEMENTS

Herein, you will find my sincere thanks to many people who filled my life as a PhD student with some best moments. First of all, I must thank my supervisor, Prof. Pedro de Paco, for giving me the opportunity to immerse in the research of BAW and SAW filters, for his encouragement and guidelines throughout this research work. Apart from his continuous support and patience, he shared his enthusiasm for improving and gave me valuable suggestions. In these four years he always had time for me.

I use this opportunity to thank Prof. Josep Parron and Prof. Gary Junkin that are members of the Antenna and Microwave Systems group. I thank my previous project supervisor Prof. Oscar Menendez for introducing me in the field of BAW filters, extending your kind support and advice.

Work apart, PhD at UAB was also fun with the Telecommunications department and the AMS group. First in the list are my current and past roommates: Alfred, Eden, Iuliia, Joan, Jordi, Monica, Rafa and Sergi. I would like to extend my thanks to my other colleagues, recent and future doctors: Albert, Alex, Juanma, Marc, Moi, Paresh and Smrati. Specially thanks to Ricard (*Richi*) for all the laughs and friendship.

I would also like to acknowledge my family for their support. My parents, Salvadora and Jose Antonio, thank you for believing in me and your help. Thanks to my brother (*Tete*), who is always there, and Sara for giving me these little gifts, Berta and Dídac.

A special thanks to Héctor for supporting my grumpy mood especially when I was writing the thesis. Thanks for giving me your optimistic perspective and for all those motivational words. I would never have been able to finish the thesis without your kind support through out my PhD.

Hoping to do not miss anyone, I would like to thank everybody who gives me his unconditional support, time and love.

EPCOS AG, a TDK Group company develops, manufactures and markets electronic components, modules and systems, focusing on fast-growing leading-edge technology markets, which include information and communications technology, automotive electronics, industrial electronics and consumer electronics. SAW and BAW components are key components of modern information and communications systems.

TDK-EPC funds and follows with great interest the results of the research activities carried out in the Universitat Autònoma de Barcelona through Dr. Karl Wagner, Vice-President Advanced Development Discretes.

CONTENTS

1	Introduction	1
1.1	The basics of acoustic wave filters	4
1.1.1	The BAW and SAW filter topology	6
1.1.2	The acoustic wave resonator modeling	9
1.2	Problem description and motivation	10
1.3	Solution approach	14
1.4	Outline of the thesis	16
1.5	Research contributions	17
2	Synthesis Methodology and Procedure	19
2.1	Characterization of filter networks	20
2.2	The Chebyshev class of filtering function	21
2.2.1	Relationship between ϵ and ϵ_R	22
2.2.2	Example polynomial synthesis	22
2.3	Coupled resonator filters with finite transmission zeros	24
2.4	Generalization of the coupling matrix	28
2.5	Analysis of the network represented by the Coupling Matrix	31
2.6	Synthesis of filters with NRNs by analytical expressions	33
2.6.1	Reflection Coefficients S_{11} and S_{22}	34
2.6.2	Reflection Coefficients with Phase Adjustment	37
2.6.3	Cases analysis of network element extraction	40

2.6.4	Extraction pole synthesis examples	49
2.6.5	Scaling property	56
2.7	Summary	58
3	Ladder Filters and Duplexers	59
3.1	Synthesis of acoustic-wave resonators from lowpass circuit approach	60
3.2	Acoustic wave resonators	60
3.2.1	SAW	62
3.2.2	BAW	63
3.2.3	Electrical characteristics of piezoelectric acoustic-wave resonators	65
3.2.4	Electrical Equivalent Circuit	66
3.3	LP model of acoustic-wave resonator	71
3.3.1	Zero-pole modules	77
3.3.2	Lowpass to Bandpass Model Transformation	83
3.3.3	Scaling property on the extracted pole sections which models acoustic-wave resonators	88
3.3.4	Two equivalent topologies of a lowpass acoustic-wave resonator: the singlet and the dangling resonator	89
3.3.5	Bandpass prototype filter adapted to feasible acoustic wave technology	91
3.4	Ladder filter of acoustic-wave resonators	94
3.4.1	Methodological design procedure for ladder-type filters based on acoustic wave resonators	97
3.4.2	Technological interactions of acoustic wave filters	101
3.4.3	Automatic search engine to design ladder-type filters based on acoustic-wave technologies	108
3.4.4	Physical implementation of asymmetrical filters	117
3.5	Ladder duplexer of acoustic-wave resonators	119

3.5.1	Mechanisms to overcome the duplexer degradation caused by the loading effect	120
3.5.2	Automatic search-engine for Duplexer design	123
3.6	Summary	130
4	Hybrid filter designs	131
4.1	Hybrid filters with combined topology	132
4.2	Structures of acoustically coupled resonators	135
4.2.1	Coupled Resonator Filter	136
4.2.2	Dual Mode SAW	138
4.3	Synthesis of hybrid prototypes	142
4.3.1	Example of design of a hybrid topology combination of ladder and CRF	145
4.4	Summary	148
5	Filtering power dividers	151
5.1	Introduction to filtering power dividers	152
5.2	Power divider ladder topology	153
5.2.1	Fully Canonical Filtering Power Divider	155
5.2.2	Examples and the analysis of miniaturized filtering power dividers	156
5.2.3	Design of an equal power divider	157
5.2.4	Design of unequal power divider	160
5.3	Power divider CRF topology	165
5.3.1	Coupling matrix synthesis of filtering power divider	165
5.3.2	T-topology power divider implemented with CRF sections	168
5.3.3	Topology I: No-shared resonators	171
5.3.4	Topology II: Two-shared resonators	174

5.3.5	Comparison of two topologies for power divider based on CRF sections	177
5.4	Summary	178
6	Conclusions and Future work	181
6.1	Conclusions	181
6.2	Future research recommendations	185

LIST OF FIGURES

1.1	Filter configurations of electrically connected resonators: (a) ladder-type filter and (b) lattice-type filter.	6
1.2	SAW Filter configurations of acoustically coupled resonators: (a) transversely and (b) longitudinally.	7
1.3	BAW Filter configurations of acoustically coupled resonators: (a) Stacked Crystal Filter and (b) Coupled Resonator Filter.	8
1.4	BVD electrical equivalent model of a BAW/SAW resonator.	9
1.5	Integrated designs face emerging filtering challenges.	15
2.1	Lowpass prototype transfer and reflection characteristics of the 5th-degree Chebyshev filter with two prescribed transmission zeros at $s_1 = +j2.1$ and $s_2 = -j1.3$	23
2.2	Lowpass prototype transfer and reflection characteristics of the 5th-degree Chebyshev filter with five prescribed transmission zeros at $s_1 = +j2.4$, $s_2 = -j1.72$, $s_3 = -j1.72$, $s_4 = j1.76$ and $s_5 = j1.76$	24
2.3	Nodal representation for lowpass prototype circuits based on coupled resonators. Two fifth-order inline filters ($N = 5$): (a) with two real transmission zeros $n_{fz} = 2$ and (b) with fully canonical response $n_{fz} = N = 5$	26
2.4	Low-pass prototype circuit of a third-order inline filter introducing two NRNs without dangling resonator.	28
2.5	Admittance matrix $[\mathbf{A}]$ of the general multicoupled circuit of parallel resonators operating between a source conductance G_S and a load conductance G_L	31

2.6	Schematic representation of a doubly loaded extracted pole filter of a fifth-order with two real transmission zeros. . . .	33
2.7	Circuit with the first node from the input (output) a resonator.	35
2.8	Circuit with the first node from the input (output) an NRN with dangling resonator.	36
2.9	Circuit with the first node from the input (output) an NRN alone without dangling resonator.	38
2.10	Circuit to extract a resonator. The elements are the inverter J and the reactance jb	40
2.11	Circuit to extract an NRN with dangling resonator. The elements are J , jB and J_1	42
2.12	Circuit to extract the parameters of the last resonator: J , jb and J_1	44
2.13	Circuit to extract the parameters of the last NRN with dangling resonator: J , jB , J_1 and J_2	45
2.14	Circuit to extract the parameters J , jB_1 , J_1 , J_2 , J_3 and jB_2 of the two last NRNs and a load conductance different to the unit.	46
2.15	Circuit to extract the parameters J and jB_1 of an NRN alone following a resonator.	48
2.16	Circuit to extract the parameters J and jB_1 of an NRN alone following an NRN.	49
2.17	Lowpass prototype circuit of a fifth-order inline filter with two real transmission zeros $n_{fz} = 2$	50
2.18	Lowpass prototype transfer and reflection responses of the extracted filter of Fig. 2.17 with TZ at $s_1 = +j2.1$ and $s_2 = -j1.3$ rad/s.	51
2.19	Lowpass prototype circuit of a fifth-order inline filter with five real transmission zeros $n_{fz} = 5$	52
2.20	Lowpass prototype transfer and reflection responses of the extracted filter of Fig. 2.19 with TZ at $s_1 = +j1.76$, $s_2 = -j1.72$, $s_3 = j2.4$, $s_4 = -j1.72$ and $s_5 = j1.76$ rad/s.	52

2.21	Lowpass prototype phase reflection response of the 5th-degree Chebyshev filter with five prescribed transmission zeros. The phase term of S_{11} at the frequency $s_1 = j1.76$ of the first transmission zero from the input is zero.	53
2.22	Lowpass prototype circuit of a fifth-order inline filter with fully canonical response $n_{fz} = N = 5$ and two extra NRN input/output elements to make phase adjustment.	54
2.23	Lowpass prototype phase reflection response of the 5th-degree fully canonical Chebyshev filter with a phase adjustment of $\theta_e = 18.97^\circ$ respect the phase response on Fig. 2.22.	55
3.1	Surface Acoustic Wave (SAW) Resonator. The acoustic wave propagates on the surface of the piezoelectric substrate. . .	62
3.2	Bulk Acoustic Wave (BAW) Resonator. The acoustic wave propagate through the interior of the piezoelectric substrate. . .	63
3.3	BAW resonators: (a) Film bulk acoustic resonator (FBAR) free standing structure, (b) Solidly Mounted Resonator (SMR) structure.	64
3.4	Magnitude and phase of input electric impedance as a function of frequency on a BAW resonator [60].	65
3.5	Lumped-element electrical equivalent circuit of an acoustic-wave resonator, the BVD model.	66
3.6	Modified Butterworth Van-Dyke equivalent circuit of an acoustic-wave resonator considering losses mechanisms.	68
3.7	Magnitude response of an acoustic-wave resonator configured in shunt.	72
3.8	Magnitude response of an acoustic-wave resonator configured in series.	73
3.9	Lowpass circuit schematic of a shunt resonator, (a) a nodal diagram representation of the extracted pole section, (b) equivalent circuit schematic.	73
3.10	Equivalent lowpass circuit BVD model of a shunt resonator	73

3.11	Lowpass circuit schematic of a series resonator, (a) a nodal diagram representation of the extracted pole section, (b) equivalent circuit schematic.	75
3.12	Equivalent circuit schematic of Fig. 3.11 using lowpass BVD circuit representation.	75
3.13	Equivalent lowpass circuit model for a series resonator in Y-network form.	76
3.14	$Y - \Delta$ network transformation: (a) Y circuit representation, (b) Δ circuit representation and equivalent lowpass circuit BVD model for series resonator.	77
3.15	Schematic representation of a doubly-loaded extracted pole section of Fig. 3.9 for a shunt equivalent resonator.	78
3.16	Schematic representation of a doubly-loaded extracted pole section of Fig. 3.11 for a series equivalent resonator.	81
3.17	Frequency transformation applied to the lowpass prototype BVD model to the bandpass BVD model of an acoustic-wave resonator.	84
3.18	Input impedance of an acoustic-wave resonator modeled with the bandpass BVD model, when normalizing the frequency, (dashed line) and with the lowpass extracted pole section prototype (solid line).	86
3.19	Singlet lowpass equivalent model of a series acoustic-wave resonator: (a) nodal representation, (b) circuital schematic.	89
3.20	Δ -Y network transformation applied to the bandpass BVD model of a resonator.	92
3.21	(a) General configuration for a ladder-type filter, (b) equivalent prototype.	95
3.22	Performance principle of one basic ladder-cell, $N = 2$	95
3.23	Computed power density of each resonator in the ladder filter for Tx B3 application at 1.785 GHz frequency.	100
3.24	Simulated frequency response of an 5th-degree ladder filter for Tx B3 application.	100

3.25	Passband simulation Insertion Loss and Return Loss of designed 5th-degree ladder filter.	101
3.26	For different return loss on a 7th-degree ladder filter with predefined transmission zeros, computed (a) the capacitance ratio r of each resonator and (b) the series resonance frequency f_s . For the symmetric ladder network, results are equivalent for Res 1 with Res 7, Res 2 with Res 6 and Res 3 with Res 5.	104
3.27	Capacitance ratio of each resonator (a) and series resonance values (b) for each resonator of the filter when all the transmission zeros are predefined except the one corresponding to 2nd and 6th resonator. Computed over the normalized frequency of the TZ.	106
3.28	Design procedure overview.	110
3.29	Filtering frequency response of the optimized design for Tx WCDMA Band 1 computing (a) the feasibility of the constraints (b) the maximization of the return loss. The quality factor used on the circuit simulations is $Q=1500$	115
3.30	Power density response of the optimized design for Tx WCDMA Band 1 at 1.98 GHz according to solution (a) from Fig. 3.29(a) (b) and from Fig. 3.29(b).	116
3.31	Filtering frequency response of the optimized design for Rx WCDMA Band 1 computing the maximization of the return loss. The quality factor used on the circuit simulations is $Q=1500$	117
3.32	Schematic of a duplexer with matching networks.	120
3.33	Nodal representation of a circuit with I/O external elements for phase adjustment.	122
3.34	Simulation of the frequency response and detail of insertion loss of the WCDMA band 1 receiver filter. The quality factor used on the circuit simulations is $Q=1500$ for resonator and $Q=25$ for I/O inductors.	125
3.35	Simulation of the reflection phase of the WCDMA band 1 receiver filter.	126

3.36	Simulation of the frequency response and detail of the insertion loss of the WCDMA band 1 transmitter filter. The quality factor used on the circuit simulations is $Q=1500$ for resonator and $Q=25$ for I/O inductors.	127
3.37	Simulation of the reflection phase of the WCDMA band 1 transmitter filter.	127
3.38	Nodal representation of a duplexer with an 7th-degree filter for the Tx joined with a 7-th degree Rx filter in the antenna port.	128
3.39	Network of the synthesized WCDMA band 1 duplexer with ladder filters with input and output inductors.	128
3.40	Simulation of the synthesized WCDMA band 1 duplexer, with $Q=1500$ for resonator and $Q=25$ for I/O inductors. . .	129
3.41	Insertion loss detail for WCDMA band 1 duplexer in the Tx and Rx bands, with $Q=1500$ for resonator and $Q=25$ for I/O inductors.	129
4.1	Prototypes with hybrid topology, part of the structure with ladder building blocks and part with (a) one-pole section, (b) two-pole section, (c) a triplet section and (d) cross-coupled section.	133
4.2	Triplet transformation into inline extracted pole building block.	134
4.3	Equivalent bandpass circuits of building blocks: (a) one-pole section, (b) two-pole section and (c) a triplet section.	135
4.4	Side view of a CRF (a) a single section, and (b) two sections connected electrically in series to allow input and output at the top layers.	136
4.5	Equivalent circuit model of a Coupled Resonator Filter. . .	137
4.6	DMS filter configuration: (a) structure of a DMS, and (b) passband performance of a DMS filter for GSM-Rx [51]. . .	139
4.7	Equivalent circuit model for operation of a DMS filter. . . .	140
4.8	Inline nodal diagram of a 2-pole DMS filter with reactive ports and the equivalent bandpass filter LC series circuit. .	141

4.9	Nodal diagram representations for 3-mode DMS interpretation with one transmission zero.	141
4.10	Topologies of the filtering structure prototype network of $N=6$ and 4 TZs at finite frequencies to be implemented with a CRF block connected (a) with shunt resonators, and (b) with series resonators.	143
4.11	A FIR element is shared by the NRN of a shunt resonator and the I/O of a CRF when they are connected in a hybrid filter.	144
4.12	Proposed hybrid filter combining two ladder cells and in between a CRF structure of 2-poles.	145
4.13	Simulated transmission and reflection response of the designed hybrid filter for Band 3 Tx combining ladder and CRF cells.	148
4.14	Passband simulation Insertion Loss and Return Loss of designed hybrid filter for Band 3 Tx.	149
5.1	Structure and analysis of the presented bandpass-response power divider.	154
5.2	Topology of the filtering structure prototype network for $N = 4$ allowing different source and load normalized conductances.	155
5.3	Filtering equal power divider for RX W-CDMA with BAW resonators for miniaturization.	157
5.4	Simulated transmission and reflection responses with loss for the proposed 3-dB filtering power divider on W-CDMA band.	159
5.5	Simulated isolation and phase imbalance responses between outputs for the proposed 3-dB filtering power divider.	160
5.6	Filtering unequal power divider for Rx W-CDMA Band 1 application. (a) Schematic network configuration for power division ratio $\alpha^2 = 2$ with a total of 6 acoustic wave resonators. (b) Prototype network nodal diagram with the topology proposed for each filtering block of order $N = 3$	161

5.7	Simulated transmission and reflection responses with loss for the proposed unequal filtering power divider on W-CDMA band.	163
5.8	Simulated reflection frequency response in the passband region and both transmission responses with different power split corresponding to a power division ratio $\alpha^2 = 2$	164
5.9	Simulated Isolation of ports 2 and 3 of the BAW unequal power divider	164
5.10	Nodal representation of a T-topology power divider.	167
5.11	Two power dividers with bifurcated topologies proposed for 4-th order filtering function. (a) Topology with no-shared resonator, $k = 0$. (b) Topology with two-shared resonators $k = 2$	168
5.12	4-pole CRF filter. (a) Nodal representation of the corresponding main-line configuration. (b) Response for the 4-pole CRF centred at 2140 MHz with 60 MHz of bandwidth.	169
5.13	Filtering equal power divider with no-shared resonators build up of two identical 4 order CRF branches and a total of 4 CRF basic sections.	171
5.14	Filtering equal power divider response with topology I for W-CDMA application.	174
5.15	Filtering equal power divider with two-shared resonators based on 3 CRF basic sections.	175
5.16	Filtering equal power divider response with topology II for W-CDMA application.	177

LIST OF TABLES

2.1	Corresponding polynomials of a Chebyshev filter function with two prescribed transmission zeros.	23
2.2	Corresponding polynomials of a Chebyshev filter function with five prescribed transmission zeros.	24
2.3	Corresponding input admittance polynomials of prototype filter like in Fig. 2.17.	50
3.1	Properties of piezoelectric materials	68
3.2	Adaptation of an extracted bandpass resonator with $r_0 > r_{max}$ the technological feasible value for acoustic wave resonators by means of an external element.	93
3.3	Adaptation of an extracted bandpass resonator with $r_0 < r_{min}$ the technological feasible value for acoustic wave resonators by means of an external element.	94
3.4	Resonator parameters extracted from the synthesized ladder for Tx Band 3 application.	99
3.5	WCDMA Tx and Rx Band 1 filter specifications.	113
3.6	Synthesized BVD bandpass elements of the Tx WCDMA Band 1 filter for Feasibility design.	113
3.7	Synthesized BVD bandpass elements of the Tx WCDMA Band 1 filter for an RL maximization design.	114
3.8	Synthesized BVD bandpass elements of the receiver filter of a WCDMA Band 1 Duplexer.	124
3.9	Synthesized BVD bandpass elements of the transmitter filter of a WCDMA Band 1 Duplexer.	126

4.1	Band 3 Tx filter specifications.	146
4.2	Elements of designed Ladder-CRF combined filter for application to Band 3 Tx.	147
5.1	Design parameters for the resonators for W-CDMA equal power divider.	159
5.2	Design parameters for the resonators for W-CDMA unequal power divider.	162
5.3	Requirements for the Rx WCDMA example CRF.	169
5.4	Properties of selected materials [80].	170
5.5	Layer thickness of the considered power divider for the topology I of no-shared resonators.	174
5.6	Layer thickness of the considered power divider for the topology II of two-shared resonators.	176

1 | INTRODUCTION

Mobile services have transformed the world and our life-style in recent decades and they will play a key role in the future evolution of communication systems. According to Cisco's report, the global mobile data traffic increased by 69 % in 2014 [1]. In 2014 the data traffic reached 2.5 exabytes/month and it is expected to increase by almost tenfold in the next five years. The research firm, Strategy Analytics, stated that handset shipment had grown 8 % annually and exceeded 445 million units at the start of 2015, driven by demand for 3G and 4G mobile phones across developing regions [2].

Smartphones shipped worldwide represented 70 % of total devices in the Q3 of 2014. To date, the total number of LTE smartphones accounts for 30 % of total handsets. In 2014, the total number of smartphones subscriptions was 2.7 billion. Furthermore, a forecast of smartphone subscriptions predicts 6.1 billion by 2020 [3]. This will result in a market growth of over 25 % per year in the RF filter of cellular devices from 2014 to 2019.

Global System for Mobile communication (GSM) and Wideband Code Division Multiple Access (WCDMA), which are respectively the 2G and 3G cellular standards, were developed as voice networks with improvements to support data. The GSM took 12 years to reach 1000 million connections. Between 2000 and 2010, the evolution of the 3G with High Speed Downlink Packet Access (HSDPA) technology started to be implemented. The HSPA+ processes faster and has more efficient use of bandwidth to increase available speed up to 42 Mbps in downlink. The global mobile broadband industry in 2009 realized 3G did not have sufficient capacity to handle the growth of applications requiring greater bandwidths. Therefore, speed improvements ten times higher were sought with 4G technology. The Long Term Evolution (LTE) is the latest cellular standard introduced to reach data-optimization and increase the throughput of data transmission.

LTE was the first to use IP packets for communications and enables better usage of the available spectrum, with higher data rates and reduced latency.

The use of 3G and 4G mobile broadband networks continues to increase and the amount of data downloaded almost doubles each year. The driving force behind this increasing rate are the new applications and services developed by the mobile industry. In the smartphone business, the major problems to overcome are the straining of the mobile broadband infrastructure. Thus, mobile broadband infrastructure must be constantly adapting and upgrading the networks to handle the capacity demanded by high-bandwidth and data-intensive multimedia applications. Despite the fact that global transition to 4G is just beginning, network operators are already planning to deploy the next major evolution of the mobile network which is 5G technology.

The evolution in mobile applications and network traffic is shifted to RF Front-End Module (FEM) in a handset aiming at global coverage with high-bandwidth connections. The assigned bands of operation for a mode are different in each region of the world. Advanced multi-mode multi-band terminals operate in 3 different modes (GSM, WCDMA and LTE) and may support more than 16 frequency band allocations. Transceiver complexity accounts in part for the need to support an ever increasing number of bands. For example, a smartphone model for international use might need to filter transmission and reception paths of 2G, 3G and 4G modes, cover up to 16 bands and coexisting with WiFi, Bluetooth and GPS systems. Consequently, the increase in the number of bands leads to a growth in the number of filters and duplexers within each device. Filters and duplexers are key elements in the RF FEM because they select the specific bands of the desired signals and reject the noise. A current smartphone may have between 30 or 40 filters and future generations will have up to 50, creating new challenges in the architectural design of FEMs to offer a small form factor while improving performance [4].

Moreover, the market pushes for RF solutions with high levels of integration. The trend towards target integration provides more capabilities in less space, which requires design abilities to package more functionalities such as integrate filters, power amplifiers (PA) and switches in a single module, or multi-band PA-duplexer modules. Additionally, the integration of FEMs reduces production costs and has better production yield than products using discrete component designs. In [5], the authors use examples for the modularization of a multi-standard multi-band front-end in order

to miniaturize it and to integrate module functions. The different partitioning of the module functions results in technically equivalent solutions but differing in size, cost, number of components, complexity and time to market aspects.

Frequency division is used for full-duplex communication, hence the handset receives and transmits simultaneously enforcing the use of a duplexer at the antenna port. A duplexer consists of highly selective filters for receiver (Rx) and transmitter (Tx) frequencies, hence the isolation between the two filters is very important. The coexistence of multiple RF bands in an LTE device creates the need for substantial isolation between signal pathways in order to avoid interferences. Due to spectral crowding, the frequency spacing between adjacent bands has become very tight. Some bands in LTE require 10 MHz narrow filters with sharper corners than 3G WCDMA. Therefore, filters with extremely sharp skirt selectivity and superior out-of-band rejection are used to overcome the highly challenging frequency band plans and multiple band operation. On the other hand, low insertion loss filters increase the data throughput and minimize the waste of transmitted power because the incoming signal strength is maximized. In LTE, the enhanced signal detection feature is important to increase data rates and, in turn, to provide a better user experience and higher data capacity per cell site. R. Aigner points out the filter requirements that arise from adapting filters/duplexers/quadplexers to different standards in [6, 7] as well as the challenges to address if adopting tunable filters in [8].

The technology to ideally suit LTE high performance specifications is the micro-acoustic filters. The Surface Acoustic Wave (SAW) filters up to about 1.5 GHz and the Bulk Acoustic Wave (BAW) filters for above this frequency deliver exceptional performance with low insertion loss, sharp roll-off and high isolation. In [9], a chart maps out this application space of SAW and BAW technologies for LTE band filters and duplexers. In their review of critical duplexer requirements for advanced systems, the authors in [10] identifies the duplexer characteristics for several WCDMA bands and discuss the realizations options with micro-acoustic technologies in order to make the suitable decision.

While the highlighted advantages of acoustic wave filters leads to the acceptance by all of the leading smartphone manufacturers, they also allow to obtain the highly compact package for the entire RF FEM. For instance, an BAW filter for LTE Band 7 exhibit a small size of $3 \times 3 \times 1.02$ mm [11].

1.1 The basics of acoustic wave filters

Acoustic wave technologies have gone mainstream in recent few decades because they have evolved to meet the challenges of cellular network transitions. To date, SAW and BAW filter technologies are used to solve many of the most complex mobile device filtering problems. A current key element in acoustic technologies is the resonator based on piezoelectric materials. The piezoelectric effect explains that when a voltage is applied to a piezoelectric crystal, it deforms, converting the electrical energy into mechanical, or the inverse conversion can occur. The exchange of energy between the electrical and the mechanical domain is produced with very low energy loss. The mechanical deformations generate acoustic waves that travel at velocities a factor roughly 10000 times lower than that of the electromagnetic waves. The relatively slow propagation velocity of acoustic waves guarantees a high level of miniaturization on the devices. In acoustic resonators, the waves are confined, generating standing waves with extremely high quality factors (Q). The high Q resonances is a key feature to target selectivity and low loss. It is important to consider each technology according to the target because each one has strengths and weaknesses in terms of performance, cost, productivity complexity and device size. The SAW and BAW technologies differ in the type of vibration mode.

Although SAW technology is still growing with improved performances, it is a mature technology used almost since the appearance of mobile phones. The surface wave is transduced by the use of interdigital transducers (IDTs) which are a periodic array of metal electrodes deposited on a piezoelectric layer over the supporting substrate. The application of an electric field on the electrodes excites surface acoustic waves. The piezoelectric substrate are for example quartz, lithium tantalate (LiTaO_3), or lithium niobate (LiNbO_3).

BAW technology has emerged during the last two decades. The intense evolution of piezoelectric materials and deposition processes have made it possible to achieve yield and cost targets in BAW devices. The most basic BAW resonator is composed of a piezoelectric plate sandwiched between metallic electrodes and having reflecting boundaries to confine the acoustic wave. The acoustic wave in a BAW filter propagates vertically in the bulk of the structure. It allows them to be effective at high frequencies. There is a variety of commonly available piezoelectric materials that can be used in BAW technology; aluminium nitride (AlN) and zinc oxide (ZnO) are some common examples. The aluminium nitride (AlN) is widely used in

BAW technology due to its lower temperature coefficient and its compatibility with CMOS processing, while the ZnO has a better intrinsic coupling coefficient.

SAW technology is good for low cellular bands for a frequency range of up to 2 GHz. The advantages of BAW vanishes at frequencies below 1.5 GHz because the thick piezo films results in large area resonators. The Q of BAW resonators is better because the wave is trapped inside the material while in SAW it is on the surface and the cavity length is of many wavelengths compared with the $\lambda/2$ of BAW. The ohmic losses are higher in the IDT of SAW than in BAW electrodes. These characteristics make the achievable Q for BAW resonators higher than in SAW, especially at high frequencies (> 2 GHz). The Q factor is typically higher than 1000 for BAW resonators [12].

SAW devices present an advantage over BAW in the complexity process of manufacturing. SAW are built using two or four masks for deposition. However, the challenge is the lithography and patterning at frequencies above 2 GHz because the IDT gaps required are of $0.3 \mu\text{m}$. The mask-count for BAW filters is about ten, which requires more effort and time for manufacturing. The BAW technology offers the possibility of realizing the filters with other wafer processing such as silicon or gallium arsenide (GaAs). SAW filters are suitable for creating balanced to unbalanced conversion. There is a huge number of possible implementations. Then, it is easy to realize filters including balun conversion in the acoustic structure. Conventional BAW does not allow single-ended to balanced conversion.

Compared to SAW technology, BAW solutions provide higher power handling (36 dBm versus 31 dBm) because the parallel plate geometry is more advantageous than the thin IDTs for power durability. Nevertheless, the cost of SAW chips is lower due to the cost-effective production process. An extensive comparison for both SAW and BAW technologies with detail of their strengths and weaknesses is presented in [13].

The electrical impedance of a SAW and BAW resonators has two characteristic frequencies, the series resonance and parallel resonance frequencies. Common for both technologies is that the coupling coefficient of the piezoelectric transducer (k_{eff}^2) defines the frequency separation of resonance frequencies and thus the maximum achievable filter bandwidth of the traditional ladder-type topology. For instance, for AlN-based BAW resonator the coupling coefficient is generally limited to a maximum of 7.5 %, which restricts the BAW filter relative bandwidth to about 4 %. A

deficient k_{eff}^2 makes it impossible to achieve flat passband and good wide-band rejection. Particularly in duplexers, the filter skirts are optimized for steepness introducing external elements in series or shunt to the branches of the ladder filter, because this relieves the requirement on k_{eff}^2 for the resonators. However, it increases the necessary footprint and degrades the far stopband frequency range rejection. Moreover, for a resonator considered as an electrical one-port device, its impedance is directly linked to the static capacitance of the resonator and, by this means, the active area.

1.1.1 The BAW and SAW filter topology

Usual filter implementations with acoustic resonators are classified into two main groups according to whether they are built of electrical connections (Fig. 1.1) or if they are acoustically coupled (Fig. 1.2 and Fig. 1.3).

Ladder-type filters belong to the first approach, where resonators are electrically interconnected in series or shunt to form a circuit topology Fig. 1.1(a). Other topologies, such as lattice-type are possible [14]. Lattice filters are

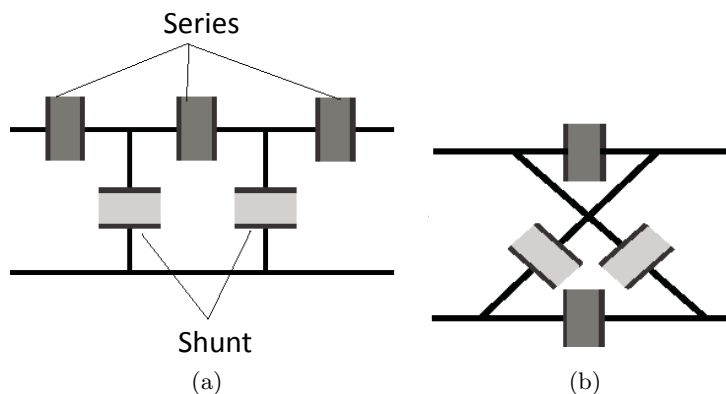


FIGURE 1.1: Filter configurations of electrically connected resonators: (a) ladder-type filter and (b) lattice-type filter.

composed of a bridge structure of 4 resonators: 2 series resonators are placed on the upper and lower branches of the bridge and 2 parallel resonators are connected to the diagonal branches Fig. 1.1(b). Either configuration is applicable for both SAW and BAW technologies. The basic principle in both electrically connected approaches is to use two different types of resonators, of different resonance frequencies, to synthesize the required passband response. Ladder filters obtain high selectivity but low

out-of-band rejection, which is controlled by the number of resonators. A balanced ladder is a mirror image of a single-ended ladder. Lattice filters are balanced networks which obtain good out-of-band rejection, but low selectivity.

The second approach of acoustically coupled resonators involves building blocks of resonant transducers with controlled mechanical coupling strength that establish the desired filter response. Thanks to the acoustic coupling between resonators, filter response yields more or less classical filter responses and it helps to enhance some aspects such as wider bandwidth. The possible conversion between single-ended to differential, as well as impedance transformation is due to the indirect coupling. The impedance transformation characteristic, provided by the acoustically coupled filter approaches, eliminates the matching networks. The acoustic coupling takes form in the thickness mode, in BAW technology, or in the surface mode, in the SAW technology.

In SAW components, the Dual Mode SAW (DMS) or Multi-Mode SAW (MMS) are building blocks based on the transverse or longitudinal acoustical coupling between IDTs Fig. 1.2. Their operational performance lies in the excitation and coupling of different resonance modes. In the longitudinal coupling case the interaction level between IDTs is stronger than in the transverse resulting in wider passband responses. Because of the exclusive acoustic coupling between input and output, DMS filters allows converting the single-ended antenna signal into a balanced transceiver input when used in the receiver path [15].

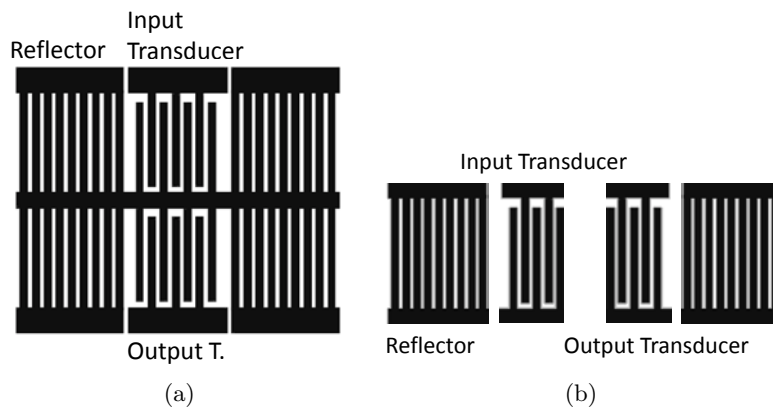


FIGURE 1.2: SAW Filter configurations of acoustically coupled resonators: (a) transversely and (b) longitudinally.

In BAW technology, there also exist filters that can accomplish the balun function. The acoustically coupled resonator BAW components require a significantly more complex process using two piezoelectric layers, although smaller sizes are obtained. There are two different devices in BAW technology based on acoustic couplings: the Stacked Crystal Filter (SCF) with direct coupling and the Coupled Resonator Filter (CRF) with indirect coupling.

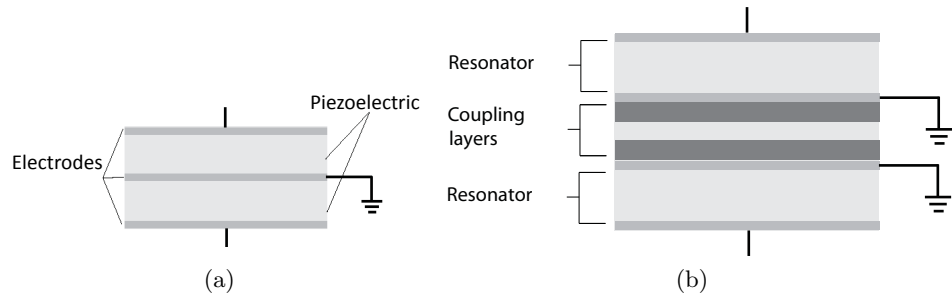


FIGURE 1.3: BAW Filter configurations of acoustically coupled resonators: (a) Stacked Crystal Filter and (b) Coupled Resonator Filter.

The SCF configuration is shown in Fig. 1.3(a); it is composed of 2 BAW stacked resonators which are acoustically connected by the direct contact of a common ground plane electrode. The whole stack behaves as a two-port resonator rather than two coupled resonators because there is no acoustic decoupling. As a result, the SCF acts as a single overmodes resonator. The structure can be excited with three different main resonance modes. However, it must be pointed out that the filter exhibits the widest bandwidth and lowest insertion loss at the second overtone.

The CRF was proposed in order to improve the limited bandwidth of SCF configurations. By decoupling the vertically stacked resonators through a set of coupling layers, Fig. 1.3(b), they can act independently and the filter behaves like an order 2. CRF structures are beneficial for wider bandwidths and excellent out-of-band rejection compared with ladder filter. When the input and output resonators are electrically isolated, BAW CRF can provide mode conversion as well as impedance transformation [16, 17].

Despite all the diverse acoustic filter architectures, the ladder configuration is the most common. Generally, BAW filter design suffer from having only two different series and parallel resonance frequencies for each series and shunt resonator, because it do not increase the manufacturing process

complexity.

1.1.2 The acoustic wave resonator modeling

There are different types of models used for BAW and SAW resonators and the design of filters. The equivalent circuit based Butterworth Van Dyke (BVD) model and the physical-based one-dimensional Mason model have been used extensively to simulate resonator performance or impedance in a narrow frequency range because they are very efficient in calculation and, therefore, useful in filter optimization iterations. However, other 2-D/3-D models such as Finite Element Method (FEM) model are useful for understanding the physics of the resonators and characterizing undesired mode loss of the resonator and accurately predicts its performance. More details about these methods can be found in [18–20].

The use of electronic design optimization is possible with the electric equivalent circuit of the BVD model if only considering the desired propagation mode. For the analysis of filtering responses, the BVD model allows for extracting the resonator parameters or modeling the filter configuration in order to carry out optimization [21]. The parameters extracted from the BVD model may be introduced into the Mason or 2-D models to enhance the accuracy. The BVD model working as impedance elements describing resonators of BAW and SAW technology is shown in Fig. 1.4, although they have quite different structures.

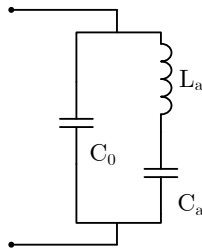


FIGURE 1.4: BVD electrical equivalent model of a BAW/SAW resonator.

Based on the equivalent circuit for electromechanical transducer presented by Mason, it is possible to develop the equivalent circuit for IDT-composed sections or constructing the BAW layer stack equivalent circuit [22]. The Mason model is useful for calculating the characteristic parameters which are dimension and material dependent, such as the resonance frequency, the

efficient coupling coefficient, harmonic responses or the reflection coefficient of the acoustic mirror. The Mason model is derived from the 1-D acoustic wave equation [23]. The application of this model is the cascading of the equivalent electrical circuit of each finite thickness layer. It models the behavior of an acoustic slab by means of a T of impedances or a transmission line model. And for the piezoelectric layers, the Mason model is a three-port circuit which contains an electrical port and two acoustic ports. A shunt capacitor C_0 models the static capacitance, and a transformer with a negative series capacitor $-C_0$ represents the electro-acoustic conversion in the piezoelectric material.

1.2 Problem description and motivation

The user segment of wireless communication systems takes advantage of the outstanding performance of filtering devices based on acoustic wave resonators. The realization of miniaturized high performance RF filters and duplexers is using SAW and BAW technology. The classical design procedure of acoustic ladder filters is based on the arrangement of series and shunt resonators by using a primary but successful pole-zero approach and defining a whole structure that is then numerically solved. It should be noted that besides resonators, other reactances could be used in addition to resonators. A major drawback in the synthesis process is to have the filter elements bound by the electromechanical coupling coefficient, k_{eff}^2 , or equivalently by the r capacitance factor, which is the motional over the static capacitance ratio.

To meet the sharp cut-off and high out-of-band rejection characteristics on a filter response, filters exhibiting finite frequency transmission zeros are most commonly used. They can be described by general Chebyshev filtering function. Classical designs synthesize such responses using coupled resonator filter topologies with direct and cross-couplings between resonators. The synthesis of coupled resonator filters lies in a previous selection of the transfer filtering function. Nowadays, the design of band pass filters, with attenuation poles at finite frequencies, is quite well understood. A band pass filter can be designed according to a low pass model based on cross-coupled resonators schemes or by means of the well-known extracted pole technique. Moreover, it was shown recently that the introduction of non-resonating nodes (NRNs), in both of the general synthesis methods, eliminates some of their inherent limitations.

The complexities of filtering requirements, with extremely high rejection of adjacent bands combined with low insertion loss, increase the need of advanced filtering techniques. A lowpass prototype with NRNs coupled with dangling resonators is widely used for the generation of finite frequencies transmission zeros in the synthesis of coupled resonators filters. The way nodes are coupled is imposed by realizability issues dependent on the technology of filter implementation. Moreover, in the case of acoustic wave technology, it will also be important to deal with coupled schemes feasible for the acoustic technology. The stringent technological constraints make the design a more and more complex and challenging task.

Commonly, in the design of a SAW/BAW filters, there is a first approximation design with acoustic simulation of the filtering response where the topology, and resonant characteristic of the resonators is determined. The research of this thesis targets this first-pass design. Finally, it is always necessary to take into account all the parasitic and coupling effects by means of 3D electromagnetic simulations, even though this is not the overall objective.

To date, optimization has been the widespread technique used to assist in the design of bandpass filters with acoustic wave technologies for the acoustic analysis. The resonant characteristics of acoustic wave resonators are modeled by means of its electrical impedance or by the equivalent circuit (BVD model). Both of them are correlated with primary parameters, such as the resonance frequency, the capacitance ratio r and the static capacitance information. Therefore, the transfer function of an acoustic wave filter has a strong dependence on the primary parameters and, hence, on the physical dimensions and materials of the structure. However, in a practical realization they are not completely free. This is why the static capacitance, the resonance frequency and, above all, the capacitance ratio, which is strongly linked with the piezoelectric material, are constrained by one single value or by minimum and maximum values.

On the other hand, there are trade-off considerations between the pass-band return loss and the stopband attenuation, which are independent of the physical realization of the filter network, as R. Cameron states in the appendix 3A in [24]. It must be analyzed to specify realistic requirements for filter responses. Since the sum of the inband equiripple level and the out-of-band rejection is always constant, given an order and a set-array of transmission zeros, therefore, any rise in the stopband attenuation generates a reduction in the passband return loss. For instance, given an order and a set-array of transmission zeros, a 5 dB rise in the stopband attenua-

tion generates a 5 dB reduction in the passband return loss. Therefore, it will never be possible to achieve an attenuation increase and return loss increase for fixed order and transmission zeros.

The common definition of the optimization problem is to minimize a cost error function which considers the defined filtering pattern and the current Scattering-parameters of the filter. The filtering pattern gives maximum and minimum transmission and reflection values in frequency intervals of passband and stopband regions. The output is the variable BVD parameters of each resonator or in other cases the whole physical dimensions. Given a filter architecture, the goal of the optimization is to iteratively minimize the value of the cost function, reaching a situation where the current S-parameters are lower than a maximum or greater than a minimum specified to find the optimum minimum. Added to that, there exist other guidelines for a feasible implementation according to the acoustic wave technology. Therefore, the control over the requirements of the filter response are lost, because the return loss and attenuation tradeoff is not being considered. Moreover, the search direction of the optimizer can be dissimilar considering the spectrum mask and the technological criteria. The number of variables to optimize and the definition of the cost function as a weighted sum of error functions result in slow convergence, with times of about 3 hours, and convergent solution issues. In the case of the spectrum mask optimization approach, the solver is not adapted to deal with the technology but with the filtering pattern of specifications.

The way in which we formulate the synthesis approach is different; we focus on the technological feasibility. The filtering pattern is a compliance, so there is no optimization to find the best solution. There is a second criteria to search for and select a solution taking into account the technological feasibility. Therefore, the solution is not the best in fulfilling the spectrum mask, although it is in fulfilling a different technological target but at the same time complying with the mask.

The initial step in the approach is the definition of the Chebyshev filtering function from the return loss level and the finite frequencies of the transmission zeros. The input variables set up (return loss and transmission zeros) is according to the fulfillment of the spectrum mask with the resulting filtering function. Since a lowpass prototype network can be associated to the already obtained Chebyshev function, there are also associated the technological parameters of the corresponding bandpass implementation of the prototype.

Accordingly, infinite solutions exist which fulfill the filtering pattern. But among all the possibilities, how do we select one? Each one of the solutions has a set of associated technological parameters. For instance, two filtering functions, which fulfill the mask, only differ in the return loss, but they bring two different solutions regarding the technological parameters. A different example occurs when, for the same filtering function suitable to comply with the frequency response requirements, the prototype synthesis can be done with different sorting of the transmission zero array. Consequently, they bring solutions with different technological parameters.

The fact of controlling the filter response mathematically in order to fulfill the defined spectrum mask generates a set of infinite possible input parameters. These can be extracted in a very fast way because the synthesis of the filtering function is direct and exact when using numerical computing software, which employs a calculation time of just few seconds. Consequently, the solver can focus on the technology because each input set leads to a technologically different solution.

Then, we have the freedom to apply a new selection criteria according to the acoustic wave technology implementation. The target can be different for each case or several simultaneously. The goals can be different, such as a uniform capacitance ratio among the resonators, minimizing the whole number of external elements required, a solution with the smaller static capacitance of its resonators because it concerns the area, a flatter group delay response, or a response where the stored energy distribution within the resonator would be more uniform. Hence, those can be the searching purposes for a solution which, fulfilling the spectrum mask, will be technologically feasible with acoustic wave resonators. This search can be automatically performed. In that case, the solver is more efficient in time than an optimization focused on the spectrum mask since the polynomial synthesis and the lowpass prototype derivation is fully analytical. This also allows for starting the automatic search with different seeds with very low time consumption.

Finally, the solver is developed to be able to deal with the technology because we begin from functions accomplishing the filtering specifications. The mask can be defined arbitrarily according to necessity, and, consequently the optimum solution is not required, only the solutions which fulfill the mask are needed.

The motivation for the thesis was to develop a design methodology where filter synthesis approaches, accommodation of acoustic wave technology and

advanced topologies are all integrated.

1.3 Solution approach

The application of lowpass prototype synthesis techniques accommodating a polynomial expression to satisfy the electrical specifications has been already implemented. However, the implementation of a methodological synthesis approach for application with acoustic wave filters will provide a direct link between the filtering function and the resonators parameters. In addition, the problem is not stated as an optimization of the frequency response, but rather stated from the application of filter synthesis theory to accommodate the technology which reduces the complexity of advanced filtering designs.

The development of a lowpass prototype model adequate for acoustic wave resonators with pole-zero characteristics allows us to implement inline topologies composed of NRNs with dangling resonators for representation of SAW and BAW filters and duplexers, while fulfilling the stringent technological constraints.

The main advantages of inline extracted pole filters with NRNs are features that can be observed in the well-established acoustic wave based ladder structures: they exhibit the property of modularity, since the position of transmission zeros can be controlled independently by tuning resonant frequencies of the resonators and they are able to create a fully canonical filter without the need of a direct coupling, which exists through a reactive path, between source and load.

The analytical synthesis of inline configurations where a resonator is responsible for each transmission zero and permits fully canonical functions helps to overcome the complexities of filtering requirements. Moreover, the stringent constraints imposed by the acoustic wave technologies are directly dealt with by the lowpass prototype due to the association of a lowpass coupled node section with a bandpass acoustic wave resonator.

This thesis explores the possibilities of the design and realization of acoustic wave filters with outstanding performance to address challenges for 4G (LTE) RF filters and duplexers. Taking advantage of cross-coupled resonator filter theory achievements, such as the modular filtering design approach using NRN and inline extracted pole filters, it has been possible to analyze advanced filter architectures which accommodate technologically feasible

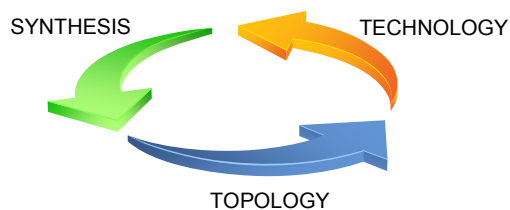


FIGURE 1.5: Integrated designs face emerging filtering challenges.

realizations.

To date, the acoustic wave technologies selected have been able to meet the challenging filter requirements. But current trends require outstanding solutions which can be achieved with technological improvements, but also by focusing on design improvements which integrate technology, synthesis and topology. We address a solution in the basis of micro-acoustic wave resonators. However the pole-zero response of resonators causes big limitations that make design a challenging task. We must consider these technological constraints imposed by the material system. Synthesis must allow us to work with the technology and the topology simultaneously. We need a methodology, so equivalent models are required to apply filter synthesis approaches according to the features of the technology and topology. It is important to innovate with new filtering architectures to enhance filter performance. If the technology is integrated on the synthesis in an efficient way, it easier to analyze a huge number of implementations even with hybrid combination of existing structures.

In conclusion, our development of filters, duplexers and other passive elements, fully leveraged on a systematic and flexible synthesis, is native to accommodate acoustic wave technological constraints, because of the integration of technology, synthesis and topology.

The implemented design methodology is systematic and native oriented to accommodate electromechanical coupling constraints, ready for SAW and BAW technologies besides fulfillment of required spectrum mask. In addition, it is native oriented to design a DPX structure as a unique device, which enables the computation of external reactive elements, consideration of losses, and monitoring of reactive power density.

1.4 Outline of the thesis

This thesis presents the work carried out for a period of almost four years, between 2011 and 2015. Subsequently, the core of the thesis presents the following contributions of work, specifying the corresponding chapters. The document is organized into six chapters.

Chapter 2 is dedicated to the description and review of synthesis procedures for inline extracted pole filters with coupled resonating and nonresonating nodes able to generate a number of transmission zeros equal to the order of the filter. The chapter outlines the basic concepts and definitions of filtering networks as well as a general definition of the coupling matrix representation introduced for NRN. The technique employed for the derivation of arbitrary lowpass prototypes from the filtering function as a base of all the designs proposed is detailed.

Chapter 3 introduces the principles of operation and technological parameters of acoustic wave resonators. It states the lowpass model sections for acoustic wave resonators for its application in the design of a lowpass inline topology composed of NRNs with dangling resonators which is an equivalent representation of a filter/duplexer based on acoustic resonators with a ladder topology. The elements of the lowpass prototype that can be synthesized analytically are linked by explicit equations in terms of acoustic wave resonators parameters. Next, we show how a direct synthesis technique of ladder filters can be devised to accommodate the stringent constraints of acoustic technologies based on BAW or SAW resonators, while at the same time ensuring that the filter response fulfills the spectrum mask specifications.

The concept of adapting the input/output reflection phase condition according to two different targets is applied. The first goal is for avoiding the use of external reactive elements at the input and output ports, commonly used to improve matching. The second purpose is for assembling the Tx and Rx filters in a duplexer, a suitable consideration of the reflection phase corrects the loading effect of each channel filter over the other.

Chapter 4 discusses the implementation of inline extracted pole filters using an arbitrary combination of electrically and acoustically coupled resonator modules in acoustic wave technology. Proposed hybrid ladder-CRF or ladder-DMS architectures entail design improvements. The hybrid configuration synthesis is also addressed by means of a methodological approach which is native in order to accommodate the acoustic wave technology.

Consequently, the application of lowpass models in the hybrid filter design for each module are required.

Chapter 5 examines the application of the techniques developed for T-junction power dividers integrated in acoustic wave technologies. The design task is addressed from a methodological point of view; first defining a suitable network topology in order accommodate the properties of the transmission responses, and second relating the prototype with an equivalent bandpass acoustic wave structure. Two different realization are considered: one is based on ladder architecture and dealt with inline extracted pole synthesis techniques and the other is based on CRF stacks where the optimization method of the coupling matrix is used for synthesis.

Chapter 6 summarizes the main conclusions of the thesis, and presents some future work recommendations in the direction of the study presented in this thesis.

The reader should note that the aim of the designed filters is to illustrate the flexibility, the suitability and the powerful properties of the synthesis methodology develop, rather than providing outstanding performance final designs which are limited by the intellectual property.

1.5 Research contributions

This dissertation collects the work that has been carried out during the Ph.D. program. Next, a list of the publications is presented.

- Jimenez, M.; Gimenez, A.; Corrales, E.; de Paco, P., "Synthesis of advanced filters with hybrid topology combinations based on Acoustic Wave technology," presented at the *International Workshop on Microwave Filters*, Toulouse, France, March 2015.
- Gimenez, A.; Jimenez, M.; Corrales, E.; de Paco, P., "On The Design of Advanced Filtering Responses Based on Acoustic Wave Technology," presented at the *International Workshop on Microwave Filters*, Toulouse, France, March 2015.
- Jimenez, M.; Gimenez, A.; Corrales, E.; de Paco, P., "Miniaturized power dividers with integrated bandpass response based on BAW coupled resonator filters," in *IEEE Proc. 14th Mediterranean Microwave Symposium (MMS)*, pp.1-6, Dec. 2014.

- Jimenez, M.; Gimenez, A.; Corrales, E.; de Paco, P., "The Role of Acoustic Wave Technology in Passive Components for User-terminals on Satellite Telecommunication Systems," presented at the *Micro- and Millimetre Wave Technology and Techniques Workshop*, Noordwijk, the Netherlands, Nov. 2014.
- Gimenez, A.; Jimenez, M.; Corrales, E.; de Paco, P., "Lowpass Equivalent Models of a Micro- Acoustic Resonator Based on Non-Resonant Nodes," presented at the *Micro- and Millimetre Wave Technology and Techniques Workshop*, Noordwijk, the Netherlands, Nov. 2014.
- Jimenez, M.; Gimenez, A.; Corrales, E.; de Paco, P., "A Filtering Power Divider Based on Bulk Acoustic Wave Technology," in *Proceedings of MEMSWAVE 2014, (15th International Symposium on RF-MEMS and RF-Microsystems)*, La Rochelle, France, July 2014.
- Jimenez, M.; Corrales, E.; de Paco, P.; Menendez, O., "Design of a Coupled Resonator 3dB power divider based on BAW technology," in *Proc. Ultrasonics Symposium (IUS), 2013 IEEE International (2013 Joint UFFC, EFTF and PFM Symposium)*, pp.2155-2158, July 2013.
- Jimenez, M.; Corrales, E.; de Paco, P.; Menendez, O., "A dual-band resonator in Bulk Acoustic Wave technology," in *Proc. Ultrasonics Symposium (IUS), 2012 IEEE International*, pp.1-4, Oct. 2012.
- Jimenez, M.; Corrales, E.; de Paco, P.; Menendez, O., "High-Selectivity Coupled Resonator Filters Based on BAW Technology," presented at the *5th International Workshop on Microwave Filters*, Toulouse, France, Oct. 2012.

2 | SYNTHESIS METHODOLOGY AND PROCEDURE

The physical implementation of a microwave filter can be carried out with several types of configurations and technologies driven by the application. However, the design procedure is usually based on the same two steps. The first step is the association of a lumped-element lowpass prototype network to a given frequency response. The prescribed frequency response is a polynomial filtering function that fulfills the electrical specifications. The second step consists of relating each prototype element with individual physical components of the filter. Here, frequency transformations are used to denormalize the lowpass elements into bandpass structures.

This chapter details this first step, the explanation of general coupled resonator synthesis networks using a wider class of nodes such as non-resonant nodes and hence the definition of a new type of coupling matrix. The direct synthesis approach, based on the extraction of elements is exploited for inline configurations with arbitrary number of transmission zeros. Transmission zeros are generated by dedicated blocks including non-resonating nodes. The extraction of the network comprises the determination of the type of elements, their arrangement as well as their values. The different extracted-pole situations for each building block on the nodal approach are formulated in mathematical terms.

2.1 Characterization of filter networks

A filter is a passive and reciprocal network. Therefore, the scattering parameters associated are expressed in a general polynomial form:

$$S = \begin{bmatrix} S_{11} & S_{12} \\ S_{21} & S_{22} \end{bmatrix} = \frac{1}{E(s)} \begin{bmatrix} \frac{F(s)}{\epsilon_R} & \frac{P(s)}{\epsilon} \\ \frac{P(s)}{\epsilon} & \frac{(-1)^N F(s)^*}{\epsilon_R} \end{bmatrix} \quad (2.1)$$

where N is the filter order and the number of resonators. The polynomials $P(s)$, $F(s)$ and $E(s)$ have complex coefficients for the complex frequency variable $s = j\omega$. $F(s)$ and $E(s)$ are N degree polynomials. $P(s)$ is n_{fz} degree polynomial where n_{fz} is the number of finite-position transmission zeros of the transfer function and $n_{fz} \leq N$. When $n_{fz} = N$, the filtering function is referred as fully canonical. The real constant ϵ_R allows to normalize the polynomials $E(s)$ and $F(s)$ to be monic and the real constant ϵ normalizes $P(s)$. The denominator polynomial $E(s)$ is strictly Hurwitz and it is the unique polynomial satisfying the conservation of energy equation of a lossless passive network:

$$E(s)E(s)^* = \frac{F(s)F(s)^*}{\epsilon_R^2} + \frac{P(s)P(s)^*}{\epsilon^2} \quad (2.2)$$

The numerator polynomial $P(s)$ satisfies the condition $P(s) = (-1)^{N+1}P(s)^*$ which ensures that the set of transmission zeros has symmetry about the imaginary axis.

Considering the orthogonality equation of the S-parameters in a two port passive, lossless and reciprocal network gives an important relationship of the phases of S_{11} , S_{22} and S_{21} polynomials, which are θ_{11} , θ_{22} and θ_{21} respectively [24]:

$$\theta_{21} - \frac{(\theta_{11} + \theta_{22})}{2} = \frac{\pi}{2} (2k \pm 1). \quad (2.3)$$

The right-hand side of the equation, for k an integer, is an odd multiple of $\pi/2$ radians and frequency independent. This equation states that a phase shift on the input reflection response will affect the phases of the output reflection and/or the transmission responses.

The relation of polynomials $P(s)$, $F(s)$ and $E(s)$ allows to determine one of the polynomials while the other two are known (2.2). Hence, S-parameters

can be determined by the two numerator polynomials $F(s)$ and $P(s)$:

$$|S_{21}(j\omega)|^2 = \frac{1}{1 + \left| \frac{F(j\omega)}{P(j\omega)} \right|^2} \quad (2.4)$$

where the ratio of polynomials $F(s)$ and $P(s)$ is the filtering or characteristic function.

2.2 The Chebyshev class of filtering function

The methods presented in the thesis include the design of characteristic functions which belongs to the general Chebyshev filtering function class. The useful features of Chebyshev filtering function is the possibility of asymmetric characteristics, the prescribed inband equi-ripple amplitude, the generation of even- and odd-degree filters and the close-to-band rejection slopes.

The filtering function expressed in (2.4) is defined as:

$$kC_N(\omega) = \frac{F(\omega)}{P(\omega)} \quad (2.5)$$

where k is a constant and $C_N(\omega)$ is the filtering function of degree N with general Chebyshev characteristic form given by [25]:

$$C_N(\omega) = \cosh \left[\sum_{n=1}^N \cosh^{-1}(x_n) \right], \quad x_n = \frac{\omega - 1/\omega_n}{1 - \omega/\omega_n} \quad (2.6)$$

where $s_n = j\omega_n$ are the n -th prescribed transmission zeros in the complex s -plane.

By analyzing $C_N(\omega)$ [24], it can be shown that it is a rational function whose denominator has the same zeros as $P(\omega)$ and is generated by the product $\prod_{n=1}^N (1 - (\omega/\omega_n))$ from the prescribed transmission zeros. Moreover, it can be observed from (2.5) that the numerator of $C_N(\omega)$, referred to $G_N(\omega)$, has the same zeros than $F(\omega)$. From (2.5), it is observed that k is just a normalizing constant, considering the fact that polynomials $F(\omega)$ and $P(\omega)$ are assumed monic but the polynomials of $C_N(\omega)$ do not have to have their highest-degree coefficients normalized.

In order to compute the coefficients of the numerator polynomials $G_N(\omega)$ of a lowpass prototype Chebyshev filtering function, S. Amari developed a

simpler recursive relation in [26] than that given by Cameron in [27]. S. Amari get the following recursive formula:

$$G_{N+1}(\omega) = -G_{N-1}(\omega) \left(1 - \frac{\omega}{\omega_N}\right)^2 \frac{(1 - 1/\omega_{N+1}^2)^{1/2}}{(1 - 1/\omega_N^2)^{1/2}} + G_N(\omega) \left[\omega - \frac{1}{\omega_{N+1}} + \left(\omega - \frac{1}{\omega_N}\right) \cdot \frac{(1 - 1/\omega_{N+1}^2)^{1/2}}{(1 - 1/\omega_N^2)^{1/2}} \right] \quad (2.7)$$

The starting polynomials $G_0(\omega)$ and $G_1(\omega)$ are:

$$G_0(\omega) = 1, \quad G_1(\omega) = \omega - \frac{1}{\omega_1}. \quad (2.8)$$

2.2.1 Relationship between ϵ and ϵ_R

The real constant ϵ for any Chebyshev filter composed of N intercoupled resonators can be expressed as:

$$\epsilon = \frac{1}{\sqrt{10^{RL/10} - 1}} \left| \frac{P(s)}{F(s)/\epsilon_R} \right|_{s=\pm j}, \quad (2.9)$$

where RL is the return loss defined in dB units. ϵ_R is different to the unit only on fully canonical filtering cases, at that cases

$$\epsilon_R = \frac{\epsilon}{\sqrt{\epsilon^2 - 1}}. \quad (2.10)$$

Giving as input parameters: the arbitrary location of the transmission zeros, the degree of the filter and the return loss level; then, the recursive relation presented in [26] is completely general and efficient to obtain the coefficients of the polynomials with Chebyshev filtering function for a broad class of lowpass prototype networks.

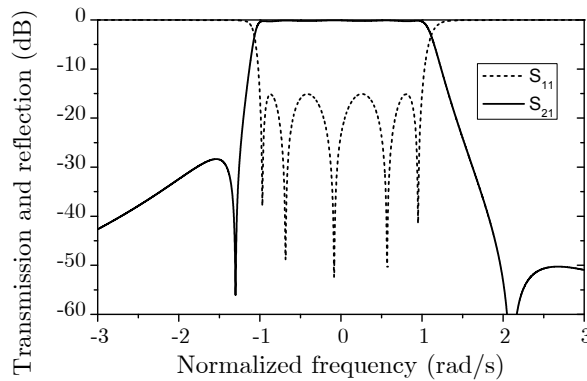
2.2.2 Example polynomial synthesis

To illustrate the procedure for the synthesis of characteristics polynomials, it is applied to two examples of 5th-degree with equiripple return loss level of 15 dB, and each one with a different number of prescribed zeros.

TABLE 2.1: Corresponding polynomials of a Chebyshev filter function with two prescribed transmission zeros.

$s^i, i =$	$E(s)$	$F(s)$	$P(s)$
0	$0.414 + j0.176$	$j0.030$	2.730
1	$1.342 + j0.403$	0.349	$j0.800$
2	$2.173 + j0.529$	$j0.222$	1
3	$2.580 + j0.365$	1.298	
4	$1.602 + j0.216$	$j0.216$	
5	1	1	
$\epsilon_R = 1$		$\epsilon = 6.078$	

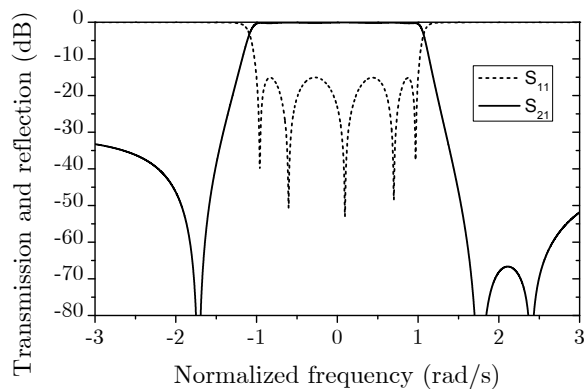
1. The first filter is designed with two finite transmission zeros ($n_{fz} = 2$) assigned at normalized frequencies $+j2.1$ and $-j1.3$ in rad/s. Applying the technique for synthesis of Chebyshev filters yields to the characteristics polynomials $F(s)$, $P(s)$ and $E(s)$. The corresponding polynomials coefficients are listed in Table 2.1. The plots of the transfer and reflection characteristics for the synthesized filter are shown in Fig. 2.1.


 FIGURE 2.1: Lowpass prototype transfer and reflection characteristics of the 5th-degree Chebyshev filter with two prescribed transmission zeros at $s_1 = +j2.1$ and $s_2 = -j1.3$.

2. A second case of fully canonical filter ($n_{fz} = 5$) is designed with assigned finite transmission zeros at $-j1.72$, $-j1.72$, $j2.4$, $j1.76$ and $j1.76$ in rad/s. The characteristic polynomials are synthesized, yielding the values shown in Table 2.2. The graph of Fig. 2.2 exhibits the 5th-degree filter with five transmission zeros.

TABLE 2.2: Corresponding polynomials of a Chebyshev filter function with five prescribed transmission zeros.

$s^i, i =$	$E(s)$	$F(s)$	$P(s)$
0	$0.487 - j0.212$	$-j0.037$	21.994
1	$1.432 - j0.369$	0.384	$j8.583$
2	$2.235 - j0.497$	$-j0.221$	14.769
3	$2.610 - j0.325$	1.342	$j5.861$
4	$1.592 - j0.202$	$-j0.201$	2.480
5	1	1	1
$\epsilon_R = 1.0003$		$\epsilon = 41.4772$	

FIGURE 2.2: Lowpass prototype transfer and reflection characteristics of the 5th-degree Chebyshev filter with five prescribed transmission zeros at $s_1 = +j2.4$, $s_2 = -j1.72$, $s_3 = -j1.72$, $s_4 = j1.76$ and $s_5 = j1.76$.

2.3 Coupled resonator filters with finite transmission zeros

Once the rational transfer and reflection polynomials are derived, the next step is to translate them into a prototype electrical circuit. Such filters can be designed from a normalized coupled resonator lowpass network. First using coupled resonator filters was Cohn in [28].

Nowadays, coupled resonator filters are complex structures where resonators are sequentially and non-sequentially coupled. Rhodes in [29] and Atia and Williams in [30] made relevant publications on the use of coupling resonator circuits. A specific topology employing coupled resonators circuits

must be selected to synthesize the prescribed filtering function regarding the transmission zeroes.

Microwave filters with very high selectivity are possible if their transfer functions incorporates finite transmission zeros. The implementation of finite transmission zeros at real frequencies generally is realized through two different approaches.

First scheme used is a general folded cross-coupling between non-adjacent resonators [31, 32]. Some synthesis are realized by means of cascaded quadruplets [33], cascaded trisections [34] or other specialized topologies [35]. The case where N transmission zeros are introduced into an N -order filter, requires a direct coupling between source and load in cross-coupled schemes [36, 37]. Cross-coupled approaches often result in complicated structures where there is no direct correspondence between zeros and the cross-couplings. Due to the loss of control over the positions of the zeros, cross-coupled structures are very sensitive and difficult to adjust.

The second scheme employed for the design of filters with attenuation poles are extensions of the extracted pole technique synthesis [38]. Implementation by the extracted pole technique allows an independent extraction and control of every transmission zero which is an important feature to reduce sensitivity. The realization of simple inline prototypes with transmission zeros was proposed using different techniques which introduce non-resonating nodes (NRN) to replace the phase-shifter [39–41].

In these proposals, frequency independent reactances extracted at the input and output generate one or two transmission zeros. An important step was the possibility of generating N real transmission zeros in in-line configurations by using NRNs, but without using cross-couplings [42]. Nevertheless, a general and direct technique for arbitrarily placed attenuation poles is developed in [43].

The inclusion of NRNs gives the possibility of designing filters with the maximum number of finite transmission zeros without implementing direct couplings between the source and load. It supposes an advantage when this coupling is not feasible or it affects all the transmission zeros in higher orders. Another advantageous property is the modularity since the position of transmission zeros can be controlled independently by tuning the resonators and it turns into a reduced sensibility. Furthermore, the inline configuration with NRN allows to extract the elements analytically.

Particularly for the work of this research, we are going to show that an inline

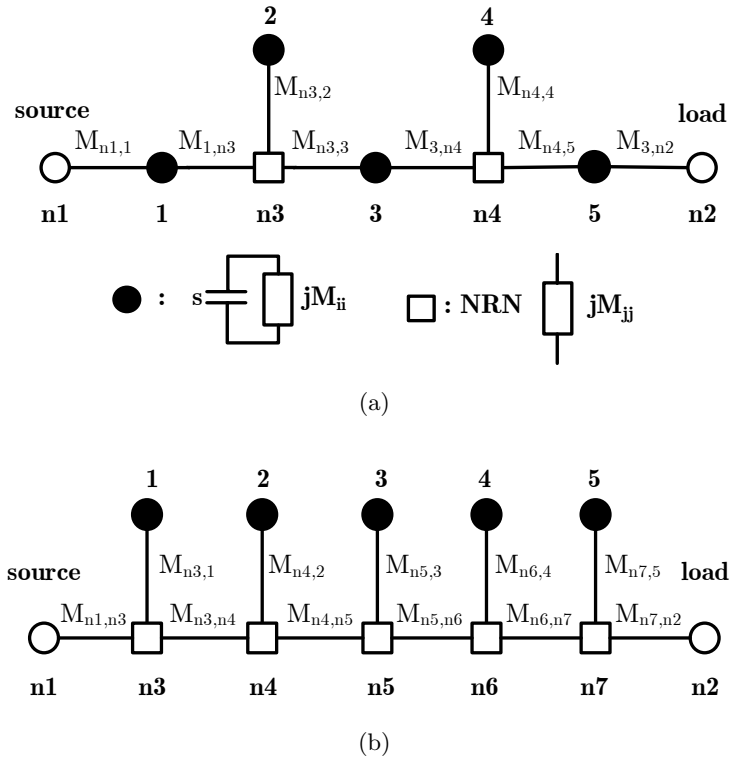


FIGURE 2.3: Nodal representation for lowpass prototype circuits based on coupled resonators. Two fifth-order inline filters ($N = 5$): (a) with two real transmission zeros $n_{fz} = 2$ and (b) with fully canonical response $n_{fz} = N = 5$.

topology composed of NRNs with dangling resonators is a good equivalence for the synthesis of a lowpass prototype of filters based on acoustic wave resonators. Therefore, the mentioned strengths of inline extracted pole filters with NRNs apply for acoustic wave structures. The modularity is specially evident on the ladder topology where each transmission zero is generated by a dedicated acoustic wave resonator, as we will verify later.

Possible prototype topologies of coupled resonators using symbolic nodal representation are shown in Fig. 2.3 which describe structures of inline filters with NRNs and dangling resonators. The connecting lines represent the couplings between nodes. We deal mainly on lowpass prototypes with attenuation poles at infinite shown in Fig. 2.3(a) and with fully canonical response shown in Fig. 2.3(b).

In the nodal diagrams (Fig. 2.3), filled nodes represent the resonators

of the filter and there are N resonators. Each resonator node is a unit frequency-dependent reactive element connected in series or in parallel with the frequency-invariant immittance (M_{ii}). Straight lines represents the inverters (M_{ij}). Each empty node represents a non-resonant node, a frequency-invariant immittance (M_{jj}) that could be a port or an internal node in a generalization of the network.

The different components used on a general coupled resonator network are:

- Frequency-dependent reactive elements: usually unit capacitors or inductors for convenience.
- Frequency-invariant reactive (FIR) elements: required for asymmetric frequency response filters. A FIR represents an offset in the resonant frequency of a resonator when connected to a capacitor or inductor.
- Coupling inverters: typical ideal admittance or impedance inverters which act as coupling elements between nodes. Each different type of inverter is used according to get series or shunt topology.

Hereafter, we will consider networks with parallel resonators (a shunt-connected capacitor and a FIR susceptance) coupled by means of admittance inverters to simplify results, even though the following results are equivalent to series resonators with impedance inverters due to the duality property.

Summarizing, the type of filters we have investigated are inline configurations in which a resonator responsible for a transmission zero at normalized frequency $s_i = j\omega_i$ is a dangling resonator connected to one NRN by an inverter. The NRNs are connected between them by inverters. When an N -order filter presents n_{fz} transmission zeros, there are $N - n_{fz}$ resonators, a part from the dangling resonators, along the path between the source and load and they are inline with NRNs.

However, as will be argued at the necessary moment, in some inline structures the inclusion of NRN in the inline path without dangling resonators, as shown in Fig. 2.4, will be necessary. The number of NRNs introduced on a filter does not modify the filter order.

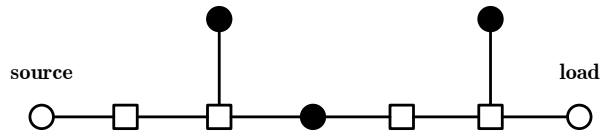


FIGURE 2.4: Low-pass prototype circuit of a third-order inline filter introducing two NRNs without dangling resonator.

2.4 Generalization of the coupling matrix with internal non-resonant nodes

A coupled resonator lowpass prototype is mathematically characterized by its coupling matrix (\mathbf{M}). The coupling matrix completely gathers all the possible couplings in the filter. Modeling a filter with the coupling matrix is useful to apply precise performance simulations and matrix operations such as transformations or reconfigurations of the topology [35]. Each element in the network is uniquely identified with a coefficient in the coupling matrix. Therefore, the coupling matrix allows computation of electrical characteristics of each element, for example, the stored energy on a resonator [44].

The coupling matrix is a suitable representation of a 2-port network made up of coupled resonators, which describes the topology of the coupling. The common $N + 2$ coupling matrix of a filter refers to the extended prototype which includes the source and load ports. It allows to consider fully canonical cases with direct source and load couplings or the transversal representation with multiple source/load couplings [35]. There exist algebraic procedures to reconfigure the matrix in a different one with identical response [45].

The prototype network above mentioned considers two different nodes according to their frequency behavior. Then, the common $N + 2$ coupling matrix, limited to only resonant nodes, needs a formulation extension in order to apply the matrix representation on general coupled resonator filters which takes into account non-resonant nodes. Consequently, the general coupling matrix will have different dimensions than $N + 2 \times N + 2$.

In the circuit three different couplings are possible and each one is characterized in a submatrix block of \mathbf{M} with different dimensions:

- $\mathbf{M}_N \in \mathbb{R}^{N \times N}$: coupling matrix between resonant nodes. The diagonal elements $[\mathbf{M}_N]_{ii}$ represents the self-couplings of the resonators, that

is FIR elements shunt-connected to the capacitors.

- $\mathbf{M}_P \in \mathbb{R}^{P \times P}$: coupling matrix between non-resonant nodes. The elements of the diagonal are also self-couplings representing the invariant susceptances.
- $\mathbf{M}_{PN} \in \mathbb{R}^{P \times N}$: coupling matrix between non-resonant nodes and resonant nodes of the network. In general $P \neq N$, and the matrix is non-square and asymmetric because connects different set of nodes.

The submatrices \mathbf{M}_N and \mathbf{M}_P are symmetric.

A convenient sorting of all the nodes according to their resonant type allows a compact definition of the coupling matrix by blocks. Consequently, a sorted set integrated by all the nodes is numerated, considering first the non-resonant nodes ($n1, n2, \dots, nP$) and second the resonant nodes ($1, 2, \dots, N$). The general coupling matrix $\mathbf{M} \in \mathbb{R}^{(P+N) \times (P+N)}$ defined by blocks is formulated characterizing network like in Fig. 2.3:

$$\mathbf{M} = \begin{bmatrix} \mathbf{M}_P & \mathbf{M}_{PN} \\ \mathbf{M}_{PN}^T & \mathbf{M}_N \end{bmatrix} \quad (2.11)$$

At the same time, \mathbf{M}_P contains two different types of non-resonant nodes: external and internal. The first ones are the source and load ports, in a two-port network like a filter. The ports are loaded with impedances and also with the external excitations. However, the second ones have no access from outside.

To face next coupling matrix formulations, it is necessary to take into account how the sorted nodes on the non-resonant set ($n1, n2, \dots, nP$) are numerated. It is necessary to follow the same criteria when numerating the source and load nodes for coherence on the results. Therefore, we state the input port as $n1$ and the output port as $n2$ from here on, which respectively correspond to the first and the second rows and columns of \mathbf{M} . And next, the $P - 2$ non-resonant nodes are numerated.

Furthermore, from the definition of the input and output ports as non-resonant nodes, the prototype network representing a filter can have reactive ports when $[\mathbf{M}]_{n1, n1} \neq 0$ and/or $[\mathbf{M}]_{n2, n2} \neq 0$.

In the case that a three-port or a multi-port network is considered, the general coupling matrix definition is also suitable. We extend the formulation and numeration sorting of the nodes explained for \mathbf{M}_P , for example in a

three-port device, with 3 external nodes ($n1, n2, n3$) in the first rows and columns and $P - 3$ internal nodes.

The coupling matrices corresponding to circuits Fig. 2.3(a) and Fig. 2.3(b) are expressed in (2.12) and (2.13), respectively, in order to illustrate the \mathbf{M} formulation clearly.

$$\mathbf{M}_1 = \left[\begin{array}{cccc|ccccc} 0 & 0 & 0 & 0 & M_{n1,1} & 0 & 0 & 0 & 0 \\ \dots & 0 & 0 & 0 & 0 & 0 & 0 & 0 & M_{n2,5} \\ & & M_{n3,n3} & 0 & M_{n3,1} & M_{n3,2} & M_{n3,3} & 0 & 0 \\ & & & M_{n4,n4} & 0 & 0 & M_{n4,3} & M_{n4,4} & M_{n4,5} \\ \hline & & & & M_{1,1} & 0 & 0 & 0 & 0 \\ & & & & \ddots & M_{2,2} & 0 & 0 & 0 \\ & & & & & & M_{3,3} & 0 & 0 \\ & & & & & & & M_{4,4} & 0 \\ & & & & & & & \dots & M_{5,5} \end{array} \right] \quad (2.12)$$

$$\mathbf{M}_2 = \left[\begin{array}{cccccc|cccccc} 0 & 0 & M_{n1,n3} & 0 & 0 & 0 & 0 & 0 & 0 & 0 & 0 \\ \dots & 0 & 0 & 0 & 0 & 0 & M_{n2,n7} & 0 & 0 & 0 & 0 \\ & & M_{n3,n3} & M_{n3,n4} & 0 & 0 & 0 & M_{n3,1} & 0 & 0 & 0 \\ & & & M_{n4,n4} & M_{n4,n5} & 0 & 0 & 0 & M_{n4,2} & 0 & 0 \\ & & & & M_{n5,n5} & M_{n5,n6} & 0 & 0 & 0 & M_{n5,3} & 0 \\ & & & & & M_{n6,n6} & M_{n6,n7} & 0 & 0 & 0 & M_{n6,4} \\ & & & & & \ddots & M_{n7,n7} & 0 & 0 & 0 & M_{n7,5} \\ \hline & & & & & & & M_{1,1} & 0 & 0 & 0 \\ & & & & & & & & M_{2,2} & 0 & 0 \\ & & & & & & & & & M_{3,3} & 0 \\ & & & & & & & & & & M_{4,4} \\ & & & & & & & & & & \dots \\ & & & & & & & & & & M_{5,5} \end{array} \right] \quad (2.13)$$

The coefficients of the matrix contain the values of all the couplings in the network including couplings between each of the nodes (resonant or non-resonant) and the input/output couplings with the ports. The coupling matrix is symmetrical about its main diagonal, because a filter is a passive and reciprocal network.

The FIR elements representing the frequency offset of the resonators or the invariant immittances of non-resonant nodes are associated with the diagonal coefficients of \mathbf{M} . From the diagonal coefficients of both cases it is observed that the I/O ports are not reactive.

The narrowband approximation of the coupling matrix model, which assumes the couplings frequency independent, is its main drawback. The coupling matrix use extents to narrow bandwidths up to 5% approximately.

2.5 Analysis of the network represented by the Coupling Matrix

Although \mathbf{M} contains all relevant information about the network, it is not a complete circuitual representation when excitation sources are applied. There are additional elements such as the conductances or the parallel capacitors connected to the susceptances. A two-port network, like in Fig. 2.3, is fed with a current unit source, i_s of internal conductance G_S and is loaded with a conductance G_L as shown in Fig. 2.5.

With the circuit arrangement of parallel resonators, the voltage at each node is denoted by v_i . The vector \mathbf{v} , of length $P + N$, gathers the voltages v_i . The excitation vector is $\mathbf{i}_s^T = [1, 0, \dots, 0]$ since only the source node is considered excited. The corresponding nodes equations from Kirchhoff's law for this circuit can be formulated with the matrix equation:

$$\begin{aligned} [\mathbf{A}] [v_1, v_2, \dots, v_{P+N}]^T &= [1, 0, \dots, 0]^T \\ [\mathbf{A}] [\mathbf{v}] &= [\mathbf{i}_s] \end{aligned} \quad (2.14)$$

where $[\mathbf{A}] \in \mathbb{C}^{(P+N) \times (P+N)}$ is the nodal admittance matrix defined by:

$$\mathbf{A} = \mathbf{G} + s\mathbf{W} + j\mathbf{M}. \quad (2.15)$$

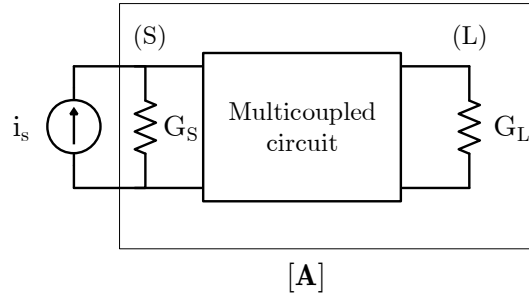


FIGURE 2.5: Admittance matrix $[\mathbf{A}]$ of the general multicoupled circuit of parallel resonators operating between a source conductance G_S and a load conductance G_L .

Note that a dual circuit of the Fig. 2.5 circuit, based on the impedance matrix, can be more convenient according to the filter structure, but the ruling equations of both dual circuits are identical.

The definition of \mathbf{A} implies the matching of the rows and columns regarding the $P + N$ nodes of this matrix to be equal to the \mathbf{M} matrix. The \mathbf{M} , \mathbf{W} and \mathbf{G} matrices completely determine the overall network elements. The matrices \mathbf{W} and \mathbf{G} are diagonal.

- \mathbf{W} : Each coefficient $[\mathbf{W}]_{kk}$ is equal to unit for the cases where k is the index of a resonant node, that means it contains a unit capacitance, and is equal to zero otherwise. Therefore, the resonance characteristic of each node is reflected in the matrix, because whether each node is variant in frequency or it is invariant is determined by means of the complex frequency s . Following the defined \mathbf{M} formulation, the matrix of capacitances, \mathbf{W} , is defined by blocks of $P \times P$ and $N \times N$ dimensions as:

$$\mathbf{W} = \begin{bmatrix} \mathbf{0} & \mathbf{0} \\ \mathbf{0} & \mathbf{I}_N \end{bmatrix} \quad (2.16)$$

where the matrix \mathbf{I}_N is equal to the $N \times N$ identity matrix.

- \mathbf{G} : The conductances at the port nodes are equal to the loading or reference conductances which strictly are not elements of the network and depend on the loading conditions. The matrix of conductances, \mathbf{G} , reflects the terminating conductances of the ports. Following the defined \mathbf{M} formulation and considering a lossless 2-port network, it is defined as:

$$\mathbf{G} = \begin{bmatrix} \mathbf{G}^{SL} & \mathbf{0} \\ \mathbf{0} & \mathbf{0} \end{bmatrix} \quad (2.17)$$

where the diagonal elements are all zero, except the first and the second one, which are $G_{11}^{SL} = G_S$ and $G_{22}^{SL} = G_L$.

The voltage on each node is computed by solving the lineal system of (2.14). To obtain the S-parameters of a 2-port network, it is enough to compute the voltages at the input and output port nodes. As the S-parameters are defined with the ports loaded at the reference impedance, in our case we assume normalized circuits of unitary reference impedance and so, $G_S = 1 \Omega^{-1}$ and $G_L = 1 \Omega^{-1}$. Consequently, the S-parameters of the two-port network of Fig. 2.5 are computed by means of the admittance matrix.

- Reflection responses ($k = l$):

$$S_{kk}(s) = -1 + 2 [\mathbf{A}^{-1}]_{kk} \quad k \in \{1, 2\}. \quad (2.18)$$

- Transmission response ($k \neq l$):

$$S_{kl}(s) = 2 [\mathbf{A}^{-1}]_{kl} \quad k, l \in \{1, 2\}. \quad (2.19)$$

In (2.18) and (2.19) and by our definition of \mathbf{M} , the input and the output ports are represented by the first and second rows and columns. The results can be expanded to a multi-port network following the proper formulation.

For further reference on the coupling matrix, [24] is a relevant reference. Additionally, [46] is suggested for the formulation of a general coupling matrix.

2.6 Synthesis of inline extracted pole filters with NRNs by analytical expressions

In the following section, the analytical equations for the element extraction of an arbitrary inline circuit are detailed. We follow a synthesis procedure based on expressions which are derived from analysis of extracted pole sections. We have tried to analyze all possible situations that can be found later on the studied designs with acoustic wave filters. The analyzed situations form the base from which a wide variety of prototype designed circuits, such as filters, duplexers and even combiners, have been derived. It will be discussed in next chapter that the acoustic wave technology accommodates inline extracted pole networks.

In Fig. 2.6, an equivalent schematic circuit of extracted pole filter corresponding to the inline nodal diagram of Fig. 2.3(a) is presented. The circuit exemplify the types of extracted sections that will be determined and are interacting in the circuit.

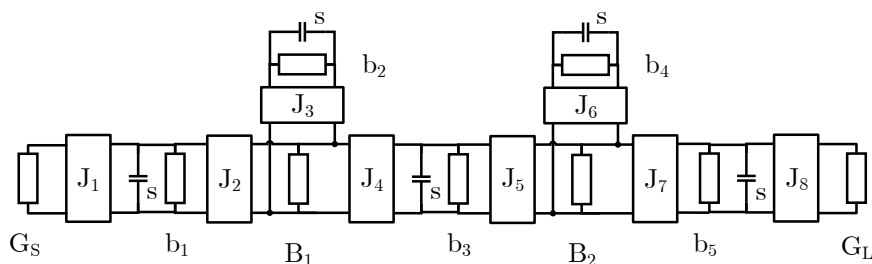


FIGURE 2.6: Schematic representation of a doubly loaded extracted pole filter of a fifth-order with two real transmission zeros.

Four different elements are possible sections to be extracted and are present in the inline filter as: admittance inverters of value J_i , resonators modeled

by unit capacitances connected in parallel with frequency invariant reactances with susceptance value b_i , non-resonating elements of constant reactance jB_i and input and output loads that for the case of no reactive ports they are normalized conductances $G_S = G_L = 1$. In a general case, for different values of G_S and G_L an appropriate change on the connecting inverters values is sufficient to change the desired impedance normalization. The building block that contains one dangling resonator coupled with an NRN generates one TZ at real frequency.

The approach to synthesize general inline prototypes of extracted pole filters describing general Chebyshev functions relies essentially on a Darlington technique. Authors in [43] established the main rules for the extraction of the elements. However, we also give the expressions for the analytical and direct extraction of elements considering additional cases not studied in [43].

The recursion relations on (2.7) yield to a general Chebyshev filtering function $C_N(\omega)$. The standard pole-zero approach determines the scattering parameters S_{11} and S_{21} from $C_N(\omega)$. However their phases are not determined, they are just related by the unitary condition (2.3).

2.6.1 Reflection Coefficients S_{11} and S_{22}

In a lossless two-port network the input and output reflection coefficients, $S_{11}(s)$ and $S_{22}(s)$ have the same poles and zeros, thus they are equal in magnitude. The reflection coefficients can be expressed as a relation of their zeros s_{zi} and their poles s_{pi} for $i = 1, 2, \dots, N$:

$$S_{11}(s) = e^{j\theta_{11}} |S_{11}(\infty)| \frac{\prod_{i=1}^N (s - s_{zi})}{\prod_{i=1}^N (s - s_{pi})} = e^{j\theta_{11}} \frac{M(s)}{D(s)} \quad (2.20)$$

$$S_{22}(s) = e^{j\theta_{22}} |S_{11}(\infty)| \frac{\prod_{i=1}^N (s - s_{zi})}{\prod_{i=1}^N (s - s_{pi})} = e^{j\theta_{22}} \frac{M(s)}{D(s)} \quad (2.21)$$

Here, the asymptotic term $|S_{11}(\infty)|$ is only different to unit when $n_{fz} = N$, i.e., it is a fully canonical response. $e^{j\theta_{11}}$ and $e^{j\theta_{22}}$ are the phase terms which do not affect the return or insertion losses and the phases θ_{11} and θ_{22} are real numbers. Additionally, the consideration of the phase terms is fundamental in the extraction process.

Lets relate the input (output) admittance seen from the source (load) with the input (output) reflection coefficient, considering that the internal conductance of the source (load) is normalized to unity:

$$y_{in}(s) = \frac{1 - S_{11}(s)}{1 + S_{11}(s)} = \frac{D(s) - e^{j\theta_{11}} M(s)}{D(s) + e^{j\theta_{11}} M(s)} \quad (2.22)$$

$$y_{out}(s) = \frac{1 - S_{22}(s)}{1 + S_{22}(s)} = \frac{D(s) - e^{j\theta_{22}} M(s)}{D(s) + e^{j\theta_{22}} M(s)} \quad (2.23)$$

The inclusion of the phase term changes the admittance seen from the source and load and, consequently, vary the prototype network extracted. The inline extracted pole prototype network that will yield the desired response must have its input (output) admittance equal to the one given by (2.22) ((2.23)). Therefore, the network implementing the filter is examined to determine the phase terms.

There are two different cases to obtain θ_{11} (θ_{22}) depending if the first (last) element is a resonant node or a non-resonant node.

1. *First Node from the input (output) is a Resonator.* If the circuit presents a first resonant node at the input like the situation described in Fig. 2.7, the phase of the reflection coefficient is obtained evaluating the admittance asymptotically. In this case, the input admittance representing the overall circuit is:

$$y_{in}(s) = \frac{J_1^2}{s + jb + \frac{J_2^2}{y'(s)}} \quad (2.24)$$

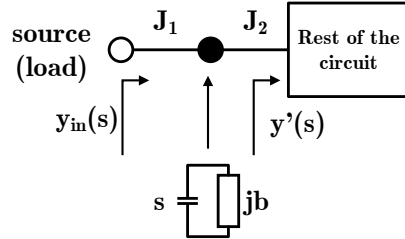


FIGURE 2.7: Circuit with the first node from the input (output) a resonator.

The asymptotic behavior of the admittance is dominated by the unit capacitance of the resonator, it is evident that when the complex

frequency variable approaches to infinity $s \rightarrow \infty$, the admittance is $y_{in} \rightarrow 0$ and gives:

$$e^{j\theta_{11}} = \frac{D(s)}{M(s)} \Big|_{s=\infty} = 1, \quad \theta_{11} = 0. \quad (2.25)$$

The result is because the numerator and denominator polynomials $M(s)$ and $D(s)$ are of degree N and the number of transmission zeros at finite frequencies, n_{fz} , is smaller than N . The equivalent analysis is done if the first node from the output is a resonator. Determining the phase of the output reflection coefficient, the result is similar:

$$e^{j\theta_{22}} = \frac{D(s)}{M(s)} \Big|_{s=\infty} = 1, \quad \theta_{22} = 0. \quad (2.26)$$

2. *First Node from the input (output) a NRN with dangling resonator.*
The situation of a circuit which presents at the input a first non-resonant node of reactance jB coupled, by an inverter J_2 , with a dangling resonator generating a transmission zero at $s = j\omega_z$ is depicted in Fig. 2.8. In this case, the expression for the input admittance is:

$$y_{in}(s) = \frac{J_1^2}{jB + \frac{J_2^2}{s - j\omega_z} + \frac{J_3^2}{y'(s)}}. \quad (2.27)$$

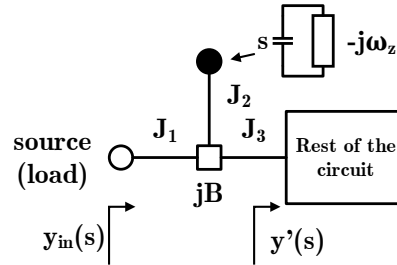


FIGURE 2.8: Circuit with the first node from the input (output) an NRN with dangling resonator.

In order to get the phase of the reflection coefficient, we use the condition that the input admittance has a zero at the position of the TZ:

$$e^{j\theta_{11}} = \frac{D(s)}{M(s)} \Big|_{s=j\omega_z}. \quad (2.28)$$

A similar expression is obtained from the output when the first element connected is a NRN coupled with a dangling resonator generating a TZ at $s = j\omega'_z$:

$$e^{j\theta_{22}} = \left. \frac{D(s)}{M(s)} \right|_{s=j\omega'_z}. \quad (2.29)$$

We can observe what happens to the input (output) reflection coefficient evaluated at the transmission zero frequency $j\omega_z$ ($j\omega'_z$) of the first (last) dangling resonator using the condition of (2.28) ((2.29)) in the expression (2.20) ((2.21)). At that specific frequency, the reflection coefficient is equal to the unit, i.e., all the power is reflected and none is transmitted. Moreover, it is also important to note that the phase at this specific frequency is zero, because the phase term θ_{11} (θ_{22}) is canceled by the term $\frac{M(j\omega_z)}{D(j\omega_z)} = e^{-j\theta_{11}}$ ($\frac{M(j\omega'_z)}{D(j\omega'_z)} = e^{-j\theta_{22}}$). This means that the filter at the transmission zero normalized frequency behaves as an open circuit.

2.6.2 Reflection Coefficients with Phase Adjustment

We have just seen how to evaluate the phase term for the reflection coefficients to equate the input/output admittance of the network in order to be synthesized. Nevertheless, the phases of S_{11} and S_{22} can be modified without affecting the magnitude and, hence, the return and insertion losses. Later, we will show the benefits of the phase match approach in filters implementing duplexers. The fact of adjusting the reflection coefficient phases avoids the use of phase shifts sections.

Following, we detail the expressions and the procedure used to include an additional phase term to the reflection coefficient on an inline extracted pole network. The procedure described here gives the expressions for the input reflection coefficient, although similar expressions can be written for S_{22} by analogy.

We assume that the first extracted pole section to determine in the inline circuit is an NRN with dangling resonator. Therefore, we are in a situation similar to the circuit described in Fig. 2.8. The reflection coefficient is written as (2.20), where θ_{11} is a real quantity and, for this case, it can be obtained by (2.28) under the condition given at (2.22), that the admittance has a zero at the position of the transmission zero $s = j\omega_z$.

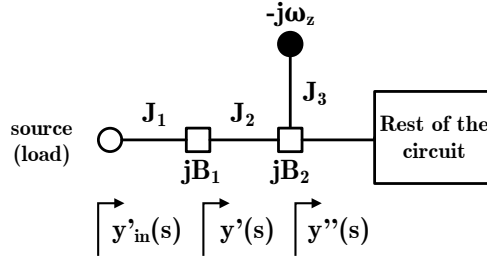


FIGURE 2.9: Circuit with the first node from the input (output) an NRN alone without dangling resonator.

With the reflection coefficient fully specified, we add an extra phase term $e^{j\theta_e}$, which will only modify the phase of the initial reflection coefficient.

$$S'_{11}(s) = e^{j\theta'_{11}} \frac{M(s)}{D(s)} = e^{j\theta_{11}} e^{j\theta_e} \frac{M(s)}{D(s)}, \quad \theta_e = \theta'_{11} - \theta_{11}, \quad (2.30)$$

where θ_e is a real quantity. With the new expression of S_{11} , we determine the new input admittance $y'_{in}(s)$ as

$$y'_{in}(s) = \frac{1 - S'_{11}(s)}{1 + S'_{11}(s)} = \frac{D(s) - e^{j(\theta_{11} + \theta_e)} M(s)}{D(s) + e^{j(\theta_{11} + \theta_e)} M(s)} = \frac{\frac{D(s)}{M(s)} - e^{j(\theta_{11} + \theta_e)}}{\frac{D(s)}{M(s)} + e^{j(\theta_{11} + \theta_e)}} \quad (2.31)$$

Note that the new admittance expression can be evaluated at the frequency of the transmission zero $s = j\omega_z$, where (2.28) is substituted and then resulting in

$$y'_{in}(s = j\omega_z) = \frac{e^{j\theta_{11}} - e^{j(\theta_{11} + \theta_e)}}{e^{j\theta_{11}} + e^{j(\theta_{11} + \theta_e)}} = \frac{1 - e^{j\theta_e}}{1 + e^{j\theta_e}} = -j \tan\left(\frac{\theta_e}{2}\right). \quad (2.32)$$

To implement an inline extracted pole circuit with phase adjustment on the reflection coefficient, it is necessary to extract, first, an inverter of J_1 admittance value and a shunt FIR of reactance value jB_1 . The cascaded connection of these new elements with the assumed circuit without adjustment of the phase is shown in Fig. 2.9. We observe that the first node is an NRN without dangling resonator, which is at the same time connected to another NRN of reactance jB_2 . The FIR B_2 is coupled to a dangling resonator, generating the transmission zero at $s = j\omega_z$. In the described

situation of the circuit (Fig. 2.9), the input admittance takes the form

$$y'_{in}(s) = \frac{J_1^2}{jB_1 + y'(s)}, \quad (2.33)$$

where the admittance expression $y'(s)$ for the rest of the circuit after the FIR without dangling resonator is

$$y'(s) = \frac{J_2^2}{jB_2 + \frac{J_3^2}{s - j\omega_z} + y''(s)}. \quad (2.34)$$

By evaluating the input admittance of (2.33) at the frequency of the first transmission zero of the circuit, $s = j\omega_z$, it results in

$$y'_{in}(s = j\omega_z) = \frac{J_1^2}{jB_1} = -j\frac{J_1^2}{B_1}, \quad (2.35)$$

because the term $y'(s)$ of (2.34) is canceled at this characteristic frequency $s = j\omega_z$. From (2.35), J_1^2 can get any arbitrary value in order to determine B_1 . Now, equating (2.35) with (2.32) allows to establish a direct relation between the included extra phase on S_{11} and the additional circuit extracted elements, which are used to accommodate the phase adjustment.

$$\tan\left(\frac{\theta_e}{2}\right) = \frac{J_1^2}{B_1}. \quad (2.36)$$

The previous finding, (2.36), shows that a network with an input configuration like shown in Fig. 2.9 is comparable to a phase shift at the input.

In the case that we assume that the first node after the NRN without dangling resonator is resonant, we need to do some variations on the above described procedure and given expressions, respect the case of a NRN with dangling resonator.

Therefore in this second case, the circuit of Fig. 2.9 changes just after the shunt FIR alone by a circuit similar to the scheme of Fig. 2.7. The remaining input admittance $y'(s)$ in (2.33) is that of a circuit with an inline resonant node, following (2.24). Hence, $y'(s)$ vanishes at infinity and resulting $y'_{in}(s)$, when evaluated at infinity ($s \rightarrow \infty$), equal to the result of (2.35).

Moreover, given that the phase θ_{11} of S_{11} of a circuit with a resonator as a first node is zero, we can follow the same procedure done above to obtain

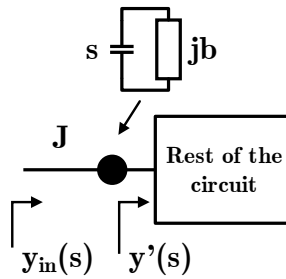


FIGURE 2.10: Circuit to extract a resonator. The elements are the inverter J and the reactance jb .

a reflection coefficient S'_{11} with phase adjustment. Now, we only have to consider in (2.30) that the phase term $e^{j\theta_{11}} = 1$ and evaluate (2.31) at $s \rightarrow \infty$, where the term $\frac{D(s)}{M(s)} \rightarrow 1$. Finally, the relation of (2.36) is also fulfilled.

2.6.3 Cases analysis of network element extraction

The rest of the subsection describes the main possible situations for the extraction of the elements in an inline extracted pole filter based on the Darlington technique. For each situation, aspects such as the nature of the node of the extraction, if it is resonant or non-resonant, are important. The arrangement on the inline circuit and the nature of the following node are also considered. Previously to the extraction, the definition of the reflection coefficient and the input admittance must be completed, following section 2.6.1. The input admittance, expressed as a rational function, is the tool employed in the extraction process. The extraction of the elements on the prototype network is carried out successively.

A. Extraction of a Resonator

If we are in one stage in the extraction procedure and the prototype circuit looks like the form in Fig. 2.10 when doing extraction from the input (or the output), the remaining admittance at that cycle requires the extraction of a resonator.

$$y_{in}(s) = \frac{J^2}{s + jb + y'(s)} \quad (2.37)$$

The resonator is extracted from the input (or the output) admittance

$y_{in}(s)$, which represents the remaining circuit for the filter, consisting in a two-stages operation.

First, the inverter J is extracted by means of the asymptotic behavior of the input admittance:

$$J^2 = sy_{in}(s)|_{s=\infty}. \quad (2.38)$$

The remainder input admittance, after removing the inverter and the shunt-connected unit capacitance, contains the constant reactance jb as leading element.

$$y_{in}(s) \leftarrow \frac{J^2}{y_{in}(s)} - s = jb + y'(s). \quad (2.39)$$

Second, the reactance of the shunt resonant pair is determined. For it, we use the admittance left after the previous step (2.39), and we evaluate it at a zero of the admittance $y'(s)$. Regarding the rest of the circuit admittance $y'(s)$, two different cases are possible.

1) *First Node in $y'(s)$ is a Resonator*

At this situation, the admittance $y'(s)$ vanishes as the complex frequency approaches to infinity.

$$y'(s = \infty) = 0, \quad y_{in}(s = \infty) = jb, \quad (2.40)$$

and

$$b = \text{Im}[y_{in}(s)|_{s=\infty}] \quad y_{in}(s) \leftarrow y_{in}(s) - jb. \quad (2.41)$$

2) *First Node in $y'(s)$ is an NRN*

In the case that the NRN is connected to a dangling resonator, it generates an open-circuit admittance at the transmission zero, $y'(s = j\omega_z) = 0$, then

$$b = \text{Im}[y_{in}(s)|_{s=j\omega_z}] \quad y_{in}(s) \leftarrow y_{in}(s) - jb. \quad (2.42)$$

At that point, the resonator has been removed and the remaining network to be extracted is represented by $y_{in}(s)$.

B. Extraction of an NRN

We assume that, at a given process cycle, the remaining network seen presents the form shown on Fig. 2.11. Hence, the input admittance

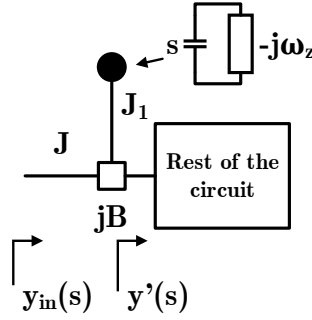


FIGURE 2.11: Circuit to extract an NRN with dangling resonator. The elements are J , jB and J_1 .

is expressed as

$$y_{in}(s) = \frac{J^2}{\frac{J_1^2}{s - j\omega_z} + jB + y'(s)} \quad (2.43)$$

where

$$\frac{J^2}{y_{in}(s)} = \frac{J_1^2}{s - j\omega_z} + jB + y'(s) \quad (2.44)$$

presents a partial fraction form in the left-side. The residue of the pole $s = j\omega_z$ is related with the inverter J_1 :

$$J_1^2 = J^2 \operatorname{residue} \left(\frac{1}{y_{in}(s)} \right) \Big|_s = j\omega_z. \quad (2.45)$$

An interesting feature of NRNs is that we only can determine the ratio between J and J_1 , but not both. Therefore, given a synthesis problem, the use of NRN allows multiple solutions.

From that point, we specify to use J as the free parameter and arbitrarily set to a value. A convenient value is to set $J = 1$, because after the synthesis has finished we can use scaling rules, explained later, to suit the elements of the circuit to the most feasible values regarding the intended realization.

Once the inverters and the dangling resonator are removed, the remaining admittance is

$$y_{in}(s) \leftarrow \frac{J^2}{y_{in}(s)} - \frac{J_1^2}{s - j\omega_z} = jB + y'(s). \quad (2.46)$$

Again, to determine the reactance of the NRN, we consider zeros of the admittance $y'(s)$ in order to evaluate the admittance left after the previous step ($y_{in}(s)$). So, we consider the two possibilities of the first node in $y'(s)$.

1) *First Node in $y'(s)$ is a Resonator*

In this case, the admittance $y'(s = \infty) = 0$, giving

$$B = \text{Im} [y_{in}(s)|_{s=\infty}], \quad y_{in}(s) \leftarrow y_{in}(s) - jB. \quad (2.47)$$

2) *First Node in $y'(s)$ is an NRN*

In the case that another NRN with dangling resonator, generating a transmission zero at $s = \omega'_z$, is connected, we obtain the reactance value evaluating at this new characteristic frequency:

$$B = \text{Im} [y_{in}(s)|_{s=\omega'_z}], \quad y_{in}(s) \leftarrow y_{in}(s) - jB. \quad (2.48)$$

Finally, we have completed the extraction of an NRN and (2.47) and (2.48) obtain the input admittance for next components.

C. *Extraction of the Last Node*

When dealing with large inline networks it is always more suitable to perform simultaneously an extraction from the input and from the output to avoid collected round off errors, which otherwise are collected over the stages in the extraction. Even though, we illustrate the extraction procedure for the last node according to the required cases. If the last node we see, either from the input or the output, is a resonator, an NRN with dangling resonator or an NRN alone without dangling resonator, the approaches used for the extraction are different.

The last situation requires special mention because our synthesis procedure contemplates having an NRN without dangling resonator and [43] does not deal it. In this case, the inclusion of an NRN alone in the inline path aims to provide a freedom parameter for a convenient solution.

In the research realized in the thesis with acoustic wave technology, we have faced some filtering structures which required the introduction of an NRN alone to consider normalized conductances at the source and the load not equal, and keep the inverter with a convenient solution,

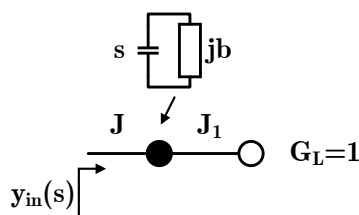


FIGURE 2.12: Circuit to extract the parameters of the last resonator: J , jb and J_1 .

for example $J = 1$. When we place this NRN at the last node, it gives the required degree of freedom to implement a network where different G_S and G_L are considered.

It is true that, previously, we assumed both conductances normalized $G_S = G_L = 1$, justified by the fact that arbitrary values of G_S and G_L are got by changing the connected inverters. Nevertheless, if in the microwave intended realization is more practical to avoid the use of inverters, like it happens with acoustic wave technology, our option is the inclusion of an extra FIR element in the lowpass prototype.

In order to accomplish the relation between the reflection coefficients and the input or output admittance, we assume $G_S = 1$ when extraction is from the input and $G_L = 1$ when it is from the output. Therefore, the other input or output conductance is considered different to unity.

Now the three possible situations for extraction of the last node are described.

1) *Last Node is a Resonator*

In the situation depicted in Fig. 2.12, the parameters to determine are J , jb and J_1 , which couples the resonator with the load $G_L = 1$ (or the source $G_S = 1$). All them determine the remaining admittance at the last cycle

$$y_{in}(s) = \frac{J^2}{s + jb + J_1^2}. \quad (2.49)$$

To get the first inverter, asymptotic evaluation is carried out

$$J^2 = sy_{in}(s)|_{s=\infty} \quad (2.50)$$

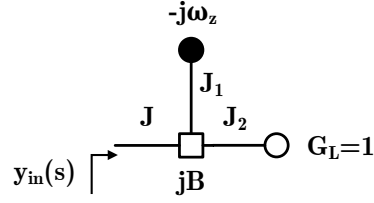


FIGURE 2.13: Circuit to extract the parameters of the last NRN with dangling resonator: J , jB , J_1 and J_2 .

and we get

$$y_{in}(s) \leftarrow \frac{J^2}{y_{in}(s)} - s = jb + J_1^2. \quad (2.51)$$

At that point, the remaining admittance is directly related as

$$b = \text{Im}[y_{in}(s)], \quad J_1^2 = \text{Re}[y_{in}(s)]. \quad (2.52)$$

2) *Last Node is an NRN with dangling resonator*

In the case that the last node is formed by an NRN with a dangling resonator, generating the transmission zero at complex frequency $s = j\omega_z$, the remaining input admittance is of the form (Fig. 2.13):

$$y_{in}(s) = \frac{J^2}{jB + \frac{J_1^2}{s - j\omega_z} + J_2^2}. \quad (2.53)$$

The inverter J_1 is related to the residue of the pole $s = j\omega_z$, then we get

$$J_1^2 = J^2 \text{residue} \left(\frac{1}{y_{in}(s)} \right) \Big|_{s=j\omega_z}, \quad (2.54)$$

where the value of J is arbitrarily set to get a practical value. The extraction is completed determining B and J_2 as follows:

$$B = J^2 \text{Im} \left[\frac{1}{y_{in}(\infty)} \right], \quad (2.55)$$

$$J_2^2 = J^2 \text{Re} \left[\frac{1}{y_{in}(\infty)} \right]. \quad (2.56)$$

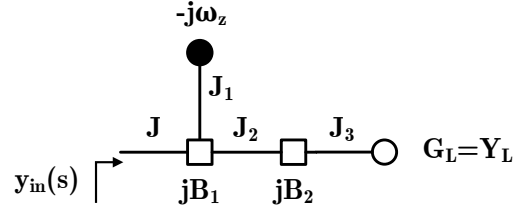


FIGURE 2.14: Circuit to extract the parameters J , jB_1 , J_1 , J_2 , J_3 and jB_2 of the two last NRNs and a load conductance different to the unit.

3) Last Node is an NRN Alone

In the case that the last node is an NRN without a dangling resonator, we give the close expressions to extract the last two nodes of the circuit taking into account that the load admittance termination is different than the source.

We need to consider the nature of the second-to-last node because at this given stage the remaining input admittance is different. Nevertheless, in this thesis, we deal only with the case that the next-to-last node is an NRN with dangling resonator, which generates a transmission zero at $s = j\omega_z$.

The circuit used for the extraction of the described situation is represented in Fig. 2.14. The parameters to extract the last two nodes are the reactance jB_1 of the NRN coupled by J_1 with the dangling resonator, the reactance jB_2 of the NRN alone, the inverter J_2 coupling both NRNs, and the inverter J_3 coupling the NRN alone with the defined load of admittance value Y_L .

The remaining input admittance for this last cycle is

$$y_{in}(s) = \frac{J^2}{jB_1 + \frac{J_1^2}{s - j\omega_z} + \frac{J_2^2}{jB_2 + \frac{J_3^2}{Y_L}}} \quad (2.57)$$

Note that the value of J is arbitrary in this case. Therefore,

$$J_1^2 = J^2 \operatorname{residue} \left(\frac{1}{y_{in}(s)} \right) \Big|_{s=j\omega_z} \quad (2.58)$$

and

$$y_{in}(s) \leftarrow \frac{J^2}{y_{in}(s)} - \frac{J_1^2}{s - j\omega_z} = jB_1 + \frac{J_2^2}{jB_2 + \frac{J_3^2}{Y_L}}. \quad (2.59)$$

Then, (2.59) can be expressed as a complex number

$$y_{in}(s) = \text{Re}[y_{in}(s)] + j\text{Im}[y_{in}(s)] = A + jD. \quad (2.60)$$

Also here, the value of J_2 and J_3 are arbitrary and they can be set to unity following the agreed solution for the extraction and later scaled. When $J_2 = J_3 = 1$,

$$B_2 = \pm \sqrt{\frac{1}{AY_L} - \frac{1}{Y_L^2}}, \quad (2.61)$$

$$B_1 = D + B_2 Y_L A. \quad (2.62)$$

On one hand, it is interesting to note that whether we chose the positive or the negative sign in (2.61), the result of (2.62) is different, although the both solutions implement the same filtering function.

On the other hand, the disadvantage is that, when the real part of the remaining admittance, $\text{Re}[y_{in}(s)] = A$, is higher than Y_L , B_2 becomes pure imaginary, i.e., a real FIR element. However, it can be solved adding more output reactive elements or matching the filter to a proper load impedance such that B_2 becomes real in equation (2.61).

D. Extraction of an NRN alone

The situation of an NRN alone, without dangling resonator, can occur, for example, in inline extracted pole circuits with phase adjustment on the reflection coefficient, as we have shown in Fig. 2.9. If we are in one stage in the extraction procedure where the node to extract is an NRN alone, we need, first, to extract the inverter J connected to the reactance. Second, in order to determine the constant reactance jB , two cases are considered, regarding the admittance left after the reactance.

Fig. 2.15 shows the circuit where the node after the NRN alone is a resonant node, and Fig. 2.16 shows the circuit where the node is an NRN with dangling resonator.

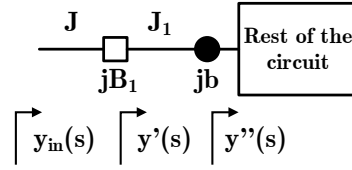


FIGURE 2.15: Circuit to extract the parameters J and jB_1 of an NRN alone following a resonator.

The admittance in both cases can be expressed as

$$y_{in}(s) = \frac{J^2}{jB_1 + y'(s)} \quad (2.63)$$

and

$$\frac{J^2}{y_{in}(s)} = jB_1 + y'(s), \quad (2.64)$$

where $y'(s)$ takes different forms depending whether the next node is a resonator or an NRN with dangling resonator. Note that the inverter J can be set to an arbitrary value.

1) *First Node in $y'(s)$ is a Resonator*

In this case, the admittance

$$y'(s = \infty) = \frac{J_1^2}{s + jb + y''(s)} \Big|_{s=\infty} = 0 \quad (2.65)$$

giving

$$B_1 = \text{Im} \left[\frac{J^2}{y_{in}(s)} \Big|_{s=\infty} \right] \quad y_{in}(s) \leftarrow \frac{J^2}{y_{in}(s)} - jB_1 = y'(s). \quad (2.66)$$

Then, we would follow the extraction process corresponding to removing a resonator.

2) *First Node in $y'(s)$ is an NRN*

In the case that an NRN with dangling resonator is connected, the admittance after the reactance jB_1 is

$$y'(s) = \frac{J_1^2}{jB_2 + \frac{J_2^2}{s - j\omega_z} + y''(s)} \quad (2.67)$$

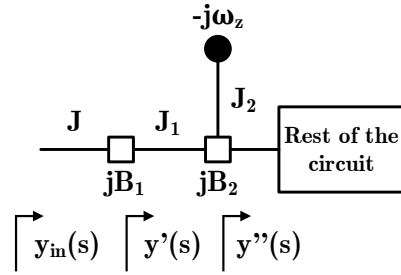


FIGURE 2.16: Circuit to extract the parameters J and jB_1 of an NRN alone following an NRN.

We obtain the reactance value evaluating at the transmission zero frequency:

$$B_1 = \text{Im} \left[\frac{J^2}{y_{in}(s)} \Big|_{s=\omega_z} \right], \quad y_{in}(s) \leftarrow \frac{J^2}{y_{in}(s)} - jB_1 = y'(s). \quad (2.68)$$

Then, we would follow the extraction process corresponding to removing an NRN.

2.6.4 Extraction pole synthesis examples

We consider four examples of synthesis using the inline extraction technique already described. The aim is to illustrate with examples the accuracy of the process according to some specifications and network topologies, given as a result the numerical values of the prototype elements.

1. The first example is a Chebyshev filter of 5th-degree with two finite frequencies transmission zeros at normalized frequencies $s_1 = +j2.1$ and $s_2 = -j1.3$ with inband return loss of 15 dB. Both transmission zeros are generated by two dangling resonators arranged within the circuit according to the topology described at the nodal diagram of Fig. 2.17. Clearly, in these cases of non fully canonical filters, there are several arrangements, beside the one selected in Fig. 2.17, that can be chosen to yield the intended response.

From the given specifications, the characteristic polynomials are the one computed at the first example in section 2.2.2. The reflection

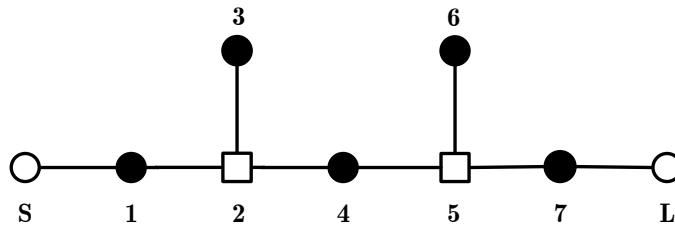


FIGURE 2.17: Lowpass prototype circuit of a fifth-order inline filter with two real transmission zeros $n_{fz} = 2$.

TABLE 2.3: Corresponding input admittance polynomials of prototype filter like in Fig. 2.17.

$s^i, i =$	$y_{in}(s)$ numerator	$y_{in}(s)$ denominator
0	$0.414 + j0.146$	$0.414 + j0.206$
1	$0.993 + j0.403$	$1.692 + j0.403$
2	$2.173 + j0.307$	$2.173 + j0.752$
3	$1.282 + j0.365$	$3.878 + j0.365$
4	1.601	$1.601 + j0.432$
5		2

coefficients are written as:

$$S_{11}(s) = e^{j\theta_{11}} \frac{M(s)}{D(s)} \quad (2.69)$$

$$S_{22}(s) = e^{j\theta_{22}} \frac{M(s)}{D(s)} \quad (2.70)$$

and the corresponding numerator $M(s)$ and denominator $D(s)$ polynomials are given by $F(s)$ and $E(s)$ in Table 2.1, respectively.

The phases of S_{11} and S_{22} must be determined according to the circuit topology arrangement. Since the first node from the input and the output is a resonator, (2.25) and (2.26) are used to yield $\theta_{11} = \theta_{22} = 0$. Using the result in (2.22) and (2.23) the input and output admittances of the circuit are obtained.

In Table 2.3, we just shown the input admittance numerator and denominator polynomial expressions because our extraction is performed from the input to the output. However, both admittances could be used when extracting the elements from the input and output simultaneously.

We follow the analytical expressions given in this section, and we get the values for the parameters of the circuit, refereed according to Fig. 2.17: $M_{S,1} = 0.895$, $M_{2,1} = 1$, $M_{2,4} = 0.772$, $M_{4,5} = 1$, $M_{5,7} = 1.348$, $M_{L,7} = 0.895$, $M_{2,3} = 2.383$, $M_{5,6} = 1.421$, $M_{1,1} = -0.316$, $M_{2,2} = -3.290$, $M_{3,3} = -2.1$, $M_{4,4} = 0.114$, $M_{5,5} = 3.0767$, $M_{6,6} = 1.3$ and $M_{7,7} = 0.578$. The resulting response of the lossless prototype circuit can be calculated and it corresponds with the one shown in Fig. 2.18.

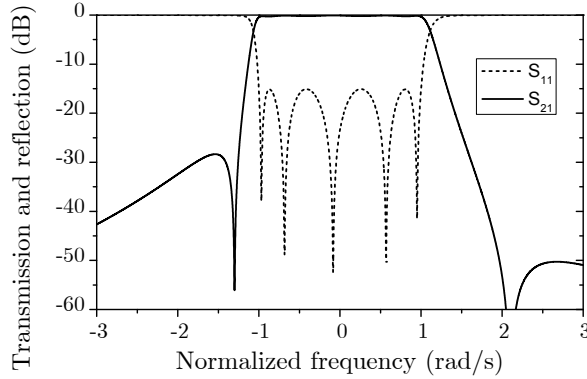


FIGURE 2.18: Lowpass prototype transfer and reflection responses of the extracted filter of Fig. 2.17 with TZ at $s_1 = +j2.1$ and $s_2 = -j1.3$ rad/s.

2. We examine the case of a fully canonical Chebyshev filter of 5th-degree with prescribed transmission zeros at $s_1 = +j1.76$, $s_2 = -j1.72$, $s_3 = j2.4$, $s_4 = -j1.72$ and $s_5 = j1.76$ and return loss of 15 dB corresponding with the second example in section 2.2.2 of the computed characteristic polynomials.

The circuit topology, according to the described filter, is the nodal diagram of Fig. 2.19. In this case the first and the last node are NRNs. We assume that the NRN of the input is connected to a resonator which generates a transmission zero at $s_1 = +j1.76$, and the corresponding phase term of S_{11} is given by (2.28) and it is $\theta_{11} = -59.4^\circ$.

Using this in (2.22) and also following the extraction steps from the input to the output, we get the circuit elements which are according to the terms used in Fig. 2.19: $M_{S,1} = 1$, $M_{1,2} = 1$, $M_{2,3} = 1$, $M_{3,4} = 1$, $M_{4,5} = 1$, $M_{L,5} = 1$, $M_{1,6} = 1.596$, $M_{2,7} = 1.673$, $M_{3,8} = 3.278$,

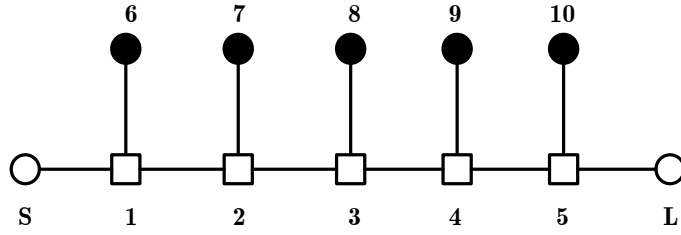


FIGURE 2.19: Lowpass prototype circuit of a fifth-order inline filter with five real transmission zeros $n_{fz} = 5$.

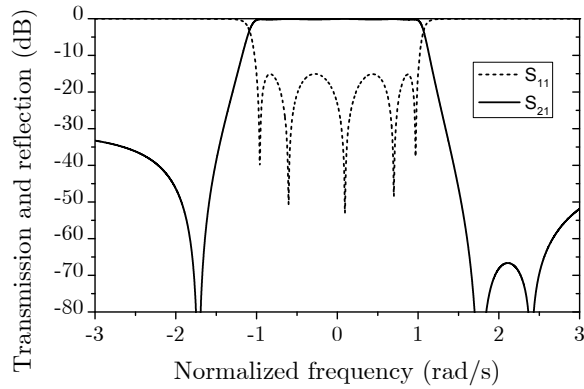


FIGURE 2.20: Lowpass prototype transfer and reflection responses of the extracted filter of Fig. 2.19 with TZ at $s_1 = +j1.76$, $s_2 = -j1.72$, $s_3 = j2.4$, $s_4 = -j1.72$ and $s_5 = j1.76$ rad/s.

$$M_{4,9} = 1.673, M_{5,10} = 1.596, M_{1,1} = -1.296, M_{2,2} = 1.971, M_{3,3} = -4.220, M_{4,4} = 1.971, M_{5,5} = -1.296, M_{6,6} = -1.76, M_{7,7} = 1.72, M_{8,8} = -2.4, M_{9,9} = 1.72, M_{10,10} = -1.76.$$

The response of this circuit is the one plotted in Fig. 2.20. The phase response of the input reflection coefficient displayed in Fig. 2.21 verifies that the S_{11} phase at the specific frequency of the first transmission zero $\omega_z = 1.76$ rad/s is null.

3. In this third example, we analyze the extraction of a filter with the same specifications $N = 5$, $n_{fz} = 5$ and $RL=15$ dB. The same circuit topology depicted in Fig. 2.19 is suitable to describe this filtering function.

The difference with the second example is the order in which we

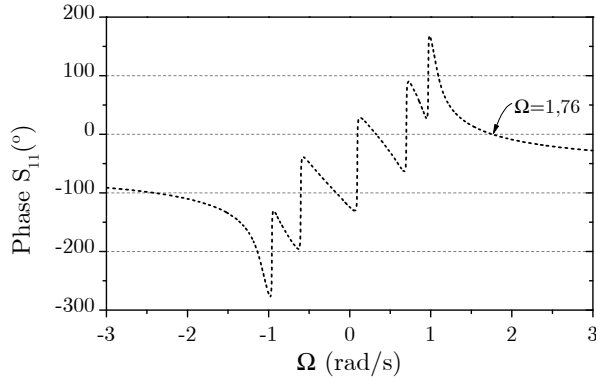


FIGURE 2.21: Lowpass prototype phase reflection response of the 5th-degree Chebyshev filter with five prescribed transmission zeros. The phase term of S_{11} at the frequency $s_1 = j1.76$ of the first transmission zero from the input is zero.

perform the extraction. This means that the array of TZs, from the input to the output, is sorted differently. For this case, the sorting selected is: $s_1 = +j1.76$, $s_2 = +j1.76$, $s_3 = -j1.72$, $s_4 = -j1.72$ and $s_5 = j2.4$ rad/s. Lets note that, regarding the second case, the normalized frequency of the first TZ is equal, therefore, the S_{11} phase is too.

Once the input admittance of this new sorted configuration is computed, we are able to perform the new extraction of the elements, following the described TZ array. The results, refereed to numeration in Fig. 2.19, are: $M_{S,1} = 1$, $M_{1,2} = 1$, $M_{2,3} = 1$, $M_{3,4} = 1$, $M_{4,5} = 1$, $M_{L,5} = 1.3852$, $M_{1,6} = 1.596$, $M_{2,7} = 1.657$, $M_{3,8} = 2.288$, $M_{4,9} = 1.201$, $M_{5,10} = 3.365$, $M_{1,1} = -2.221$, $M_{2,2} = -1.871$, $M_{3,3} = 4.390$, $M_{4,4} = 1.320$, $M_{5,5} = -4.292$, $M_{6,6} = -1.76$, $M_{7,7} = -1.76$, $M_{8,8} = 1.72$, $M_{9,9} = 1.72$, $M_{10,10} = -2.4$. The corresponding frequency response is equivalent to the one show in Fig. 2.20.

Briefly, two important features are observed. The first is that a specific sorting of the transmission zeros directly affects the values of the extracted elements and, consequently, the technological implementation of the filter will be different according to the selected sorted TZ array. Therefore, technological issues are used to make the sorting selection. The second important feature is the invariability of the filtering response, even though two different implementations have resulted.

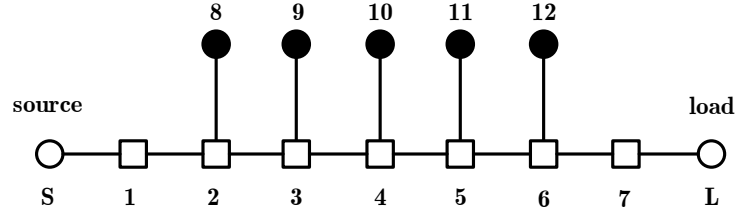


FIGURE 2.22: Lowpass prototype circuit of a fifth-order inline filter with fully canonical response $n_{fz} = N = 5$ and two extra NRN input/output elements to make phase adjustment.

Ejemplo para el sorting. Clearly, in the cases of non fully canonical filters there are several arrangements that can be chosen to yield the intended response depending on the implementation constraints of the selected technology.

4. In the last example we synthesize a fully canonical filter equal to the second example but in this case we apply a phase adjustment on the reflection coefficients. In a duplexer design, the Tx and Rx filters must behave like open-circuits for the counter-band frequencies ($\Gamma = 1$) by using the phase condition. Because of the phase condition modifies the input and/or output admittance the prototype network that implements the filter also does. Therefore, the circuit topology modifies according to Fig. 2.22 in order to implement the additional phase term. For this example, we follow the same transmission zeros arrangement than in the second example.

Contrarily to the second example, where the phase term of S_{11} is evaluated to avoid the need of an input/output NRN element alone in the design; here the input/output external NRNs are needed to adjust the zero-phase of S_{11} to a different frequency than the one of the first transmission zero. The phase term θ'_{11} on (2.30) when realizing the adjustment is determined with the condition that the reflection coefficient phase is zero at a specific frequency, referred as dual ω_{dual} . To face duplexer synthesis, this ω_{dual} will be the counter-band of the Tx or Rx center frequency band.

Therefore, we can obtain the phase term with the expression:

$$e^{j\theta'_{11}} = \left. \frac{D(s)}{M(s)} \right|_{s=j\omega_{dual}}, \quad (2.71)$$

where ω_{dual} is set by the designer according to the filter specifications and requirements. For this example, we consider arbitrarily $\omega_{dual} = 2.411$ rad/s. The resulting value of θ'_{11} is -40.42° , while $M(s)$ and $D(s)$ remain the same than the previous examples because the filtering function has not changed.

Once the reflection coefficient and the input admittance expressions are determined, the elements of the whole prototype structure are extracted according to the TZ sorting of the second example. We get the following values for the coupling matrix coefficients according to reference nodes labeled in Fig. 2.22: $M_{S,1} = 1$, $M_{1,2} = 1$, $M_{2,3} = 1$, $M_{3,4} = 1$, $M_{4,5} = 1$, $M_{5,6} = 1$, $M_{6,7} = 1$, $M_{L,7} = 1$, $M_{2,8} = 0.263$, $M_{3,9} = 10.153$, $M_{4,10} = 0.540$, $M_{5,11} = 10.153$, $M_{6,12} = 0.263$, $M_{1,1} = 5.985$, $M_{2,2} = 0.127$, $M_{3,3} = 72.596$, $M_{4,4} = -0.115$, $M_{5,5} = 72.596$, $M_{6,6} = 0.127$, $M_{7,7} = 5.985$, $M_{8,8} = -1.76$, $M_{9,9} = 1.72$, $M_{10,10} = -2.4$, $M_{11,11} = 1.72$, $M_{12,12} = -1.76$.

The response of this filter is also plotted in Fig. 2.20, which is equivalent in magnitude from that one of the second example, as it is given by the same filtering function. The phase response of the input reflection coefficient corresponding to this circuit which implements the phase adjustment is displayed in Fig. 2.23.

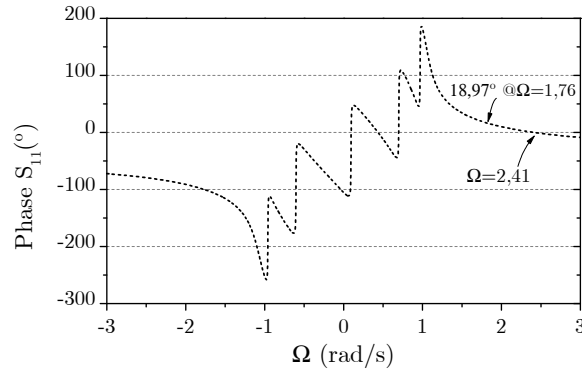


FIGURE 2.23: Lowpass prototype phase reflection response of the 5th-degree fully canonical Chebyshev filter with a phase adjustment of $\theta_e = 18.97^\circ$ respect the phase response on Fig. 2.22.

We can observe in Fig. 2.23 that the phase of S_{11} at the normalized frequency corresponding to the first TZ is now different than 0° , this is the reason why I/O FIR elements are necessary, because it is the

first reactive element which controls the resulting S_{11} phase.

From the plot we verify the fact that the circuit behaves as an open circuit at ω_{dual} , because of the condition imposed of $\theta'_{11} = -40.42^\circ$ for the phase adjustment. According to the phase relation (2.30) and given from the second example that $\theta_{11} = -59.39^\circ$, the extra phase get a value of $\theta_e = 18.97^\circ$. Because the susceptance value of the first NRN is $M_{1,1} = 5.985$ and the first admittance inverter is $M_{S,1} = 1$, we can verify the fulfillment of the relation (2.36) between the phase adjustment and the circuit elements.

In a comparison of the S_{11} phase response at the normalized frequency of the first transmission zero $\omega_z = 1.76$ rad/s of the second and last filter examples, the phase varies from being null in the second example to be approximately 19° in the third example. However, we observe that this phase difference is constant over the whole frequency range, corresponding to the phase shift of θ_e .

2.6.5 Scaling property

In a filter of extracted pole sections with NRNs, there exist infinite solutions for the elements of the circuit and without affecting the response. We have seen, for example, in the extraction process of Fig. 2.11 how in (2.45), there is only a restriction between the ratio of the admittance inverters. Giving an arbitrary value to one of them specifies the other.

The scaling property allows to scale by an arbitrary constant α all the inverters terminating at an NRN since the susceptance of the NRN is also scaled by α^2 . Indeed, in a circuit containing N NRN elements, there are N free parameters that can be chosen to allow some preferred implementation.

We give now an example to illustrate the scaling property. We take the coupling matrix corresponding to the second filter extraction example as

initial matrix:

$$\mathbf{M}_0 = \begin{bmatrix} 0 & 0 & 1 & 0 & 0 & 0 & 0 & 0 & 0 & 0 & 0 & 0 \\ \dots & 0 & 0 & 0 & 0 & 0 & 1 & 0 & 0 & 0 & 0 & 0 \\ & & -1.3 & 1 & 0 & 0 & 0 & 1.6 & 0 & 0 & 0 & 0 \\ & & & 1.97 & 1 & 0 & 0 & 0 & 1.7 & 0 & 0 & 0 \\ & & & & -4.22 & 1 & 0 & 0 & 0 & 3.3 & 0 & 0 \\ & & & & & 1.97 & 1 & 0 & 0 & 0 & 1.7 & 0 \\ & & & & & & \ddots & -1.3 & 0 & 0 & 0 & 1.6 \\ & & & & & & & & -1.76 & 0 & 0 & 0 \\ & & & & & & & & & 1.72 & 0 & 0 \\ & & & & & & & & & & -2.4 & 0 \\ & & & & & & & & & & & 1.72 \\ & & & & & & & & & & & 0 \\ & & & & & & & & & & & \dots \\ & & & & & & & & & & & & -1.76 \end{bmatrix} \quad (2.72)$$

If we multiply by α a row p and a column p for \mathbf{M}_0 simultaneously, we get all the inverters terminating at the NRN, which correspond with matrix coefficients $M_{p,i}$ for $i = S, L, 1, 2, \dots$, scaled by α . At the same time, the susceptance of the NRN itself is scaled by α^2 , which corresponds with the matrix coefficient $M_{p,p}$.

The outcome after scaling the NRN numerated, according to Fig. 2.19, as 1 by α_1 and the NRN numerated as 2 by α_2 is:

$$\mathbf{M}_\alpha = \begin{bmatrix} 0 & 0 & \alpha_1 & 0 & 0 & 0 & 0 & 0 & 0 & 0 & 0 & 0 \\ \dots & 0 & 0 & 0 & 0 & 0 & 1 & 0 & 0 & 0 & 0 & 0 \\ & & -1.3\alpha_1^2 & \alpha_1\alpha_2 & 0 & 0 & 0 & 1.6\alpha_1 & 0 & 0 & 0 & 0 \\ & & & 1.97\alpha_2^2 & \alpha_2 & 0 & 0 & 0 & 1.7\alpha_2 & 0 & 0 & 0 \\ & & & & -4.22 & 1 & 0 & 0 & 0 & 3.3 & 0 & 0 \\ & & & & & 1.97 & 1 & 0 & 0 & 0 & 1.7 & 0 \\ & & & & & & \ddots & -1.3 & 0 & 0 & 0 & 1.6 \\ \hline & & & & & & & & -1.76 & 0 & 0 & 0 \\ & & & & & & & & & 1.72 & 0 & 0 \\ & & & & & & & & & & -2.4 & 0 \\ & & & & & & & & & & & 1.72 \\ & & & & & & & & & & & 0 \\ & & & & & & & & & & & \dots \\ & & & & & & & & & & & & -1.76 \end{bmatrix} \quad (2.73)$$

According to the defined terminology of the coupling matrix, we observe that only the submatrix between NRNs \mathbf{M}_P , and the submatrix between NRNs and resonant nodes \mathbf{M}_{PN} are modified. The submatrix between resonant nodes \mathbf{M}_N is never affected by the scaling property.

2.7 Summary

This chapter describes the characteristic polynomials which represent a filtering function. Making use of the polynomials, we have derived the generalized Chebyshev function generating equiripple with arbitrary transmission zeros and applicable to lossless symmetric and asymmetric filters. We have reviewed important concepts for the relations, in magnitude and phase, of the S-parameters in filters. Next, the polynomials have been translated into a prototype electrical circuit based on coupled resonators structures, for our considered approach, because it suits well with the representation in a coupling matrix form.

We include here the definition of a general class of coupling matrix with non-resonant nodes and resonant ones, and also extended to multiple ports. The input admittance of a two-port network, such a filter, can be calculated from the knowledge of the S-parameters.

In the work, the generation of finite transmission zeros at real frequencies by the introduction of NRNs in an inline configuration has been followed. NRNs specially gives the possibility to create fully canonical inline topologies without a direct source-load coupling and the modularity feature, which is important to control independently the location of transmission zeros.

The synthesis methodology of completely general inline prototypes with NRNs is based on electrical parameter extraction. In this chapter we addressed the issue by deriving analytical expressions for the extraction with respect to the specific filtering function for the most general situations of lowpass prototype filters. This includes the discussion of the phase adjustment for the reflection coefficients, which is suitable for duplexers designs.

The chapter concludes with some synthesis examples of inline extracted pole filters with NRNs exploiting the cases of the analytical procedure. In the extraction process, the effect of the TZs sorting over the prototype elements resulting has been highlighted because of its implication for a later physical implementation. Moreover, the scaling properties of the solutions are demonstrated.

3

LADDER FILTERS AND DUPLXERS BASED ON ACOUSTIC WAVE TECHNOLOGY

In this chapter, we detail how the resonators, as basic building blocks of the prototype network, build up the bandpass acoustic-wave filters with ladder configuration. Therefore, a filter based on acoustic resonators with a ladder topology is equivalent in behavior to an inline prototype network composed of NRNs with dangling resonators. The lowpass prototype network is completely characterized in terms of its critical frequencies, which are the poles and zeros of the transfer function, and the return loss level.

Consequently, this easily leads to the possibility of generating such a ladder filter for a desired response shape by adopting the synthesis extraction technique of the prototype and optimizing its critical frequencies. However, this also means selecting, among all the mask-suitable filtering functions, the ones that are ready to be realized in acoustic wave technology considering: materials, die size, physical restrictions, power density, requirement of external elements, etc. For that reason, in this thesis we show that we are able to accommodating all the stringent constraints of acoustic wave technologies thanks to the efficiency of the developed synthesis method which properly modifies the response within the spectrum mask.

The chapter is devoted to define a direct synthesis methodology which obtains the bandpass electric parameters of a general RF filter or duplexer that is based on acoustic resonators and it includes accommodating the stringent constraints of acoustic wave technologies.

3.1 Synthesis of acoustic-wave resonators from low-pass circuit approach

Once the prototype elements of the electric network are extracted according to a given frequency response, the second step on the design of microwave filters is the correspondence between the elements of the prototype and individual physical components of the filter. At a first glance, the second step is not independent of the applied technology, because at that point the distributed microwave filter is dimensioned for a practical realization.

The lumped-element prototype network might be converted into bandpass filters using frequency transformations for physical elements with an analogous electrical response. Therefore, the numerical values of the lowpass prototype elements are related with the dimensions of the physical elements.

Acoustic wave technology is the microwave filter technology of choice for the user segment of wireless communication systems. The excellent properties of acoustic wave resonators are primarily effect of operating with piezoelectric films.

When applying an electric field between the electrodes on a piezoelectric layer produces a mechanical deformation caused by the inverse piezoelectric effect which generates an acoustic-wave propagation on the electric field direction. Because of different modes of propagation, mainly, two different types of resonators exist. The typical resonator model of BVD electrical circuit is used for bulk acoustic wave and one-port surface acoustic wave resonators.

The appropriate association of the lowpass prototype network with the bandpass BVD model is put into effect by a frequency transformation with equivalence at the bandpass center frequency and finally an impedance transformation. In this chapter, the attempting to find the resonators equivalent prototype circuit model and the justification is extensively detailed.

3.2 Acoustic wave resonators

The term acoustic-wave resonator can be used to indicate a number of significantly different devices. Their common characteristic is the fact that

acoustic waves are involved in their operating principle by means of piezoelectric crystal materials. The piezoelectric material is the cause of generating an acoustic wave. Piezoelectricity is a property own by some crystals which are able to generate a voltage when a mechanical strain (S) is generated.

The coupling between the electric properties and the mechanical deformations is described in general by the piezoelectric constitutive equations [47]:

$$T = cS - eE, \quad (3.1)$$

$$D = eS + \varepsilon E, \quad (3.2)$$

where T is the stress, c is the mechanical stiffness, e is the piezoelectric coefficient, E is the electric field and ε is the permittivity.

Due to the piezoelectric effect, the total strain in the transducer is the sum of mechanical strain induced by the stress and strain caused by the presence of an external electric field. The relation in (3.1) express the inverse piezoelectric effect, and the relation in (3.2) deals with the direct effect describing the created displacement current (D). The transduction between electric and acoustic fields requires the application of an electric field, generally by means of metal electrodes, to the piezoelectric material film.

The electromechanical coupling factor K^2 is a parameter that determines the efficiency of the piezoelectric material to convert energy between the electric and the acoustic fields:

$$K^2 = \frac{e^2}{c^E \varepsilon^S}. \quad (3.3)$$

The superindex E and S indicate that the stiffness has been measured at constant electric fields and that the permittivity has been measured at constant strain, respectively.

However, K^2 is merely related with the material, so the efficient coupling coefficient k_{eff}^2 is often a more used parameter. The k_{eff}^2 measures the efficiency of the electromechanical conversion as a ratio of the stored energy in the electric field and the energy stored in the acoustic field. It is a device property which is related with the material properties, the stack material system and the resonator configuration as well.

The combination of electrodes interfaces and piezoelectric plate configure a transducer. The resonance process requires that the energy is confined

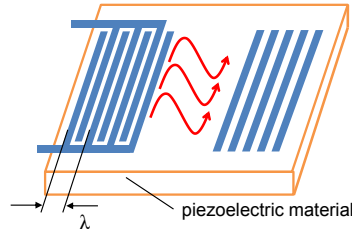


FIGURE 3.1: Surface Acoustic Wave (SAW) Resonator. The acoustic wave propagates on the surface of the piezoelectric substrate.

within the outer surfaces of the electrodes of the transducer. The acoustic waves reflect off mechanical boundaries and stay confined. The basic principle of operation for an acoustic-wave resonator is a traveling wave combined with a confinement structure to produce a standing wave. The frequency of the wave depends on the velocity of the traveling wave and the dimensions of the structure.

Acoustic-wave resonators handled in our research are the following two types that differ on the nature of the acoustic waves and vibration modes involved [48]. On one hand, for Surface Acoustic Wave (SAW) resonators, the acoustic wave propagates on the surface of the substrate. On the other hand, for Bulk Acoustic Wave (BAW) resonators, the traveling wave is a bulk acoustic wave propagating through the interior of the substrate. Therefore, the resonators take the name as the dominant wave in the device.

3.2.1 SAW

A surface acoustic wave travels along the x-y-plane of a piezoelectric substrate wherein the thickness of the substrate is much larger than the wavelength of the SAW [49]. The operation mode is represented in Fig. 3.1. The electrodes are deposited on the surface of the piezoelectric crystal. Interdigital transducers (IDTs) consist of spatially periodic electrodes alternately connected to two bus bars that generate or receive waves synchronous at center frequency with the periodicity of the electrodes (λ) [50]. The frequency of SAW (f) is related with the velocity of propagation v_p and λ , the IDT period defined according Fig. 3.1:

$$f = v_p/\lambda. \quad (3.4)$$

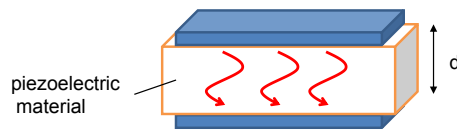


FIGURE 3.2: Bulk Acoustic Wave (BAW) Resonator. The acoustic wave propagate through the interior of the piezoelectric substrate.

As a consequence, the frequency operational range of SAW devices is limited by the photolithographic process.

Because of the alternating connections of the electrodes, the gaps between electrodes have electric fields and, by the piezoelectric property, mechanical stresses also alternate in sign generating surface waves. The frequency of the generated waves is controlled by the pitch of the IDT electrodes, because when the wavelength equals the transducer pitch, the waves for all the gaps are in phase. A SAW propagates in both directions along the surface until incident SAWs arrive at another IDT. Reciprocally, if the IDT and SAWs match, an electrical signal is generated between the IDT electrodes. Typically, the electrodes are quarter-wavelength long in the propagation direction and much wider on the direction normal to propagation [51–53].

Gratings are basic SAW device components which reflect a SAW and are placed at both sides of IDTs. They act as mirrors and together with the transducers form resonant cavities. Within a SAW transmission line, incident and reflected waves interfere with each other yielding a standing wave between the gratings. The regular spacing of the gratings is chosen so that the acoustic wave with a wavelength λ incident on the grating is reflected backward. The length of the gaps between IDT and reflector significantly affects the resonance characteristics. If the resonance frequency of the IDT and reflector are designed to match, so the IDT can detect a very steep resonance [54].

3.2.2 BAW

Two parallel metallic electrode plates, which are separated by a piezoelectric thin film, form the vertical layer stack of a BAW transducer, as depicted in Fig. 3.2. A bulk wave propagates in the z -direction inside the piezoelectric when applying a high frequency signal to the transducer. Consequently, the waves propagates parallel to the electric field direction.

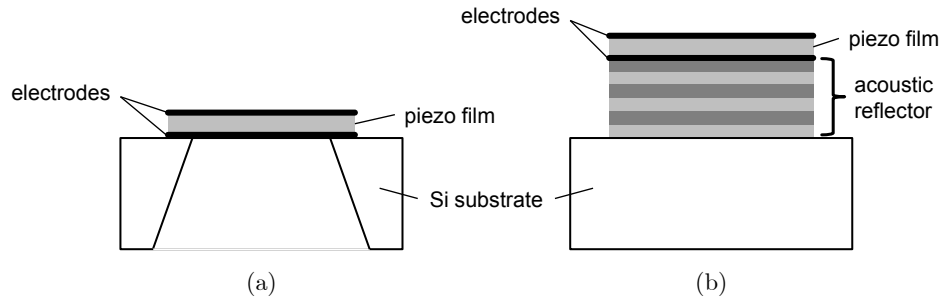


FIGURE 3.3: BAW resonators: (a) Film bulk acoustic resonator (FBAR) free standing structure, (b) Solidly Mounted Resonator (SMR) structure.

The top and bottom surfaces bounce the acoustic waves to form a standing wave. In a first approximation, the mechanical resonance is generated when the thickness of the thin film equals a half-wavelength of the acoustic wave [55].

In order to achieve confinement of BAW within the structure, acoustic isolation of the resonator is required from the substrate because the acoustic mirror at the top is already the air interface. Two configurations are possible to get highly reflective boundaries (Fig. 3.3) [12, 56].

Film bulk acoustic resonator (FBAR) utilizes, as reflective boundaries for the acoustic waves, air because it is considered to get the higher reflection [57]. FBAR etches an air cavity underneath the active area, creating suspended membranes as shown in Fig. 3.3(a).

Another approach to isolate the resonator from the substrate is to use a Bragg reflector below the bottom electrode shown in Fig. 3.3(b), so called Solidly Mounted Resonator (SMR) [58]. SMRs stack thin layers of quarter-wavelength thick and alternate high and low acoustic impedance layers as a distributed acoustic mirror.

For BAW resonators, lateral plate dimensions are larger than the thickness (d), in order to ensure that it mainly operates in the longitudinal mode. With this assumption, the one-dimensional approximation brings out the derived impedance equation [59]

$$Z_{in} = \frac{1}{j\omega C} \left(1 - K^2 \frac{\tan \phi}{\phi} \right) \quad (3.5)$$

$$\phi = \frac{kd}{2} = \frac{\pi}{2} \left(\frac{f}{f_p} \right) \quad (3.6)$$

$$f_p = v_p/2d \quad (3.7)$$

where v_p is the velocity of propagation, k is the propagation constant in the acoustic wave and C the capacitance between the boundaries of the plate.

The analytical expression for the input impedance of a simple resonator assumes infinitesimal thin electrodes. When the frequency (f) is the parallel resonance frequency (f_p) occurs that $kd/2 = \pi/2$, and Z_{in} reaches the maximum value. The minimum value of Z_{in} is produced at the series resonance frequency (f_s) when $K^2 = \phi/\tan \phi$. Although the resonance frequency is determined by the piezoelectric film thickness, in complex resonators the additional layers influence the resonance.

In a BAW resonator the parallel plate capacitance, proportional to the active area A , is given by

$$C = \epsilon^S A/d. \quad (3.8)$$

3.2.3 Electrical characteristics of piezoelectric acoustic-wave resonators

From the interaction of the applied voltage and the generated current flow, a complex impedance is seen through the electrical terminals of an acoustic-wave resonator, either BAW or SAW. If we extract the input impedance of an acoustic-wave resonator as a function of frequency, the typical response is similar to the one shown in Fig. 3.4.

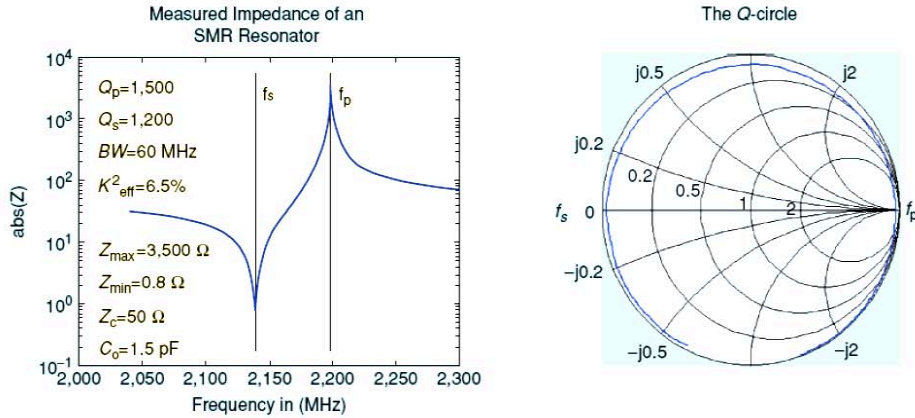


FIGURE 3.4: Magnitude and phase of input electric impedance as a function of frequency on a BAW resonator [60].

The input impedance of a resonator exhibits a zero and a pole. The zero of the input impedance defines the series frequency f_s and the pole the parallel frequency f_p . Respectively, the resonances frequencies are sometimes referred as resonant and antiresonant.

The magnitude of the impedance gets its minimum value at f_s approaching to a short-circuit and the maximum value at f_p approaching to an open-circuit. In acoustic wave resonators, the series resonance is always lower than the parallel resonance. The behavior between the two resonances is inductive; the phase angle of the impedance (ϕ) is 90° . Outside the range between resonances the behavior is capacitive with an angle -90° mainly generated by the static capacitance.

The effective electromechanical coupling coefficient k_{eff}^2 of the resonator, previously defined as a measure of the electromechanical conversion is directly linked to the distance between the resonance frequencies. The k_{eff}^2 is defined as:

$$k_{eff}^2 = \frac{\pi f_s}{2 f_p} \cot \frac{\pi f_s}{2 f_p}. \quad (3.9)$$

3.2.4 Electrical Equivalent Circuit

A typical way of representing the impedance of a piezoelectric resonator is to use an electrical equivalent circuit. The circuit depicted on Fig. 3.5 corresponds to equivalent model for BAW resonators [23, 59] and for one-port SAW resonators as well [51]. The model, known as the Butterworth Van-Dyke (BVD), has been found accurate over narrow bands near the resonance frequency.

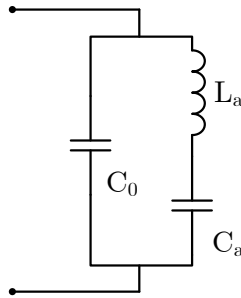


FIGURE 3.5: Lumped-element electrical equivalent circuit of an acoustic-wave resonator, the BVD model.

The lossless BVD circuit models the contribution of the mechanical motion as a series L-C. The capacitance C_a and the inductance L_a from the motional branch are in parallel with the static capacitance C_0 . The static capacitance is due to the parallel electrode plates in BAW resonators, as shown in (3.8), and to the static capacitance of the IDT in SAW resonators. The lossless version of the BVD circuit is of second order.

A BVD model input impedance describes the main resonances of acoustic wave resonators. The expression of the resonator input impedance can be obtained in pole-zero form by analyzing the circuit

$$Z_{in}(\omega) = \frac{j \left(\omega L_a - \frac{1}{\omega C_a} \right)}{1 - \omega^2 C_0 L_a + C_0 / C_a}. \quad (3.10)$$

At the pole and zero frequencies evaluation the two resonances are obtained:

$$f_s = \frac{1}{2\pi\sqrt{L_a C_a}} \quad (3.11)$$

$$f_p = \frac{1}{2\pi} \sqrt{\frac{C_0 + C_a}{L_a C_a C_0}} = f_s \sqrt{1 + \frac{C_a}{C_0}} \quad (3.12)$$

Note that $(f_p - f_s)$ is proportional to the ratio of C_a/C_0 . We verify that f_p is always greater than f_s because the term $\sqrt{1 + \frac{C_a}{C_0}}$ in (3.12) is always greater than one, as the capacitances are always positives values. Moreover,

$$\left(\frac{f_p}{f_s} \right)^2 = \frac{C_0 + C_a}{C_0} = \frac{C_{LF}}{C_0} \quad (3.13)$$

where $C_{LF} = C_0 + C_a$ is defined as the measured low-frequency capacity of the resonator. More often in SAW resonators, the capacitance ratio parameter r , given by

$$r = \frac{C_0}{C_a} = \frac{1}{(f_p/f_s)^2 - 1}, \quad (3.14)$$

is frequently used to determine the resonator performance.

From impedance measurements, f_s , f_p and C_{LF} can be extracted. Therefore, the fundamental parameter of capacitance ratio can be extracted as

well. To the relation in (3.9) the effective electromechanical coupling coefficient can be simplified applying the second order Taylor series approximation [61] and then, related with the definition of r , we can express [21]:

$$k_{eff}^2 = \frac{\pi^2}{8} \left(\frac{1}{r} \right) \left(1 - \frac{1}{r} \right). \quad (3.15)$$

The last relation shows the inverse correspondence between r and k_{eff}^2 .

Some common piezoelectric materials, AlN, ZnO and LiTaO₃, possess varying material parameters, such as the electromechanical coupling coefficient. Table 3.1 compares the summary of material properties.

TABLE 3.1: Properties of piezoelectric materials

Parameter		<i>AlN</i>	<i>ZnO</i>	<i>LiTaO₃</i>
v_p	(10 ³ m/s)	11.5 [62]	6.08 [63]	3.29 [64]
k_t^2	(%)	6.5 [65]	7.5 [65]	15 [66]
r		19.9	17.4	9.1

The lumped element model helps to analyze resonator performance and design filters. However, BVD model does not predict the harmonic responses. Nonetheless, the use of equivalent lumped circuit model is widespread because few parameters are required for modeling the resonator and it is easy to introduce losses due to finite quality factors (Q).

Many authors [21, 67, 68] have tried to improve the BVD model by including resistive elements seeking a substantial agreement of the circuit model to the measured data of acoustic-wave resonators. The Modified BVD (MBVD) model, pointed out in [21], has demonstrated to produce a good agreement to the measured data. Six elements form the MBVD equivalent circuit which is depicted in Fig. 3.6. The resistive elements model the degraded resonance behavior due to the different sources of losses. The

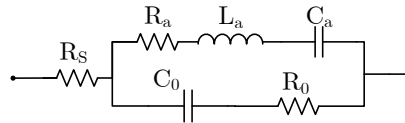


FIGURE 3.6: Modified Butterworth Van-Dyke equivalent circuit of an acoustic-wave resonator considering losses mechanisms.

motional resistance R_a is associated with the acoustic losses in the system.

With the introduction of the series resistance R_s at the input, the model takes into account the metal electrode losses which are always present even if their resistance is a small value. Adding a resistor R_0 in series with the static capacitance C_0 , the material losses are included.

The quality factor Q parameter measures losses for a resonator. Originally, Q factor is defined as the ratio of the stored energy to the dissipated energy in a half-cycle. The quality factor at the series and parallel resonance frequencies are denoted by Q_s and Q_p , respectively. At the series resonance the stored energy in the motional branch is given by L_a and the dissipated energy by R_a and the series resistance R_s . Then, the series quality factor Q_s , defined in terms of the equivalent circuit, follows the relation

$$Q_s \approx \frac{2\pi f_s L_a}{R_a + R_s} \quad (3.16)$$

Similar analysis at the parallel resonance is carried out to extract the quality factor Q_p in terms of circuit elements

$$Q_p \approx \frac{2\pi f_p L_a}{R_a + R_0} \quad (3.17)$$

For the characterization of the Q it is convenient to compute the slope of the impedance phase (ϕ_Z) evaluated at each resonance frequency. Using equations

$$Q_s = \frac{f_s}{2} \left. \frac{\partial \phi_Z}{\partial f} \right|_{f=f_s} \quad (3.18)$$

$$Q_p = \frac{f_p}{2} \left. \frac{\partial \phi_Z}{\partial f} \right|_{f=f_p} \quad (3.19)$$

we define the Q factors in terms of the slope of the phase. When Q is enough large, the frequency giving the specified ϕ_Z does not change under variation of ϕ_Z (Fig. 3.4). Larger Q factors means smaller power dissipation. Observe that the gradient of the phase corresponds to the group delay. If not resistive elements are present any losses are taken into account in the MBVD circuit. Therefore, the Q factor of series and parallel resonances will be infinite.

From measurements and parameter extraction of f_s , k_{eff}^2 , C_{LF} , Q_s , Q_p and R_s of an acoustic-wave resonator, the other five MBVD circuit parameters are derived by analytical expressions.

$$f_p = \sqrt{\left(1 + \frac{1}{r}\right) f_s^2} \quad (3.20)$$

$$C_0 = C_{LF} \left(\frac{f_s}{f_p} \right)^2 \quad (3.21)$$

$$C_a = C_{LF} - C_0 = \frac{C_0}{r} \quad (3.22)$$

$$L_a = \frac{1}{(2\pi f_s)^2 C_a} \quad (3.23)$$

$$R_a = \frac{2\pi f_s L_a}{Q_s} - R_s \quad (3.24)$$

$$R_0 = \frac{2\pi f_p L_a}{Q_p} - R_a \quad (3.25)$$

where relations (3.14), (3.13), (3.11), (3.16), (3.17) have been considered. The computed MBVD circuit values are used to find relationship between physical parameters for resonators.

3.3 Lowpass equivalent models for acoustic wave resonators

From the previous section we have seen that the BVD circuit is used to extract network models that reflects the basic electromechanical behavior of individual acoustic-wave resonator, but also characterizes the physical structure. The BVD model allows accuracy for the electromechanical analysis of an acoustic resonator, avoiding 3D solvers of the whole physical device which experience long simulation times, large memory consume and high computational effort. The BVD electrical model is widely accepted and it is faithful input impedance characterization of the physical acoustic resonator in the main resonance vicinity. This is the reason why we have based our target of synthesis outcome the primary elements of the BVD model.

Our goal is to establish a straightforward synthesis methodology to obtain the bandpass electric parameters based on acoustic resonators of a general RF acoustic wave filter. The filter synthesis algorithm described in Chapter 2 begins with an ideal inline lowpass prototype circuit represented by its coupling matrix which defines the topology. Therefore, our question is if we can use the lowpass prototype of a general inline coupled resonator filter as a model for acoustic wave resonators.

In this section, we focus on the association of the inline lowpass NRN structure representation with the BVD model-based acoustic wave resonator. Consequently, we will make use of the analytical extracted pole synthesis procedure from a desired mathematical filtering function in order to determine the circuitual BVD model of the resonators. We apply direct extraction for synthesis and simplify the design.

Next, we describe the lowpass equivalent BVD resonator. The frequency translation of the BVD model has an analogous frequency response to the one of acoustic-wave resonators in the lowpass frequency domain.

For simplicity, we carried out the association neglecting the resistance components of the MBVD model, we deal with the lossless model because the lossess can be introduced later with a complex frequency variable according to the Q factor.

The conventional ladder filter has alternating cascading of series and shunt elements. An acoustic-wave resonator in shunt connection designed to have a series resonance frequency f_{sSH} , a capacitance ratio r_{SH} and static ca-

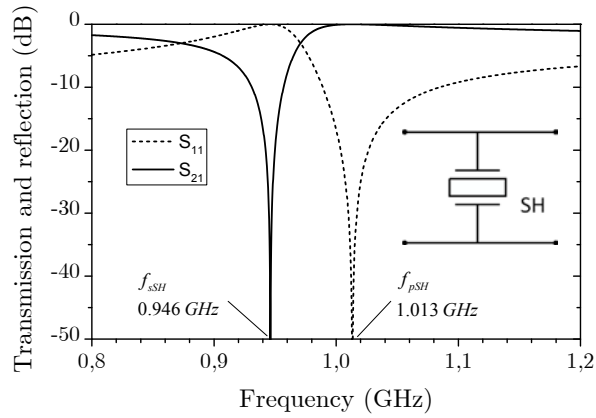


FIGURE 3.7: Magnitude response of an acoustic-wave resonator configured in shunt.

capacitance C_{0SH} is modeled by means of the circuit elements L_{aSH} , C_{aSH} and C_{0SH} of the BVD equivalent network. The transmission and reflection magnitude responses of the shunt resonator are represented at Fig. 3.7. A transmission zero is observed at the lower side-band, agreeing with the series resonance frequency f_{sSH} . The reflection zero agrees with f_{pSH} .

Meanwhile, an acoustic-wave resonator configured in series connection having a series resonance frequency f_{sSE} , a capacitance ratio r_{SE} and a static capacitance C_{0SE} is modeled by means of the circuit elements L_{aSE} , C_{aSE} and C_{0SE} of the BVD equivalent network. The transmission and reflection magnitude responses of the series resonator are represented at Fig. 3.8. A transmission zero is observed at the upper side-band, agreeing with the parallel resonance frequency f_{pSE} . The reflection zero agrees with f_{sSE} .

Lets now analyze two different extracted pole sections from a lowpass inline prototype circuit. An NRN coupled with a dangling resonator by means of an admittance inverter constitute the first lowpass section as it is represented in the nodal diagram of Fig. 3.9(a). The equivalent circuit of this section, in Fig. 3.9(b), shows the elementary resonating structure (dangling resonator) represented by a unit capacitor (admittance $Y = s$) in parallel to a constant susceptance b and both elements connected through an admittance inverter to an NRN of frequency invariant susceptance value B . After analyzing the dangling resonator model of Fig. 3.9(b) it is proved its equivalence with the circuit based on two parallel branches shown in Fig. 3.10.

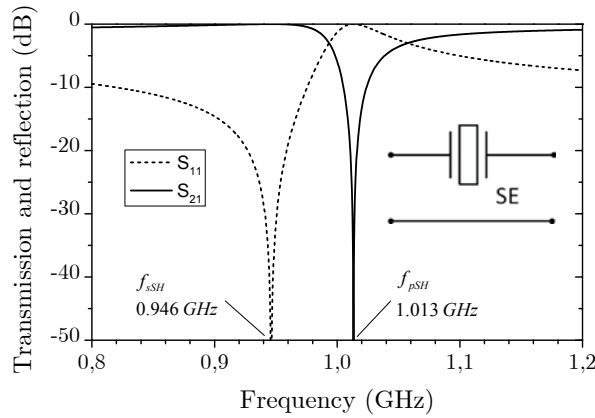


FIGURE 3.8: Magnitude response of an acoustic-wave resonator configured in series.

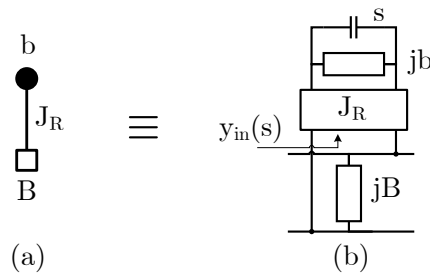


FIGURE 3.9: Lowpass circuit schematic of a shunt resonator, (a) a nodal diagram representation of the extracted pole section, (b) equivalent circuit schematic.

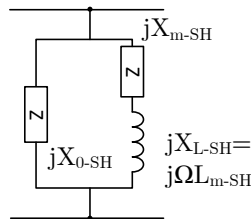


FIGURE 3.10: Equivalent lowpass circuit BVD model of a shunt resonator

The elements, defined as impedances, form the two parallel branch equivalent circuit: one shunt FIR element X_{0-SH} , another branch composed of series inductor, which produces a reactance X_{L-SH} , and a FIR X_{m-SH} .

The label 'Z' on the FIR elements of the circuit in Fig. 3.10 have been set to indicate they are defined as impedances.

When expressing the input admittance in Fig. 3.9(b) at the point the admittance inverter connects to the FIR forward the dangling resonator, we have

$$y_{in}(s) = \frac{J_R^2}{s + jB} \quad (3.26)$$

which is an impedance

$$z_{in}(s) = \frac{s}{J_R^2} + j\frac{b}{J_R^2}. \quad (3.27)$$

The impedance presents a term frequency-dependent, which could be X_{L-SH} and a FIR which could be X_{m-SH} . Similarly, the shunt susceptance B of circuit Fig. 3.9(b) can be expressed as a reactance X_{0-SH} , all establishing the relationships with the impedance elements of circuit Fig. 3.10:

$$X_{0-SH} = \frac{-1}{B} \quad (3.28)$$

$$X_{L-SH} = \frac{\Omega}{J_R^2} = \Omega L_{m-SH} \quad (3.29)$$

$$X_{m-SH} = \frac{b}{J_R^2}, \quad (3.30)$$

where Ω is the real normalized frequency. Now, it is straightforward the equivalence of both circuits Fig. 3.9 and Fig. 3.10, which relates an NRN with dangling resonator directly with a lowpass equivalent BVD resonator in shunt connection.

The circuit in Fig. 3.10 is a relatively new idea of lowpass BVD resonator, as it is evident by the arrangement and composition regarding the BVD model defined in Fig. 3.5.

Lets study now the second extracted pole section considered which is a dangling resonator with NRN, like the first section, placed between two admittance inverters of value $\pm J_{ML}$ and it is represented by the nodal diagram of Fig. 3.11(a).

The equivalent circuit of Fig. 3.11(b) is clearly, a lowpass BVD circuit of elements X_{0-SH} , X_{L-SH} and X_{m-SH} placed between the admittance inverters J_{ML} and $-J_{ML}$, which is depicted in Fig. 3.12.

For the analysis of the resulting circuit, we can multiply the cascading of $ABCD$ matrices of the two inverters at both sides of the central admittance,

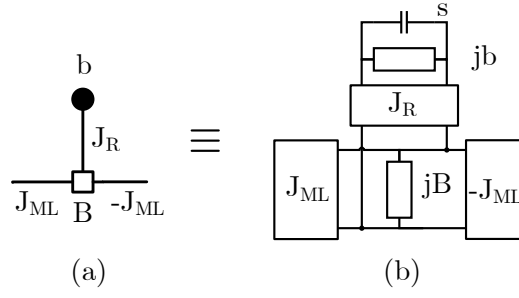


FIGURE 3.11: Lowpass circuit schematic of a series resonator, (a) a nodal diagram representation of the extracted pole section, (b) equivalent circuit schematic.

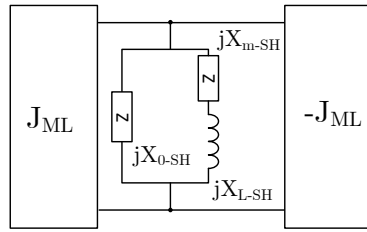


FIGURE 3.12: Equivalent circuit schematic of Fig. 3.11 using lowpass BVD circuit representation.

and the resulting $ABCD$ matrix is:

$$\begin{bmatrix} 1 & \frac{1}{J_{ML}^2} \left(jB + \frac{1}{jX_{L-SH} + jX_{m-SH}} \right) \\ 0 & 1 \end{bmatrix} \quad (3.31)$$

Note that we are assuming the two admittance inverters of equal value J_{ML} and opposite sign, if not the resulting $ABCD$ matrix would be more general.

The resulting $ABCD$ matrix of the studied network corresponds with the $ABCD$ matrix of an impedance element Z , which impedance value is:

$$Z = j \frac{B}{J_{ML}^2} + \frac{1}{\frac{s}{J_R^2} J_{ML}^2 + j \frac{b}{J_R^2} J_{ML}^2}. \quad (3.32)$$

A network describing such impedance is a series reactance X'_{0-SE} in series with a two-parallel branches, one with a frequency variant susceptance B_C

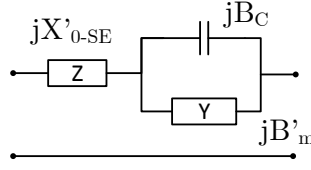


FIGURE 3.13: Equivalent lowpass circuit model for a series resonator in Y-network form.

and the other with a frequency invariant susceptance B'_m as depicted in Fig. 3.13.

The values of the elements on the Y-network of Fig. 3.13, according to (3.32), are:

$$X'_{0-SE} = \frac{B}{J_{ML}^2} \quad (3.33)$$

$$B_C = \Omega \frac{J_{ML}^2}{J_R^2} = \Omega C'_m \quad (3.34)$$

$$B'_m = b \frac{J_{ML}^2}{J_R^2} = \frac{-1}{X'_m} \quad (3.35)$$

In order to convert the circuit of Fig. 3.13 into a more convenient network, we apply the $Y-\Delta$ transform which gives the equivalence of the two circuits in Fig. 3.14 when the following relations are established:

$$X_{0-SE} = X'_{0-SE} = \frac{B}{J_{ML}^2} \quad (3.36)$$

$$X_{m-SE} = - \left(X'_{0-SE} + \frac{(X'_{0-SE})^2}{X'_m} \right) = \frac{bB^2}{J_{ML}^2 J_R^2} - \frac{B}{J_{ML}^2} \quad (3.37)$$

$$L_{m-SE} = C'_m X'_{0-SE} = \frac{B^2}{J_{ML}^2 J_R^2} \quad (3.38)$$

It is noticeable that the Δ circuit after the transformations equals the lowpass BVD model in series connection.

Therefore, the expressions (3.28), (3.29) and (3.30) gives the relation between the first extracted pole section of Fig. 3.9 and the lowpass BVD circuit in shunt, whereas the expressions (3.36), (3.37) and (3.38) relates the second extracted pole section of Fig. 3.11 and the lowpass BVD circuit

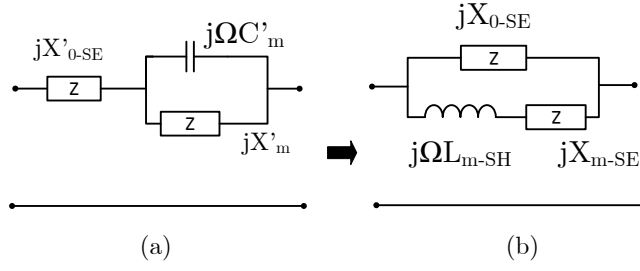


FIGURE 3.14: $Y-\Delta$ network transformation: (a) Y circuit representation, (b) Δ circuit representation and equivalent lowpass circuit BVD model for series resonator.

in series. Elements relations can be studied for both BVD circuits, series and shunt, regarding the parameters of the extracted pole network:

$$\frac{X_{0-SH}}{L_{m-SH}} = -\frac{J_R^2}{B} \quad (3.39)$$

$$\frac{X_{m-SH}}{L_{m-SH}} = b \quad (3.40)$$

$$\frac{X_{m-SH}}{X_{0-SH}} = \frac{-bB}{J_R^2} \quad (3.41)$$

and

$$\frac{X_{0-SE}}{L_{m-SE}} = \frac{J_R^2}{B} \quad (3.42)$$

$$\frac{X_{m-SE}}{L_{m-SE}} = (bB - J_R^2) \quad (3.43)$$

$$\frac{X_{m-SE}}{X_{0-SE}} = \frac{bB}{J_R^2} - 1 \quad (3.44)$$

3.3.1 Zero-pole modules

Now we are going to analyze how the two last extracted pole modules generate a pole-zero pair, in order to verify that an acoustic-wave resonator acts as one of the two extracted pole sections, according if its position is series or shunt.

The reflection coefficient can be expressed as a function of $F(\Omega)$, which is

the inverse function of the characteristic function,

$$S_{11}(\Omega) = \pm \frac{1}{1 - jF(\Omega)}. \quad (3.45)$$

For the normalized lowpass frequency variable Ω , the function $F(\Omega)$ has a zero at Ω_Z , $F(\Omega_Z) = 0$, where $|S_{11}| = 1$ and $|S_{21}| = 0$ for the conservation of energy condition. Therefore, Ω_Z is a transmission zero. The function $F(\Omega)$ has a pole at Ω_P , $F(\Omega_P) = \infty$, where $|S_{11}| = 0$ and $|S_{21}| = 1$ and hence Ω_P is a reflection zero. The positive or negative sign is just a phase term which does not affect the zero and pole frequencies.

Zero-pole response for the extracted pole section of a shunt resonator

Firstly, we analyze the equivalent schematic circuit of a single NRN with dangling resonator of Fig. 3.9 doubly-loaded with unit loads G_S and G_L to extract the S-parameters as shown in Fig. 3.15.

We can apply the even-odd mode technique by using the symmetry of the circuit. The reflection coefficient expressed as a function of the even admittance (Y_e) and the odd admittance (Y_o) is:

$$S_{11} = \frac{1 - Y_e Y_o}{(1 + Y_e)(1 + Y_o)} \quad (3.46)$$

The admittance at the A point of the circuit in Fig. 3.15 is

$$Y_A = jB + \frac{J_R^2}{s + jb}, \quad (3.47)$$

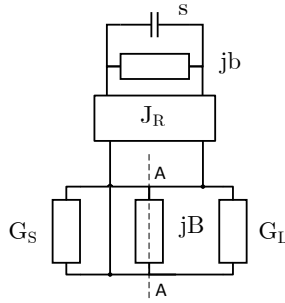


FIGURE 3.15: Schematic representation of a doubly-loaded extracted pole section of Fig. 3.9 for a shunt equivalent resonator.

which is equal to the parallel of two admittances of value $Y_A/2$, in order to apply symmetry.

Therefore, $Y_e = Y_A/2$ and $Y_o = \infty$. When applying L'Hôpital rule, the reflection coefficient is

$$S_{11} = -\frac{1}{1 + 1/Y_e} = -\frac{1}{1 + 2 \left(\frac{s + jb}{(s + jb)jB + J_R^2} \right)}. \quad (3.48)$$

When it is expressed as a function of the real normalized frequency

$$S_{11} = -\frac{1}{1 - j \frac{2}{B} \left(\frac{\Omega + b}{\Omega + b - \frac{J_R^2}{B}} \right)}. \quad (3.49)$$

For the corresponding function $F(\Omega)$ in (3.49), the root of the numerator represents the frequency of transmission zero and the root of the denominator is the frequency of the reflection zero:

$$\Omega_Z = -b \quad (3.50)$$

$$\Omega_P = \frac{J_R^2}{B} - b. \quad (3.51)$$

The ratio $\frac{J_R^2}{B}$ controls the frequency distance between the pole and zero, and the sign of B controls the order of the zero-pole, because

$$\Omega_P - \Omega_Z = \frac{J_R^2}{B} \quad (3.52)$$

and we observe that if $B > 0$, then the frequencies $\Omega_P > \Omega_Z$ at the frequency response of circuit Fig. 3.15.

We next explain the implications of the results when B is a positive value, according to the fact that the analyzed extracted pole section of Fig. 3.9 is equivalent to the lowpass BVD circuit model in shunt position of Fig. 3.12 proved before. Aiming to equate the lowpass BVD circuit in shunt position with an acoustic wave resonator model, on one hand the input electrical impedance properties of an acoustic resonator must be fulfilled, which means that the parallel resonance f_p of maximum impedance is greater than the

series resonance f_s of minimum impedance. On the other hand, the unique nature of the static capacitance C_0 on the BVD model, must be also considered in the lowpass BVD circuit.

The desired situation in order to ensure the first equivalence is when $\Omega_P > \Omega_Z$. The transmission zero at Ω_Z is the frequency of maximum attenuation, there is no transmission between the source and the load, therefore this is only possible if the input impedance of the resonator is at its minimum value and behaves such a short-circuit driving the signal to ground. The minimum impedance of an acoustic resonator occurs at its f_s which is lower than f_p .

The reflection zero at Ω_P is the frequency of maximum transmission between the source and the load, and the frequency corresponds with the point where the impedance of the resonator in shunt position is maximum. The situation approaches to an open circuit for the resonator, producing maximum signal transmission to the load. The maximum impedance of an acoustic resonator occurs at its f_p frequency.

Moreover, the simulated transmission and reflection frequency responses of an acoustic wave resonator placed in shunt on Fig. 3.7 corroborate the equivalence with the extracted pole section in Fig. 3.9 for a $B > 0$. The bandpass frequency response confirms the transmission zero is at a lower frequency than the reflection zero.

Zero-pole response for the extracted pole section of a series resonator

Secondly, we analyze the reflection response of the equivalent schematic circuit of a single NRN with dangling resonator between two admittance inverters of Fig. 3.11 when it is doubly-loaded, aiming to support its equivalence with a series acoustic wave resonator. The lowpass circuit to analyze is shown in Fig. 3.16.

We also apply circuit symmetry defined at the A point and the even and odd admittances are:

$$Y_e = \frac{2J_{ML}^2}{jB + \frac{J_R^2}{s + jb}} = \frac{2J_{ML}^2}{B} \frac{s + jb}{j(s + jb) + \frac{J_R^2}{B}} \quad (3.53)$$

$$Y_o = 0 \quad (3.54)$$

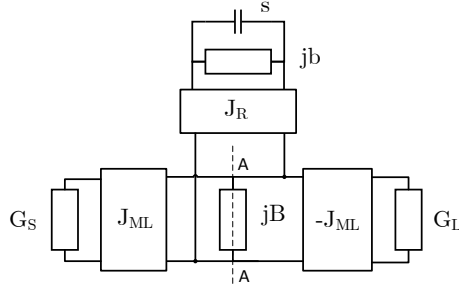


FIGURE 3.16: Schematic representation of a doubly-loaded extracted pole section of Fig. 3.11 for a series equivalent resonator.

Then, according to the reflection parameter as a function of the even-odd admittance (3.46),

$$S_{11} = \frac{1}{1 + Y_e}. \quad (3.55)$$

We get the equivalence $Y_e(\Omega) = -jF(\Omega)$ by using (3.45). Consequently, the $F(\Omega)$ of this circuit can be written as follows:

$$F(\Omega) = \frac{2J_{ML}^2}{B} \frac{\Omega + b}{\Omega + b - \frac{J_R^2}{B}} \quad (3.56)$$

and the frequencies of the transmission zero and the reflection zero are:

$$\Omega_Z = -b \quad (3.57)$$

$$\Omega_P = \frac{J_R^2}{B} - b. \quad (3.58)$$

Calculating the zero-pole distance gives

$$\Omega_Z - \Omega_P = -\frac{J_R^2}{B} \quad (3.59)$$

which results in $\Omega_Z > \Omega_P$ when $B < 0$ for the frequency response of the circuit of Fig. 3.16.

The value of B negative is the desired case, when this extracted pole section is equivalent to a lowpass BVD circuit in series position, to be the model of an acoustic-wave resonator.

With an analysis similar to the case of shunt extracted pole section carried out we observe that, the pole of $F(\Omega)$, Ω_P , which is at a lower frequency

than Ω_Z , corresponds to a minimum of the input impedance of the extracted pole section of Fig. 3.11. With Ω_Z which corresponds to a higher frequency happens contrarily, producing maximum input impedance. The minimum impedance of an acoustic resonator occurs at its f_s which is lower than f_p , of maximum impedance.

In addition, the simulated transmission and reflection responses, in Fig. 3.8 ,for an acoustic-wave resonator placed in series confirms the equivalence with the studied extracted pole section and a series resonator when $B < 0$.

After these two cases have been studied, we can conclude that in order to generate TZs at both passband sides, it is only possible if alternating between series and shunt extracted pole sections. The reason is because the filter realized on the basis of acoustic wave resonators is restricted for the resonance frequencies condition $f_s < f_p$. The reader should observe the relation with the common ladder topology and its frequency response.

The transmission zero generated by each of both extracted pole sections in normalized frequency results to be at $\Omega_i = -b$. The frequency of the transmission zero Ω_i can be either positive or negative.

For the extracted pole section of a shunt resonator (Fig. 3.15) being part of a filter, first, the reflection zero lies along the normalized frequency range $[-1, 1]$; second, the reflection zero is placed at a greater frequency than the transmission zero. Consequently, the transmission zero normalized frequency of a shunt resonator is $\Omega_i < -1$, located at the lower stopband. It means the FIR element b is positive, according to the definitions of sign set up.

A similar reasoning carried out for the extracted pole section of a series resonator (Fig. 3.16) results in a normalized transmission zero $\Omega_i > 1$ and placed at the upper stopband. It means the FIR element b is negative.

It can be concluded from the analysis of both extracted pole sections, that we can arrange a transmission zero above and below the passband. At the same time, (3.52) and (3.59) shows that space between the pole and zero on both cases is determined by the value of the coupling between the NRN and the dangling resonator and the inverse of the NRN susceptance.

3.3.2 Lowpass to Bandpass Model Transformation

Following, we give further proof that the characteristics of extracted pole sections with dangling resonators are equivalent to those of a bandpass BVD model by applying a frequency transformation and impedance denormalization.

At that point, we have verified the concept that both circuits, the extracted pole section form and the lowpass BVD referred circuit are equivalent. Straightforward analysis gave the set of relations between elements of both configurations. The two shunt and series lowpass equivalent circuits transformed each from extracted pole sections are controlled by different sets of relations taking into account the series or shunt interpretation.

The equivalent lowpass circuit BVD model is defined for Ω the normalized frequency variable for a unity bandwidth and zero center frequency. Hence, in order to provide link between the bandpass filter circuit and the model, the lowpass to bandpass frequency transformation is used:

$$\Omega = \alpha \left(\frac{\omega}{\omega_0} - \frac{\omega_0}{\omega} \right), \quad (3.60)$$

where α is defined as the inverse of the fractional relative bandwidth (FBW). It is defined as

$$\alpha = \frac{1}{FBW} = \frac{\omega_0}{\omega_2 - \omega_1}. \quad (3.61)$$

The variable ω is the unnormalized frequency variable and ω_0 the center frequency obtained as the geometric mean of the specified bandwidth with edges at ω_1 and ω_2 .

The frequency transformation, represented in Fig. 3.17, is carried out as an approximation suitable for narrow bands; where the series branch of the lowpass prototype with L_m and X_m is matched with the series resonator (L_a and C_a) of the motional branch in the bandpass BVD model. And the branch of the static capacitance C_0 is also matched with X_0 .

First, in order to analytically express the correspondence of the motional branch given the frequency transformation in (3.60), we get:

$$j\alpha \left(\frac{\omega}{\omega_0} - \frac{\omega_0}{\omega} \right) L_m + jX_m = j\omega L_a + \frac{1}{j\omega C_a}. \quad (3.62)$$

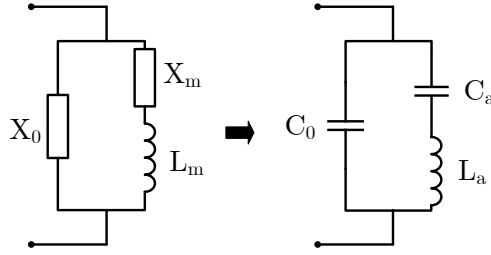


FIGURE 3.17: Frequency transformation applied to the lowpass prototype BVD model to the bandpass BVD model of an acoustic-wave resonator.

To compute the capacitance C_a and the inductance L_a it is necessary a second equation, which is obtained determining the first derivative of (3.62) with respect to ω :

$$j\alpha \left(\frac{1}{\omega_0} - \frac{\omega_0}{\omega^2} \right) L_m = jL_a + \frac{1}{j\omega^2 C_a}. \quad (3.63)$$

Both equations must be accomplished for any ω value around the center frequency ω_0 . Then, they are evaluated at $\omega = \omega_0$, which yields to the following system of equations:

$$X_m = L_a \omega_0 - \frac{1}{C_a \omega_0} \quad (3.64)$$

$$\frac{2\alpha}{\omega_0} L_m = L_a + \frac{1}{C_a \omega_0^2}. \quad (3.65)$$

Now, the determination of the reactances placed at the static branch is provided by considering a narrowband approximation around ω_0 expressed as:

$$jX_0 = \frac{1}{j\omega C_0} \Big|_{\omega=\omega_0}. \quad (3.66)$$

The outcome of solving the (3.64), (3.65) and (3.66) are the values of the bandpass circuit elements L_a , C_a and C_0 as a function of the lowpass prototype elements. Although, the frequency transformation allows mapping the lowpass BVD prototype to the bandpass domain, the denormalization of the unity source and load impedances to any required characteristic impedance value Z_0 (or the inverse Y_0 for admittance) is performed by means of impedance scaling of the elements conveniently.

The relationship between the lowpass and bandpass elements are:

$$L_a = Z_0 \frac{(\alpha L_m + \frac{1}{2} X_m)}{\omega_0}, \quad (3.67)$$

$$C_a = \frac{1}{Z_0 \omega_0} \frac{1}{(\alpha L_m - \frac{1}{2} X_m)}, \quad (3.68)$$

$$C_0 = -\frac{1}{Z_0} \frac{1}{\omega_0 X_0}. \quad (3.69)$$

Indeed, we use quadratic approximation computing the second derivative. The accurate transformations result in BVD model elements which better match with the prototype filtering function.

The relation (3.69) clearly indicates that the unique nature of C_0 implies $X_0 < 0$. In a shunt equivalent extracted pole section, $X_{0-SH} = \frac{-1}{B}$, resulting that B must be positive like we already pointed out previously from the analysis of (3.52). In a series equivalent extracted pole section, $X_{0-SE} = \frac{B}{J_{ML}^2}$ resulting that B must be negative like we stated from the analysis of (3.59).

From the description of the acoustic wave technology we have expose that some resonator characteristics are limited, specially the electromechanical coupling coefficient, by technological parameters of the implementation (materials, wave propagation nature, supporting structure, resonator composition, etc.). The electromechanical coupling coefficient constrains the f_s - f_p distance of an acoustic wave resonator, and its range depends on the material system and the technology.

The r capacitance ratio parameter is defined as the ratio of the motional branch capacitance C_a over static capacitance C_0 . Similarly to the way that the electromechanical coupling coefficient is taken into account in the bandpass domain with the standard definition of r , it is possible to use r in its definition in the lowpass frequency domain:

$$r = \frac{C_0}{C_a} = \frac{1}{2} \frac{X_m}{X_0} - \frac{\alpha L_m}{X_0}. \quad (3.70)$$

Using the equivalence of the X_m , L_m and X_0 parameters with respect the extracted pole section elements, the capacitance ratio presents two different definitions, one for each cases: the shunt circuit (r_{SH}) and the series circuit (r_{SE}).

$$r_{SH} = \frac{B}{J_R^2} \left(\alpha - \frac{b}{2} \right) \quad (3.71)$$

$$r_{SE} = \frac{B}{J_R^2} \left(\frac{b}{2} - \alpha \right) - \frac{1}{2} = -r_{SH} - 1/2 \quad (3.72)$$

By simple observation of expression (3.71) and (3.72), it is observed, first, the dependence of the capacitance ratio with the relative bandwidth, second, the dependence with the zero-pole distance in the lowpass prototype. The higher the relative bandwidth, the lower the capacitance factor or equivalently, the higher the electromechanical coupling coefficient.

The inverse of the factor $\frac{B}{J_R^2}$ directly controls the distance between the pole and zero of the extracted pole sections for series or shunt resonators which completely make sense because its equivalence with distance of the resonance frequencies f_s and f_p in the bandpass domain as r is affected by the fractional bandwidth.

From (3.72), it is observed that the r is not affected by the value of the two admittance inverters J_{ML} . In fact, when the inverters are scaled, following the rules which keep the filter response, the ratio $\frac{B}{J_R^2}$ keeps constant and hence, r does not change.

The relation concept between the lowpass prototype model and the bandpass BVD model assures to satisfy the acoustic filter key design conditions, such as r of the material system technology, making use of the proposed lowpass prototypes. At the same time the BVD passband model constitute a link between the mathematical modeling of an acoustic wave filter and the physical dimensions of its structure.

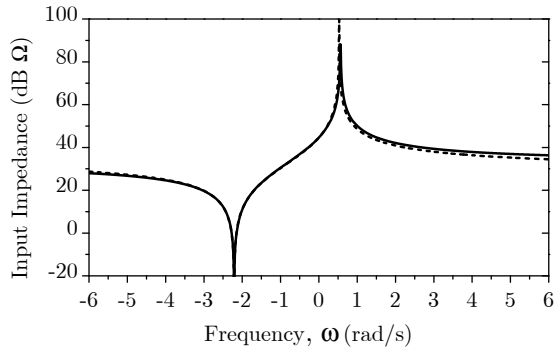


FIGURE 3.18: Input impedance of an acoustic-wave resonator modeled with the bandpass BVD model, when normalizing the frequency, (dashed line) and with the lowpass extracted pole section prototype (solid line).

The equivalence between the lowpass prototype section modeling a resonator and the resonator modeled with BVD lumped circuit is verified with the computation of the input impedance of both circuits. The comparison of the input impedance responses is shown in Fig. 3.18 to validate the equivalence of the models, where we carried out frequency normalization in order to overlap the input impedances.

Consideration of the resonator losses effect for a designed filter

We have dealt with the lossless BVD model of an acoustic-wave resonator when giving its equivalence with the lowpass prototype extracted pole sections. However, the inherent mechanisms of losses in a physical realization of a filter network produce dissipation of energy. The expected transfer function is different than the response with lossless elements.

All the poles and zeros of the transfer function are displaced along the real axis in the complex frequency plane. The displacement is referred as the dissipation factor or loss tangent $\tan \delta$. The effect of the dissipation factor is considered converting the complex frequency variable $s \rightarrow s + \tan \delta$.

For the identification of the losses in the circuit the unloaded quality factor is related with the loss tangent by:

$$Q = \frac{1}{\tan \delta}. \quad (3.73)$$

The unloaded quality factor defines the ratio between the energy stored by the energy dissipated per cycle.

In terms of the lowpass prototype normalized to $\Omega_c = 1$ rad/s, the change of variable to consider the losses on the filtering response is [24]:

$$\Omega \longrightarrow \Omega - \frac{j}{Q_{LP}}. \quad (3.74)$$

In terms of the bandpass practical resonators, the effect of the loss can be considered to the response by replacing the resonant frequency with a complex effective frequency [69]:

$$\omega \longrightarrow \omega \left(1 + \frac{j}{2Q_{BP}} \right). \quad (3.75)$$

The relation between the quality factor in terms of lowpass and bandpass frequencies is [24]:

$$Q_{LP} = Q_{BP} \frac{\Delta\omega}{\omega_0}. \quad (3.76)$$

Therefore, by considering a solution for the lossless case, the change of variable procedure is useful to add the effect of the loss. We simulate the complete filter characteristic of the obtained resonators as well as including the additional reactive components, by cascading the $ABCD$ component matrices. It allows to consider for each particular component any unloaded Q , and even different Q for series and parallel resonance frequencies of the resonators.

For instance, inductors exhibit lower Q , in the range of 20 to 50, while Q of acoustic wave resonators could reach 100 times higher order values. Q values of 2000 for BAW resonators at 2 GHz represents the state-of-art.

3.3.3 Scaling property on the extracted pole sections which models acoustic-wave resonators

The scaling property of inverters described in section 2.6.5 in prototype circuits with NRN is analyzed for each particular case of the two extracted pole sections modeling a series and a shunt resonator.

In a extracted pole section of a shunt resonator like in Fig. 3.9, when scaling by γ^2 the susceptance B of the NRN, the admittance inverter J_R terminating in the NRN must be scaled by γ to keep the filtering function. Therefore, the capacitance ratio r_{SH} is written by

$$r_{SH} = \frac{B\gamma^2}{(J_R\gamma)^2} \left(\alpha - \frac{b}{2} \right) = \frac{B}{J_R^2} \left(\alpha - \frac{b}{2} \right), \quad (3.77)$$

which is the same expression than (3.71).

When applying the scaling property the ratio B/J_R^2 is constant. The effect of the scaling on the parameters X_{0-SH} , L_{m-SH} and X_{m-SH} is like an impedance scaling of factor $1/\gamma^2$.

In a extracted pole section of a series resonator like in Fig. 3.11, when scaling by γ^2 the susceptance B of the NRN, all the inverters terminating at the NRN J_{ML} , $-J_{ML}$ and J_R are scaled by γ .

There is no variation over the parameters X_{0-SE} , L_{m-SE} and X_{m-SE} when applying the scaling, because the scaling factor is canceled due to their relations with B , J_{ML} , $-J_{ML}$ and J_R . Therefore, the capacitance ratio r_{SE} is the same value than before the scaling (3.70).

Summarizing, the capacitance ratio of the acoustic wave resonators in shunt and series positions are never affected by the scaling property when it is carried out in the way explained here.

3.3.4 Two equivalent topologies of a lowpass acoustic-wave resonator: the singlet and the dangling resonator

A part from the lowpass representation of an NRN with dangling resonator shown in Fig. 3.11, a second model is also proposed in order to extend the design possibilities of devices based on acoustic-wave technologies. Such second lowpass representation consists on a variant of the trisection, referred as the singlet in [70].

A trisection scheme is widely used for the design of advanced filters topologies [71] and its structure consists of a three nodes coupled with each other. However, the singlet building block couple one resonator and two NRNs with each other, as it is shown in Fig. 3.19.

The singlet is a canonical network and able to introduce one transmission zero Ω_Z . Although in the extracted pole section the generated transmission zero is directly associated with the resonant node $\Omega_Z = -b$, it is not possible to have a direct interpretation of the transmission zero in the singlet structure.

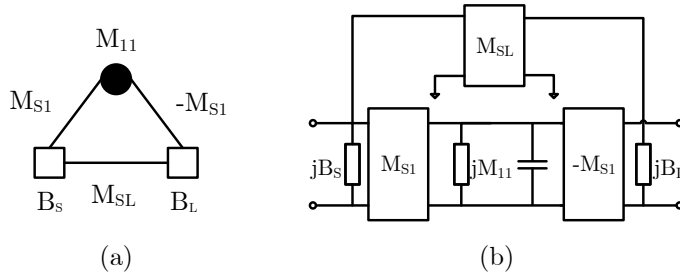


FIGURE 3.19: Singlet lowpass equivalent model of a series acoustic-wave resonator: (a) nodal representation, (b) circuitual schematic.

We are going to show that this scheme is equivalent to the previous extracted pole section of a series resonator, but the singlet could be more convenient for a representation which differentiates between the electrical behavior and the acoustical one.

On one hand, the direct path between the source and the load, comprising the admittance inverter M_{SL} and the input/output shunt NRNs B_S and B_L , is directly linked with the static capacitance C_0 of the bandpass acoustic-wave resonator. As we compute the $ABCD$ matrix of this path like

$$\begin{bmatrix} 1 & 0 \\ jB_S & 1 \end{bmatrix} \begin{bmatrix} 0 & j/M_{SL} \\ jM_{SL} & 0 \end{bmatrix} \begin{bmatrix} 1 & 0 \\ jB_L & 1 \end{bmatrix} = \begin{bmatrix} \frac{-B_L}{M_{SL}} & \frac{j}{M_{SL}} \\ jM_{SL} - \frac{jB_L B_S}{M_{SL}} & \frac{-B_S}{M_{SL}} \end{bmatrix}, \quad (3.78)$$

we can compare the $ABCD$ matrix with a series static capacitance of the bandpass BVD model matrix:

$$\begin{bmatrix} -B_L/M_{SL} & j/M_{SL} \\ jM_{SL} - jB_L B_S/M_{SL} & -B_S/M_{SL} \end{bmatrix} = \begin{bmatrix} 1 & -j/\omega C_0 \\ 0 & 1 \end{bmatrix}. \quad (3.79)$$

The following relations are obtained to satisfy the equivalence at a frequency $\omega = \omega_0$:

$$B_S = B_L = -M_{SL} \quad (3.80)$$

$$C_0 = \frac{-M_{SL}}{\omega_0}. \quad (3.81)$$

The cross-coupling between the source and the load M_{SL} is directly proportional to the static capacitance, and hence is also of the active area of the resonator.

The source-load coupling must be negative to assure a positive capacitance. Even though the singlet is able to generate a TZ in the lower or the upper stopband, for the relation with an acoustic resonator, the capacitive nature of the coupling M_{SL} , avoids this duality. The sign of the coupling is limited and consequently also is the location of the TZ in the upper side band.

On the other hand, the alternative path between the source and the load that includes the resonant node belongs to the motional branch of an acoustic wave resonator. Here, there is a shunt resonator of a unit capacitance with a FIR M_{11} element between two admittance inverters of value $\pm M_{S1}$.

Easily, the network can be converted into a series resonator comparable to the LC resonator of the bandpass BVD model regarding the conventional lowpass to bandpass frequency transformation of (3.60).

The $ABCD$ matrix of the acoustical branch is found by cascading the each element matrices:

$$\begin{bmatrix} 1 & (j\Omega + jM_{11})/M_{S1}^2 \\ 0 & 1 \end{bmatrix}. \quad (3.82)$$

The expression (3.82) has the form of an impedance and it is comparable to the impedance obtained from the series resonator with L_a and C_a on the acoustic branch of the BVD model. The condition is to do both impedances equivalent at the center frequency and also their derivatives, in order to obtain the values of L_a and C_a .

The components of the bandpass BVD model for an acoustic-wave resonator can be expressed in terms of the lowpass singlet model by a variable change of the lowpass frequency to the bandpass and solving for $\omega = \omega_0$ given:

$$L_a = \frac{1}{2} \frac{2\alpha + M_{11}}{M_{S1}^2 \omega_0} \quad (3.83)$$

$$C_a = 2 \frac{M_{S1}^2}{\omega_0 (2\alpha - M_{11})} \quad (3.84)$$

3.3.5 Bandpass prototype filter adapted to feasible acoustic wave technology

The major drawback when implementing a filter is to have the acoustic-wave resonator, BAW or SAW, bounded by the electromechanical coupling coefficient. When realizing the filter synthesis methodology of the extracted pole technique for the fulfillment of desired specifications, the resulting prototype filter after the frequency transformation and impedance conversion can result in a resonator with k_{eff}^2 of any value, which can be or not between the bounds of the viability of the manufacturing process of the specific acoustic technology.

To overcome the k_{eff}^2 limitation and, hence, the bounded capacitance ratio, external inductances and capacitances, either in series or in shunt with the acoustic resonators, are used.

The adaptation of a bandpass prototype network constituted by bandpass sections like in Fig. 3.17 lie in finding a new network composed exclusively

of resonators with r comprised within the feasible technological range, and of external elements when necessary.

A lowpass prototype of extracted pole sections, outcome of the synthesis methodology presented in Chapter 2, is frequency translate into a bandpass prototype circuit. The capacitance ratio r_0 for each section of the bandpass circuit corresponding to a series or shunt resonator, modeled by L_a , C_a and C_0 , is extracted. The capacitance ratios are analyzed to determine if it is necessary the association of any external element or if the resonator can be directly implemented by the acoustic wave technology in consideration.

As the connected element can be a capacitance C_{ext} or an inductor L_{ext} in series or in shunt, there are four possible configurations regarding the need of increasing or reducing the capacitance ratio. The Table 3.2 and Table 3.3 review the passive external element with resonator configurations and the equations for the technology adaptation. When the elements are connected in series is useful to employ the $\Delta - Y$ transformation for the network of the BVD model which is summarized in Fig. 3.20.

The capacitance ratio of the extracted resonator r_0 must be adapted to range between a minimum capacitance ratio r_{min} and a maximum value r_{max} defined by the technology considered. The feasible acoustic wave resonator adapted to the technology is modeled by the BVD circuit of parameters L'_a , C'_a and C'_0 (or L'_{sh} , C'_{sh} and C'_{se}) and its resonance frequencies are f'_s and f'_p which can differ from the f_s and f_p of the extracted bandpass

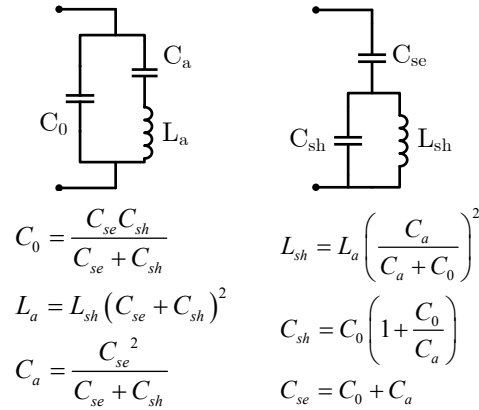


FIGURE 3.20: Δ -Y network transformation applied to the bandpass BVD model of a resonator.

resonator.

In the case that the condition of an r_0 greater than the r_{max} , the solution to adapt the resonator to the technology is to associate a series or shunt capacitance C_{ext} . Table 3.2 gives the equation which relates the value of the external capacitance with the extracted resonator and the feasible capacitance ratio r_{max} .

The table also shows that the resonance frequencies are modified in the implemented acoustic resonator regarding the extracted bandpass resonator. In the configuration of a resonator in series with C_{ext} , a high capacitance value is often required.

In the case that the condition of an r_0 lower than the r_{min} , the solution to adapt the resonator to the technology is to associate a series or shunt inductance L_{ext} . Table 3.3 gives the relationship for the value of L_{ext} with the extracted resonator and the feasible capacitance ratio r_{min} . The variation of the resonance frequencies in the implemented acoustic resonator according to the extracted bandpass resonator is also summarized. In both configurations of Table 3.3 the tunable range is high, large variations on f'_p or f'_s can be achieved within a small range of inductance values.

TABLE 3.2: Adaptation of an extracted bandpass resonator with $r_0 > r_{max}$ the technological feasible value for acoustic wave resonators by means of an external element.

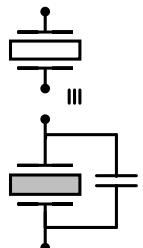
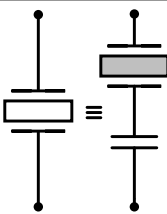
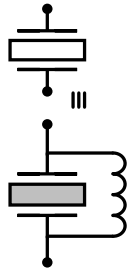
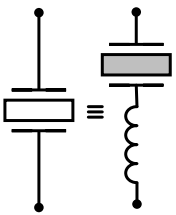
Configuration	Adapted parameter	Resonance frequencies
	$L'_a = L_a$ $C'_a = C_a$ $C'_0 = r_{max}C_a$ $C_{ext} = C_0 - r_{max}C_a$	$f'_s = f_s$ $f'_p > f_p$
	$L'_{sh} = L_{sh}$ $C'_{sh} = C_{sh}$ $C'_{se} = C_{sh}/r_{max}$ $C_{ext} = \frac{C_{sh}C_{se}}{C_{sh} - C_{se}r_{max}}$	$f'_s < f_s$ $f'_p = f_p$

TABLE 3.3: Adaptation of an extracted bandpass resonator with $r_0 < r_{min}$ the technological feasible value for acoustic wave resonators by means of an external element.

Configuration	Adapted parameter	Resonance frequencies
	$L'_a = L_a$ $C'_a = C_a$ $C'_0 = \frac{r_{min} C_a}{1 - C_0}$ $L_{ext} = \frac{1}{\omega^2 (r_{min} C_a - C_0)}$	$f'_s = f_s$ $f'_p < f_p$
	$L'_{sh} = L_{sh}$ $C'_{sh} = C_{sh}$ $C'_{se} = \frac{C_{sh}}{r_{min} - C_{sh}}$ $L_{ext} = \frac{1}{\omega^2} \frac{C_{se} r_{min} - C_{sh}}{C_{sh} C_{se}}$	$f'_s > f_s$ $f'_p = f_p$

3.4 Ladder-type filters based on acoustic-wave resonators

This section discuss about the classical ladder-type filter based on acoustic-wave resonators of SAW or BAW technology electrically coupled. The key feature of ladder filters are the close to passband-edge transmission zeros which produce a slope steepness important to fulfill selectivity requirements.

The conventional topology describing a ladder filter based on acoustic-wave resonators is shown in Fig. 3.21(a). Ladder filters are organized alternatively connecting series resonators with shunt resonators. The notation *SE* and *SH* is used to refer to the position in the filter network. The basic cell to form a ladder filter is a series resonator cascaded by a shunt resonator. Several cells are connected to provide a filter of greater order N , where N denominates the total number of resonators arranged in the filter.

The performance principle to achieve the passband is leveraged on a slightly lower frequency tuning of the shunt elements. In a conventional filter, the

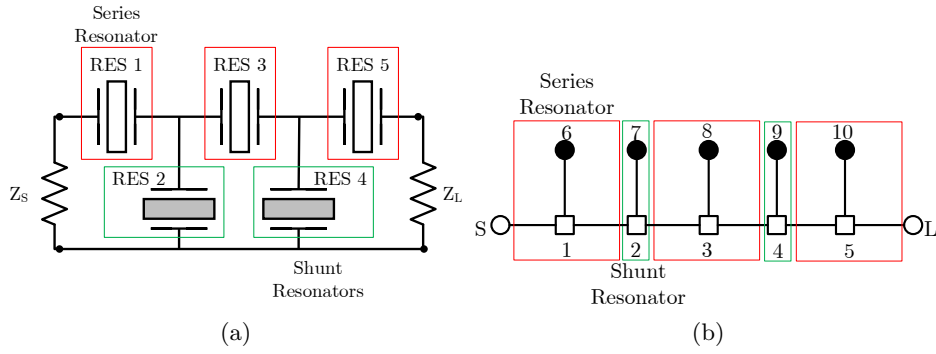


FIGURE 3.21: (a) General configuration for a ladder-type filter, (b) equivalent prototype.

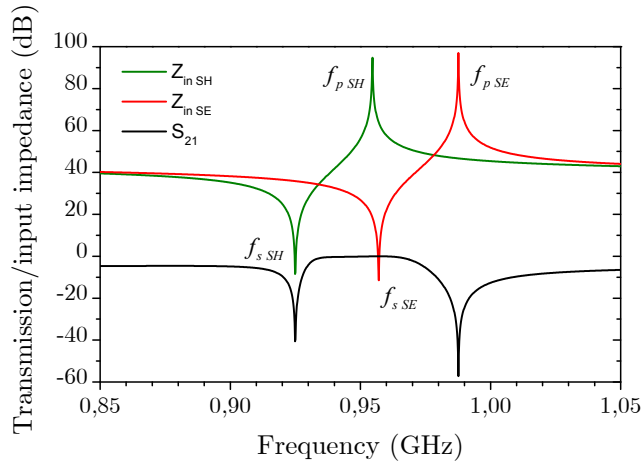


FIGURE 3.22: Performance principle of one basic ladder-cell, $N = 2$.

series resonators resonate at the frequencies f_{s-SE} and f_{p-SE} , and the shunt at f_{s-SH} and f_{p-SH} .

The frequency response of a filter jointly with the input electrical impedances of a series and shunt resonator are displayed in Fig. 3.22. There are four resonance frequencies arranged from lower to higher as f_{s-SH} , f_{p-SH} , f_{s-SE} and f_{p-SE} .

At the frequency f_{s-SH} , the input impedance of shunt resonators get the minimum value, defining a transmission zero at the lower side of the filter passband. Increasing the frequency to f_{p-SH} , the input impedance of shunt resonators is at the maximum value which means that the signal

transmission is maximum and the attenuation very low. At the frequency f_{s-SE} , there is also maximum signal transmission because the series resonator impedances are very low. The frequencies f_{p-SH} and f_{s-SE} are approximately placed at the center of the band to generate the filter passband. The frequency f_{p-SE} defines the transmission zero at the upper side of the passband because the impedance of series resonators are at the maximum value. Thus, the common ladder filter topology leads to high selectivity responses owing to the close location of f_p and f_s of acoustic-wave resonators.

For frequencies below f_{s-SH} and above f_{p-SE} , both set of resonators have capacitive behavior. As a consequence, the out-of-band rejection of the filter is defined by the power division of the static capacitances of series and shunt resonators.

The weakness of ladder responses is the poor rejection far from the band. They suffer from the out-of-band flyback of the transmission response which is a problem in applications that requires attenuation of certain bands above and below the passband. Even though the out-of-band rejection can be increased with a higher number of resonators, the insertion loss also increases.

The maximum achievable filter bandwidth is limited by the electromechanical coupling coefficient k_{eff}^2 or the capacitance ratio r of resonators because they are parameters linked with the distance of the resonance frequencies. For high performance filter applications, the filter response can be modified by means of external reactances. Using inductor or capacitors connected in series or shunt to resonators modifies the distance between series and parallel resonance frequencies, as we discussed in section 3.3.5.

The problem of the approach is that the number of external elements and their values are limited by the requirements of overall filter size and the number of interconnections for the external elements into the filter circuit. Moreover, the filter transfer function is sensitive to the low quality factors of inductors too.

From the performance description for a ladder, we have seen that each transmission zero generated on the transmission response is independently controlled by one resonator. That feature gives the modularity property to the ladder structures. Indeed, ladder-type filters describe a fully canonical response as the number of transmission zeros at finite frequencies equal the degree of the filter (N). Ladder networks create fully canonical filters without need of direct coupling between source and load, although it exists

though a reactive path.

These pair of advantageous characteristics have been also highlighted in the well-established inline extracted pole filters with NRNs which make the link with the acoustic wave technology.

Consequently, it can be proof that an inline topology composed of NRNs with dangling resonators is an equivalent lowpass representation of a filter based on acoustic resonators with ladder topology. One should note that the synthesis technique for inline extracted pole filters with NRNs and dangling resonators applied to obtain a determined frequency response can be exploited to design acoustic wave filters with ladder topology.

3.4.1 Methodological design procedure for ladder-type filters based on acoustic wave resonators

The aim of the design in an acoustic wave filter is to fulfill a given set of frequency response specifications. The direct design method for ladder filters is leveraged on the analytical synthesis of inline extracted pole filters with NRN describing Chebyshev functions.

First step in the design is to set up the position of the transmission zeros and the inband return loss level defining a generalized N -degree Chebyshev filtering function for a given spectrum mask. The condition for the inline lowpass prototype network is to accommodate an N fully canonical response by means of the appropriate element arrangement. Since the filter is made up of a concatenation of dangling resonators between inverters, the extraction technique is recursive.

Notice that the extraction order of the transmission zeros does not affect the transmission response, but will affect to the lowpass elements and, hence, to the bandpass electrical elements. Therefore, for the implementation of a ladder-type filter, the transmission zeros at normalized frequencies must be suitably arranged, that is alternating between positive and negative values. This consideration is essential to accommodate the acoustic technological requirements during the design.

The shunt resonator behavior is modeled by the extracted pole section of an NRN and a dangling resonator which generates a transmission zero at a normalized frequency lower than -1. An NRN with dangling resonator between two opposite value admittance inverters, generating a transmission zero at a frequency higher than 1, models the series resonator behavior.

Fig. 3.21 reflects the relationships between the inline extracted pole prototype of N sections with the bandpass series and shunt acoustic wave resonators of a ladder filter.

Once all the dangling resonators are extracted, the second step is to carry out suitable associations of the lowpass prototype cells with the bandpass BVD model by means of the lowpass to bandpass transformation with equivalence at the bandpass center frequency and the impedance denormalization.

Finally, with the BVD elements of each resonator, the primary elements f_s , r and C_0 are obtained for all the resonators building up the ladder filter and can be analyzed in order to accommodate the technological constraints.

Indeed, once we have made the systematic design of the filter which fulfills a frequency pattern, we are able to analyze many aspects related with the design and evaluate them, such as the number of external elements required, the uniformity among the f_s of resonators, the group delay, the power density, reliability issues, etc.

To validate and show the advantages of the synthesis methodology for acoustic-wave resonators we design a filter for application in the Tx band 3 with passband 1.71-1.785 GHz. The acoustic-wave technology considered allows capacitance ratio values included between $r_{min} = 14$ and $r_{max} = 15$. For a filter of degree $N = 5$ and two transmission zeros placed at the lower rejection band $f_{z2,4} = 1.683$ GHz and three placed at the upper band $f_{z1,5} = 1.804$ GHz, $f_{z3} = 1.808$ GHz, the return loss level is specified at 13 dB. The filter is designed to have the first element a series resonator, as we can observe from the frequency of transmission zero f_{z1} placed at the upper transition band.

The relation of the transmission zeros with the normalized frequencies $\Omega_1 = 1.54$, $\Omega_2 = -1.82$, $\Omega_3 = 1.65$, $\Omega_4 = -1.82$ and $\Omega_5 = 1.54$ in rad/s, is obtained through (3.60). From the mathematical synthesis the characteristic polynomials are extracted given an expression for the input admittance of a prototype like the one depicted in Fig. 3.21(b).

Subsequently, the extraction steps over the lowpass prototype results in the definition of the following circuit elements: $M_{S,1} = M_{1,2} = M_{2,3} = M_{3,4} = M_{4,5} = M_{5,L} = 1$, $M_{1,1} = M_{5,5} = -1.189$, $M_{2,2} = M_{4,4} = 2.062$, $M_{3,3} = -2.690$, $M_{1,6} = M_{5,10} = 1.367$, $M_{2,7} = M_{4,9} = 1.849$, $M_{3,8} = 2.090$, $M_{6,6} = M_{10,10} = -1.54$, $M_{7,7} = M_{9,9} = 1.82$ and $M_{8,8} = -1.65$.

TABLE 3.4: Resonator parameters extracted from the synthesized ladder for Tx Band 3 application.

BVD Elements	RES 1&5	RES 2&4	RES 3
L_a (nH)	80.34	36.45	175.7
C_a (pF)	0.103	0.245	0.047
C_0 (pF)	1.53	3.48	0.68
r	14.79	14.20	14.37
f_s (GHz)	1.746	1.683	1.748

The numeration of the nodes used for the elements in the lowpass prototype and the numeration of the resonators in the acoustic-wave filter is according to Fig. 3.21. We observe the sign correspondence of the prototype elements, according to the definition of the extracted pole section like series or shunt.

The next step in the process is determining the bandpass BVD network from the extracted lowpass elements. The solution for the transformed elements is shown in Table 3.4. The lumped element values of BVD model are directly related with the primary parameters of acoustic wave resonator, and they are also in the table.

The resulting design fulfill the condition of technological implementation, because the whole set of values are within the feasible values $[r_{min}, r_{max}]$ allowed by the technological process. Resonators 2 and 4, which are shunt, present the higher static capacitance. That fact implies larger areas for shunt resonators than for series, however they will better handle the power with lower reactive power densities (W/pF). Resonators with low static capacitances in designs for power durability require cascading of some resonators.

The bar graph Fig. 3.23 presents the computed power density for the designed filter at the higher passband edge frequency (1.785 GHz), where the relations of the stored reactive power and static capacitances of each resonator are observed. It is observed that the middle series resonator 3 with the lower capacitance has the higher density.

Thanks to the use of the fast systematic approach to obtain one filter design fulfilling the spectrum mask, we can analyze a big variety of aspects apart from the r , f_s , area or stored reactive power of the resonators.

Fig. 3.24 shows the simulation of the response for the synthesized bandpass

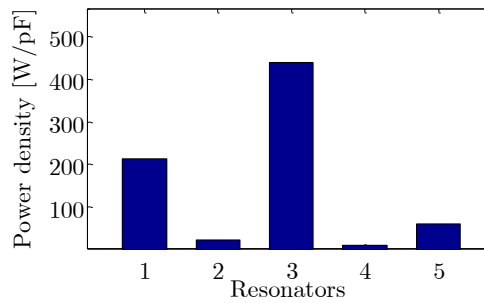


FIGURE 3.23: Computed power density of each resonator in the ladder filter for Tx B3 application at 1.785 GHz frequency.

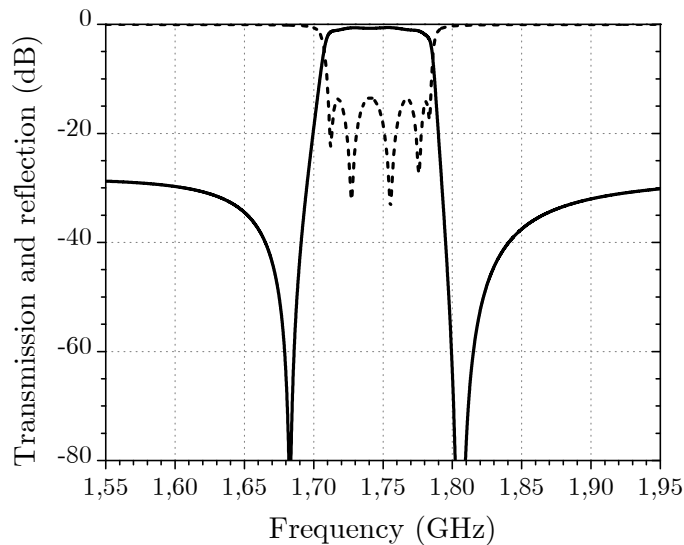


FIGURE 3.24: Simulated frequency response of an 5th-degree ladder filter for Tx B3 application.

filter with the elements of Table 3.4, where a lossless simulation has been considered. The narrowband transmission and reflection characteristics are obtained. This $N = 5$ configuration provides the steepness in the transition bands and a maximum attenuation out-of-band of 30 dB which depends on the static capacitances.

The inband performance is displayed in Fig. 3.25. The equiripple is observed for the reflection response, which defines a relative bandwidth of 4.3 % at 13 dB level. Consequently, the planar passband transmission features the filter. It is observed that the upper passband edge degrades more the

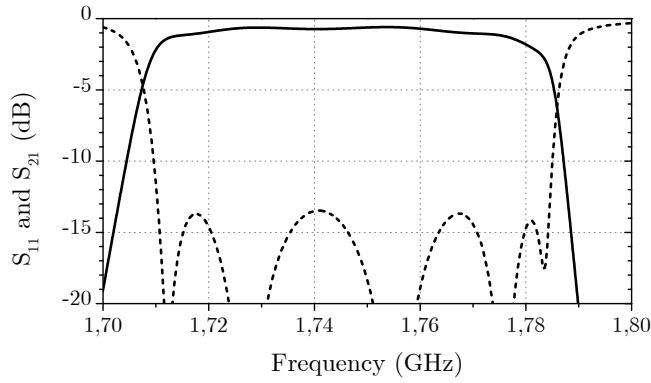


FIGURE 3.25: Passband simulation Insertion Loss and Return Loss of designed 5th-degree ladder filter.

insertion loss. The maximum ripple is of 3.1 dB and the maximum IL is of 3.7 dB.

If we consider the same design just with a modification on the $RL = 12$ dB, the capacitance ratio of the resonators are then $r_{R1\&R5} = 15.37$, $r_{R2\&R4} = 14.03$ and $r_{R3} = 14.37$. Their values have changed, although the resonators $R2$, $R3$ and $R4$ can be implemented as their r is within the technological range. However, the association of a external shunt capacitance to resonators $R1$ and $R5$ is required to reduce their r equal to $r_{max} = 15$ for the considered technology. The value of the external capacitance is equal to 33 pF, meanwhile the implemented acoustic resonators $R1$ and $R5$ are set to $r'_{R1\&R5} = 15$ and $C'_0 = 1.36$ pF.

3.4.2 Technological interactions of acoustic wave filters

The synthesis methodology applied over the last filter example does not constrain the acoustic-wave resonators considering the technology (capacitance ratio limitations). It is after we have finished the synthesis that we are able to analyze the obtained resonators and verify the condition for technological implementation.

However, we have seen that for a defined array of transmission zeros, just a variation on the return loss level defined for the Chebyshev filtering function makes the resonators feasible to be implemented with the technology avoiding external elements or not.

On top of that, the design of a filter for a desired application starts with

the definition of the passband and the spectrum mask with attenuation and reflection levels for the response. Therefore, there exists multiple possible filtering functions as suitable solutions for the filter application set of specifications.

Nevertheless, it is very important to take into account the tradeoff which exists between the return loss in the passband and the transmission attenuation in the stopband [24]. For one order filter specified, there is a relation dB for dB between the corresponding maximum ripple in the passband and the corresponding minimum attenuation in the stopband, so that, if one increases the other decreases.

Once the filter degree is predefined, each filtering function solution consist of an array of TZs and the RL level. Despite all solutions fulfilling the spectrum mask, only some of them accommodate the capacitance ratio restriction in order to avoid or minimize the number of lumped elements.

A good practice for the manufacturing of acoustic-wave filters, is to hold a certain uniformity through the r or k_{eff}^2 parameter of the resonator set, because these parameters directly depends on the technology. Instead of defining a capacitance ratio range of values for feasible implementation, only one value is considered for the technological constraint of resonators.

In addition, sometimes acoustic wave technologies impose constraints about the number of different resonance frequency, for example, allowing one f_s for all shunt resonators and two different f_s among the set of series resonators. The resonant frequency uniformity constraint is more often required in BAW resonators as the parameter is directly linked with the thickness dimension.

There is a dependency of the r value of each resonator over the specified inband RL level and the array of transmission zeros. Moreover, there is also dependency of the resonators f_s value over the RL and array of TZs.

As we employ a direct design technique much faster than the optimization of the frequency pattern, we are able to analyze those dependencies over a large set of feasible solutions for a filtering application.

A good example to represent this interesting property is to sweep the RL level of a 7th-degree ladder-type filter where the array of transmission zeros is $\Omega_z = [1.40, -1.79, 1.60, -1.62, 1.60, -1.79, 1.40]$ rad/s, following this arrangement for the extraction. Since the transmission zeros normalized frequencies are symmetrical, the resulting ladder network and capacitance ratio of acoustic resonators are too. The design has considered a filter

application with frequency passband [1.164 – 1.214] GHz.

In Fig. 3.26 there are represented the values of the capacitance ratios and the values of the series resonance frequencies for different values of return loss. Note that the graphs of the capacitance ratio or the series resonance frequency over the return loss are controlled by each set of filter degree and transmission zero array.

The graph Fig. 3.26(a) shows that there is a capacitance ratio change over the RL for all the resonators. The capacitance ratio of resonators *Res1* and *Res7* has a marked decline, consequently, the spread of r values is large. The result consequently means that the most external resonators have a stronger effect on the return loss.

Contrarily, the r of resonators *Res3*, *Res4* and *Res5* present non-appreciable variations over the RL which means that their values are more dependent on the array of transmission zeros. For positions of resonators more internal, such as *Res3*, *Res4* and *Res5*, the return loss do not experiment appreciable effects caused by their capacitance ratios.

A similar analysis on the graph Fig. 3.26(b) shows that the series resonance frequencies of all resonators stay steady over the RL, except for *Res1* and *Res7* whose f_s 's decrease exponentially. This result is partially expected as the f_s of shunt resonators corresponds to their transmission zero frequency which has been maintained for the RL sweep. Then, the resulting graph is more dependent on the filter specifications.

Some interesting findings from the obtained data are listed and indicated into the graph:

1. The r 's trends show that there is a region of return loss approximately equal to 15 dB with uniformity through the r parameter of value 15. If we consider technological resonator implementations of $k_{eff}^2 = 7.6$ % which equates to an $r \approx 15$, the synthesized filter would not require external elements since the resonators capacitance ratios satisfy the material system constraints.
2. The study highlights that when we make use of the optimization technique for a frequency pattern of specifications, where the RL is fixed, it can disable the possibility of reaching uniformity on the r of resonators.
3. Enabling one resonator of having an r different from the others generates an improvement of the filter response with higher RL.

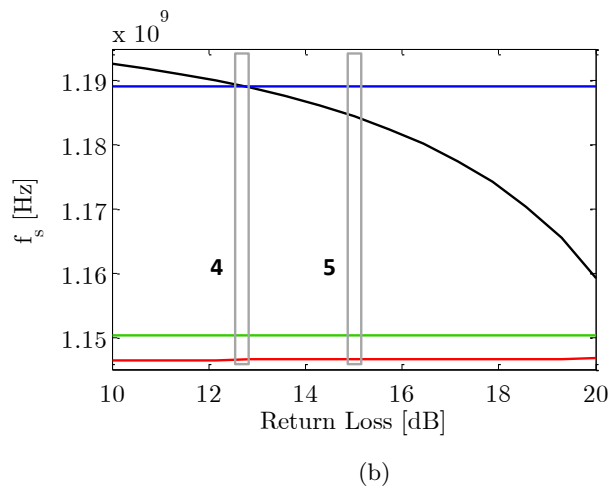
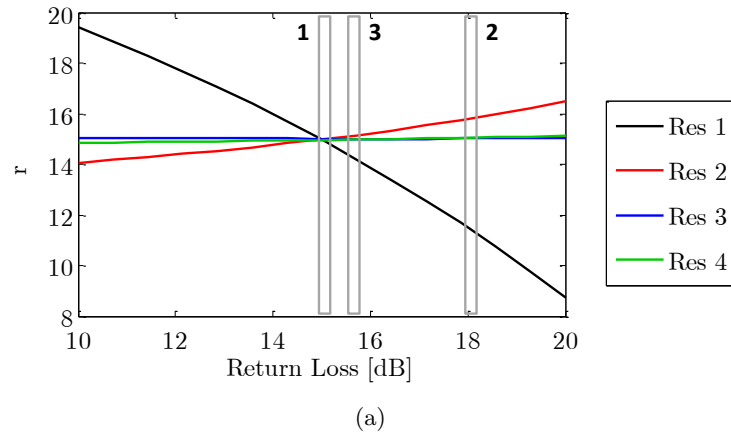


FIGURE 3.26: For different return loss on a 7th-degree ladder filter with predefined transmission zeros, computed (a) the capacitance ratio r of each resonator and (b) the series resonance frequency f_s . For the symmetric ladder network, results are equivalent for Res 1 with Res 7, Res 2 with Res 6 and Res 3 with Res 5.

4. Among the series resonators $Res1$, $Res3$, $Res5$ and $Res7$ is possible to find uniformity on f_s around a value of 13 dB of RL. However, uniformity among the shunt resonators can not be reached without a change on the transmission zero array.

5. The optimum RL level for uniformity in r must not be equal to the

optimum RL level where a lower number of different f_s are required. For this particular example of Fig. 3.26 with predefined transmission zeros, it will be impossible to have both a uniform coupling constant and only three different resonant frequencies.

It should be noted that these studies of the filter and resonators properties and parameters address with optimization will suppose a big time of simulation. However our systematic method can obtain the result quickly because the filter we deal with is already fulfilling the mask. For instance, we have considered now the repercussion of changing the array of transmission zeros.

For the study we use a 7th-degree ladder-type filter with predefined transmission zeros except for the normalized frequencies of *Res2* and *Res6*, $\Omega_{z2} = \Omega_{z6}$, whose values are sweep. In the transmission zero dependence studied example, the capacitance ratios and the series resonance frequencies are obtained for a sweep over the transmission zero frequency range from -2.6 to -1.4 rad/s of the resonators *Res2* and *Res6*.

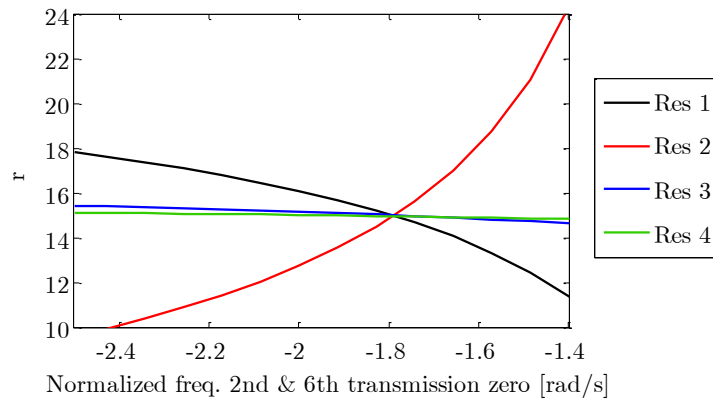
We have assumed transmission zeros normalized frequencies symmetry, hence the sweep range and results are equivalent for both resonators *Res2* and *Res6* simultaneously. The rest of values of the array of transmission zeros is assumed the same than in the study of the RL sweep. The same application with frequency passband $[1.164 - 1.214]$ GHz is considered in the study. The return loss level is now set to 15 dB.

In Fig. 3.27, there are represented the the values of the capacitance ratios and the values of the series resonance frequencies.

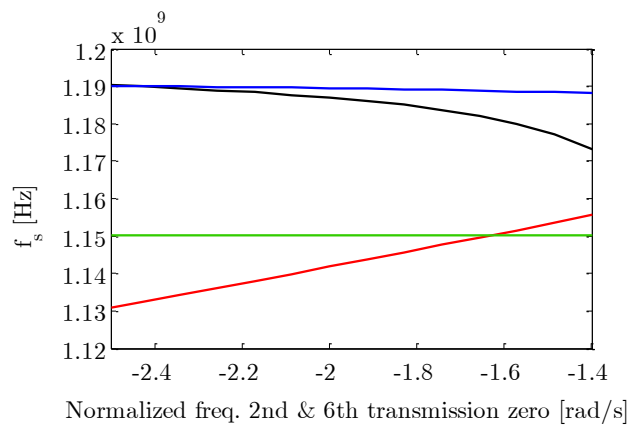
The graph Fig. 3.27(a) shows that the capacitance ratio of all the resonators change when does the location of the transmission zero corresponding to resonators *Res2* and *Res6*. Even if, variations over the transmission zero array help to get uniformity among the r 's and fulfill the technological constraints, we will have to consider the spectrum mask requirements of the filter.

The capacitance ratio of resonators *Res2* and *Res6* grows rapidly as the TZ is closer to the passband edge, as expected, because the two resonance frequencies become closer. The capacitance ratio trend for resonators *Res1* and *Res7* is opposite, the r parameter falls gradually as the variables $\Omega_{z2} = \Omega_{z6}$ approach to -1 rad/s. The r of resonators *Res3*, *Res4* and *Res5* change very slowly, remaining almost stable over the sweep of the TZ.

We can observe how the variation of the location of the transmission zero



(a)



(b)

FIGURE 3.27: Capacitance ratio of each resonator (a) and series resonance values (b) for each resonator of the filter when all the transmission zeros are predefined except the one corresponding to 2nd and 6th resonator. Computed over the normalized frequency of the TZ.

generates an optimum point regarding the technological requirements, which in this example occurs for $\Omega_{z2} = \Omega_{z6} = -1.79$ rad/s.

Consequently, modifications along the complete array of TZs provide further possibilities to reach the optimum value of r according to the technological constraints to implement a resonator.

The evaluation of the results on the graph Fig. 3.27(b) indicate that the variation of the transmission zero over resonators *Res2* and *Res6* modifies the series resonance frequency of resonators *Res1* and *Res7*. The f_s reduction on *Res1* and *Res7* becomes more considerable when the location of the swept TZs approaches to the passband edge, and this trend on resonators *Res1* and *Res7* obeys to the trend observed at the r parameter of same resonators, because their corresponding TZs are maintained while the r parameter falls.

As logically expected for shunt resonators, the f_s of *Res2* and *Res6* steady proportional increase when approaching $\Omega_{z2} = \Omega_{z6}$ to the passband edge (-1 rad/s), and the f_s of *Res4* stay constant as the corresponding Ω_{z4} is not modified. Also, the f_s of series resonators *Res3* and *Res5* remain constant.

Two special different points characterize this plot. The first one is at the normalized frequencies $\Omega_{z2} = \Omega_{z6} = -2.4$ rad/s, where the series resonators *Res1*, *Res3*, *Res5* and *Res7* have only one f_s value. The second optimum point is at $\Omega_{z2} = \Omega_{z6} = -1.6$ rad/s, where the shunt resonator *Res2*, *Res4* and *Res6* have uniform f_s .

Consequently, it is concluded that for the studied example a minimum of only three different resonant frequencies will be possible, because uniformity of f_s among series and shunt resonators does not occur at the same TZ frequency value.

Moreover, the two points of f_s uniformity do not agree with the point of feasible technological r implementation for all the resonators which is around a normalized frequency of -1.79 rad/s.

Summarizing, the most interesting results shown in Fig. 3.26 and Fig. 3.27 is that there are different ways to find out the most adequate transmission zeros set and return loss. For a predefined array of TZs, a sweep of the RL shows at which value most of the resonator r 's are close to a desired r value or other technological constraints regarding f_s . On the other hand, if the return loss is a predefined parameter, a sweep for the transmission zeros is needed to find technological requirements. In most of the cases, there is a trade off between the uniformity of the capacitance ratio and the number of different series resonance frequencies. Without using these kind of analysis for the synthesis of a filter, we can assign arbitrary RL and set of TZs which lead to employ lumped elements since the resonators r 's differ from the feasible value demanded for the implementation of acoustic-wave resonator.

The information that we can manage on the systematic design are the return loss, the set of finite transmission zeros and the sorting of such TZs. The design task lies to find out the suitable combination of this information which results on a filter that meets the technological requirements and fulfills the filter response specifications (rejection, minimum insertion loss and bandwidth). By technological constraints it could be considered, depending on the case, the value of the resonators r parameter, a minimum number of external elements, a minimum number of different f_s , failure mode, reliability, or even, specific minimum or maximum values of static capacitances (C_0) as the parameter is related with the active area of the acoustic-wave resonators, or for controlling the maximum levels of stored energy in the resonators. All of this without worry of the filtering response, because it is completely controlled.

The conclusion is that it is not obvious and challenging to design a BAW/SAW ladder filter given the specifications because acoustic-wave resonators impose stringent technological constraints to be considered on the design process. In general, the r of a set of resonators is a fixed parameter because all of them are on the same wafer process. The r is strictly bounded by the technological process and depends on the choice of the piezoelectric material as well as resonator configuration.

Giving that acoustic-wave filters are a very restrictive technology, the deep understanding of the particular interactions between the technological parameters (r , f_s or C_0) and the device performance (N , RL and Ω_z) drive us to tackle a systematic, efficient and precise procedure in order to design ladder filters.

3.4.3 Automatic search engine to design ladder-type filters based on acoustic-wave technologies

The synthesis of microwave filters based on acoustic-wave resonators starts with the filtering function definition which attains the electrical specifications. Since we have manufacturing constraints, it implies the set of realizable filtering functions is delimited. The class of realizable filtering functions is constrained by the close zero-pole resonant frequencies. Additionally, more often in BAW technology, the filter characteristics flexibility is also limited when fixing the same resonance frequencies for each type of resonators series or shunt. Therefore, the degrees of freedom for synthesizing a filter are restricted by both the intrinsic behavior of acoustic

wave resonators and parameters of an appropriate manufacturing technology.

In spite of the technological constraints, we can still perform a direct synthesis from the filtering function. The appropriate technological characteristics of each resonator are considered in the synthesis because they can be derived straightforward from the nodal approach of resonating and non-resonating nodes. Using this information is possible to design a filter, for example, without external elements, since the design procedure accommodate the technological parameters for the implementation of acoustic wave resonators.

We have built up a systematic synthesis method which extracts the elements of the NRN prototype and link them with the equivalent electrical model of an acoustic wave filter completely consistent with a suchlike scenario; it takes into account the technological constraints presented by acoustic wave resonators, either BAW or SAW. Indeed, we can provide design results which show uniformity among the k_{eff}^2 of the resonators.

The challenging task is tackled leveraging on a systematic synthesis methodology. That is the reason that we take as core module the design technique described in section 3.4.1. We upgrade it to provide a filter solution that combines a complete spectrum mask fulfillment with topologies ready to accommodate acoustic-wave technological constraints automatically.

It consists on a combination of the filter synthesis routine with an automatic search engine that finds automatically the right/best input parameters satisfying the electrical specifications and technological feasibility for a given optimization criteria, such as RL or static capacitances.

Fig. 3.28 presents an overview of the systematic technological design procedure implemented. For an specific application, we define the range of frequencies at which an specific insertion loss level is desired in the pass-band, and similarly, we define frequency ranges for different attenuation levels in the stopband. The whole set constitutes the spectrum mask requirement for the filter response we will design.

The available technological manufacturing process will impose the resonators capacitance ratios to implement that we define as the material system. It must be remained that a wide variety of technological characteristics would be indicated as constraints, not only the capacitance ratios. This will depend on the preferences of the design.

The designer selects a filter order and the arrangement of the resonators

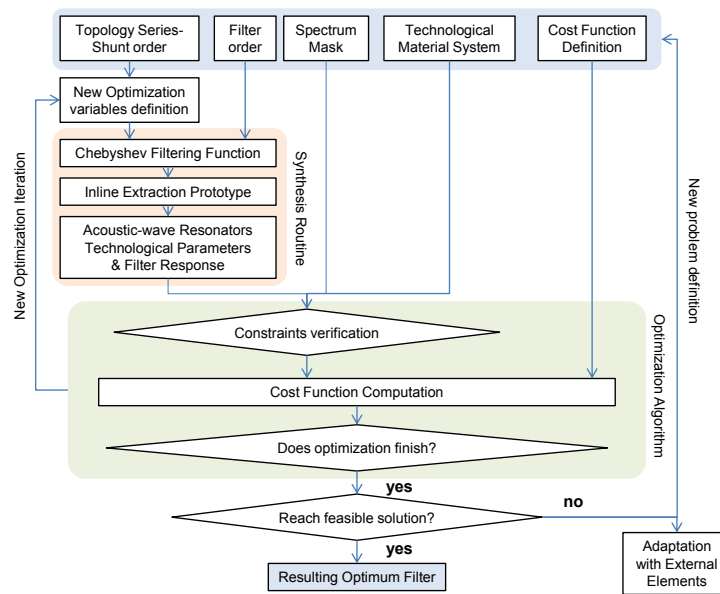


FIGURE 3.28: Design procedure overview.

in series of shunt position. The optimization variables are the return loss and the array of transmission zeros defined at normalized frequencies. An initial set up of optimization variables is necessary for the first iteration, and jointly with the filter degree, results in a expression of the Chebyshev filtering function defined by the characteristics polynomials.

Subsequently, the S-parameters and the input admittance are obtained. The input admittance expression is employed for the synthesis routine, where we first extract the elements of the lowpass prototype filter and secondly we obtain the acoustic wave filter by applying the network denormalization.

The acoustic wave filter outcome of the synthesis routine could have resonators whose technological parameters satisfy the material system or not and could also present a response which attains the predefined spectrum mask or not. Then, after the synthesis routine we make the verifications of these constraints.

Moreover, there is a definition of a cost function to minimize (maximize) an objective variable. There are different options to define the objective variable according if the principal objective is maximize the return loss level, minimize the static capacitance of the resonators or just verify the feasibility

of the constrained problem, among many other possibilities. Therefore, the optimization problem looks for an optimized input variable set which minimizes the defined cost function and accomplishes the spectrum mask and the material system simultaneously.

When the constraints of specifications or technological implementation are not fulfilled, a new iteration on the optimization algorithm is produced. For each optimization a new set of RL value and array of transmission zeros is set up for the input of the synthesis routine. When the constraints are satisfied but the cost function is not a the minimum value, a new iteration is also produced in the optimization.

There are two reasons why the optimization can finish. One option is because the set up parameters have generated a filter solution which has the minimum value of the evaluated cost function and the resonators of the filter accommodate the technological material system. In that case, the filter solution results in an optimum filter for the application taking into account the specifications and the technology. The other option is because the optimization algorithm has reached the maximum number of iterations without generating a feasible solution.

When the optimization procedure does not reach a feasible solution the designer can choose between different options in order to reach the requirements of the filter. If the resonators are derived from the material system, the capacitance ratio of resonators can be adapted with external reactive elements, where the nature and the value are controlled.

However, there could be constraints about the total number of external elements, their values, and the arrangement with in series or shunt with resonators because they can change the frequency of the transmission zeros of the filter response. If a solution is not possible with external elements for the adaptation to the required manufacturing technology, then we need to start a new problem which means, for example, relaxing some of the specifications for the filter response, defining a new filter order or filter topology, modifying the objective variable to minimize, or change the requirements of the technology.

This explanation of the systematic design procedure given is a general description to introduce the main performance of the technique developed. Nevertheless, the method has been packed into a software tool that gives an integrated solution, where more complex functions have been integrated in order to consider more cases or to give to the platform more interoperability. We avoid to give here the full description of the software functions

and variables. Further available options or functions will be described along the document at the specific section or with examples.

The automatic search of the parameters for a realizable filter is made at the first step, previous to the definition of the characteristic polynomials. The total number of parameters for the procedure is limited to the return loss and the array of transmission zeros which enforce in some cases to not accomplish the technological constraints but we have the alternative of using external elements.

The systematic design technique has been developed as a software tool to face the design of filters in acoustic wave technology. The program has been created in MATLAB® language and we have used the optimization toolbox to solve the minimization problem with nonlinear constraints. Challenges of efficiency and simulation time reduction are overcome by the synthesis methodology of the software tool.

The software framework allows the study of multiple topologies which is the first approximation design step along the whole manufacturing process of a filter. The topology selection task is reliable and fast, because the software obtain the best parameter values satisfying design specifications in an average simulation time lower than 30 seconds using a 3.1 GHz CPU. Additionally, more complex and accurate simulations, that for example considers the electromechanical behavior and the performance in package, have a prohibitive computational cost and time which make them unfeasible for the agile study of a wide range of topologies or filter properties.

An example to validate the design methodology is developed next. The methodology enables the control of the structure and balances the performance with the technological constraints or the requirements of external elements. Two stand-alone filters for 3G WCDMA Band 1 (Tx and Rx) need to satisfy the technological requirements of a material system with $r = 18$ ($k_{eff}^2 = 6.4\%$) and the specifications shown in Table 3.5.

In the software program the specifications of the Tx filter are introduced to be considered on the design outcome, and also a 7th-degree filter with a first element a series resonator is set up. The software program has the option to select symmetric filter regarding the arrangement of the transmission zeros array in odd degree filters. In this example we disable the symmetry option. Next, we designate the technological constraints in the software framework to have an $r = 18$ along the seven filter resonators. Finally, the program requires the definition of a cost function to minimize (maximize). As we have mentioned there are different options for the cost function.

TABLE 3.5: WCDMA Tx and Rx Band 1 filter specifications.

<i>Requirement</i>	<i>Freq. Band (MHz)</i>	<i>Value (dB)</i>
Insertion Loss	1920-1980 (Tx)	< -2
	2110-2170 (Rx)	< -2
Isolation	1920-1980 (Tx)	> -50
	2110-2170 (Rx)	> -50
OoB Rejection	1710-1755 (B4Tx)	> -40
	2400-2500 (WiFi)	> -40

TABLE 3.6: Synthesized BVD bandpass elements of the Tx WCDMA Band 1 filter for Feasibility design.

BVD Elements	RES 1&7	RES 2&6	RES 3&5	RES 4
L_a (nH)	137.41	35.90	247.56	34.81
C_a (pF)	0.048	0.197	0.027	0.202
C_0 (pF)	0.87	3.54	0.48	3.64
r	18	18	18	18
f_s (GHz)	1.950	1.894	1.950	1.897

Firstly, we are going to set up an empty cost function for the methodological design. Consequently, the outcome will be a feasible or not solution. The program runs looking for one solution which satisfies the constraints.

For the example of the transmitter filter following the above initialization parameters gives the normalized frequencies of the transmission zeros at $\Omega_1 = \Omega_7 = 1.81$, $\Omega_2 = \Omega_6 = -1.94$, $\Omega_3 = \Omega_5 = 1.81$ and $\Omega_4 = -1.82$ in rad/s for an $RL = 12$ dB configuration. Therefore, we have one solution suitable for the frequency pattern among many others, however, this one also accomplish the specified r .

In Fig. 3.29(a) there is represented the response of the filter when the optimization program verifies the feasibility of the selected topology according to the defined constraints. As it is observed in the graph, the obtained filter response fulfills the spectrum mask specifications and the synthesized acoustic wave resonators, presented in Table 3.6 accomplish the technological capacitance ratio. Therefore, the use of additional external reactive elements is not needed. We observe how the systematic tool has found a solution with symmetrical transmission zeros even though we disabled this option.

TABLE 3.7: Synthesized BVD bandpass elements of the Tx WCDMA Band 1 filter for an RL maximization design.

BVD Elements	RES 1&7	RES 2&6	RES 3&5	RES 4
L_a (nH)	72.26	34.54	220.18	32.39
C_a (pF)	0.093	0.205	0.030	0.217
C_0 (pF)	1.67	3.68	0.54	3.91
r	18	18	18	18
f_s (GHz)	1.944	1.893	1.950	1.897

As the optimization constrained routine has found a feasible solution accomplishing the specification mask and the technological material system, we can think that many other solutions can be feasible for the established constrained problem. However, along all the solutions there would be one which would be better in terms of RL level, greater than 12 dB.

Secondly, we define a cost function which maximizes the RL for the systematic design, following the previous initialization parameters. As we already know there is a feasible solution for the constrained problem, the outcome will be a feasible solution with the highest RL level.

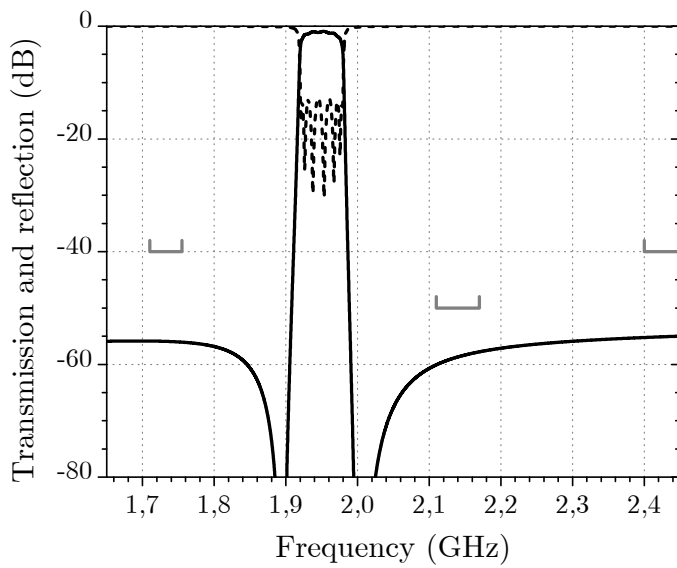
After we run the program for the example of the transmitter filter the obtained normalized frequencies of the transmission zeros are $\Omega_1 = \Omega_7 = 1.59$, $\Omega_2 = \Omega_6 = -2.00$, $\Omega_3 = \Omega_5 = 1.81$ and $\Omega_4 = -1.83$ in rad/s configured with $RL = 17$ dB.

The graph in Fig. 3.29(b) of the simulated frequency response verifies that the spectrum mask for the desired application is satisfied.

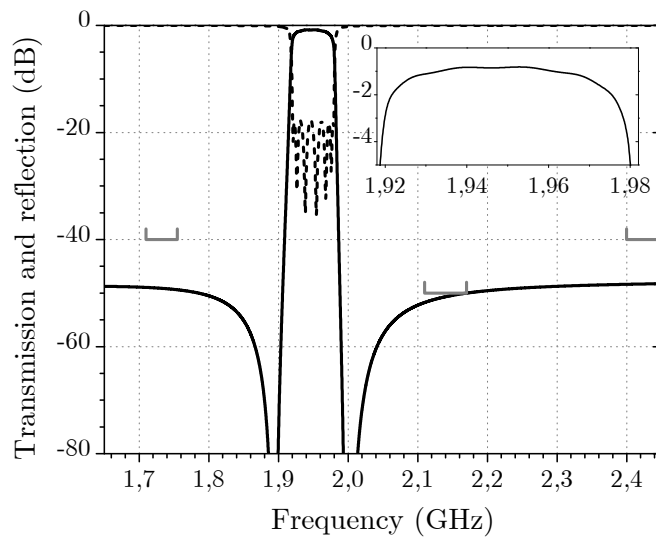
The plots in Fig. 3.29 have been simulated considering the losses of the resonators with Qs of 1500, but in the search of the solution, the model was considered lossless, in this example. Consequently, the rounding effect produced at the passband edges leads to do not attain the IL specification for the whole passband.

The synthesized acoustic-wave resonators with the values of Table 3.7 shows the accommodation of the material system for the resonators without need of external elements.

When comparing the two filter responses displayed in Fig. 3.29 it is appreciated the previously mentioned trade-off between the return loss in the passband and the attenuation in the stopband. The optimization problem

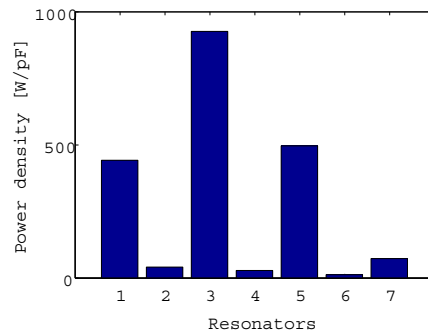


(a)

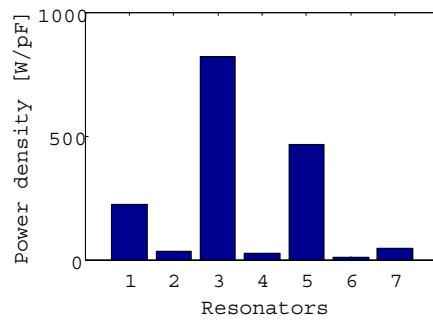


(b)

FIGURE 3.29: Filtering frequency response of the optimized design for Tx WCDMA Band 1 computing (a) the feasibility of the constraints (b) the maximization of the return loss. The quality factor used on the circuit simulations is $Q=1500$.



(a)



(b)

FIGURE 3.30: Power density response of the optimized design for Tx WCDMA Band 1 at 1.98 GHz according to solution (a) from Fig. 3.29(a) (b) and from Fig. 3.29(b).

solution when maximizing the RL, gives a solution with an increased RL level which has the rejection adjusted to the more restrictive attenuation specification.

Although the design has not optimized the power distribution over the filter resonators, Fig. 3.30 displays the resonator power density of the two Tx B1 designed filters of Table 3.6 and Table 3.7 with respectively frequency responses of Fig. 3.29(a) and Fig. 3.29(b). The resonators power density differences between the two solutions which accomplish the spectrum mask and the restriction on the r are observed. So that, there exist different options which will be more suitable depending on the application requirement.

The specifications of the Rx filter according to Table 3.5 are now introduced for a new filter the design. Defining also a 7th-degree filter with a first

element a series resonator and material system constraint of $r = 18$ along the resonators. With cost function defined to maximize the return loss, the outcome after running the software design tool is a symmetric filter. The receiver filter obtained has normalized frequencies of the transmission zeros are $\Omega_1 = \Omega_7 = 1.51$, $\Omega_2 = \Omega_6 = -2.22$, $\Omega_3 = \Omega_5 = 1.97$ and $\Omega_4 = -2.02$ in rad/s configured with $RL = 20$ dB. For this example the frequency response obtained is displayed in Fig. 3.31 where the resulting filter attain the application specifications and the implementation material system constraints with all the resonators at $r = 18$.

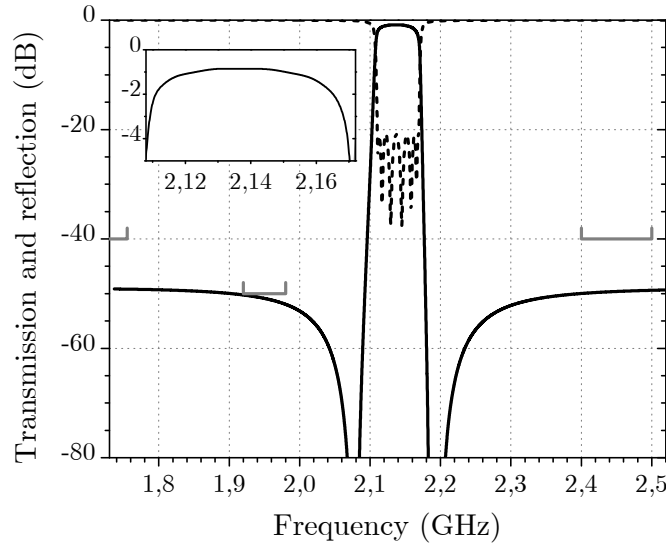


FIGURE 3.31: Filtering frequency response of the optimized design for Rx WCDMA Band 1 computing the maximization of the return loss. The quality factor used on the circuit simulations is $Q=1500$.

3.4.4 Physical implementation of asymmetrical filters

At that point, we have given the filter design systematic tools. The nodal diagram selected from the fulfillment of response specifications determines the topology. For instance, the arrangement of the transmission zeros determines the connection of series and shunt resonators in a the ladder configuration. The proposed models enable to apply the synthesis theory from the nodal diagram of coupled resonators with NRN to a realizable filter with acoustic-wave resonators and external elements.

When the arrangement of the array of transmission zeros defined for the inline NRN network is not symmetrical, seen from the input and output, then one of the coupling inverters at mainline positions has a value different than unity.

In an inline NRN network of N -th degree and N transmission zeros, like in 3.21(b), there are $N + 1$ mainline inverters. Along the circuit element extraction analytical procedure, N inverters are arbitrarily chosen as they are free parameters but the value of one inverter is not arbitrary. In a general inline network, the number of arbitrary parameters that can be chosen is equal to the number of NRNs that the circuit contains.

Asymmetrical filters are generated by all even degree filters or for the odd degree filters whose transmission zero array is not arranged symmetrically. In both cases, the array of transmission zeros is not symmetrical and neither is the resultant implemented filter. The phase term of the input reflection coefficient is different than the output reflection coefficient. In a symmetrical odd degree filter, the non-arbitrary inverter results always unitary.

Applying the scaling properties (section 2.6.5) the inverter coupling different than one can be placed at any mainline coupling position of the network. In order to physically implement a filter, the proposed nodal diagram must be corresponding with a realizable filter. Therefore, the inverter coupling different than one has to be considered with any implemented network behaving as inverter.

If the extraction is done from the input to the output with unitary source and load, the non-unitary inverter appears at the output, which is more coherent, in the context of acoustic wave technology, than appearing in the middle of the network. The non-unitary inverter at the output is took into account straightforward by adding external output components. Another possibility is to use an unitary inverter and move the the condition to the load, hence, we can assume the natural mismatching at the expense of degrading the in-band return loss when source and load are maintained equal or we can afford a source and load different.

In the case of performing the matching with additional components, the extraction methodology requires that, at the stage of the remaining admittance is of the last resonant node Ω_N , we consider an additional NRN without dangling resonator before the load to offer new degrees of freedom, as depicted in Fig. 2.14. Thus, the reactance of such output element is analytically determined. Since B_1 depends on the selected sign of B_2 , the

resulting value of the capacitance ratio r of the last resonator will also depend on it. The selection decision can be made upon the resulting r most similar to the technologically required one. However, when at that extraction point the remaining admittance is higher than one, B_2 results pure imaginary if the load impedance is unitary. The situation can be solved adding more output reactive elements or matching the filter to a suitable load impedance to change the condition of the remaining admittance.

3.5 Ladder-type duplexers based on acoustic-wave resonators

A duplexer separate simultaneously the receiving (Rx) signals from the antenna and the transmitting (Tx) signals to it. They are indispensable devices at front-end sections for WCDMA Frequency Division Duplex (FDD) mobile phones. A duplexer consists of two filters parallel connected to the antenna, as illustrated in Fig. 3.32.

Indeed, duplexers like filters for mobile communications exhibit high isolation between the Tx and Rx ports and high performance. The specifications such as center frequencies, duplex spacing, relative bandwidths are different considering the operation band, while stringent requirements terms such as passband characteristics, attenuation at other frequency ranges, isolation and shape factor are very stringent for 3G/4G frequency bands.

Regarding the complex and challenging performance to attain, duplexer devices can be tailored using acoustic-wave filtering technologies: BAW and SAW. Of course advantages like device size, weight and price are also important for their use. Currently, duplexers with the two filters SAW-based or BAW-based as well as duplexers combining SAW and BAW chips have been implemented. The most often realization is the ladder topology for filters composed of one-port SAW and BAW resonators, although other building blocks are feasible. Therefore, we firstly deal with the design of both the RX and TX filters single-ended input and outputs.

Fig. 3.32 shows an RF duplexer scheme. The weak received signals at the antenna port are filtered by a bandpass filter to reject the unwanted signals at the Low Noise Amplifier (LNA). The strong emitted signals, about 1W, from the Power Amplifier (PA) are filtered by a bandpass filter to suppress unnecessary signals at the antenna generated in the PA. The frequency range of the Tx pass band (F_{Tx}) is apart from the frequency range of the

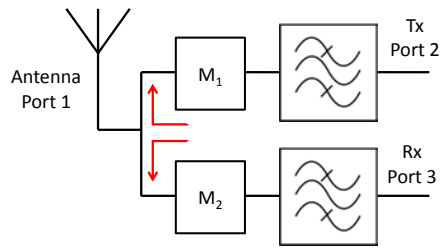


FIGURE 3.32: Schematic of a duplexer with matching networks.

Rx pass band (F_{Rx}). The Rx filter attenuation at the Rx band must be minimized as much as possible in order to detect the weak Rx signals which are comparable to the noise. Meanwhile, the Rx filter attenuation at the Tx band must be maximized to suppress power leakage of the Tx signal from the PA to the LNA. The Tx filter attenuation at the Tx band must be also minimized because it leads to a reduction on the battery power consumption and heating. But, the Tx filter attenuation at the Rx band must be maximized to avoid power leakage from the PA.

A common isolation value of 55 dB is required, because the 30 dBm of transmitted power plus the -20 dBm blocking power level of the receiver, with a 5 dB margin gives this isolation level.

3.5.1 Mechanisms to overcome the duplexer degradation caused by the loading effect

For Tx and Rx filters of Fig. 3.29(b) and Fig. 3.31, the reflection coefficient phases in the F_{Rx} and F_{Tx} , respectively, are arbitrary. Therefore, a degradation effect occurs increasing the IL of the duplexer when it is made up with these two filters directly connected to the antenna port. In a duplexer operating at F_{Tx} , we aim that the Tx signal do not leakage to the Rx filter, which is solved if the Rx filter in F_{Tx} behaves as an open-circuit device, and vice versa with the Tx filter.

If the open-circuit condition is accomplished for both reflection coefficients at the Tx filter output and the Rx filter input from the antenna junction, a minimum insertion loss will be achieved in F_{Tx} and F_{Rx} . This indicates that the transmitting and receiving signals are not interfering with each other.

The idea of a suitable phase correction agrees with the method described

in section 2.6.2 for the reflection coefficients phase adjustment in prototype networks of coupled resonators with NRNs. An additional NRN alone is introduced, therefore the phase of the reflection coefficient θ_{11} can be adjusted to be null at a specified normalized frequency Ω_{dual} :

$$e^{j\theta_{11}} = \left. \frac{D(s)}{M(s)} \right|_{s=j\Omega_{dual}} = 1. \quad (3.85)$$

The determined Ω_{dual} corresponds in a duplexer to the center frequency of F_{Tx} normalized in rad/s for the case of the Rx filter and to the center frequency of F_{Rx} normalized in the Tx filter.

In this thesis, the necessary reflection phase at the antenna junction to provide open-circuit condition is used to reduce loading effects between the duplex bands, obtaining the nature and value of the reactive element in the junction. The pole extraction with NRN methodology, along with the lowpass to bandpass BVD model equivalence are applied to design the acoustic wave filters gathered on a duplexer device. Simulations results indicate that with a convenient design regarding the reflection phase for impedance matching, a duplexer with very low IL can be made up using SAW and BAW devices.

The susceptance value of the first NRN in the lowpass prototype will have equivalence with a reactive element employed as matching network in the bandpass filter. The inductive or capacitive nature of the reactive element depends on the separation between bands and the position of the first transmission zero for each filter.

To overcome the loading effect matching networks are needed at the antenna port to properly correct the magnitude and phase of the individual filtering functions, see Fig. 3.32. A common matching configuration employed is a quarter wavelength transmission line used to transform low input impedances [72]. In order to miniaturize the component, a Π -network of two shunt capacitors and a series inductor replaces a transmission line. The most popular solution among acoustic-wave filters is to use one shunt inductor at the output of the Tx and another at the input of the Rx, which are merged in one coil at the antenna port. The inductor implements the properly phase correction necessary to attain the open-circuit condition.

Following the extraction procedure detailed in section 2.6 we get the prototype network describing the lowpass response of a Tx or Rx filter on a duplexer. In the design of stand-alone filters the phase term of the reflection coefficient is calculated to avoid the need of lumped input/output elements

enforcing zero-phase at first implemented transmission zero. In contrast to stand-alone filters, in the design of filters for a duplexer, the zero-phase is adjusted at a different frequency than in the first transmission zero, hence the prototype extraction from the input admittance is not possible if susceptances at the source and load ports are not considered. Input/output external NRN elements will be needed, as show in Fig. 3.33. This elements on the prototype are equivalent to external lumped reactive elements in the implemented filter.

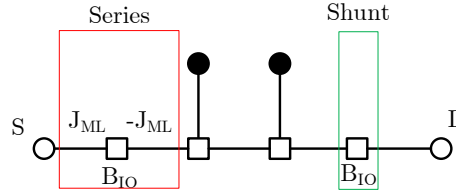


FIGURE 3.33: Nodal representation of a circuit with I/O external elements for phase adjustment.

The lowpass prototype elements of a section that implements the correction phase may corresponds two one of the two following cases: one section could be a shunt FIR element (susceptance value B_{IO}) between two opposite sign admittance inverters ($\pm J_{ML}$) and the other section could be a shunt FIR element (susceptance B_{IO}). In the first case, the equivalent network for the section of the FIR between the inverters is an series impedance of value $j \frac{B_{IO}}{J_{ML}^2}$. In the second case, the network for the section of the shunt FIR is already a shunt admittance of value jB_{IO} .

Once the lowpass I/O reactive elements are extracted, the next step is to apply the narrowband frequency transformation and the impedance de-normalization to obtain the bandpass elements. The lowpass to bandpass frequency transformation (3.60) is used and imposing the approximation at the passband center frequency of the filter f_0 . The transformation is done by matching the impedances of the lowpass prototype to a series inductor L_{series} , for the case of impedance $j \frac{B_{IO}}{J_{ML}^2}$, or a shunt inductor L_{shunt} , for the case of admittance jB_{IO} , with the corresponding expression:

$$L_{series} = \frac{-Z_0 B_{IO}}{2\pi f_0 J_{ML}^2} \quad (3.86)$$

$$L_{shunt} = \frac{-Z_0}{2\pi f_0 B_{IO}}, \quad (3.87)$$

where Z_0 is the normalizing impedance.

As the external elements are defined for the lowpass to bandpass equivalence as inductors, when one of the obtained inductors has a negative value it means a change in the nature of the reactive element, and the element in fact is a capacitance. For these cases, the obtained inductor value L , including the negative sign, is converted to a capacitance C for a practical implementation given by:

$$C = \frac{-1}{(2\pi f_0)^2 L}. \quad (3.88)$$

In asymmetrical Tx/Rx filters for duplexers the phase term of the input reflection coefficient is different from the output reflection one. The external I/O reactances in the prototype, equivalently input and output capacitances or inductors are not equal. When the extraction is performed from the input to the output, the output reflection phase will be non-zero at Ω_{dual} .

3.5.2 Automatic search-engine for Duplexer design

The described methodology for designing Tx/Rx filters of duplexers has been developed in the software tool for automatic search of filtering function solutions that accomplish a constrained problem. The script allows the design of Tx/Rx filters assembled in a duplexer taking into account the Rx and Tx interaction and includes the necessary phase matching elements and then accommodates the required material system of the resonators while attaining the specifications.

The operation procedure is equal to the previous described for stand-alone filters, with the only variation in the network composing the prototype filter of extracted pole sections. For this case, the prototype network would be similar to the one in Fig. 3.33, but with the appropriate order.

In the case of the Rx filter output or the Tx filter input, the phase term can be calculated at Ω_{dual} or at the normalized frequency of the first transmission zero corresponding to that port. Therefore, the extraction technique for each situation would lead to having external elements or not. Observe that with the structure we have the control of the design.

We focus on an example to validate the duplexer design technique developed, with the specifications of WCDMA Band 1 presented in Table 3.5. The frequency spacing between Tx and Rx bands is 30 MHz with Tx and Rx attenuation of 50 dB. The design assumes a technological $r = 18$. For

TABLE 3.8: Synthesized BVD bandpass elements of the receiver filter of a WCDMA Band 1 Duplexer.

BVD Elements	Res R1&R7	Res R2&R6	ResR3&R5	Res R4
L_a (nH)	70.31	16.53	105.08	16.11
C_a (pF)	0.077	0.357	0.053	0.363
C_0 (pF)	1.38	6.42	0.95	6.53
$L_{in/out}$ (nH)	3.685			
r	18	18	18	18
f_s (GHz)	2.163	2.073	2.140	2.082

each case, it is considered the input and output elements for design a duplexer, imposing zero phase at the Tx center frequency $f_{0Tx} = 1.95$ GHz for the receiver filter, and zero phase at the Rx center frequency $f_{0Rx} = 2.14$ GHz for the transmitter filter.

The automatic methodology directly carries out the study of the set of transmission zeros and RL for a design which must accomplish the spectrum mask and any considered implementation issue, in our case the resonator capacitance ratio. The cost function of the search allows to perform a second order analysis along multiple solutions, where the optimizer settles on the ones belonging to the defined second order interest, such as maximum RL, lower power densities, minimum area, flater group delay, etc.

For the receiver filter when maximizing RL, the following normalized transmission zeros are obtained $\Omega_1 = \Omega_7 = 2.81$, $\Omega_2 = \Omega_6 = -2.32$, $\Omega_3 = \Omega_5 = 1.98$ and $\Omega_4 = -1.99$, for $RL = 32.6$ dB. The phase term of the reflection parameter has to be evaluated at the normalized frequency $\Omega_{dual} = -6.58$ rad/s. This phase term in S_{11} is found to be $\theta'_{11} = 26.36^\circ$. Following the extraction steps for the prototype network, all the couplings between NRNs are set to unitary admittance inverters, and the input/output NRNs result in external susceptance $B_{in} = B_{out} = -1.0089$.

The transformed elements corresponding to acoustic wave resonators to constitute the bandpass ladder filter for the receiver are shown in Table 3.8. The technological capacitance ratio is uniform for all the resonators without need of external elements. The $L_{in/out}$ external elements corresponding to B_{in} is show in the table, too.

Plots in Fig. 3.34 display the simulated frequency response 7th-degree bandpass receiver filter. We can observe now how the requirement of IL is ful-

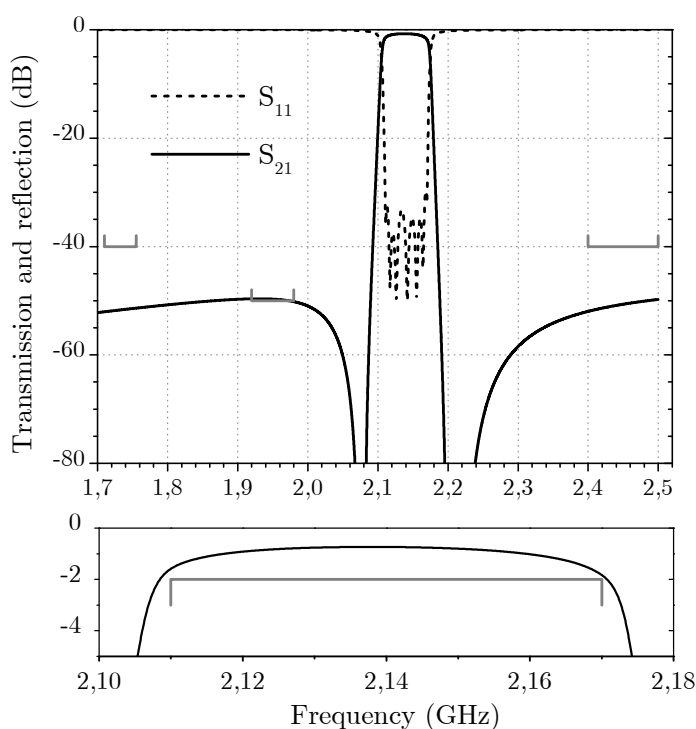


FIGURE 3.34: Simulation of the frequency response and detail of insertion loss of the WCDMA band 1 receiver filter. The quality factor used on the circuit simulations is $Q=1500$ for resonator and $Q=25$ for I/O inductors.

filled, because in the search of a solution, the filter model was considered with losses and, hence, the response is suitable for the IL demanded.

The phase reflection response for the synthesized filter in Fig. 3.35 shows at the F_{Tx} band it is close to the 0° phase, although not exactly at f_{0Tx} because of the bandpass approximations.

With the receiver designed, we need to compute the transmitter to obtain the suitable set of transmission zeros and RL for the duplexer when maximizing the RL and constrained by the specifications and the technological requirements.

The corresponding normalized transmission zeros are $\Omega_1 = \Omega_7 = 1.87$, $\Omega_2 = \Omega_6 = -1.84$, $\Omega_3 = \Omega_5 = 1.66$ and $\Omega_4 = -1.66$, for $RL = 17$ dB. The phase term of the reflection parameter has to be evaluated at the normalized frequency $\Omega_{dual} = 5.46$ rad/s. This phase term in S_{11} is found

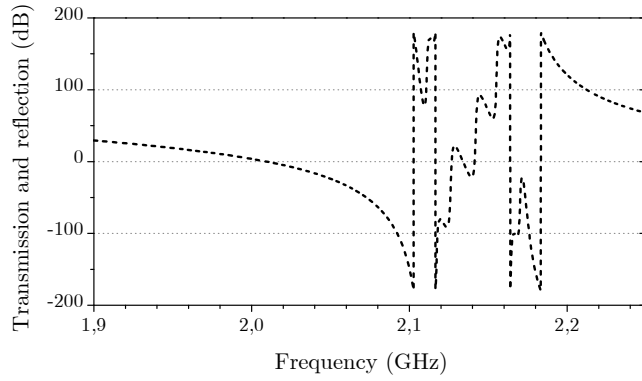


FIGURE 3.35: Simulation of the reflection phase of the WCDMA band 1 receiver filter.

TABLE 3.9: Synthesized BVD bandpass elements of the transmitter filter of a WCDMA Band 1 Duplexer.

BVD Elements	Res T1&T7	Res T2&T6	Res T3&T5	Res T4
L_a (nH)	110.09	34.38	177.45	34.74
C_a (pF)	0.060	0.206	0.037	0.202
C_0 (pF)	1.08	3.70	0.67	3.64
$L_{in/out}$ (nH)	10.994			
r	18	18	18	18
f_s (GHz)	1.958	1.893	1.951	1.898

to be $\theta'_{11} = -18.21^\circ$. From the prototype extraction, the input/output NRNs result in external susceptance $B_{in} = B_{out} = -0.3710$.

The bandpass BVD elements defining the resonators of the obtained design are shown in Table 3.9. Also, for the transmitter, the technological capacitance ratios are uniform. We observe that a high input/output impedance is required in order to control the reflection phase.

Fig. 3.36 displays the magnitude response of the transmission and reflection. With the design the filter exhibits inband insertion loss better than 2 dB.

The phase reflection response for the synthesized filter in Fig. 3.37 at F_{Rx} is close to the zero degrees.

The network representing the resulting duplexer in the lowpass nodal rep-

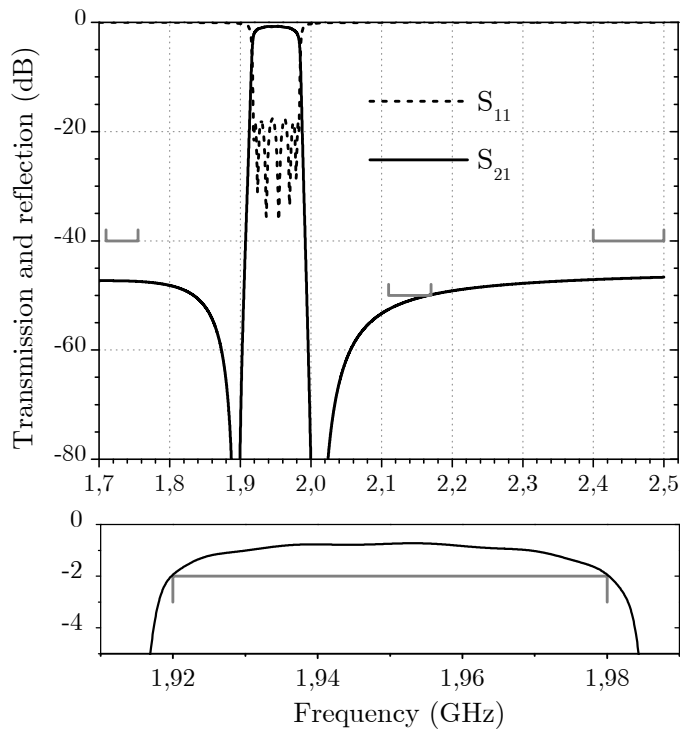


FIGURE 3.36: Simulation of the frequency response and detail of the insertion loss of the WCDMA band 1 transmitter filter. The quality factor used on the circuit simulations is $Q=1500$ for resonator and $Q=25$ for I/O inductors.

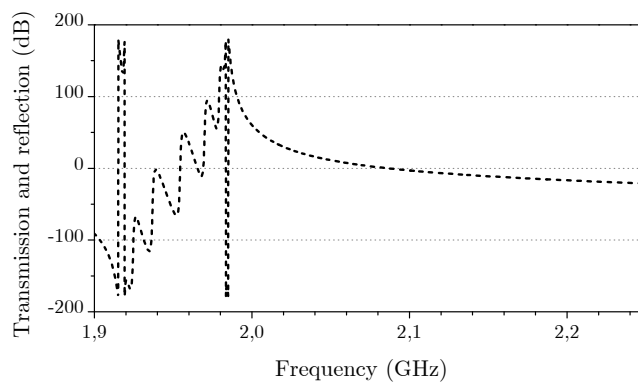


FIGURE 3.37: Simulation of the reflection phase of the WCDMA band 1 transmitter filter.

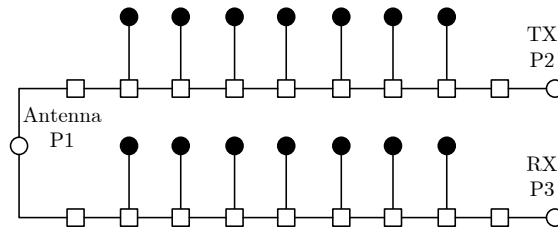


FIGURE 3.38: Nodal representation of a duplexer with an 7th-degree filter for the Tx joined with a 7-th degree Rx filter in the antenna port.

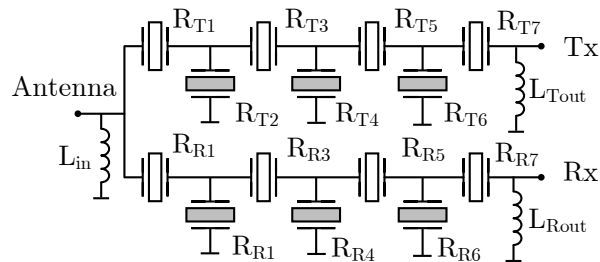


FIGURE 3.39: Network of the synthesized WCDMA band 1 duplexer with ladder filters with input and output inductors.

resentation after assembling each Rx and Tx ladder filter of the synthesis is shown in Fig. 3.38.

The corresponding bandpass acoustic wave duplexer topology is depicted in Fig. 3.39. At the antenna port the two shunt inductors are merged into one reactive element.

The simulated performance of the duplexer with both two transmission frequency response and the input reflection response at the antenna port is illustrated in Fig. 3.40. In the graph we verify that the mask specifications are fulfilled, as well as the implementation of the resonators attain the technological capacitance ratio. The rejection in the frequency range of each counterband for each transmission response has improved respect the rejection on the filter stand-alone.

The two filters designed with the phase condition, when performing in a duplexer, exhibit insertion loss levels in both Rx and Tx passbands according to the specifications, as shown in Fig. 3.41. The insertion loss has not been degraded because the loading effect of the Rx or Tx filter in the counterband has been cancel with the control of the reflection phases.

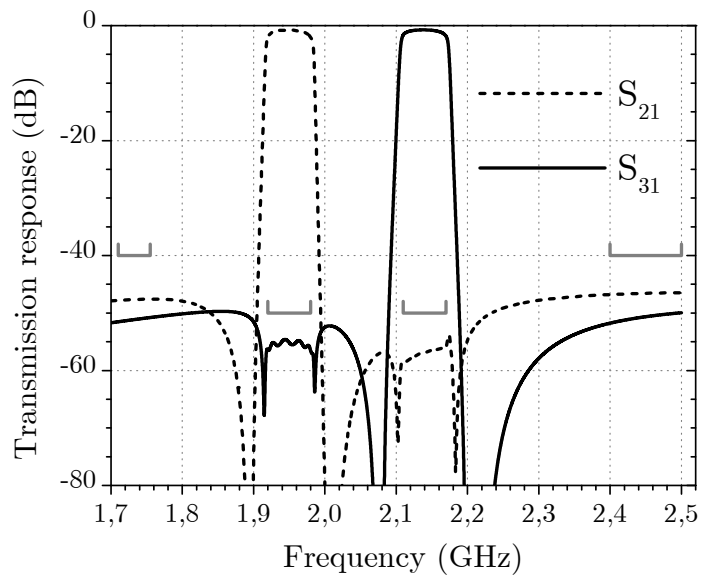


FIGURE 3.40: Simulation of the synthesized WCDMA band 1 duplexer, with $Q=1500$ for resonator and $Q=25$ for I/O inductors.

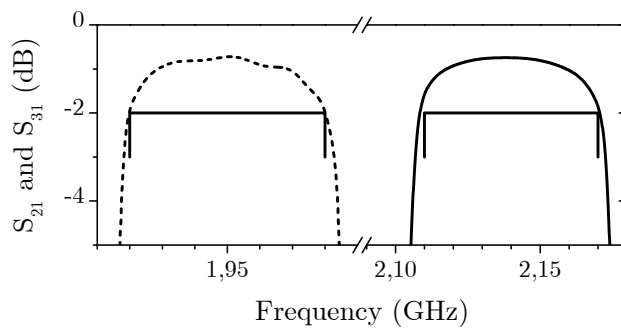


FIGURE 3.41: Insertion loss detail for WCDMA band 1 duplexer in the Tx and Rx bands, with $Q=1500$ for resonator and $Q=25$ for I/O inductors.

3.6 Summary

Given the association between an acoustic resonator and the lowpass model of the extracted pole prototype, it allows that the stringent constraints imposed by limited realization possibilities of acoustic wave technology can be already taken into account when designing the reference lowpass filter. Then, the synthesis of ladder topologies can be dealt by direct analytical extraction of a nodal approach based on resonating and nonresonating nodes and application of frequency transformations together with impedance conversion.

The study of particular interactions between resonators parameters and variations of critical frequencies of transmission zeros or return loss reveals that they are the variables to manage on a design to meet the technological requirements and desired response shape. Indeed, the speed and efficiency of this kind of implementation characteristic studies is possible thanks to the systematic methodology.

The starting point design success of filters shall be simple and robust to allow a batch processing with high yield in the fabrication. We describe the methodology used for an integrated software solution that can improve productivity and significantly reduce costs on the implementation of a filter, particularly, in the stage of topology definition because of the effective and fast solutions provided. The methodology offers a solution that combines a complete spectrum fulfillment with topologies ready to accommodate technological constraints of micro-acoustic technologies. Moreover, the approach is native oriented to design a duplexer structure as a unique device because the adjustment of reflection phase is done regarding the mitigation of the loading effect, it includes losses and it is ready for SAW and BAW technologies. The nature, value and position of all external elements are directly obtained.

The design methodology has been successfully evaluated with the synthesis of examples for application of WCDMA band 1 filters without input/output reactive elements, as well as to face a duplexer synthesis of band 1 where the reflection phase term has been properly computed to meet the right phase condition to avoid destructive interferences.

4

HYBRID FILTER DESIGNS BASED ON ACOUSTICALLY COUPLED RESONATOR TOPOLOGIES

Current demands for advanced wireless communications systems tend to filters with extremely low insertion loss, higher skirt steepness, stringent rejection levels and in some cases wide bandwidths while still shrinking sizes. As a consequence, the suitability of acoustic wave technologies due to the high miniaturization and high quality factor features depends on the capability to develop sophisticated filter topologies.

Besides, inline topologies, other than the fully canonical, will have resonance frequencies at infinite. Interesting features that are not found in the fully canonical network for ladder topologies are obtained. Filtering functions performing simultaneously high selectivity and good out-of-band rejection are implemented with functions that introduce a number of finite transmission zeros but less than the order of the filter. The finite TZs tend to increase the selectivity without increasing the order, and the corresponding TZs located at infinite yield to stopband rejection.

Given the strengths of ladder and acoustically coupled resonators configurations, the combinations of both can overcome new challenges of high-performance in filters. Filter configurations with both configurations combined are studied in this chapter in order to merge their corresponding valuable features in a single hybrid filter. For the application of a direct synthesis approach, it is an undeniable requirement to provide a lowpass coupled resonator prototype interpretation of its operation.

The lowpass models of different configurations of coupled resonators building blocks based on acoustic wave technologies are detailed for later use in

hybrid filters. Furthermore, in the synthesis process the features of the technology and the topology are important issues to take into account.

4.1 Hybrid filters with combined topology

Although the fully canonical inline circuit forms the base from which the ladder filter configuration can be derived, there are a wide variety of useful filter configurations that are not synthesized by fully canonical networks. In this chapter we shall follow the inline extracted pole synthesis methodology with coupled NRNs and resonators and its application to bandpass.

The inclusion of resonating nodes in the mainline path for the formation of the prototype circuit plays an important role in order to generate transmission zeros located at infinite frequencies, hence the transmission response shape drops monotonically at far stopband regions. The resonating nodes sections may be realized as building blocks cascaded with other sections or not necessarily.

In Chapter 2, the general technique for synthesizing non-fully canonical inline networks, such as a circuit in Fig. 2.3(a), from the characteristic polynomials of a desired filtering function was described. Nevertheless, the resonating nodes sections may find its implementation in the context of acoustic wave technologies. As a consequence, there exist requirements, regarding the network arrangement, to provide adequate and feasible realization of the prototype circuit by the acoustic wave technologies.

For instance, in a circuit represented by the nodal diagram Fig. 2.3(a), the two sections of NRN with dangling resonator are implemented with series or shunt resonators, however the other three resonating nodes in the mainline, we may think to implement them with lumped parallel LC resonators.

In the context of SAW and BAW, this solution is not suitable because of the problems it arise, such as large space for inductors and capacitors integrated externally on a PCB, as well as they exhibit very low Q in comparison to acoustic resonators.

An alternative approach is to look at new filter configurations that exploit the behavior of resonating nodes by means of piezoelectric transducers. The key to implement such required building blocks, without the use of inductors, is acoustically loading and coupling by means of propagating

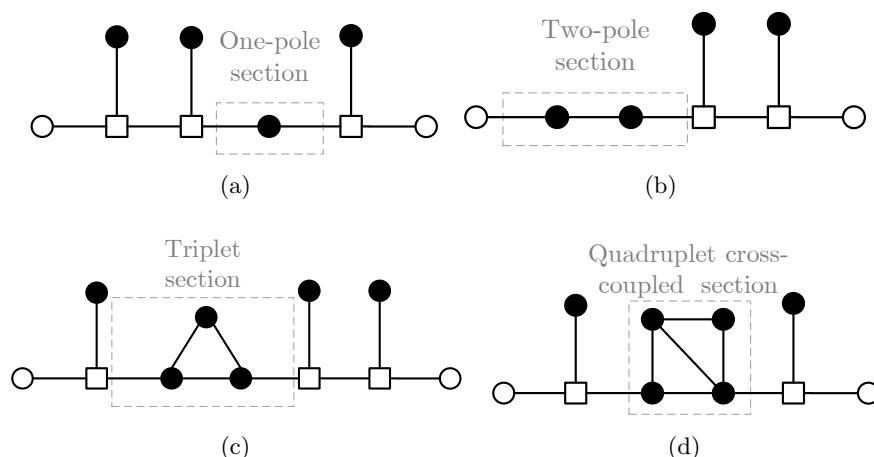


FIGURE 4.1: Prototypes with hybrid topology, part of the structure with ladder building blocks and part with (a) one-pole section, (b) two-pole section, (c) a triplet section and (d) cross-coupled section.

acoustic waves rather than just the electrical interaction of resonators as circuit elements.

The most pertinent examples of wave coupling for SAW and BAW technologies are the Dual Mode SAW (DMS), Multi-Mode SAW (MMS), Stacked Crystal Filter (SCF) and Coupled Resonator Filter (CRF) in BAW. For instance, a SCF is a structure wherein two transducers act as a single over-moded resonator. As a consequence, the SCF structure operate as a single resonator.

In order to generalize, the inline circuit should not have only one resonating node coupled between two NRN or one NRN an one port. It is possible to find SAW or BAW practical implementations which represent two coupled resonating nodes, or more, or even particular sections, such as trisections, different than the already presented sections of NRN with dangling resonators. In this case, all of them can be cascaded with sections behaving as ladder stages, such as the examples represented in Fig. 4.1.

In [73], the authors describe how to synthesize a filter with hybrid topologies realizing one part of the filter with extracted pole techniques and the other part with cross-coupled configuration using the methods available for N -tuplets [74].

However, for cases, such as Fig. 4.1(a) and Fig. 4.1(b), the direct synthesis

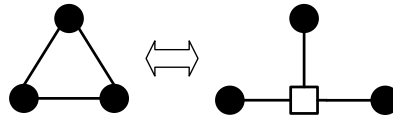


FIGURE 4.2: Triplet transformation into inline extracted pole building block.

methodology of inline coupled resonators and NRNs that we have presented is completely valid, even with Fig. 4.1(c).

The triplet block can analytically be transformed to an inline section of an NRN with dangling resonator in between two resonating nodes, see Fig. 4.2. The derivation of the $Y - \Delta$ transformation relationships is in [75].

All of the possible cases do not feature a practical realization with acoustic wave technologies. The work presented is confined to some of those building sections that are feasible in acoustic wave technology. Hybrid topology filters like the one presented in Fig. 4.1(d) may be beyond the scope of the micro-acoustic technologies.

As a consequence, the design of hybrid topologies starts from the synthesis of lowpass prototype. The NRN with dangling resonator building block was already associated with the equivalent electrical BVD circuit in Chapter 3. The association of the other presented building blocks in Fig. 4.1 has not been done yet. Therefore, suitable frequency transformation and network relations to reconfigure series and parallel resonators are applied to deduce the bandpass circuit corresponding to the lowpass prototype sections of Fig. 4.3.

Then, the values of inverters or lumped elements should be normalized to the characteristic impedance Z_0 . Later, the bandpass circuit will be associated as the electrical equivalent circuit of physical structures considering the fabrication technology.

We can assume that the studied building blocks are connected to NRN composing the whole hybrid topology, in the equivalent bandpass circuit this element is transformed to shunt capacitances. The I/O NRNs of the building blocks shown in Fig. 4.3 are important in order to consider the phase of the corresponding structure, which constitute one part of a whole filter. We have already discuss how important is to consider the phase of two blocks that are going to be connected.

Among the different kinds of resonating building blocks presented, for ex-

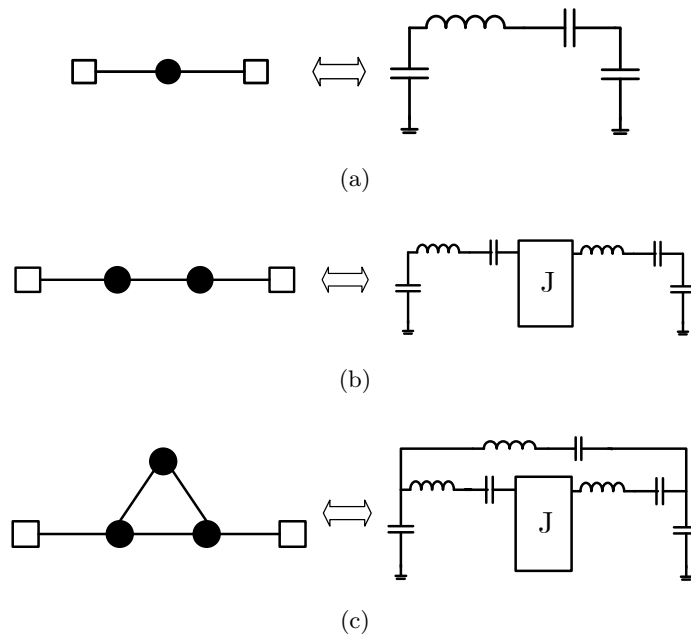


FIGURE 4.3: Equivalent bandpass circuits of building blocks: (a) one-pole section, (b) two-pole section and (c) a triplet section.

ample, the bandpass network in Fig. 4.3(a) is, by definition, the resulting equivalent circuit which models an SCF derived from the Mason model [76]. Also building blocks with two or more resonant modes are feasible; they are well established in acoustic wave technologies as coupled resonator filters. In the most simple case (Fig. 4.3(b)), two transducers are acoustically coupled by means of SAW or BAW mechanisms, which represent the equivalent circuit of a CRF or simple model of a DMS [77].

4.2 Structures of acoustically coupled resonators

Acoustic filter networks are designed by the connection of resonating acoustic structures. SAW and BAW technologies allow the implementation of different types of resonating building blocks. In a ladder-type configuration the electrically connected acoustic structures are one-port resonators which have one resonant mode. Building blocks with two or more resonant modes consist of resonant transducers that are acoustically coupled. The control of the acoustical coupling strength establishes the filtering function.

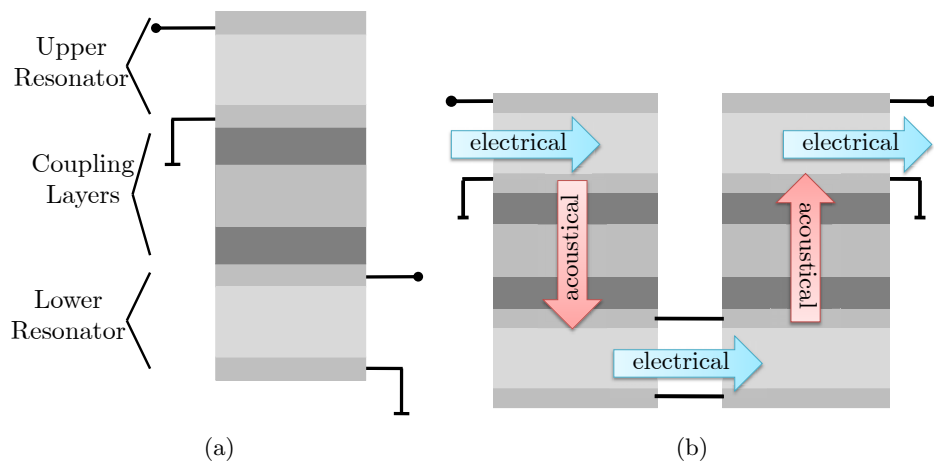


FIGURE 4.4: Side view of a CRF (a) a single section, and (b) two sections connected electrically in series to allow input and output at the top layers.

Filters implemented with acoustically coupled resonators overcome the limited bandwidth issue in ladder filters caused by the pole-zero distance link. DMS or CRF achieve wider-bandwidth low-loss filters. Despite the fact that the transmission zeros provide slope steepness on ladder filter responses, which is important to fulfill selectivity requirements, ladder topologies suffers from the out-of-band flyback of the transmission response. This feature can be a weakness in applications that requires attenuation of certain bands above and below the passband. Typically, the acoustically coupled approaches present transmission zeros at infinite which provide a response with good out-of-band rejection.

After a brief structure and features description of both dual mode building blocks for SAW and BAW technologies, we discuss the convenient equivalent circuit for the two structures regarding their operation.

4.2.1 Coupled Resonator Filter

In BAW components, the basic CRF section, in Fig. 4.4(a), is composed by two BAW resonators, each one with two electrodes and a piezo film. The resonators are acoustically coupled by means of a set of coupling layers [78, 79].

The coupling layers make that the resonators to work independently and

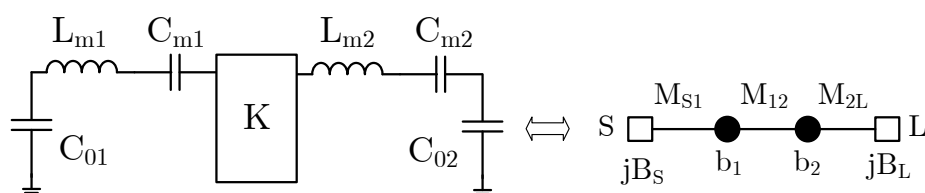


FIGURE 4.5: Equivalent circuit model of a Coupled Resonator Filter.

behave like a 2nd-degree filter. The transmission response of a basic CRF presents two transmission zeros placed at infinite. Consequently, CRF structure allows to obtain good out-of-band rejection, but has poor selectivity. In order to increase the rejection, CRF sections can be connected. See, e.g., the popular 4-pole CRF filter with two sections electrically connected through the electrodes of the lower resonators, in Fig. 4.4(b).

Applying an electrical field on the electrodes of the input upper resonator produces an acoustic wave due to the electromechanical transduction produced by the piezoelectric layer sandwiched between the electrodes. Then, the interaction between the upper and lower resonator is produced in the acoustic domain as the longitudinal wave propagates across the coupling layers. The coupling between the lower resonators takes place in the electric domain and is in part produced by the intrinsic capacitances of the resonators. Going forward to the output, an equivalent behavior between electric and mechanical fields is produced from the lower to the upper resonator.

Due to the vertical stacking of resonators, CRF is more compact in area than ladders. Nevertheless, its drawback lies on the accurate processing demanded for the big amount of layers which makes the manufacturing very challenging.

In our work, we are not interested in a CRF as an individual filter, we consider it as a section of a whole filter composed by order sections, such as ladder cells.

In [80], the fully electrical equivalent circuit model is developed in detail to gather the filter behavior along with its internal coupling and resonating mechanisms. Fig. 4.5 shows the electrical equivalent model of the CRF which anticipates the topology of a filter of order 2. It is similar to the SCF model with the difference of having two LC resonators separated by means of an impedance inverter controlling their acoustic coupling strength.

The proposed model captures the performance of any CRF at frequencies around f_p . It is composed of electrical elements: inductors, capacitors and an impedance inverter. The shunt capacitor C_0 implements the static capacitance between the electrodes of the structure, while the motional branch (L_m and C_m) of the transducers are located in the series position. The impedance inverter K represents the coupling between the two resonant cavities. The equivalent model facilitates working with the CRF in a straightforward way from a completely electrical standpoint.

The electrical circuit representation of the device is connected to the mature electromagnetic filter design theory exploiting its techniques to analyze and synthesize a CRF. As a consequence, full design and sizing of BAW CRFs can be performed to meet specifications. The strength of the technique is that it can deal with complex multi-layered structures. Additionally, a set of closed-form expressions for the design of the CRF coupling layers are presented in [80]. The expressions relate the geometry of the layers with the value of the inverter that is part of the CRF models.

The concept of CRF can be extended to include more complex structures having multiple acoustically coupled resonators where the order of the filter is determined by the number of acoustically resonating plates. For example, the near band rejection of a CRF response could be increased by adding a third acoustic resonator resulting in a filtering block of order 3 [81,82].

4.2.2 Dual Mode SAW

In SAW components, the DMS is implemented by setting two spaced interdigital transducers (IDT) enclosed between two reflecting gratings which form a resonating cavity [83]. As can be seen in Fig. 4.6(a), the profile of the first and second modes, which are the symmetrical and antisymmetrical resonances arising over the length of the structure, are the resonance modes supported in a simple model for DMS. Two identical resonators are acoustically coupled in the propagation direction of the SAW, thus they are longitudinally coupled. The resonance modes interact to create the filter response.

In longitudinal-coupled DMS filters, the frequency difference between the two modes is adjusted by means of the gap between the input and output IDTs. By properly defining the strength of the acoustic coupling, the filter bandwidth is determined. Strong couplings enlarge the frequency separation between the resonances for broadband applications.

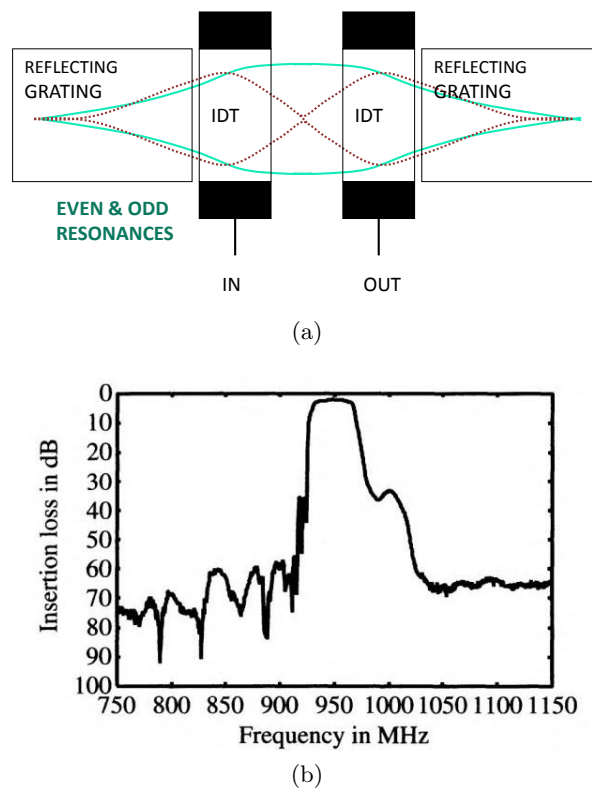


FIGURE 4.6: DMS filter configuration: (a) structure of a DMS, and (b) pass-band performance of a DMS filter for GSM-Rx [51].

In a simple model, one-track DMS filter exhibits two transmission zeros at infinite producing good far stopband rejection. Due to the superposition of the two modes, DMS structures realize broadband bandwidths, likewise, the simple structure has very low insertion loss. Fig. 4.6(b) shows the transmission frequency response of a DMS filter with low insertion loss. The characteristic hump on the high transition band of a DMS which limits the rejection can be overcome by use a series connection of DMS.

In order to outline the operation mechanisms of a DMS filter, for simplicity, we consider a structure with 2 IDTs, although in practice DMS with 3 or 5 IDTs are extensively used [84]. The structural symmetry derives in resonance modes of symmetrical and antisymmetrical field distribution [85, 86]. Hashimoto proposed a two port equivalent circuit [77] to describe the operation of DMS filters and it is shown in Fig. 4.7(a). There are two shunt admittances: Y_{me} the motional admittance of the symmetrical mode and

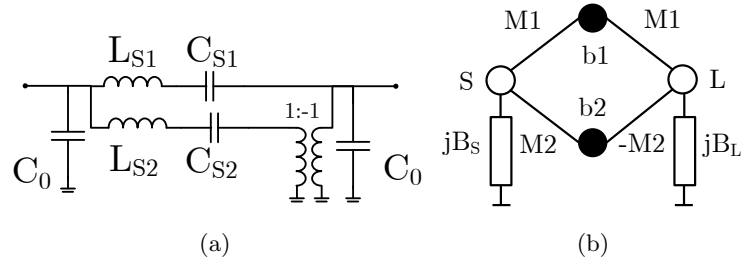


FIGURE 4.7: Equivalent circuit model for operation of a DMS filter.

Y_{mo} motional admittance of the antisymmetrical one. C_0 is the IDT static capacitance.

The transversal equivalent circuit model uses the eigenmodes of the complete filter (even and odd). One resonance corresponds to the contributions of the shunt admittance $Y_{mo} = 2(j\omega L_{S1} + 1/j\omega C_{S1})$ between the two terminals, while the second resonance does to the shunt admittance $Y_{me} = 2(j\omega L_{S2} + 1/j\omega C_{S2})$ cascaded with an ideal 1:-1 transformer. The shunt admittance $j\omega C_0$ is connected from each terminal to ground.

It is clear that the equivalent circuit Fig. 4.7(a) can be mapped into a transversal nodal representation, as depicted in Fig. 4.7(b). The transformer is represented by the change of sign on the coupling observed in Fig. 4.7(b). In order to control the input-output phase, affected by C_0 , it is necessary to include input-output frequency invariant reactive (FIR) elements.

The transversal representation enables an interpretation with a transformed inline path formed by 2 coupled resonators, corresponding to the coupled IDTS. The equivalence between both nodal representations is carried out by means of similarity transformations which are just a fundamental change of basis of the coupling matrix representation [45]. The similarity transformations or rotations preserve the port parameters and internal state variables.

The inline nodal diagram representation, like shown in Fig. 4.8, makes easy a physical interpretation, as two acoustic branches associated to each coupled IDT. It shows up that the total device performs as a 2-pole filter, which represents the bandpass lumped element equivalent circuit of Fig. 4.8. Consequently, the modified equivalent circuit of two-port DMS filter is integrate by the two motional impedances of resonant cavities and

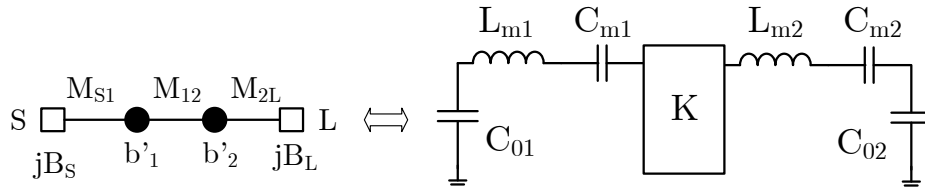


FIGURE 4.8: Inline nodal diagram of a 2-pole DMS filter with reactive ports and the equivalent bandpass filter LC series circuit.

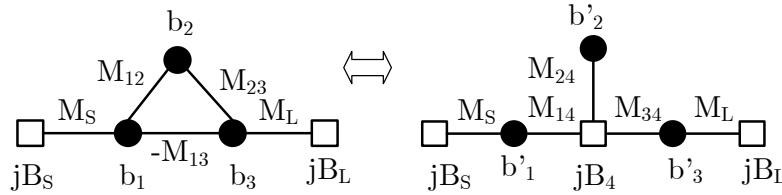


FIGURE 4.9: Nodal diagram representations for 3-mode DMS interpretation with one transmission zero.

the acoustic inverter is coupling them. Also the shunt static capacitances are connected at both terminals.

Despite the 2-pole model for a DMS, authors in [77] pointed out that, in a conventional DMS filter, three resonance modes are used for the design of the filter passband. While two of the modes resonate between the two reflectors, even and odd modes caused by the symmetrical structure, the third mode is supposed to resonate between the two IDTs. In this case, the IDTs act as reflectors for the resonance frequency of the third mode which is mainly controlled by the gap between them, even though the length of the IDTs have also influence. Authors also remarked on a null in the transmission response caused by a resonance in a half section of an IDT and a reflector. The resonance, in the half section, blocks the SAW signal to the other IDT. The signal is not transferred from one IDT to the other and, hence, there is no transmission.

Regarding the proposed advanced model of a DMS with 3 resonances and one transmission zero, a trisection nodal diagram representation, as shown in Fig. 4.9, can be suitable for it. The trisection enables an interpretation with one mainline path formed by the 2 coupled IDTs and a parallel path formed by the cavity resonance that is excited from the IDTs nodes. In order to control the input-output phase it is necessary to include input-

output FIR elements.

The equivalent model corresponds to a 3rd-degree response with one transmission zero, provided that one on the couplings at the trisection has opposite sign in order to generate the TZ. A direct relationship is kept for the trisection with the NRN extracted-pole representation, already presented in Fig. 4.9. Extracted-pole with NRN may be better suited doing the parameter extraction.

The advanced model of the DMS with 3 resonances and different equivalent models, have been perfectly adjusted to the DMS performance and a complete study of the different interpretations has been developed. Nevertheless, the activity results can not be presented because intellectual property factors.

4.3 Synthesis of hybrid prototypes

At that point we have the tools to deal with the synthesis of an hybrid topology and assuring technological feasibility. General networks, different that fully canonical cases, can also be designed regarding the base of the acoustic wave technology and applying the methodology of direct extraction synthesis. We have the nodal diagram circuits associated with the equivalent filters implemented in micro-acoustic technology.

It has been proved how the methodology of design already described in Chapter 3 for ladder filters take into account systematically the constraints imposed by the spectrum mask specifications and the manufacturable technology as well. Consequently, the same technique is consistently extended to be applied now to the proposed hybrid configurations with different acoustic building blocks combined. In this case, given the inline nodal diagram representation, the synthesis process takes as input variables the frequency singularities of the filtering function and the return loss looking for converging to the technological limitations and filtering response.

A highlighted characteristic of the synthesis procedure for hybrid topologies is that it is detached from the nature of the couplings produced in the physical filter. It is observed that in the hybrid filters proposed exist different natures of couplings. Acoustical and electrical couplings are combined on the same assembled filter to take advantage of valuable features of each approach, however the nodal diagram representation deal with the whole set independently of the coupling domain.

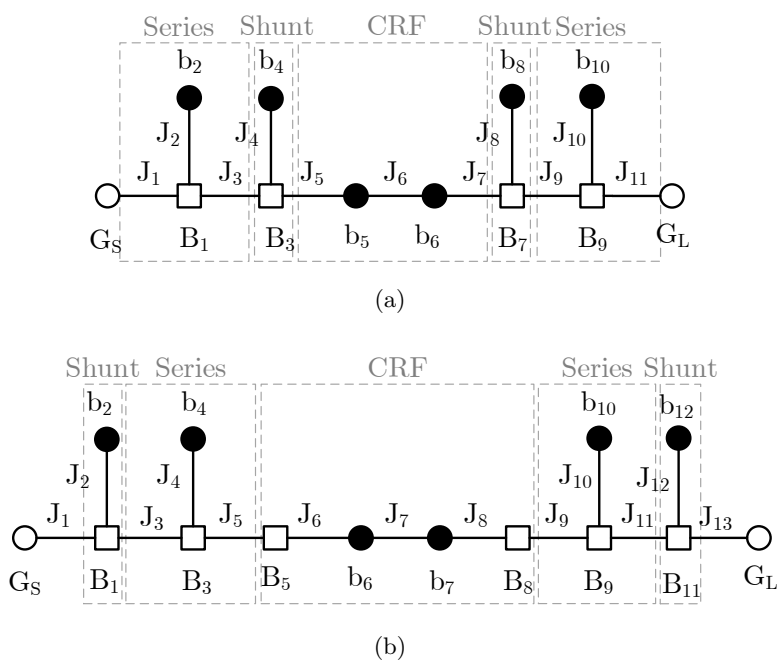


FIGURE 4.10: Topologies of the filtering structure prototype network of $N=6$ and 4 TZs at finite frequencies to be implemented with a CRF block connected (a) with shunt resonators, and (b) with series resonators.

It is important the fact that the combined structure is a whole entity that accommodates one transfer function, although we use different acoustic modules cascaded. Therefore the modules are designed jointly. In [87], it is show how the independent design of modules for a later combination leads to degradation of the filtering function, increasing the inband insertion loss.

Therefore, to apply the systematic synthesis it is necessary an appropriate topology according with the established filtering function of the desired assembled filter. When transmissions zeros are required for the filtering function, a suitable implementation is by means of ladder cells.

The choice of one particular arrangement configuration for the inline prototype circuit must be carefully evaluated regarding the extraction and the derived micro-acoustic modules, because it has impact on the achievable electrical characteristics and issues related with the physical filter practical filter. Lets describe it with an example.

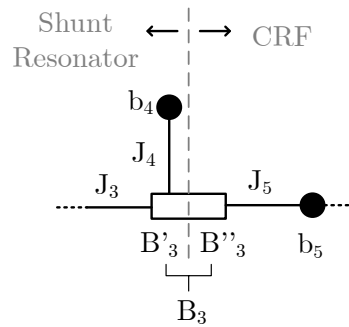


FIGURE 4.11: A FIR element is shared by the NRN of a shunt resonator and the I/O of a CRF when they are connected in a hybrid filter.

Both of the nodal diagrams in Fig. 4.10 feature a 6th-degree filter with four transmission zeros, two TZs above the passband and two TZs below. But they differ in the way, they are associated to the physical filter based on acoustic-wave modules. Doing the association of the extracted pole section on the nodal diagram with practical cells, reveals that the assembled filter for each of the two cases will be different. Therefore, the physical dimensions or technological characteristics of each cell will be also different, comparing both implemented filters.

After analyzing the prototype nodal diagram in Fig. 4.10(a), the first module is a ladder cell consisting of a series resonator connected with a shunt resonator. The same ladder cell is viewed from the output. Thus, the third module place in the middle could correspond with a CRF, which connects with the shunt resonators.

As a CRF equivalent prototype circuit has been defined with reactive ports, the FIR element of the NRN of each shunt resonator section is, in fact, shared by the shunt resonator and the input or output of the CRF, like it is exemplified in Fig. 4.11. Once the prototype extraction is carried out, the FIR element has to be split between the shunt resonator and the CRF when denormalizing to the bandpass networks.

The way to conduct the FIR division is influenced by the technology; because the particular value in each module arise from the remaining split-FIR element values, resulting or not in accommodating the technological constraints.

By the other hand, if it is desired to implement a filter with ladder sections and a middle CRF which is connected thought series resonators, as depicted

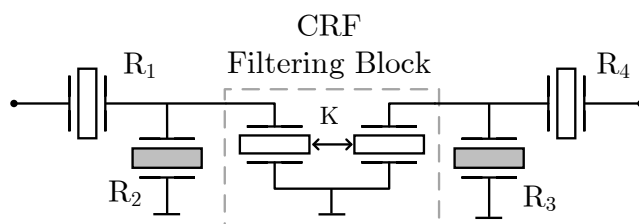


FIGURE 4.12: Proposed hybrid filter combining two ladder cells and in between a CRF structure of 2-poles.

in Fig. 4.10(b), internal NRN without dangling resonators are necessary to accommodate the reactive ports of the CRF block.

4.3.1 Example of design of a hybrid topology combination of ladder and CRF

Following, a ladder and CRF combined structure based on BAW resonators is presented. The bandpass circuit of the proposed topology is shown in Fig. 4.12. From source to load, a basic section of ladder, one series and one shunt resonators, is cascaded to a CRF block and it does to another ladder cell of shunt and series resonators. The two shunt resonators connect, for this example, with the CRF block. The resultant circuit has a response with four transmission zeros, each one controlled by the two shunt and two series ladder resonators.

Our proposed topology has network symmetry from input to output. However, the systematic tool for synthesis can afford any other mixed topology without symmetry or connecting with series resonators to a CRF.

An in-line structure with NRN, like the nodal diagram of Fig. 4.10(a) can synthesize the proposed hybrid filter of Fig. 4.12. The prototype network, detached from the couplings nature, is able to describe a general Chebyshev filtering response of order $N = 6$ with four transmission zeros at finite frequencies and two TZs at infinite.

The shunt BAW resonators for ladder cells are lowpass modeled by NRN with a dangling resonator and, for series resonators, an NRN with dangling resonator between two admittance inverters. In order to implement ladder-type sections, the normalized resonance frequencies at the resonant nodes should be suitably arranged alternating their sign.

TABLE 4.1: Band 3 Tx filter specifications.

<i>Requirement</i>	<i>Freq. Band (MHz)</i>	<i>Value (dB)</i>
Insertion Loss	1710-1785 (Tx)	< -2
OoB Rejection	1805-1880 (Rx)	> -40
	1920-1980 (B1Tx)	> -23
	2110-2170 (B1Rx)	> -30
	2400-2500 (WiFi)	> -40

The CRF structure is modeled by two resonant nodes coupled by means of admittance inverters. The FIRs of the I/O nodes on the CRF structure are merged with the NRN reactance value of the side-placed ladder resonator, when it is connected to the two shunt resonators at each side. The proposed general synthesis technique of Chapter 2 for analytical and direct extraction of the prototype elements has been followed.

To validate the synthesis methodology, a proposed design is a Band 3 Tx. A bandpass with effective bandwidth of 4.3 % in the range of 1.710 GHz to 1.785 GHz is required. Main specifications are minimal waste of transmit power, more than 40 dB RX isolation and more than 40 dB WiFi band attenuation, resulting respectively in low bandpass IL, high selectivity and good out-of-band rejection. A detailed list of demanded specifications is in Table 4.1. The k_{eff}^2 is assumed to a value of 7.7 % for BAW ladder resonators, corresponding to $r = 14.7$.

In the filter synthesis, the aim is to obtain the set of transmission zeros and the return loss level of a generalized Chebyshev filtering function that fulfills the spectrum mask and the technological constraints imposed by the material system.

Our developed synthesis method has given a return loss level of 12 dB and transmission zeros at 1.683 and 1.804 GHz, which best suit the r and the masks constraints.

Next, the prototype elements have been extracted: $J_1 = 1$, $J_2 = 1.1043$, $J_3 = 1$, $J_4 = 1.5274$, $J_5 = 0.7347$, $J_6 = 0.5335$, $J_7 = 0.7347$, $J_8 = 1.5274$, $J_9 = 1$, $J_{10} = 1.1043$, $J_{11} = 1$, $B_1 = -0.8713$, $B_3 = 2.0575$, $B_7 = 2.0575$, $B_9 = -0.8713$, $b_2 = -1.36$, $b_4 = 1.57$, $b_5 = 0.201$, $b_6 = 0.201$, $b_8 = 1.57$ and $b_{10} = -1.36$.

The imposed spectrum mask and the material system r can be obtained allowing symmetry on the resonators of ladder cells, as we can observe from the normalized frequencies. However, in a situation with stringent

TABLE 4.2: Elements of designed Ladder-CRF combined filter for application to Band 3 Tx.

Parameters Ladder Cells			
Elements	f_s (GHz)	r	C_0 (pF)
R_1 & R_4	1.7460	14.7	2.09
R_2 & R_3	1.6827	14.7	3.14
Parameters CRF Cell			
L_{m1} & L_{m2}	C_{m1} & C_{m2}	C_{01} & C_{02}	K
175.71 nH	0.0477 pF	0.5996 pF	49.4 Ω

constraints, the synthesis tool will provide asymmetry to the structure elements to give more freedom and fulfill the specifications.

On completion of the prototype elements extraction, we are ready to make its equivalence with the physical filter. The primary elements of resonators, capacitance ratio r , resonance frequency f_s and static capacitance C_0 , building up the ladder cells (R_1 , R_2 , R_3 and R_4) can be extracted and also the elements that model the CRF according to Fig. 4.5.

Table 4.2 summarizes the parameters of the proposed filter. We can observe that the two series resonators (R_1 and R_4) are equal, and the two shunt (R_2 and R_3) are too, caused by the symmetry on the transmission zeros and network. In a general situation, resonators may be different, for example, in the case that the impedance inverter K in the CRF is limited to a manufacturable value. Then, the constraint drives the synthesis tool to an asymmetric network solution, in order to fulfill the whole set of requirements.

The hybrid configuration of ladder and CRF filter has been simulated and the frequency response of the filter designed for Band 3 Tx application is shown in Fig. 4.13. For the simulations, we take into account the loss effects by means of the Q parameter which is assumed to a value of 800 for the whole set of resonators.

Regarding the obtained filter response, we can observe that the flyback effect present in ladder filter responses has been solved with the combined topology, thus the transmission response has a decreasing tendency as it gets away from the passband. This fact is advantageous to fulfill, above all, the WiFi attenuation requirement. The number of reflection zeros within the passband is 6 equal to the filter order.

In addition, the response keeps the high selectivity feature, as the trans-

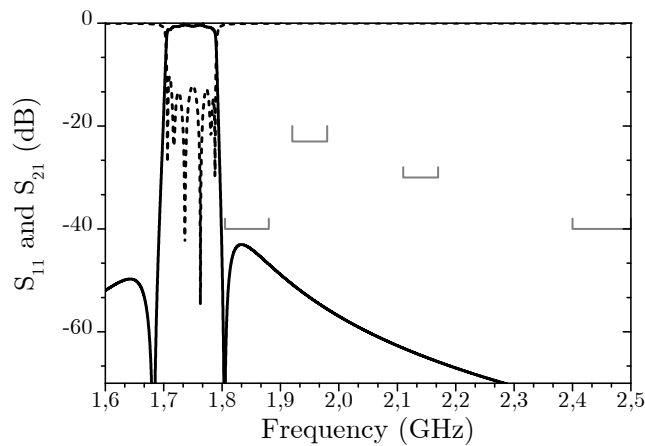


FIGURE 4.13: Simulated transmission and reflection response of the designed hybrid filter for Band 3 Tx combining ladder and CRF cells.

mission zeros of the response, produced by the ladder cells, are placed close to the band. The extreme steep roll-off overcomes the challenge of high Rx isolation of acoustic FDD duplexer, with attenuation levels better than 40 dB for the Rx frequency range.

The hybrid filter utilizes BAW technology to achieve a high isolation as well as high rejection at far stopbands. Based on this integrated design, the insertion loss has not suffer even though ladder and CRF sections are connected. Fig. 4.14 shows the return loss and the insertion loss minimum levels which are around 10.5 dB and 1.5 dB within the passband, respectively. Also, the 70 dB of attenuation at 2.3 GHz are achieved without degradation of insertion loss.

4.4 Summary

The transfer function of an inline nodal approach based on resonating and nonresonating nodes with transmission zeros at finite and infinite frequencies is key to make sure that selectivity and far out-of-band rejection is accomplished on a filter. Using a consequent relation of the lowpass prototype network with realizable building blocks by acoustic wave technology, some of the possible inline configurations can be associated with BAW or SAW technology.

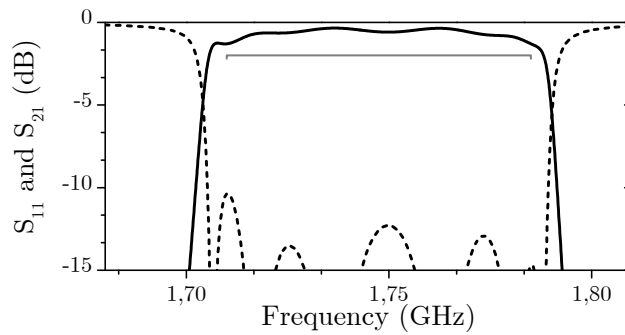


FIGURE 4.14: Passband simulation Insertion Loss and Return Loss of designed hybrid filter for Band 3 Tx.

In this chapter, we have demonstrated the suitability of our synthesis methodology extended to hybrid filters, fully leveraged on a systematic and flexible synthesis which accommodates acoustic-wave technological constraints. Therefore, we have a method that integrates technology, synthesis and topology.

We have provide equivalent circuit models in the lowpass prototype domain to be associated with acoustically coupled resonators filters, such as the Coupled Resonator Filters in BAW and the Dual Mode SAW.

In order to verify the proposed design approach, a synthesis example of a hybrid filter with ladder and CRF cells for application on Band 3 Tx has been computed, while taking into account the particular constraint of capacitance ratio imposed by the BAW technology.

The introduced hybrid integrated BAW filter helps to mitigate the flyback problem of conventional ladder filters, while it fulfills the high isolation requirements for duplexers. Although ladder and CRF blocks are used in the filter, there is no degradation effect in the IL, because the synthesis considers the integrated hybrid filter as a whole entity. The insertion losses are lower than 2 dB in the whole band.

5

ACOUSTIC WAVE FILTERING T-JUNCTION POWER DIVIDERS

Power dividers and bandpass filters are usual passive components at modern microwave systems. Power dividers are used to divide/combine signals and they are usually needed in an antenna feed network, or balanced circuits and then the RF filters select the frequency band of operation. In a conventional system, the two blocks are often connected to split and filter signals, which produce large circuits with an increase of the insertion loss. But two important features concern the design of wireless communications RF Front-end modules: the physical size reduction and the system functionality integration. Acoustic wave technologies lead more and more the important segment of RF filters and duplexers solutions for cellular systems and other mobile communications in the user segment. Acoustic wave technology is extensively used because the high level of miniaturization and scalability.

The strategy of combine an splitter and a filter has been followed in our work, where high-quality factor acoustic wave resonators are used. Utilizing acoustic wave filters to realize the filtering structures can provide the strengths of the acoustic wave technology to the power divider such as reduction in the size on a power divider. Therefore, we leverage our methodology of synthesis with acoustic-wave resonators to design power splitters with realizable configurations in BAW or SAW. In this chapter, two different filter configurations have been applied: the first one is based on ladder topologies which provide high selectivity and the second one is based on acoustically coupled resonators, such as the CRF structures to generate bandpass responses.

5.1 Introduction to filtering power dividers

An extensive and growing research has investigated on the power dividers focusing the design consideration on the size reduction and the higher functional integration. Firstly, efforts were to develop size reduced dividers with harmonic suppression. The authors in [88–90] reported a series of new configurations and structures to assemble compact designs drawn on planar and quasi-planar technologies. In [88], reduced line lengths from $\lambda/5$ to $\lambda/12$ Wilkinson power dividers, using planar transmission lines, are designed employing capacitive loading to reduce lines and to match the corresponding characteristic impedance. However, the correspondence of the impedance is only at one frequency and then the bandwidth is reduced. In [89], the suppression of two harmonics is leveraged on the two different resonance frequency signal rejections generated by two spiral-shaped Defected Ground Structures (DGS) with different size. Furthermore, the slow-wave effect of the DGS reduce the size of the $\lambda/4$ branches, but the overall Wilkinson power divider area is limited by the two DGS in cascade of each branch. In [90], by using a stepped impedance interdigital coupling element, the conventional $\lambda/4$ line sections can be replaced and then reduce size. In addition to the in-band power splitting, its response possesses harmonic suppression at both lower and upper stopbands. However it does not exhibit a satisfactory filtering characteristic.

Secondly, several studies on power dividers have integrated filtering characteristics which have efficiently resulted in a miniaturization of the whole RF system. References [91–94] reported bandpass-response power divider structures which merged the two individual components. The dual-functional approach bring about a number of benefits such as significant device size decrease, reduced insertion loss and lower power consumption. The strategy to realize a power divider embedded with bandpass filters in [91, 92] is to replace each $\lambda/4$ transformer of the conventional Wilkinson power divider with filters. The synthesis employs the even- and odd-mode method. The designs are implemented with microstrip technologies. In [91], coupled lines for the transmission structure are used as impedance inverters for bandpass response on the splitter. To get isolation between the outputs, elements are added to the output of the filters open ends. In [92], net-type resonators construct miniaturized coupled resonator filters to replace the impedance transformers. The designed dividers feature high selectivity and improve out-of-band rejection.

By using a multi-port coupled-resonator network defined in [46], an opti-

mization of the multi-port coupling matrix was performed in [93] and [94] to get the dual-functional property. As the 3-three port junction dividers in [93, 94], are lossless and reciprocal, the problem in the response is the poor output ports isolation. In [93], a synthesis method for multiple coupled resonators deals with arbitrary topologies of Chebyshev functions for multiple output circuits. The design procedure is based on a optimization of the coupling matrix to implement three-port power dividers. The waveguide-based circuits are very bulky hence the dimensions are not suitable for miniaturization, whereas they supply low insertion loss and high power handling capability.

On the basis of acoustic wave technology, the next two sections provide a detailed explanation and examples of T-junction power dividers integrated with two different configurations: one is ladder topology and the other uses CRF building blocks. The three-port T-junction divider networks developed are, according to general properties, lossless and reciprocal because it is a passive network with isotropic materials. Nevertheless, it is impossible to have the three ports matched in a three-port network to accomplish the unitary condition [69].

5.2 Power divider ladder topology

Our motivation was to apply acoustic wave technologies as candidates to size shrinkage of power dividers. We have extended the design methodology offering a solution with complete spectrum mask fulfillment and ready to accommodate technological constraints for power splitter in micro-acoustic technology with ladder configuration. In the section, the modeling and design steps of the filtering power dividers are discussed for a case with arbitrary power split ratio. Moreover, we include two examples of equal and unequal filtering power divider. Main features of the proposed devices are: arbitrary power division, integrated functionality of the power split and filtering with transmission zeros near the passband.

The approach to design three-ports dividers is based on general coupled resonators and NRN properly arranged to include the realization of acoustic resonators. Then, the synthesis of the proposed dividers employs the synthesis methodology similar to that of ladder filters.

The configuration of the proposed two-way power divider with an arbitrary power division ratio and bandpass response is depicted in Fig. 5.1. It consists of two filtering structures and its three ports are loaded in real

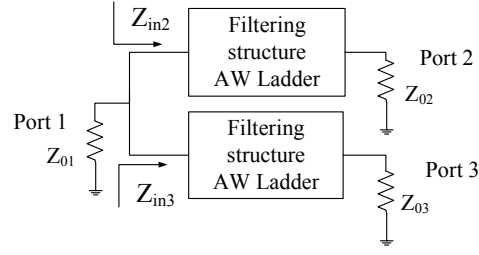


FIGURE 5.1: Structure and analysis of the presented bandpass-response power divider.

impedances Z_{01} , Z_{02} and Z_{03} . The input power from port 1 is transmitted to ports 2 and 3 through the filtering structures. Consequently, the transmission responses S_{21} and S_{31} are defined by the two filtering blocks. The input power P_1 is split between the two outputs. The division ratio, α^2 , is the relation between the output powers of ports 2 and 3, P_2 and P_3 respectively:

$$\frac{P_2}{P_3} = \alpha^2. \quad (5.1)$$

The division ratio influences on the maximum values of the insertion loss.

From Fig. 5.1, the proposed configuration allows to address the synthesis considering the two filtering blocks apart from the power divider taking into account necessities for the whole splitter. Next, we analyze how to fulfill arbitrary power ratios. In Fig. 5.1 two input impedances of Z_{in2} and Z_{in3} are indicated and they are expressed as:

$$Z_{in2} = Z_{01} \frac{1 + \alpha^2}{\alpha^2} \quad (5.2)$$

$$Z_{in3} = Z_{01} (1 + \alpha^2). \quad (5.3)$$

For each individual filtering structure, it is necessary an impedance transformation within the filtering structure. The input impedances Z_{in2} and Z_{in3} should be converted into the terminations impedances at ports 2 and 3, Z_{02} and Z_{03} respectively. By using the above-described equations the parameters of the proposed divider can be determined. Arbitrary power division ratios are obtained by setting the impedance transformation of the filtering blocks. Then, a two-way splitter can be classified into two types: the equal power division ones and the unequal power division ones.

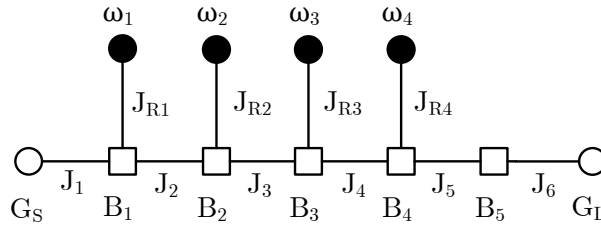


FIGURE 5.2: Topology of the filtering structure prototype network for $N = 4$ allowing different source and load normalized conductances.

5.2.1 Fully Canonical Filtering Power Divider

The characteristic transfer function of both bandpass filters is equal, only the impedance terminations have different values according to the required power division ratio. We propose to use a ladder-type filter for each output branch of the three-port network (Fig. 5.1) so we get transmission zeros on the filtering response. The synthesis methodology employed for each individual filtering structure consists on extracting the elements of the lowpass prototype network and then denormalizing to obtain the realizable ladder structure. Ladder filters describe fully canonical responses where the number of attenuation poles at finite frequencies equals the degree of the filter (N) resulting in a lowpass prototype of inline cascaded singlets of NRN coupled with resonating nodes.

In order to describe the topology of the lowpass prototype network equivalent to the ladder-type bandpass filter with impedance transformation, an inline network like the nodal representation of Fig. 5.2 is required. Because of the use of the extra NRN without a coupled resonator as a last node it is possible to perform the impedance transformation in the filtering structure. The prototype network shown in Fig. 5.2 is able to describe the fully canonical filtering characteristic for a ladder filtering configuration and it gives the required degree of freedom to implement a network where different normalized source and load conductances are considered.

The first step in the synthesis is to set the following filter parameters: the order, the bandwidth, the center frequency, the return loss, and the frequencies of the finite transmission zeros. The recursive approach allows to meet the characteristic polynomials of the general Chebyshev function. Moreover, the transfer and reflection functions of a 2-port network S_{21} and S_{11} may be written as an expression of the characteristic polynomials. The lowpass prototype equivalent network is arranged in order to deal with the

synthesis of a ladder filter. The second step is to determine the elements of the prototype circuit by means of the extraction approach of Chapter 2. The close expressions to extract last element parameters of a situation where there are an NRN coupled with a resonator and an NRN alone just coupled with the load conductance (G_L) were expounded.

On completion of the prototype circuit synthesis, we are ready to make its equivalence with the MBVD modeled filter. The prototype enables to accommodate the filtering function into the topology network of MBVD unit cells modeling the acoustic wave resonators and reactive elements. After the MBVD of each resonator is obtained, the primary elements (f_s , r and C_0) of all the resonators building up the ladder filter can be extracted and analyzed in order to accommodate technological constraints.

Despite this methodological approach, the synthesis process must consider the stringent technological constraints imposed to the resonators. A fixed capacitance ratio on a set of resonators can be imposed as a constraint on the systematic design process to procure a solution accommodating the material system.

On the prototype circuit it has been illustrated that the addition of an alone NRN node helps to make the I/O conversion of each individual filtering structure. Consequently, in a physical filter, the proper equivalence at the bandpass center frequency of this frequency-independent susceptance/reactance is a reactive element. The extraction procedure analytically computes their reactance nature and values.

Furthermore, in regard of the power divider performance, the connection of the two filtering blocks should be without a damaging interaction. To this aim, it is important that each individual filtering network provides the same reflection response phases ($\angle S_{11}$) at the point of the connection. The objective of the phase requirement is to get properly assembled the two output transmission signals.

5.2.2 Examples and the analysis of miniaturized filtering power dividers

The concept developed for synthesis of ladder-type power divider is applied here to illustrate it with two design examples with different power division ratios and different number of resonators. The first example is an equal power divider with a filtering order 4. The second example considered gets unequal power split and a 3rd-order filtering response. The two proposed

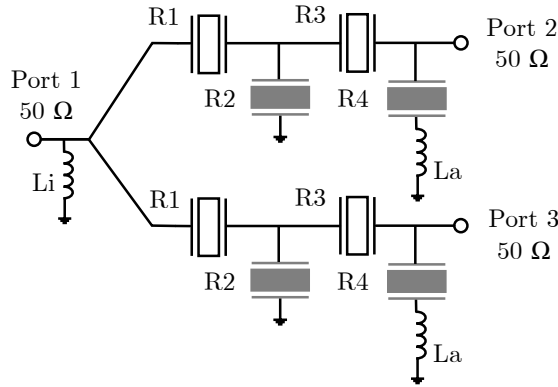


FIGURE 5.3: Filtering equal power divider for RX W-CDMA with BAW resonators for miniaturization.

implementations with bandpass response are designed to satisfy the receiver W-CDMA communication band I specifications with BAW technology. For the application, the center frequency band is 2.14 GHz and a fractional bandwidth about 3% is considered.

5.2.3 Design of an equal power divider

An eight BAW resonators 3-dB power divider has been designed and it has the topology depicted in Fig. 5.3. The resultant circuit using ladder-type BAW filters is composed by a total of 4 series and 4 shunt BAW resonators, one input shunt inductor and two inductors in series with the output shunt resonators ($R4$). The power divider has been made with two identical branches of BAW-ladder filters. Each filtering structure has been designed according to the systematic synthesis methodology proposed here and considering an I/O impedance conversion of 2:1 ratio on the filtering network, that is an $\alpha^2 = 1$. This scaling factor is required since both filter input ports are common in the power divider. External input or output reactive elements are connected to carry out the impedance conversion which is the equivalence of the NRN alone in the prototype network. Therefore, the L_i inductor is included in the network because of the topology.

The transmission zeros are placed in the specification definition process. After the allocation of transmission zeros, we generate the characteristic function of the prototype filter which for the example corresponds with the configuration presented in Fig. 5.2. Let remember that the synthesis

is realized considering the impedance transformation. Next, the prototype links with primary elements of a piezoelectric resonator: f_s , r and C_0 .

Consequently, the dependence of the r value of each extracted BAW resonator over the specified inband RL level of the synthesis, when transmission zeros are set, can be examined. Obtained results are similar to the one evaluated in section 3.4.2, however now considering a prototype configuration like the one in Fig. 5.2. The traces from the study show that for certain RL level we get an equal r value on resonators $R1$, $R2$ and $R3$.

Setting RL level to 16 dB gets a r value for the $R1$, $R2$ and $R3$ resonators of 20.7, equivalent to a $k_{eff}^2 = 5.6$ %. The selected value can be implemented with AlN, which is a piezoelectric film material commonly used in BAW technology [95] and provides effective coupling coefficients around the selected value considering the electrodes. However, the transmission response needs on $R4$ a lower r of 16.7. This reduction is accomplished by placing an inductor (L_a) in series with the mentioned BAW resonator which is observed in Fig. 5.3. Therefore, the two L_a inductors are introduced because of the technology.

Synthesis

The characteristic polynomials of the filter evaluated with the proposed RL level of 16 dB and transmission zeros at normalized frequencies $\omega_1 = -1.88j$, $\omega_2 = 1.94j$, $\omega_3 = -1.88j$ and $\omega_4 = 2.55j$ in rad/s give the normalized prototype elements according to Fig. 5.2 as follows: $B_1 = 1.3473$, $B_2 = -2.1177$, $B_3 = 2.8496$, $B_4 = -2.5603$, $B_5 = -0.6671$, $J_{R1} = 1.6703$, $J_{R2} = 1.9145$, $J_{R3} = 2.1792$, $J_{R4} = 2.1063$, $J_1 = J_2 = J_3 = J_4 = J_5 = J_6 = 1$. In order to provide the required impedance transformation we set $G_S = 1$ and $G_L = 2$, according to the terms in Fig. 5.2. To compute B_4 and B_5 the negative sign in (2.61) has been selected. An inversion between the corresponding input and output nodes between the filtering network in Fig. 5.2 and one filtering branch in Fig. 5.3 has been carried out in order to merge the two shunt inductors in just one. The value of the input inductor L_i is 2.79 nH. Each series inductor, L_a , attached to the $R4$ resonators is set to a value of 0.61 nH, for this example. Finally, the computed static capacitance (C_0) and the resonance frequency of each resonator (f_s) with the corresponding capacitance ratio (r) of the transductor are summarized in Table 5.1.

TABLE 5.1: Design parameters for the resonators for W-CDMA equal power divider.

Design Parameters	Resonators			
	$R1$	$R2$	$R3$	$R4$
f_s (GHz)	2.164	2.084	2.146	2.095
r	20.7			
C_0 (pF)	0.58	4.24	0.70	1.60

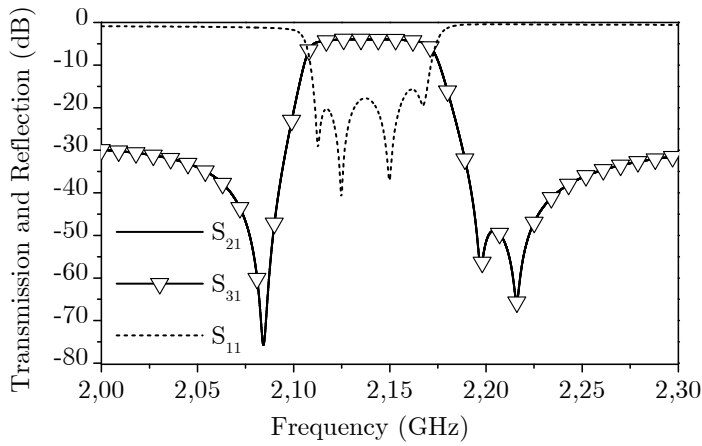


FIGURE 5.4: Simulated transmission and reflection responses with loss for the proposed 3-dB filtering power divider on W-CDMA band.

Results

Using the previously computed parameters, the 3-dB power divider has been simulated and the results are given in Fig. 5.4. For the simulation, we take into account the loss effects by means of the quality factor Q parameter which is assumed to a value of 1000 for the whole set of resonators and 25 for the inductors. From the simulated response, the performance of the power divider is in accordance with the 3 dB power division ratio and filtering bandpass response. The considered filtering blocks place a number of transmission zeros equal to the order of the filter in each individual branch (S_{21} and S_{31}). The four transmission zeros enhance the near out-of-band rejection. The resulting RL level within the passband is of 15.7 dB and an Insertion Loss (IL) level of 4 dB at the center frequency, which includes the 3 dB inherent from the split. At the lower and the upper edges

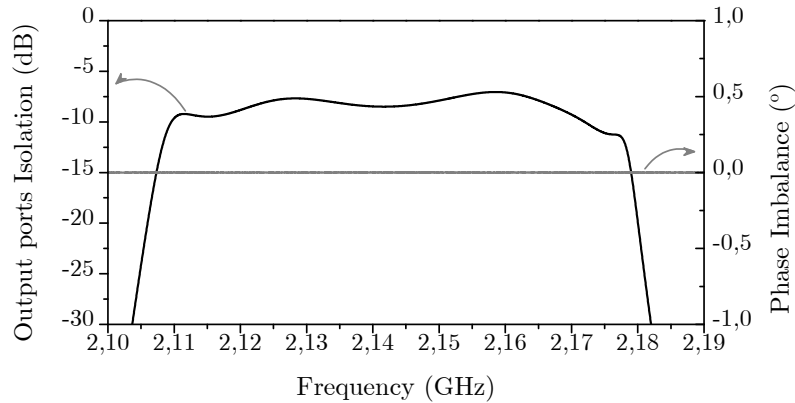


FIGURE 5.5: Simulated isolation and phase imbalance responses between outputs for the proposed 3-dB filtering power divider.

of the passband the IL are of 5 dB and 5.2 dB, respectively. Both output transmission signals are in-phase, verified by the phase imbalance graph on the right axis of Fig. 5.5. The isolation response in Fig. 5.5 over the left axis shows that the output ports are not isolated, with $|S_{32}|$ about 7 dB through the passband. The low level for the isolation and the two output ports not matched is expected, because it is as a typical feature for lossless reciprocal power dividers like the proposed here. Therefore, there will be no isolation between the two output ports and there will be a mismatch looking into the output ports.

5.2.4 Design of unequal power divider

An unequal power divider has been designed with a total of six resonators and the synthesis has been done according to the procedure proposed here for a power division ratio α^2 of 2. Following (5.2) and (5.3) for all ports at 50Ω , Z_{in2} is $3/2 \cdot 50 \Omega$ and Z_{in3} is $3 \cdot 50 \Omega$. The divider will use the topology depicted in Fig. 5.6(a). Two ladder filtering branches form the splitter, each one is made up with two shunt resonators, one series resonator and a series inductor at the output. Output inductors L_{o1} and L_{o2} are necessary for an impedance transformation on the filtering block and their values are computed by the extraction engine. The parallel capacitance C_a to resonator $R3b$ is introduced for technological material system accommodation.

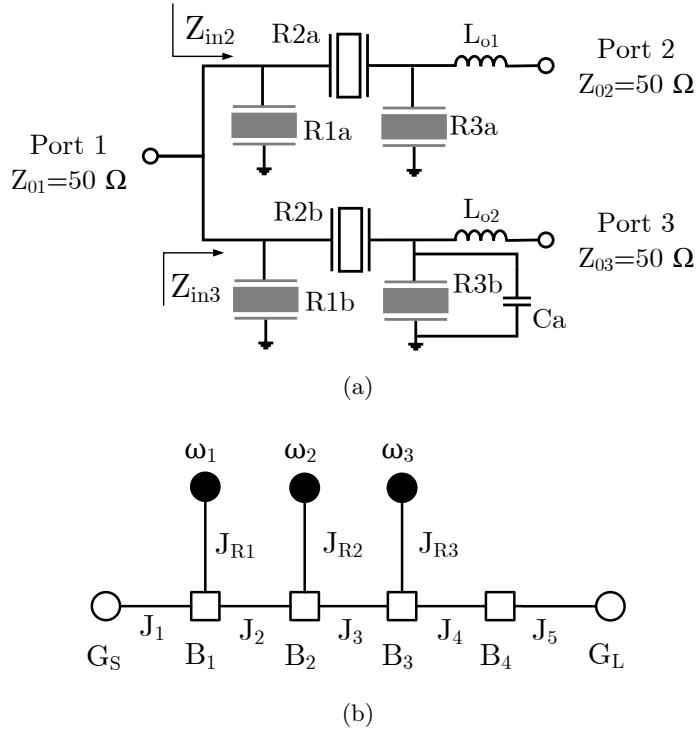


FIGURE 5.6: Filtering unequal power divider for Rx W-CDMA Band 1 application. (a) Schematic network configuration for power division ratio $\alpha^2 = 2$ with a total of 6 acoustic wave resonators. (b) Prototype network nodal diagram with the topology proposed for each filtering block of order $N = 3$.

Synthesis

We have considered two different extraction processes which are necessary for each of the filtering structures. The circuit between ports 1 and 2 should make an impedance conversion of Z_{in2} into $Z_{02} = Z_0$, so in this case we set $G_S = 1$ and $G_L = 2/3$ following Fig. 5.6(b). And the circuit between ports 1 and 3 should also convert the impedance of Z_{in3} into $Z_{03} = Z_0$, then we set $G_S = 1$ and $G_L = 1/3$. Like it was performed with the previous example, we proposed a capacitance ratio of $r = 16.4$, equivalent to k_{eff}^2 of 7%, as input parameter for our synthesis method. Moreover, the value is reasonable and feasible to get with AlN piezoelectric material. Next, by setting the transmission zeros at normalized frequencies $\omega_1 = -2.125j$, $\omega_2 = 2.44j$ and $\omega_3 = -2.58j$ in rad/s, the analysis of the r is provided

TABLE 5.2: Design parameters for the resonators for W-CDMA unequal power divider.

Design Parameters	Resonators		
	$R1a/R1b$	$R2a/R2b$	$R3a/R3b$
f_s (GHz)	2.077	2.147	2.064
r		16.42	
C_0 (pF)	2.33 /	0.41 /	3.72 /
	1.165	0.205	1.861

and the selected RL value is of 12 dB. The configured parameters lead to a situation where all the resonators, except resonator $R3b$, meet the r value of 16.4 that was proposed for this design. However, the effective r value required for $R3b$ is of 19.6. Let note in Fig. 5.6(a) that an additional capacitance, Ca , in parallel with the shunt resonator $R3b$ is introduced in order to accomplish the higher effective $r = 19.6$, while $R3b$ remains with a value $r = 16.4$ of the material system.

The extracted prototype elements according to the terms of Fig. 5.6(b) are: $B_1 = 2.2153$, $B_2 = -2.5644$, $B_3 = 3.5371$, $B_4 = 0.4968$, $J_{R1} = 2.1623$, $J_{R2} = 2.3635$, $J_{R3} = 2.7213$, $J_1 = J_2 = J_3 = J_4 = J_5 = 1$ and correspond to the circuit from port 1 to 2. For the other circuit branch, only the $B3 = 4.2196$ and $B4 = 0.4843$ values have varied due to the different conductance termination. In both cases, to compute the elements the positive sign in (2.61) has been selected. Then the magnitude transmission response on the two output power divider will present the same transmission zeroes, however, different in-band IL levels will be achieved.

Once we get the prototype elements, it is necessary an impedance de-normalization which is different in each filtering block. In the circuit from port 1 to 2, it is necessary to de-normalize with 75Ω because the I/O normalized impedance conversion is of 1:2/3, so it gives $Z_{in2} = 3/2 \cdot 50 = 75 \Omega$ and $Z_{02} = 50 \Omega$. Similarly for the circuit from port 1 to 3, an impedance of 150Ω is used to de-normalize the impedance conversion of 1:1/3 and gives $Z_{in3} = 3 \cdot 50 = 150 \Omega$ and $Z_{03} = 50 \Omega$. The equivalent impedance of the Z_{in2} and Z_{in3} in parallel is Z_{01} of 50Ω , so all the three terminating impedances at ports of the power divider are equal.

The Table 5.2 summarizes the electrical parameters of the impedance characteristic of the resulting BAW resonators after the synthesis process. As

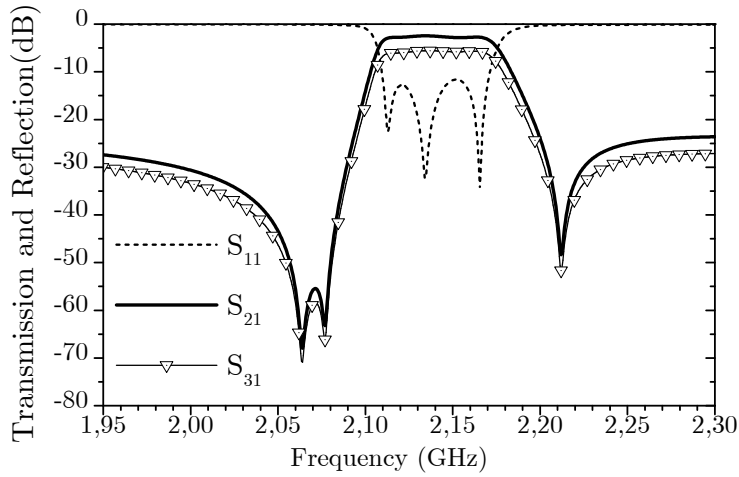


FIGURE 5.7: Simulated transmission and reflection responses with loss for the proposed unequal filtering power divider on W-CDMA band.

expected, C_0 and hence, the active areas of the resonators from the filtering structure between port 1 to 2 are the double than the values of the corresponding resonators for the structure between port 1 to 3, labeled with b . The relationship is caused by the ratio between the de-normalization impedances at both filtering blocks which is of factor 2. The values of the output series inductors are $L_{o1} = 2.77$ nH and $L_{o2} = 5.40$ nH. The capacitor C_a attached to the resonator $R3b$ is set to a value of 0.34 pF.

Results

The frequency response obtained from the simulation analysis of the unequal power divider is shown in Fig. 5.7, where a Q factor of 1000 is considered for BAW resonators and the embedded capacitance and 25 for external inductors. From the graph, we can see that for both output transmission responses S_{21} and S_{31} of 3rd-order, three transmission zeros appears at frequencies near the transition band in each response. The RL level within the passband is of 11.7 dB.

Moreover, Fig. 5.8 displays in detail the IL level for each of the transmission responses, and evidences the unequal split achieved. The IL level for the output transmission response S_{21} at the center frequency is of 2.5 dB which include the inherent 1.79 dB (2/3) split loss of the corresponding I/O branch. For the transmission response S_{31} at the center frequency

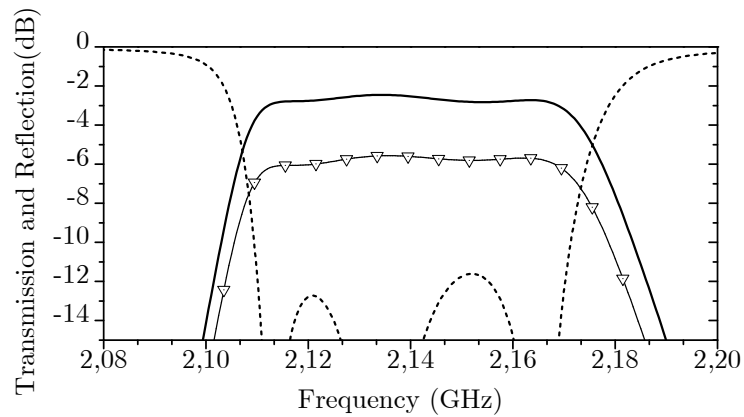


FIGURE 5.8: Simulated reflection frequency response in the passband region and both transmission responses with different power split corresponding to a power division ratio $\alpha^2 = 2$.

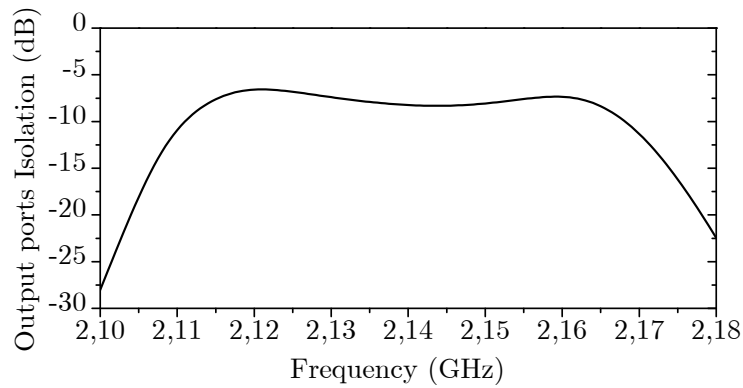


FIGURE 5.9: Simulated Isolation of ports 2 and 3 of the BAW unequal power divider

the IL level is of 5.6 dB corresponding to an inherent split loss of 4.8 dB ($1/3$).

It should be noted that designed power divider only have one of the ports matched, the input port, because it is a lossless reciprocal 3-port network which exhibits the problem that it is not matched at all the ports, likewise, the two output ports are not isolated. In Fig. 5.9, the isolation is about 6 dB around the passband. In this case, there will be also a mismatch looking into the output ports.

5.3 Power divider CRF topology

Authors in [93] introduced the concept of characteristic polynomials for the design of filtering power divider based on coupled resonator filter theory. Leveraged on this synthesis approach for power dividers, our motivation was to discuss the possibility of applying the CRF basic configuration in order to design a splitter which contributes to the stringent miniaturization demands on microwave devices. Coupled Resonator Filters (CRF) offer a compact design and are described as a network of multiple coupled resonators. We look for possible realizations including CRF sections, that based on the coupling of resonators constitute a 3-port structure with a response which is combination of power divider and filter.

The synthesis approach applied in this section follows the general idea of filter design from previous chapters. Based on a Chebyshev filtering function described by the characteristic polynomials, a prototype circuit representing the desired filtering function is extracted, and finally, the prototype is transformed according to equivalent models into an integrated structure of the selected technology. The two facts that differ primarily from previous procedure are that the design directly generates a three-port device because the characteristic polynomials are defined for a three-port network with power split and that now there is not a direct pole-extraction to build up the prototype. The prototype circuit is generated by the optimization of the multi-ports coupling matrix which defines the multiple coupled resonator network.

Synthesis and design method for the power divider with bandpass filtering response has been presented in [93]. Here we give a brief description of the coupling resonant theory for the synthesis of three-port circuits. The characteristics to model the filtering power divider according to the CRF structures is deduced.

5.3.1 Coupling matrix synthesis of filtering power divider

The coupling matrix with N coupled resonators for multi-output ports follows the generalization of the matrix of section 2.4. In this case, the two-way network to be implemented with CRFs do not exhibit NRNs, hence, there are N coupled resonators and 3 ports included on the defined sub-matrix \mathbf{M}_P . In section 2.5, the nodal admittance matrix $[\mathbf{A}]$ for such a three-port coupling matrix \mathbf{M} has been defined in (2.15) and the derived

scattering parameters as a function of $[\mathbf{A}]$ in (2.18) and (2.19), too.

The characteristic polynomials of the proposed divider are related to the S-parameters because they describe filtering functions. The definition of the transmission and reflection functions are by the same three characteristic polynomials that in a two-port filter because they are obtained from the Chebyshev transfer function. So we can express them as follows:

$$S_{11}(s) = \frac{F(s)}{E(s)}, \quad S_{21}(s) = \frac{P(s)/\epsilon_1}{E(s)}, \quad S_{31}(s) = \frac{P(s)/\epsilon_2}{E(s)} \quad (5.4)$$

the meaning of $E(s)$, $F(s)$ and $P(s)$ is not different than the described for a filter as well as its formulation. The difference now is the two new normalization constants ϵ_1 and ϵ_2 of the two transmission coefficient and how variates the equation of the conservation of energy for a 3-port network given by:

$$S_{11}(s) S_{11}^*(s) + S_{21}(s) S_{21}^*(s) + S_{31}(s) S_{31}^*(s) = 1. \quad (5.5)$$

The term division ratio α^2 from previous definition relate the two transmission:

$$|S_{21}(s)|^2 = \alpha^2 |S_{31}(s)|^2. \quad (5.6)$$

As a consequence, the denominator polynomial $E(s)$ is computed once $F(s)$ and $P(s)$ are know as well as the normalizing constants by:

$$|S_{11}(s)|^2 = (1 + \alpha^2) |S_{21}(s)|^2. \quad (5.7)$$

and substituting (5.4).

For a Chebyshev transfer function, the normalization constants ϵ_1 and ϵ_2 specify the insertion loss of the transmissions $S_{21}(s)$ and $S_{31}(s)$:

$$\epsilon_1 = \sqrt{\frac{1 + \alpha^2}{10^{RL/10} - 1}} \left| \frac{P(s)}{F(s)} \right|_{s=\pm j}, \quad (5.8)$$

$$\epsilon_2 = \sqrt{\frac{1 + \alpha^2}{\alpha^2 (10^{RL/10} - 1)}} \left| \frac{P(s)}{F(s)} \right|_{s=\pm j}, \quad (5.9)$$

Observe now that the order of the polynomials $E(s)$ and $F(s)$ define the order of the filtering function, although the order does not correspond now with the total number of resonators.

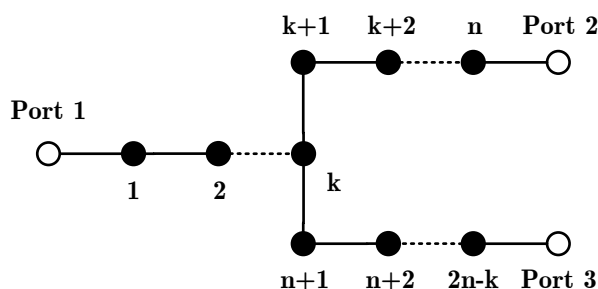


FIGURE 5.10: Nodal representation of a T-topology power divider.

The synthesis we follow uses coupling matrix optimization technique for the three-port coupled resonator divider. The optimization technique employed is very similar to the ones developed for coupled resonator filters. The variables to optimize are the coefficients of the multi-port coupling matrix. The aim is to minimize a cost function which in the literature have been reported in several ways [26, 96–98]. The cost function adopted is an update of the adopted in [26] for the inclusion of the power division ratio requirement. The optimization identify the desired response by characterizing the coupling matrix in terms of critical frequencies (poles and zeros) of the transfer function and the ripple factor. The optimization is used to find the coupling matrix of a defined topology according to the desired response.

A Matlab software has been programmed for the optimization, and it demonstrated success in generating coupling matrices for power dividers with any general Chebyshev filtering response for arbitrary topologies. Among the many possible topologies we propose to study power dividers with T-topology like the suggested in Fig. 5.10. The reason is the CRF technology selected, because single section do not generate cross-coupling topologies. Hence, filtering responses do not exhibit transmission zeros at finite frequencies, contrarily to the previous case in section 5.2. For a T-topology power divider, there is a k number of shared resonators and $n - k$ no-shared resonators at each output branch. The order of the filtering function at each output is n . The coupling coefficients $M_{k,k+1}$ and $M_{k,n+1}$ specify the power division of the two signal on each path. It has been verified among different optimizations of T-topologies power dividers, that the division ratio can be used to compute the couplings coefficients $M_{k,k+1}$ and $M_{k,n+1}$ on this topologies. Since one of the input to output paths describes a Chebyshev filtering function of n -th degree, the couplings coefficients between the corresponding n resonators for a two-port filter model can be obtained.

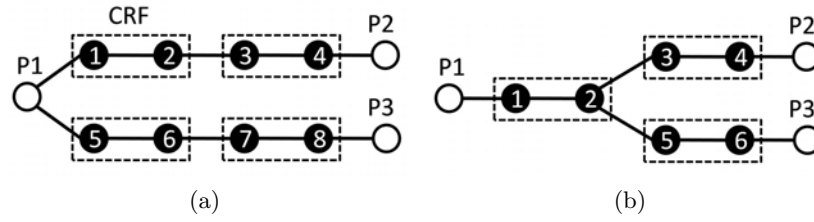


FIGURE 5.11: Two power dividers with bifurcated topologies proposed for 4-th order filtering function. (a) Topology with no-shared resonator, $k = 0$. (b) Topology with two-shared resonators $k = 2$.

The coupling M' on the two-port filter model between the resonators k and $k + 1$ presents a relationship with the couplings coefficients $M_{k,k+1}$ and $M_{k,n+1}$ of the T-topology power divider:

$$M_{k,k+1} = \sqrt{\alpha^2/(\alpha^2 + 1)}M' \quad (5.10)$$

$$M_{k,n+1} = \sqrt{1/(\alpha^2 + 1)}M' \quad (5.11)$$

5.3.2 T-topology power divider implemented with CRF sections

For the study of the BAW CRF technology expanded to the power divider idea we introduce proposals for generating 4-th order filtering functions according to Fig. 5.10, this is $n = 4$. Although with $n = 4$ there exists 4 possible T-topologies regarding to the value of $k = \{0, 1, 2, 3\}$, only the topologies with $k = 0$ and $k = 2$ have been considered because they are feasible to realize using CRF sections. For the other two cases new composition of layers would be necessary.

The two different topologies are studied and compared, they offer choices in feasible topologies for power dividers with CRF structures. Fig. 5.11 depicts the two structures of the power dividers. The first one in Fig. 5.11(a), consists of 8 coupled resonators arranged in two main-line output branches bifurcated from the input port. The second one in Fig. 5.11(b), consist of 6 coupled resonators arranged in a T-topology, where the two output branches bifurcate from an inter-resonator.

Both are 3-port networks and integrate a Chebyshev filter response for S_{21} and S_{31} . The filtering function has order 4 at each output, which is equal to the number of resonators in each input/output branch. In the case of

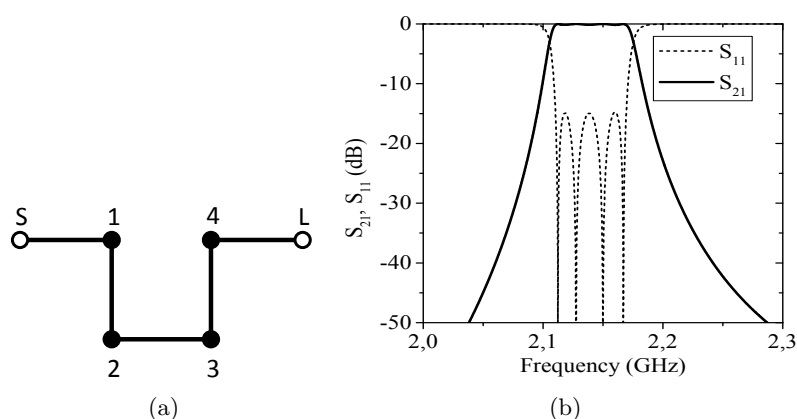


FIGURE 5.12: 4-pole CRF filter. (a) Nodal representation of the corresponding main-line configuration. (b) Response for the 4-pole CRF centred at 2140 MHz with 60 MHz of bandwidth.

TABLE 5.3: Requirements for the Rx WCDMA example CRF.

Passband Frequencies	2.11-2.17	GHz
$Z_S = Z_L$	50	Ω
Return Loss	20	dB

implementing a 3-dB power division, the couplings have equal values for both output branches. Even though, an arbitrary power division ratio can be also implemented, herein we focus on the equal ratio case for design simplicity.

In Chapter 4, we seen two CRF sections that are electrically connected through the electrodes of the lower resonators produce a 4-pole filter and constitute the most common CRF topology (Fig. 4.4(b)). The advantage is that the input and output ports are placed on the upper resonators. The nodal diagram of this main-line configuration is represented in Fig. 5.12(a) which corresponds to the 4-pole filtering structure composed by two CRF sections electrically connected.

Table 5.3 summarizes the filter specifications for an example working in Rx WCDMA band I. The values of the normalized couplings of the coupling matrix obtained are: $M_{S1} = M_{4L} = 1.0352$, $M_{12} = M_{34} = 0.9106$, $M_{23} = 0.6999$, indexed according to the nodal diagram of Fig. 5.12(a).

Once the normalized coupling matrix has been synthesized, the param-

TABLE 5.4: Properties of selected materials [80].

Material	Acoustic Impedance (10^7 kg/m ²)	Velocity (m/s)
W	9.98	5200
AlN	3.59	11000
SiO ₂	1.2	5600

eters which characterize the filter in the bandpass frequency of the microwave application are: the input/output external quality factors ($Q_{ei} = 1/(M_{Si}FBW)$) and the coupling coefficient ($k_{ij} = M_{ij}FBW$), where $FBW = 0.028$ is the fractional bandwidth. They denormalize the prototype and give a direct relationship with the physical structure of coupled resonators. The procedure followed for the first-order dimensioning is extensively developed in [80]. The CRF structure is evaluated by means of the Mason model which provides a useful equivalent circuit [23]. The good agreement of the model response and the measurements makes valid the model for BAW filters analysis and design.

Fig. 5.12(b) shows the simulated filter response of the proposed example composed of two CRF basic stages connected in series. The BAW CRF basic structure is composed by two AlN piezoelectric resonators with its electrodes of W. The coupling layers have been implemented by three layers (SiO₂-W-SiO₂). We appreciate the whole set in Fig. 4.4(b). Even if it is not represented in the figure, a Solidly Mounted Resonator (SMR) configuration has been used in all the CRF structures simulated. The set of layers on the Bragg reflector alternates SiO₂ and W films. Regarding the set of layers that form a CRF, reaching the same thicknesses among the CRF sections is aimed during all design procedures because uniformity on layer thicknesses simplifies the fabrication. Table 5.4 shows the properties of the materials used for the selected configuration of layers in a CRF. These values have been considered among all the proposed CRF structures of the paper. Furthermore the piezoelectric constant and the relative permittivity of AlN are 1.5 C/m² and 9.7, respectively.

Now we are ready to realize from a normalized coupling matrix the sizing of the CRF structure resulting. Therefore, we have the tools to implement a 3-port power divider with CRF section, such as the two topologies in Fig. 5.11.

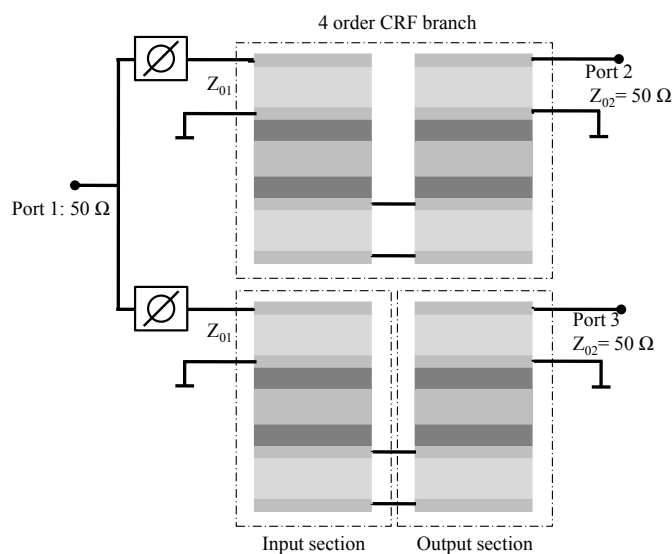


FIGURE 5.13: Filtering equal power divider with no-shared resonators build up of two identical 4 order CRF branches and a total of 4 CRF basic sections.

5.3.3 Topology I: No-shared resonators

The scheme of the physical structure for the topology of Fig. 5.11(a) is shown in Fig. 5.13. We note that two identical 4-pole CRF sections are considered for each branch which is composed by two CRF basic sections in series connection. The two identical order 4 CRFs are connected by their input ports to conform the 3-port power divider network. An input signal is applied to the upper electrode of the input resonator of each CRF branch and their lower electrodes are grounded. When the signal arrives to the output resonators of each branch they have the same amplitude and phase. Each output is produced between the pair of electrodes of the upper output resonators.

An important feature to take into account in this configuration is the impedance transformation produced in each individual branch if considered as a two-port filter. The input and two output port impedances are kept to $50\ \Omega$. Consequently, it is required to make an impedance transformation of 100:50 on each 4th-order CRF branch that forms the splitter. If the input of this 4-pole CRF is matched to an input port of impedance Z_{01} and an output port of impedance Z_{02} , then, when the two branches are connected like in Fig. 5.13, the input impedance of the resulting device

is $Z_{01}/2$. The input port of the power divider have two branch inputs in parallel, thus, the input impedance is $Z_{01}/2$. Meanwhile, the output ports have the corresponding impedance Z_{02} .

Given the particularities of the proposed power divider with no-shared resonators, a simplification on the design can be done. It consist on dimensioning one of the structures of the I/O branches, as they are identical, an deal with the impedance transformation. Therefore, if the filters of order 4 that make up each branch are designed at $Z_{01} = 100 \Omega$, the input impedance of the resulting power divider is 50Ω and if the output is designed with $Z_{02} = 50 \Omega$, both output impedances of the splitter device are 50Ω . This configuration leads in a resulting divider with the three ports at 50Ω . In the design of the CRF we control the matching of the upper resonators to different impedances. The input resonator (1), considering the two-port filter are designed to provide the required external quality factor (Q_{e1}) when they are coupled to an input port of 100Ω (Z_{01}) and the output port to provide the required external quality factor (Q_{e4}) but coupled to an output port of 50Ω (Z_{02}).

We have connected in parallel the two 4-pole CRF structures seen from the input, however for this parallel connection of the CRF structures some considerations and the addition of some external support elements are necessary. The input/output parallel capacitors of a CRF network (Fig. 4.5) are seen as NRN in the lowpass prototype (Fig. 4.3(b)) leading to a variation of the reflection phases. When several CRF sections are cascaded, we have include the corresponding effect of the static capacitors within the inverters coupling the resonators. Contrarily, when the sections are connected in parallel the assumption in incomplete.

For the parallel connection, it is required the addition of new elements, that in a way correct the phase effect produced by the static capacitance. The discussion of the problem was already dealt in [80]. For simplicity, we include ideal phase shifts according to the required phase. However, for practical implementations lumped networks or transmission lines can be considered. In order to compute the correction phase shift, we obtain, from one single CRF section before doing the connection in parallel, its reflection phase which has a value different than zero at the center frequency.

As a design example, a power divider for W-CDMA receivers has been synthesized following the topology of no-shared resonators of Fig. 5.13. The defined W-CDMA specifications follow Table 5.3. The synthesized normalized coupling matrix according to Fig. 5.11(a) obtained are: $M_{P1,1} =$

$M_{P1,5} = 0.732$, $M_{1,2} = M_{5,6} = M_{3,4} = M_{7,8} = 0.9106$, $M_{2,3} = M_{6,7} = 0.6999$ and $M_{P2,4} = M_{P3,8} = 1.0352$. Giving the coupling coefficients $M_{P1,1}$ and $M_{P1,5}$ and the division ratio $\alpha^2 = 1$, the representing coupling coefficient in the two-port filter presents a value of 1.0352, which agrees with the already synthesized 4-pole CRF filter.

In order to design this power divider with no-shared resonators we follow the simplification strategy of design only one CRF order 4 branch with impedance conversion. That fact implies that the coupling coefficient M' in the two-port model representative of $M_{P1,1}$ and $M_{P1,5}$ for the coupling between the input and the first resonator has a value of 1.0352. Hence, the same dimensioning approach that in the case of the 4-pole CRF is carried out, with the difference that Q_{e1} is computed for $Z_{01} = 100 \Omega$. Once the structure of this two-port filter model with impedance conversion computed, the simulation of the input reflection phase provide the value required for the phase shifter. The reference impedance for the phase shifter connected at the input is 100Ω , and the phase value is -120.5° .

The four CRF structures are composed by the same layer materials described for Fig. 5.12 and also considering SMR configuration. Table 5.5 shows the layer thicknesses of the CRF stacks. The four CRF stacks have the same layer configuration but different area. The area of the CRF sections corresponding to the input is $10.04 \cdot 10^{-9} \text{ m}^2$ each for this example. For each output section, the area is slightly different of the input sections; it is $10.57 \cdot 10^{-9} \text{ m}^2$. Despite the large number of layers required for the CRF structure, the thicknesses of the whole device remain equal, except for the top electrodes.

The simulated transmission and reflection responses of the power divider with the first topology are show in Fig. 5.14. Although a total of 8 resonators form the device structure the response of each output branch presents and embedded bandpass filtering response of order 4. The 20 dB input return loss and insertion loss in the passband around 3 dB agree with the specified design. The simulated inband isolation of the output around 6 dB, as can be seen in Fig. 5.14, is consistent with the 3-port network features because the device does not present good isolation. Results of phase of the two transmission response are identical, then both outputs are in phase.

TABLE 5.5: Layer thickness of the considered power divider for the topology I of no-shared resonators.

Structure part		Thickness (μm)	
		<i>Input section</i>	<i>Output section</i>
Upper resonator	Top electrode	0.216	0.208
	Piezoelectric		0.855
	Bottom electrode		0.207
Coupling layers	Top layer		0.555
	Middle layer		1.048
	Bottom layer		0.555
Lower resonator	Top electrode		0.374
	Piezoelectric		0.357
	Bottom electrode		0.374

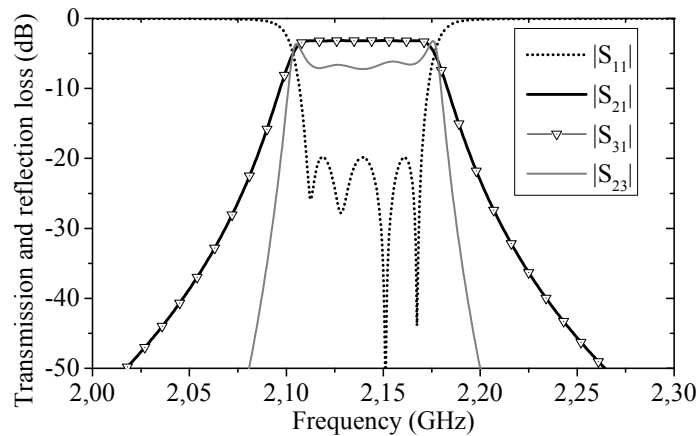


FIGURE 5.14: Filtering equal power divider response with topology I for W-CDMA application.

5.3.4 Topology II: Two-shared resonators

The scheme in Fig. 5.15 depicts the physical structure composed by 3 CRF for the topology of Fig. 5.11(b). In the two output ways, one CRF section is common for the input signal and then it is bifurcated in two identical CRFs (3-dB division) forward to the two output ports. Thus, 3 basic CRF structures are electrically connected through the electrodes of the lower resonators. Thereby, the coupling between the connected lower resonators of all the three CRF sections takes place in the electric domain, and it is caused in part by the intrinsic capacitances of the resonators. The pair

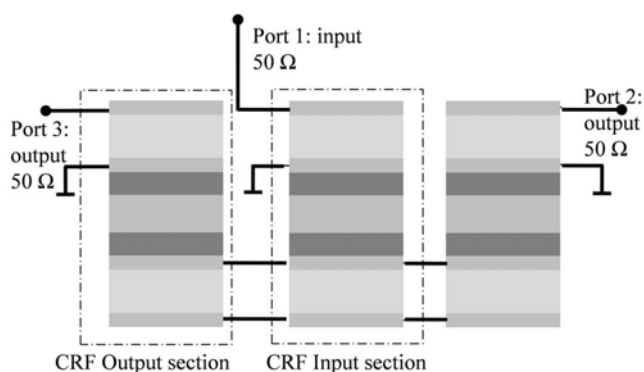


FIGURE 5.15: Filtering equal power divider with two-shared resonators based on 3 CRF basic sections.

of upper electrodes of the middle CRF (Fig. 5.15) is used as input port. The pairs of upper electrodes of the side-placed CRFs are used as output ports.

We define the input impedance from the connection point of the lower resonators forward the input port as Z_{in1} . In the same way, Z_{in2} can be defined as the input impedance from that connection point forward the output ports. In order to satisfy the symmetry in the equivalent filter response, Z_{in1} of the input section must match Z_{in2} of the output sections. As the two output CRF sections on the divider are equal and in parallel, then Z_{in2} is seen as the equivalent impedance of the parallel intrinsic capacitances of each output CRF section. Therefore, an intrinsic capacitance of double value leads to double area size.

In [99], we used the double area size feature to design the 3-dB power divider with two-shared resonators applying a simplification with a two-port filter model and then a transformation to a 3-port power divider resizing the area of the output sections. Nevertheless, this simplification is no longer required since we are able to synthesize the normalized coupling matrix and dimensioning the proposed splitter of Fig. 5.15 by means of the coupling coefficients and the external quality factors. The sizing of the layers is also based on the Mason model for direct relation.

In order to carry out an example, a CRF power divider for W-CDMA receivers has been synthesized following the topology of two-shared resonators of Fig. 5.15. The defined W-CDMA specifications also follow the listed in Table 5.3, in order to provide suitable comparisons.

TABLE 5.6: Layer thickness of the considered power divider for the topology II of two-shared resonators.

Structure part		Thickness (μm)	
		<i>Input section</i>	<i>Output section</i>
Upper resonator	Top electrode	0.214	0.205
	Piezoelectric		0.877
	Bottom electrode		0.198
Coupling layers	Top layer		0.556
	Middle layer		1.046
	Bottom layer		0.556
Lower resonator	Top electrode		0.373
	Piezoelectric		0.358
	Bottom electrode		0.373

Applying the proposed design procedure for filtering power dividers, the terms coefficients of the coupling matrix according to Fig. 5.11(b) are: $M_{P1,1} = M_{P2,4} = M_{P3,6} = 1.0352$, $M_{1,2} = M_{5,6} = M_{3,4} = 0.9106$ and $M_{2,3} = M_{2,5} = 0.4949$. Denormalizing the prototype the dimensions of the three CRF stacks can be obtained. The CRF structures are composed by the same layer materials described in the previous examples and with SMR configuration. Table 5.6 presents the layer thicknesses of the CRF stacks. The two output CRF sections have the same configuration and the input CRF section has a different one. For the designed splitter, the thicknesses of the whole stack of layers are uniform over the three CRF sections, except for the top electrodes. The area of the CRF section corresponding to the input port is $20.5 \cdot 10^{-9} \text{ m}^2$ for this example. For each output CRF section, the area is half of the input section; it is $10.2 \cdot 10^{-9} \text{ m}^2$.

The simulation has been carried out modeling the acoustic effects by the Mason model. The simulated transmission and reflection responses of the power divider are given in Fig. 5.16. The result clearly shows a Chebyshev filter response with 20 dB return loss in the passband. The transmission responses S_{21} and S_{31} validate the equal power division over the 60 MHz passband. The transmission phase responses are in-phase. The outputs isolation is not good around 6 dB level, as seen in the plot Fig. 5.16, which is an expected result for this lossless, reciprocal 3-ports network. Only the input port is matched.

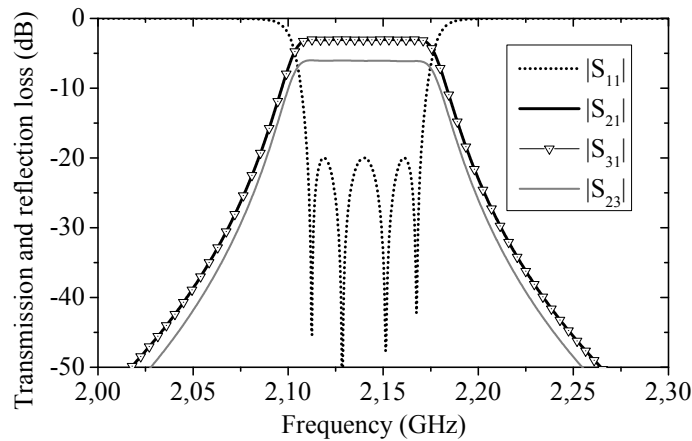


FIGURE 5.16: Filtering equal power divider response with topology II for W-CDMA application.

5.3.5 Comparison of two topologies for power divider based on CRF sections

The two different proposed topologies implement WCDMA 3dB split with inherent 4-th order filtering response and return loss of 20 dB at the input. The differences are in regard of the number of resonators shared by each output branch in a multiple coupled resonator configuration. While the first configuration has a total of 8 resonators and there is anyone shared, the second configuration has a total of 6 resonators and two of them are shared in the two input to output signal paths. Nevertheless, from the point of view of the frequency performance, differences are almost lacking, except for the isolation response, since in both configurations the two transmissions and input reflection responses are nearly identical. But, differences are observed in the isolation response, because the no-shared resonators topology exhibits a sharp roll-off in the near passband frequency regions. The $|S_{23}|$ on both configuration reflects different roll-offs. In the case of the two-shared resonator topology, the roll-off is lower than in the case of the no-shared resonator topology. The total number of resonators making up the multi-coupled resonator network is an important factor in the slope variations.

From the point of view of the of the structure, the differences are more noticeable. First one is regarding the total active area required for the structure. According the computed active area of the 2 input and 2 output

sections in the no-shared resonators configuration the total area can be estimated of $41.22 \cdot 10^{-9} \text{ m}^2$; likewise, for the two-shared resonators topology the total area of the 3 CRF stacks is of $51.20 \cdot 10^{-9} \text{ m}^2$ approximately. The difference is caused by the higher active area of the output sections on the second topology even though the whole structure requires one CRF section less.

When two CRF stacks look for uniformity among the layers but require different active areas, the coupling between to lower resonators is not affected by the different area size. The area neither affects the inter-resonator coupling of the coupling layer set. Hence, the thicknesses of the coupling layers are held, as well as the thicknesses of the lower resonators along the two different stacks. In contrast, the external quality factor and the resonance frequency for the upper resonators are dependent on the area [100]. The two different CRF stacks suffer a resonance frequency shift even though the external quality factor is slightly affected, then they are not according to the required values. As a consequence, an adjustment to tune the resonance frequency is required. The value is tuned with variations on the top electrodes thicknesses to maintain uniformity.

As a matter of fact, when analyzing the stack layer thicknesses over the two proposed configurations we found that for the lower resonators layers, as well as, the set of coupling layers are comparable. The computed thicknesses have variations of the order of 1 nm. Hence, we can consider them as equal, regarding the differences may be generated by the lack of precision on the sizing. The alike results are justified because both configurations describe the same Chebyshev function, where the terms of each topology corresponding coupling matrix are related.

5.4 Summary

The integration of a bandpass filter and a power divider allows miniaturization in RF transceivers. This chapter describes power distribution networks with filtering function embedded, composed of ladder-type filters, as well as coupled resonators filters. The technology lying behind all proposed networks is the acoustic wave technology characterized as a high-miniaturized components. Two design procedures allow the synthesis of realizable T-junction divider circuits.

The first approach using two ladder-type structures connected to generated a T-junction divider, is based on the analytical methodology of design of a

ladder-type filter with I/O impedance transformation required on the power divider circuit. Beside, the methodology considers the defined material system constraints to accommodate the resonator capacitance ratio in the resulting design. Two examples of filtering power dividers for application on W-CDMA, one with a 3-dB split and the other with a power division ratio α^2 of 2, have been synthesized and simulated based on the MBVD model for acoustic wave resonators and including losses. Transmission responses on the power divider provides filtering performance with transmission zeros near the passband, which are inherent features of acoustic wave technology in ladder configuration.

In the second approach a different methodology has been followed to use CRF structures in coupled resonator power dividers. This is accomplished by forming a multi-coupled resonators divider from the optimization of the multiple ports coupling matrix for a given characteristic polynomials of a Chebyshev filtering response. For a given prototype coupled resonator 3-port network the dimensioning of the physical CRF stacks is carried out denormalizing the prototype to values of external quality factors and coupling coefficients in the bandpass frequency domain and its association with the physical multi-layer CRF structure. We have reported two specific 3-dB power dividers for implementation with CRF blocks in Rx WCDMA band 1 application, offering compact design and contributing to the stringent miniaturization. Although both configurations exhibit same transmission responses and input reflection responses, they differ in the number of resonators re-used in the input to output paths, as well as, the total active area for each realization. The first topology, with no-shared resonators presents a large number of resonators than the second one with two-shared resonator, however the computed total active area in the first splitter is smaller and the out-of-band isolation higher. Moreover, the proposed designs simplify the fabrication process giving uniformity on the layers thicknesses for all the CRF sections.

Proposed dividers are not isolated at the output ports and therefore are not matched at all ports. The bad isolation is a feature of lossless reciprocal 3-ports junctions. For practical applications, such an isolation between the output ports of the splitter may not be adequate, hence it is possible to improve it by an appropriate choice of an isolation circuit.

In conclusion, the proposed power dividers based on different acoustic wave configurations prove to be particularly valuable to compete in the high-miniaturized components segment with outstanding filtering performance.

6 | CONCLUSIONS AND FUTURE WORK

In this final chapter, we summarize the research finding and conclusions according to a general view and the significance of the contribution. Additionally, some suggestion of improvement as well as recommendations for possible future work will be highlighted.

6.1 Conclusions

The rapid growth in mobile phones and smartphones underlies the large demand for smartphone filters and duplexers. The deployment of Long Term Evolution wireless technology of 4G systems and the expected development of 5G systems has exploded the number of filters required in handsets. The filter technologies which completely dominate cell phone market are the SAW and BAW filters based on piezoelectric acoustic resonators. Moreover, without the small size property of SAW and BAW technologies, it would have been impossible the coexistence of more than 50 filters in a front-end, along with highlighted features such as good insertion loss and steep skirts.

The forces driving the close proximity of passbands are bands proliferation and spectrum crowding. Moreover, the trend to combine bands and functionalities results in a reduction of filter count and area, but makes specifications more challenging. The way to overcome these issues is with very high-performance filters and duplexers which exhibit high-Q for extremely steep skirts.

While acoustic wave filtering solutions are maturing and providing solutions for several RF filter requirements and applications, there is enough room

for further research in topics such as: manufacturing processes, characterization of acoustic materials, device modeling, device design, new materials, new devices and structures, simulations, etc.

Within the existing filters configurations, the ladder type is the most commonly used. Usually ladder filter design techniques have not been explored in depth and have been mainly entrusted to optimization techniques. The main reason for why optimization is a widespread design approach is because the stringent constraints imposed by the capacitance ratio of piezoelectric resonators and the challenging electrical specifications makes the synthesis of acoustic filters a complex task with just few degrees of freedom. One aim of the work was focused on easing their design and making it more efficient. Consequently, the initial formulation of the problem has been focused on the technological feasibility of acoustic filters. Providing a systematic methodology is also useful to accelerate the learning curve of new entrant designers.

The fulfillment of the onerous high-selectivity specifications are addressed necessarily with the introduction of finite transmission zeros. The realization of inline prototypes with non-resonant nodes can generate finite frequency transmission zeros in the filtering response up to a number equal to the filter order. We have selected the inline configuration because of the advantages it supposes and the similarities regarding the characteristics of a ladder network of acoustic wave resonators. The observed features are the property of modularity, since the position of transmission zeros can be controlled independently by tuning resonant frequencies of resonators and capacity to offer a fully canonical response without the need of a direct coupling between source and load, but existing through a reactive path.

In Chapter 2, all the expressions and network synthesis tools, to deal with the proposed inline configuration with non-resonant and resonant nodes, are described. The object of the chapter involves all the lowpass synthesis base employed along the research. Some significant contributions are:

- The reflection phase term can be suitably obtained for a desired value at a specific frequency. The utility of the property is to face duplexers synthesis, where the phase is controlled to meet the open-circuit condition to avoid destructive interferences. The relationship between external elements required to satisfy the phase condition is analytically obtained.
- The control of situations, such as designs with I/O impedance transformation or asymmetrical networks, are evaluated for the analytical

extraction. Additionally, when the reflection parameter phase is not calculated at the first TZ, because it is calculated at the counterband of the Tx or Rx center frequency band, are also analyzed.

We have proved that microwave ladder filters with acoustic wave resonators can be modeled by inline coupled resonant or non-resonant nodes. An association of a lowpass prototype circuit with the acoustic wave resonator, involving motional and electrical resonance, has facilitated an analytical and systematic way of synthesizing it. The use of the BVD model, which is a simple lumped-element circuit, is accurately for the main vibrational mode of SAW and BAW resonators. The lowpass prototype is represented in a general definition of the coupling matrix with mixed nature of couplings. The coupling theory is a powerful technique for the formulation of the filter, which allows advanced implementations as well, for example consideration of acoustic coupled resonators and cross-couplings.

The procedure is time efficient and precise in the outcomes, likewise, it provides a deep understanding of the particular interactions between technology constraints and device performance. Assuming a set of electrical specifications and technological constraints the filter is entirely determined.

In Chapter 3, ladder-type filter circuits based on acoustic wave technologies have been accurately designed without having to use heavy-computation simulations for optimization goals. The key for a faster and higher simulation is the prediction of an accurate performance through a circuit synthesis design process that relies on coupled resonator theory. Consequently, in this chapter we explained the synthesis-based approach to quickly and easily design an acoustic wave filtering device.

Direct implications, of this main contribution involves:

- The number of design challenges and trade-offs characteristics of acoustic wave technologies can be easily evaluated in order to achieve a successful circuit implementation. There are several technological features, such as: uniform capacitance ratios, minimum number of external elements, highly reduced filter area, power durability, etc.
- The synthesis process enables filter designers to quickly achieve an optimal topology starting point design, becoming a seed for a last-step optimization.
- The automation of the solution search based on the synthesis approach is able to combine spectrum mask goals fulfillment with topologies ready to accommodate technological constraints of micro-acoustic

technologies.

- The methodology has been successfully evaluated to design stand alone filters without input/output reactive elements, as well as to face a duplexer synthesis, where the reflection phase term has been properly evaluated to meet the right phase condition to avoid destructive interferences.
- The nature, the value and the position of all the external reactive elements are directly obtained.

A direct outcome of the developed design method is a software tool which automatizes the process. The software package has been developed under a toolbox for Matlab. As a result of the work developed, SAW and BAW manufacturing firm (TDK-EPC) has already show its interest and has started to employ the software. The software is a complete set of fast, accurate and easy-to-use simulator enabling first-pass design success. Moreover, it is native oriented to accommodate electromechanical coupling constraints.

The general systematic methodology has been extended to take into consideration the design of a variety of filtering devices like hybrid filters and filtering power dividers.

In Chapter 4, the methodology has been extended for hybrid topologies that combine extracted-ole blocks with coupling resonator blocks. The synthesis of hybrid filters also accommodates acoustic-wave technological constraints. The utility considers several coupled resonator filters and the combination of ladder structures with acoustically coupled building blocks.

In Chapter 5, we developed the design which applies the acoustic wave technology to contribute on the size reduction of power dividers. The object is addressed by two different configurations: one is the ladder topology and the other is with CRF-based dividing structures. The synthesis of arbitrary ratio dividers with ladder filters which integrate filtering responses has been presented, resulting in frequency responses with transmission zeros near the passband and inherent inband transmission split. For the second approach, we give the guidelines for the design of three-port filtering dividers based on coupling theory, involving coupling matrix optimization. We illustrate the design of two 3-dB splitters based on CRF sections which differ in their structures, while presenting similar output transmission responses.

6.2 Future research recommendations

Even though, the work presented is focused in the synthesis of acoustic wave filtering devices, some extended questions and future work lines that could be addressed are identified.

The matrix representation with mixed nature nodes have shown to be very useful, however it does not allow the general application of similarity transformations for such structures with resonant and non-resonant nodes. The capacity to extend the transformations to blocks which contain simultaneously resonant and non-resonant nodes must be figured out. Moreover we must be able to define transformations between different dimension spaces in order to configure topologies efficiently and systematically.

A possible task for the future is the development of an improved technique to directly synthesis filters in bandpass, with arbitrary bandwidth, arbitrary transmission zeros and canonical structure. In comparison with other techniques already studied in the literature, the ladder topology with micro-acoustic resonators exhibits, in the transmission response, singularities at the origin which are not associated with reflection zeros singularities of polynomial F observed in the passband. These differences must be solved for the direct bandpass synthesis.

The methodology can be successfully extended to take into consideration cross-couplings circuits. Cross-couplings circuits are configured to bypass series or shunt resonators with inductors or capacitors. The methodology also shows the potential to include parasitic electromagnetic cross-couplings inside the die.

Commonly in the filtering network analysis, it is assumed that resonators have a high quality factor (Q) or are lossless. The effect of using medium- Q resonators is well known, producing a strong degradation of the filter performance. The use of lossy filters synthesis techniques are able to control a non uniform distribution of the quality factor in the network which can provide a high potential in filtering networks with acoustic wave resonators where they have not been applied yet.

As a result of the activity for the development of a design method able to synthesis hybrid topologies with ladder blocks and DMS-CRF sections, we studied models perfectly adjusted to DMS structures. We have worked in three different circuit topologies to model the DMS, however, because of intellectual property reasons we are not allow of presenting them. The advanced models absolutely match with the frequency response in magnitude

and phase and the group delay. Each one of the three models offers different characteristics in terms of synthesis and interpretation of the physical couplings in the device.

It can be also possible to explore the possibility of incorporate to the software tool, based on the systematic design, the electromagnetic (EM) simulations result of an established layout of dies and laminate. An even further perspective could be the implementation and evaluation of the EM couplings of the structure with an equivalent model.

BIBLIOGRAPHY

- [1] Cisco, “Cisco visual networking index: Global mobile data traffic forecast update, 2014–2019,” Cisco, San Jose, CA, Tech. Rep., Feb. 2015. [Online]. Available: www.cisco.com
- [2] W. Oh, “Global mobile phone shipments reach 445 million units in q1 2015,” Tech. Rep., Apr. 2015. [Online]. Available: www.strategyanalytics.com/strategy-analytics/blogs/devices/handsets/handset/2015/05/05/global-mobile-phone-shipments-reach-445-million-units-in-q1-2015
- [3] A. Ericsson, “Ericsson mobility report, on the pulse of the networked society,” Ericsson, Sweden, Tech. Rep. EAB-14:061078 Uen, Revision A, Nov. 2014. [Online]. Available: www.ericsson.com
- [4] J.-E. Mueller, T. Bruder, P. Herrero, N. Norholm, P. Olesen, J. Rizk, and L. Schumacher, “Requirements for reconfigurable 4G front-ends,” in *Microwave Symposium Digest (IMS), 2013 IEEE MTT-S International*, June 2013, pp. 1–4.
- [5] U. Bauernschmitt, C. Block, P. Hagn, G. Kovacs, A. Przadka, and C. Ruppel, “Concepts for RF Front-Ends for Multi-Mode, Multi-Band Cellular Phones,” in *Wireless Technologies, 2007 European Conference on*, Oct 2007, pp. 130–133.
- [6] R. Aigner, “Filter technologies for converged RF-frontend architectures: SAW, BAW and beyond,” in *Silicon Monolithic Integrated Circuits in RF Systems (SiRF), 2010 Topical Meeting on*, Jan 2010, pp. 136–139.
- [7] M. Li, M. El-Hakiki, D. Kalim, T.-Y. Kim, A. Link, B. Schumann, and R. Aigner, “A fully matched LTE-A carrier aggregation quadruplexer based on BAW and SAW technologies,” in *Ultrasonics Symposium (IUS), 2014 IEEE International*, Sept 2014, pp. 77–80.

- [8] R. Aigner, "Tunable Filters? Reality Check Foreseeable Trends in System Architecture for Tunable RF Filters," *Microwave Magazine, IEEE*, vol. 16, no. 7, pp. 82–88, Aug 2015.
- [9] "Leveraging advanced filter technology for regional demands," Tech. Rep., Feb. 2015. [Online]. Available: www.qorvo.com/docs/brochures/qorvo-filter-technology.pdf
- [10] U. Bauernschmitt, C. Block, P. Hagn, H. Klamm, G. Kovacs, and et al., "Advanced microwave acoustic filters enabling advanced system concepts," in *Elect. Compon. and Tech. Conf.*, May 2008, pp. 706–712.
- [11] *2535 MHz BAW Band 7 Uplink Filter*, TriQuint-Qorvo, 2014, rev. B 07-16-14.
- [12] R. Ruby, "Review and Comparison of Bulk Acoustic Wave FBAR, SMR Technology," in *IEEE Ultrasonics Symposium*, Oct 2007, pp. 1029–1040.
- [13] R. Aigner, "SAW and BAW technologies for RF filter applications: A review of the relative strengths and weaknesses," in *Ultrasonics Symposium, 2008. IUS 2008. IEEE*, Nov 2008, pp. 582–589.
- [14] G. Fattinger, J. Kaitila, R. Aigner, and W. Nessler, "Thin film bulk acoustic wave devices for applications at 5.2 GHz," in *Ultrasonics, 2003 IEEE Symposium on*, vol. 1, Oct 2003, pp. 174–177 Vol.1.
- [15] G. Endoh, M. Ueda, O. Kawachi, and Y. Fujiwara, "High performance balanced type SAW filters in the range of 900 MHz and 1.9 GHz," in *Ultrasonics Symposium, 1997. Proceedings., 1997 IEEE*, vol. 1, Oct 1997, pp. 41–44 vol.1.
- [16] G. Fattinger, J. Kaitila, R. Aigner, and W. Nessler, "Single-to-balanced filters for mobile phones using coupled resonator BAW technology," in *Ultrasonics Symposium, 2004 IEEE*, vol. 1, Aug 2004, pp. 416–419 Vol.1.
- [17] L. Mourot, P. Bar, C. Arnaud, G. Parat, and J.-F. Carpentier, "Coupled Resonator Filters for W-CDMA Duplexer Application," in *Silicon Monolithic Integrated Circuits in RF Systems, 2008. SiRF 2008. IEEE Topical Meeting on*, Jan 2008, pp. 214–217.
- [18] R. Lerch, "Simulation of piezoelectric devices by two- and three-dimensional finite elements," *Ultrasonics, Ferroelectrics, and Fre-*

-
- quency Control, IEEE Transactions on*, vol. 37, no. 3, pp. 233–247, May 1990.
- [19] M. Hofer, N. Finger, G. Kovacs, J. Schoberl, U. Langer, and R. Lerch, “Finite element simulation of bulk- and surface acoustic wave (SAW) interaction in SAW devices,” in *Ultrasonics Symposium, 2002. Proceedings. 2002 IEEE*, vol. 1, Oct 2002, pp. 53–56 vol.1.
- [20] (2015) Mems module: Software for microelectromechanical systems (mems) simulations. COMSOL, Inc. [Online]. Available: www.comsol.com/mems-module
- [21] I. Larson, J.D., R. Bradley, S. Wartenberg, and R. Ruby, “Modified Butterworth-Van Dyke circuit for FBAR resonators and automated measurement system,” in *IEEE Ultrasonics Symposium*, vol. 1, Oct 2000, pp. 863–868.
- [22] W. P. Mason, *Piezoelectric crystals and their application to ultrasonics*. Princeton, NJ: van Nostrand, 1950.
- [23] J. Rosenbaum, *Bulk acoustic wave theory and devices*. Norwood, MA: Artech House, 1988.
- [24] R. J. Cameron, R. Mansour, and C. M. Kudsia, *Microwave Filters for Communication Systems: Fundamentals, Design and Applications*. NJ, USA: Wiley-Interscience, 2007.
- [25] R. J. Cameron, “Fast generation of Chebyshev filter prototypes with asymmetrically-prescribed transmission zeros,” *ESA Journal*, vol. 6, pp. 83–95, 1982.
- [26] S. Amari, “Synthesis of cross-coupled resonator filters using an analytical gradient-based optimization technique,” *Microwave Theory and Techniques, IEEE Transactions on*, vol. 48, no. 9, pp. 1559–1564, Sep 2000.
- [27] R. J. Cameron, “General coupling matrix synthesis methods for chebyshev filtering functions,” *Microwave Theory and Techniques, IEEE Transactions on*, vol. 47, no. 4, pp. 433–442, Apr 1999.
- [28] S. B. Cohn, “Direct-coupled-resonator filters,” *Proceedings of the IRE*, vol. 45, no. 2, pp. 187–196, Feb 1957.
- [29] J. Rhodes, “A low-pass prototype network for microwave linear phase filters,” *Microwave Theory and Techniques, IEEE Transactions on*, vol. 18, no. 6, pp. 290–301, Jun 1970.

- [30] A. Atia and A. Williams, "Narrow-bandpass waveguide filters," *Microwave Theory and Techniques, IEEE Transactions on*, vol. 20, no. 4, pp. 258–265, Apr 1972.
- [31] R. Kurzrok, "General Three-Resonator Filters in Waveguide," *IEEE Transactions on Microwave Theory and Techniques*, vol. 14, no. 1, pp. 46–47, Jan. 1966.
- [32] A. Atia, A. Williams, and R. Newcomb, "Narrow-band multiple-coupled cavity synthesis," *IEEE Transactions on Circuits and Systems*, vol. 21, no. 5, pp. 649–655, Sep. 1974.
- [33] R. Levy, "Direct synthesis of cascaded quadruplet (CQ) filters," *Microwave Theory and Techniques, IEEE Transactions on*, vol. 43, no. 12, pp. 2940–2945, Dec 1995.
- [34] R. Hershtig, R. Levy, and K. Zaki, "Synthesis and Design of Cascaded Trisection (CT) Dielectric Resonator Filters," in *Microwave Conference, 1997. 27th European*, vol. 2, Sept 1997, pp. 784–791.
- [35] R. Cameron, "Advanced coupling matrix synthesis techniques for microwave filters," *IEEE Transactions on Microwave Theory and Techniques*, vol. 51, no. 1, pp. 1–10, Jan. 2003.
- [36] S. Amari, "Direct synthesis of folded symmetric resonator filters with source-load coupling," *Microwave and Wireless Components Letters, IEEE*, vol. 11, no. 6, pp. 264–266, June 2001.
- [37] J. R. Montejo-Garai and J. M. Rebollar, "Synthesis and design of N-order filters with N-transmission zeros by means of source-load direct coupling," *Microwave and Optical Technology Letters*, vol. 29, no. 4, pp. 248–252, May 2001.
- [38] J. Rhodes and R. Cameron, "General Extracted Pole Synthesis Technique with Applications to Low-Loss TE/sub011/ Mode Filters," *IEEE Transactions on Microwave Theory and Techniques*, vol. 28, no. 9, pp. 1018–1028, Sep. 1980.
- [39] S. Amari and U. Rosenberg, "A third order in-line pseudo-elliptic filter with a transmission zero extracted at its center," in *Microwave Symposium Digest, 2004 IEEE MTT-S International*, vol. 2, June 2004, pp. 459–462 Vol.2.

-
- [40] G. Macchiarella, "Synthesis of an in-line prototype filter with two transmission zeros without cross couplings," *Microwave and Wireless Components Letters, IEEE*, vol. 14, no. 1, pp. 19–21, Jan 2004.
- [41] S. Amari and U. Rosenberg, "Synthesis and design of novel in-line filters with one or two real transmission zeros," *Microwave Theory and Techniques, IEEE Transactions on*, vol. 52, no. 5, pp. 1464–1478, May 2004.
- [42] J. Montejo-Garai, J. Ruiz-Cruz, J. Rebollar, M. Padilla-Cruz, A. Onoro-Navarro, and I. Hidalgo-Carpintero, "Synthesis and design of in-line N-order filters with N real transmission zeros by means of extracted poles implemented in low-cost rectangular H-plane waveguide," *Microwave Theory and Techniques, IEEE Transactions on*, vol. 53, no. 5, pp. 1636–1642, May 2005.
- [43] S. Amari and G. Macchiarella, "Synthesis of inline filters with arbitrarily placed attenuation poles by using nonresonating nodes," *IEEE Transactions on Microwave Theory and Techniques*, vol. 53, no. 10, pp. 3075–3081, Oct. 2005.
- [44] A. Sivadas and R. Cameron, "A simplified analysis for high power microwave bandpass filter structures," in *2000 IEEE MTT-S International Microwave Symposium Digest (Cat. No.00CH37017)*, vol. 3. IEEE, 2000, pp. 1771–1774.
- [45] R. J. Cameron, "Advanced filter synthesis," *Microwave Magazine, IEEE*, vol. 12, no. 6, pp. 42–61, Oct 2011.
- [46] A. Garcia-Lamperez, M. Salazar-Palma, and T. Sarkar, "Analytical synthesis of microwave multiport networks," in *IEEE MTT-S International Microwave Symposium Digest*, vol. 2, 2004, pp. 455–458.
- [47] J. D. N. Cheeke, *Fundamentals and applications of ultrasonic waves*, 2nd ed. Boca Raton, FL: CRC press, 2012.
- [48] R. Weigel, D. Morgan, J. Owens, A. Ballato, K. Lakin, K.-Y. Hashimoto, and C. Ruppel, "Microwave acoustic materials, devices, and applications," *Microwave Theory and Techniques, IEEE Transactions on*, vol. 50, no. 3, pp. 738–749, Mar 2002.
- [49] C. Campbell, *Surface acoustic wave devices for mobile and wireless communications*. Academic press, 1998.

- [50] P. Wright, "Modeling and Experimental Measurements of the Reflection Properties of SAW Metallic Gratings," in *IEEE 1984 Ultrasonics Symposium*, Nov 1984, pp. 54–63.
- [51] K.-Y. Hashimoto, *Surface Acoustic Wave Devices in Telecommunications: Modelling and Simulation*. Berlin: Springer, 2000.
- [52] Y. Koyamada, F. Ishihara, and S. Yoshikawa, "Narrow-band filters employing surface-acoustic-wave resonators," *Proceedings of the IEEE*, vol. 64, no. 5, pp. 685–687, May 1976.
- [53] K.-Y. Hashimoto, T. Omori, and M. Yamaguchi, "Design considerations on surface acoustic wave resonators with significant internal reflection in interdigital transducers," *Ultrasonics, Ferroelectrics, and Frequency Control, IEEE Transactions on*, vol. 51, no. 11, pp. 1394–1403, Nov 2004.
- [54] K.-y. Hashimoto, *Surface acoustic wave devices in telecommunications*. Berlin: Springer, 2000.
- [55] W. Newell, "Ultrasonics in integrated electronics," *Proceedings of the IEEE*, vol. 53, no. 10, pp. 1305–1309, Oct 1965.
- [56] K. Lakin, "Thin film resonator technology," *Ultrasonics, Ferroelectrics, and Frequency Control, IEEE Transactions on*, vol. 52, no. 5, pp. 707–716, May 2005.
- [57] R. Ruby, P. Bradley, Y. Oshmyansky, A. Chien, and I. Larson, J.D., "Thin film bulk wave acoustic resonators (FBAR) for wireless applications," in *Ultrasonics Symposium, 2001 IEEE*, vol. 1, 2001, pp. 813–821 vol.1.
- [58] K. Lakin, G. Kline, and K. McCarron, "Development of miniature filters for wireless applications," *Microwave Theory and Techniques, IEEE Transactions on*, vol. 43, no. 12, pp. 2933–2939, Dec 1995.
- [59] K. Lakin, "Modeling of thin film resonators and filters," in *Microwave Symposium Digest, 1992., IEEE MTT-S International*, June 1992, pp. 149–152 vol.1.
- [60] F. Bi and B. Barber, "Bulk acoustic wave RF technology," *Microwave Magazine, IEEE*, vol. 9, no. 5, pp. 65–80, Oct 2008.
- [61] "IRE Standards on Piezoelectric Crystals: Measurements of Piezoelectric Ceramics," *Proceedings of the IRE*, vol. 49, no. 7, pp. 1161–1169, July 1961.

-
- [62] G. Carlotti, F. Hickernell, H. Liaw, L. Palmieri, G. Socino, and E. Verona, "The elastic constants of sputtered aluminum nitride films," in *Ultrasonics Symposium, 1995. Proceedings., 1995 IEEE*, vol. 1, nov 1995, pp. 353–356 vol.1.
- [63] K. Lakin, "Thin film resonators and filters," in *Ultrasonics Symposium, 1999. Proceedings. 1999 IEEE*, vol. 2, 1999, pp. 895–906 vol.2.
- [64] S. Takahashi, H. Hirano, T. Kodama, F. Miyashiro, B. Suzuki, A. Onoe, T. Adachi, and K. Fujinuma, "Saw IF Filter on LiTaO₃ for Color TV Receivers," *Consumer Electronics, IEEE Transactions on*, vol. CE-24, no. 3, pp. 337–348, Aug 1978.
- [65] R. Aigner, "MEMS in RF Filter Applications: Thin-film Bulk Acoustic Wave Technology," *Sensors Update*, vol. 12, no. 1, pp. 175–210, 2003.
- [66] O. Kawachi, G. Endoh, M. Ueda, O. Ikata, E. Hashimoto, and M. Yamaguchi, "Optimum cut of LiTaO₃ for high performance leaky surface acoustic wave filters," in *Ultrasonics Symposium, 1996. Proceedings., 1996 IEEE*, vol. 1, Nov 1996, pp. 71–76 vol.1.
- [67] "IRE Standards on Piezoelectric Crystals-The Piezoelectric Vibrator: Definitions and Methods of Measurement," *Proceedings of the IRE*, vol. 45, no. 3, pp. 353–358, March 1957.
- [68] I. Larson, J.D., R. Ruby, P. Bradley, and Y. Oshmyansky, "A BAW antenna duplexer for the 1900 MHz PCS band," in *Ultrasonics Symposium, 1999. Proceedings. 1999 IEEE*, vol. 2, 1999, pp. 887–890 vol.2.
- [69] D. M. Pozar, *Microwave Engineering*, 4th ed. New York, NY, USA: Wiley, 2011.
- [70] S. Amari, U. Rosenberg, and J. Bornemann, "Singlets, cascaded singlets, and the nonresonating node model for advanced modular design of elliptic filters," *IEEE Microwave and Wireless Components Letters*, vol. 14, no. 5, pp. 237–239, 2004.
- [71] R. J. Cameron, A. R. Harish, and C. J. Radcliffe, "Synthesis of advanced microwave filters without diagonal cross-couplings," in *IEEE Transactions on Microwave Theory and Techniques*, vol. 50, no. 12, 2002, pp. 2862–2872.

- [72] R.-Y. Lee, H.-Y. Lee, R. Ro, and H.-Y. Tung, "Design of DCS duplexer using SAW ladder filter," in *Intelligent Signal Processing and Communication Systems, 2004. ISPACS 2004. Proceedings of 2004 International Symposium on*, Nov 2004, pp. 754–757.
- [73] G. Macchiarella, M. Oldoni, and S. Tamiazzo, "Narrowband microwave filters with mixed topology," *Microwave Theory and Techniques, IEEE Transactions on*, vol. 60, no. 12, pp. 3980–3987, Dec 2012.
- [74] S. Tamiazzo and G. Macchiarella, "An analytical technique for the synthesis of cascaded N-tuplets cross-coupled resonators microwave filters using matrix rotations," *Microwave Theory and Techniques, IEEE Transactions on*, vol. 53, no. 5, pp. 1693–1698, May 2005.
- [75] S. Amari, "Direct synthesis of cascaded singlets and triplets by non-resonating node suppression," in *Microwave Symposium Digest, 2006. IEEE MTT-S International*, June 2006, pp. 123–126.
- [76] K. Lakin, "Equivalent circuit modeling of stacked crystal filters," in *Thirty Fifth Annual Frequency Control Symposium. 1981*, May 1981, pp. 257–262.
- [77] K.-Y. Hashimoto, T. Omori, and M. Yamaguchi, "Operation mechanism of double-mode surface acoustic wave filters with pitch-modulated idts and reflectors," *Ultrasonics, Ferroelectrics, and Frequency Control, IEEE Transactions on*, vol. 54, no. 10, pp. 2152–2158, October 2007.
- [78] K. Lakin, "Coupled resonator filters," in *Ultrasonics Symposium, IEEE Proceedings*, vol. 1, Oct 2002, pp. 901–908 vol.1.
- [79] G. Fattinger, R. Aigner, and W. Nessler, "Coupled bulk acoustic wave resonator filters: key technology for single-to-balanced RF filters," in *2004 IEEE MTT-S International Microwave Symposium Digest (IEEE Cat. No.04CH37535)*, vol. 2. IEEE, 2004, pp. 927–929.
- [80] E. Corrales López, "Analysis and Design of Bulk Acoustic Wave Filters Based on Acoustically Coupled Resonators," 2011.
- [81] A. Reinhardt, S. Laude, R. Lanz, P. Muralt, M. Solal, S. Ballandras, and W. Steichen, "Design of coupled resonator filters using admittance and scattering matrices," in *Ultrasonics, 2003 IEEE Symposium on*, vol. 2, Oct 2003, pp. 1428–1431.

-
- [82] E. Corrales, P. de Paco, O. Menendez, and J. Verdu, "Design of three-pole bulk acoustic wave coupled resonator filters," in *Microwave Conference, 2008. EuMC 2008. 38th European*, Oct 2008, pp. 357–360.
- [83] T. Morita, Y. Watanabe, M. Tanaka, and Y. Nakazawa, "Wideband low loss double mode SAW filters," in *Ultrasonics Symposium, 1992. Proceedings., IEEE 1992*, Oct 1992, pp. 95–104 vol.1.
- [84] G. Kovacs, W. Sauer, and T. Bauer, "DMS filter with reduced resistive losses," in *Ultrasonics Symposium, 2004 IEEE*, vol. 1, Aug 2004, pp. 294–297 Vol.1.
- [85] S. Ichikawa, H. Kanasaki, N. Akahori, M. Koshino, and Y. Ebata, "Mode analysis of longitudinal multi mode SAW resonator filter," in *Ultrasonics Symposium, 2001 IEEE*, vol. 1, 2001, pp. 101–106 vol.1.
- [86] K.-Y. Hashimoto, H. Kamizuma, M. Watanabe, T. Omori, and M. Yamaguchi, "Wavenumber domain analysis of two-dimensional SAW images captured by phase-sensitive laser probe system," *Ultrasonics, Ferroelectrics, and Frequency Control, IEEE Transactions on*, vol. 54, no. 5, pp. 1072–1075, May 2007.
- [87] K. Lakin, C. Andrus, J. Belsick, K. McCarron, and W. Thornhill, "Wide bandwidth thin film BAW filters," in *IEEE Ultrasonics Symposium, 2004*, vol. 1. IEEE, 2004.
- [88] M. Scardelletti, G. Ponchak, and T. Weller, "Miniaturized Wilkinson power dividers utilizing capacitive loading," *IEEE Microw. Wireless Compon. Letters*, vol. 12, no. 1, pp. 6–8, Jan 2002.
- [89] D.-J. Woo and T.-K. Lee, "Suppression of harmonics in Wilkinson power divider using dual-band rejection by asymmetric DGS," *Microwave Theory and Techniques, IEEE Transactions on*, vol. 53, no. 6, pp. 2139–2144, June 2005.
- [90] P. Cheong, K.-I. Lai, and K.-W. Tam, "Compact Wilkinson power divider with simultaneous bandpass response and harmonic suppression," *Microwave Symposium Digest (MTT), IEEE MTT-S International*, pp. 1588–1591, 2010.
- [91] Y. C. Li, Q. Xue, and X. Y. Zhang, "Single- and dual-band power dividers integrated with bandpass filters," *Microwave Theory and Techniques, IEEE Transactions on*, vol. 61, no. 1, pp. 69–76, Jan 2013.

- [92] C.-F. Chen, T.-Y. Huang, T.-M. Shen, and R.-B. Wu, "Design of Miniaturized Filtering Power Dividers for System-in-a-Package," *IEEE Transactions on Components, Packaging and Manufacturing Technology*, vol. 3, no. 10, pp. 1663–1672, Oct. 2013.
- [93] T. Skaik, M. Lancaster, and F. Huang, "Synthesis of multiple output coupled resonator circuits using coupling matrix optimisation," *IET Microw., Antennas Propagation*, vol. 5, no. 9, pp. 1081–1088, June 2011.
- [94] K. Song, F. Chen, F. Zhang, and Y. Fan, "Synthesis and design method of bandpass-response power divider," *Microelectronics Journal*, vol. 45, no. 1, pp. 71–77, Jan. 2014.
- [95] S. Mahon and R. Aigner, "Bulk acoustic wave devices-why, how, and where they are going," in *CS MANTECH Conf.*, 2007, pp. 15–18.
- [96] G. Macchiarella, "A powerful tool for the synthesis of prototype filters with arbitrary topology," in *Microwave Symposium Digest, 2003 IEEE MTT-S International*, vol. 3, June 2003, pp. 1467–1470.
- [97] A. Jayyousi and M. Lancaster, "A gradient-based optimization technique employing determinants for the synthesis of microwave coupled filters," in *Microwave Symposium Digest, 2004 IEEE MTT-S International*, vol. 3, June 2004, pp. 1369–1372.
- [98] W. Atia, K. Zaki, and A. Atia, "Synthesis of general topology multiple coupled resonator filters by optimization," in *Microwave Symposium Digest, 1998 IEEE MTT-S International*, vol. 2, June 1998, pp. 821–824.
- [99] M. Jimenez, E. Corrales, P. de Paco, and O. Menendez, "Design of a Coupled Resonator 3dB power divider based on BAW technology," in *IEEE Ultrasonics Symposium*, July 2013, pp. 2155–2158.
- [100] P. de Paco, O. Menendez, and E. Corrales, "Equivalent circuit modeling of coupled resonator filters," *IEEE transactions on ultrasonics, ferroelectrics, and frequency control*, vol. 55, no. 9, pp. 2030–7, Sep. 2008.